FLEXURAL ANCHORAGE PERFORMANCE AT DIAGONAL CRACK LOCATIONS

Final Report

SPR 661

FLEXURAL ANCHORAGE PERFORMANCE AT DIAGONAL CRACK LOCATIONS

Final Report

SPR 661

by

Christopher Higgins,
Mary Ann Triska and Joshua Goodall
Structural Engineering Group
Department of Civil and Construction Engineering
Oregon State University
220 Owen Hall
Corvallis, OR 97331

for

December 2010

Technical Report Documentation Page

1. Report No. FHWA-OR-RD-11-06	2. Government Accession No.	3. Recipient's Catalog No.
4. Title and Subtitle Flexural Anchorage Performance at Diagonal Crack Locations		5. Report Date December 2010
		6. Performing Organization Code
7. Author(s) Christopher Higgins, PhD; Mary Ann Triska and Joshua Goodall		8. Performing Organization Report No.
9. Performing Organization Name and Address Oregon State University Department of Civil and Construction Engineering 220 Owen Hall Corvallis, OR 97331		10. Work Unit No. (TRAIS)
		11. Contract or Grant No. SPR 661
12. Sponsoring Agency Name and Address Oregon Department of Transportation Research Section and Federal Highway Administration 200 Hawthorne Ave. SE, Suite B-240 400 Seventh Street, SW Salem, OR 97301-5192 Washington, DC 20590-0003		13. Type of Report and Period Covered Final Report
		14. Sponsoring Agency Code

15. Supplementary Notes

16. Abstract

Large numbers of reinforced concrete deck girder bridges that were constructed during the interstate system expansion of the 1950s have developed diagonal cracking in the stems. Though compliant with design codes when constructed, many of these bridges have flexural steel bars that were cut off short of the full length of the girders. When load-rating these structures, the current design specification check of tension reinforcement anchorage often controls the capacity of these bridges. The tensile force demand is controlled by the load-induced moment and shear, the number of stirrups, and the diagonal crack angle; however, little information is available regarding bond stresses developed with larger-diameter bars for full-size specimens in the presence of diagonal cracks.

This research used large-size specimens to investigate the influence of diagonal cracks near flexural cutoff locations on the behavior and strength of vintage reinforced concrete girders. Testing indicated that a diagonal crack crossing the development length of cutoff longitudinal bars may not necessarily control specimen failure. Analysis showed that the required tensile demand at a diagonal crack location as predicted by AASHTO LRFD was reasonable. Two analytical methods and a non-linear finite element method were investigated for predicting the failure mode and capacity of the laboratory beams. A procedure was developed to rate existing bridges for flexural anchorage requirements around cutoff locations. Cracking characteristics indicative of flexural reinforcement slippage were defined for bridge inspection.

17. Key Words REINFORCED CONCRETE BRIDGES, BEAMS, GIRDERS, CRACKING, FLEXURAL STRENGTH, BOND STRENGTH, PULL-OUT, ANCHORAGES	18. Distribution Statement Copies available from NTIS, and online at http://www.oregon.gov/ODOT/TD/TP_RES/

19. Security Classification (of this report) Unclassified	20. Security Classification (of this page) Unclassified	21. No. of Pages 166	22. Price

Technical Report Form DOT F 1700.7 (8-72)   Reproduction of completed page authorized   ♺ Printed on recycled paper

SI* (MODERN METRIC) CONVERSION FACTORS

APPROXIMATE CONVERSIONS TO SI UNITS

Symbol	When You Know	Multiply By	To Find	Symbol
LENGTH				
in	inches	25.4	millimeters	mm
ft	feet	0.305	meters	m
yd	yards	0.914	meters	m
mi	miles	1.61	kilometers	km
AREA				
in^2	square inches	645.2	millimeters squared	mm^2
ft^2	square feet	0.093	meters squared	m^2
yd^2	square yards	0.836	meters squared	m^2
ac	acres	0.405	hectares	ha
mi^2	square miles	2.59	kilometers squared	km^2
VOLUME				
fl oz	fluid ounces	29.57	milliliters	ml
gal	gallons	3.785	liters	L
ft^3	cubic feet	0.028	meters cubed	m^3
yd^3	cubic yards	0.765	meters cubed	m^3
NOTE: Volumes greater than 1000 L shall be shown in m^3.				
MASS				
oz	ounces	28.35	grams	g
lb	pounds	0.454	kilograms	kg
T	short tons (2000 lb)	0.907	megagrams	Mg
TEMPERATURE (exact)				
°F	Fahrenheit	(F-32)/1.8	Celsius	°C

APPROXIMATE CONVERSIONS FROM SI UNITS

Symbol	When You Know	Multiply By	To Find	Symbol
LENGTH				
mm	millimeters	0.039	inches	in
m	meters	3.28	feet	ft
m	meters	1.09	yards	yd
km	kilometers	0.621	miles	mi
AREA				
mm^2	millimeters squared	0.0016	square inches	in^2
m^2	meters squared	10.764	square feet	ft^2
m^2	meters squared	1.196	square yards	yd^2
ha	hectares	2.47	acres	ac
km^2	kilometers squared	0.386	square miles	mi^2
VOLUME				
ml	milliliters	0.034	fluid ounces	fl oz
L	liters	0.264	gallons	gal
m^3	meters cubed	35.315	cubic feet	ft^3
m^3	meters cubed	1.308	cubic yards	yd^3
MASS				
g	grams	0.035	ounces	oz
kg	kilograms	2.205	pounds	lb
Mg	megagrams	1.102	short tons (2000 lb)	T
TEMPERATURE (exact)				
°C	Celsius	1.8C+32	Fahrenheit	°F

*SI is the symbol for the International System of Measurement

ii:

ACKNOWLEDGEMENTS

DISCLAIMER

FLEXURAL ANCHORAGE PERFORMANCE AT DIAGONAL CRACK LOCATIONS

TABLE OF CONTENTS

APPENDICES

LIST OF TABLES

LIST OF PHOTOS/FIGURES

EXECUTIVE SUMMARY

Large numbers of reinforced concrete deck girder bridges that were constructed during the interstate system expansion of the 1950s have developed diagonal cracking in the stems. Compared to the present AASHTO-LRFD standards, the provisions of the 1950s allowed for higher shear stress in the concrete, thus reducing the amount of transverse steel required. Further, service loading has increased over time. When load-rating these structures, the current design specification check of tension reinforcement anchorage often controls the capacity of these bridges. This check compares the applied tensile force in the reinforcement to the tensile force available based on the reinforcement development length. The tensile force demand is controlled by the load-induced moment and shear, the number of stirrups, and the diagonal crack angle. However, the crack angle considered in the design specification is commonly flatter than the angle of the vertically-oriented cracks generally noted in field inspections. The tensile force that can be developed in the flexural reinforcing steel depends on the diameter of the bar and the embedded length; however, little information is currently available regarding bond stresses developed with larger-diameter bars for full-size specimens in the presence of diagonal cracks.

The objectives of this research were to provide bridge inspectors and rating engineers with tools to evaluate vintage reinforced concrete deck girder bridges containing diagonal cracks interacting with flexural reinforcing steel bar cutoffs. To meet these objectives, eight large-size specimens were designed, constructed, and tested to failure. Four of the specimens were T-beams and four of the specimens were IT-beams. Load application was cyclic without reversal applied in near-three-point loading symmetrically over the specimen centerline.

Three T-beam specimens were constructed using a plastic sheet to create a preformed diagonal crack, which controlled the initial diagonal crack geometry and eliminated aggregate interlock. Two preformed diagonal cracks were at 45° and one crack was at 60°, common crack angles observed in the field. The fourth specimen did not have a preformed crack, but contained similar reinforcing details to the other specimens. The cutoff bar location began at about one third the minimum development length (as defined by ACI 318-08 specification) away from where the 45° crack crossed the flexural reinforcing bars. A fourth specimen, without a preformed crack, was a control.

Four IT-beam specimens were constructed with a plastic preformed diagonal crack. Two preformed diagonal cracks were at 45° and two cracks were at 60°. Cutoff bars were provided with half the minimum design development length specified by the least conservative of the ACI 318 and AASHTO-LRFD specifications past the preformed crack.

Data were collected to assess the shear and flexural-induced tensile stresses in the reinforcing steel at various locations along the span, to verify specification analysis methods, and to assist in the development of new models for assessing anchorages in the presence of diagonal cracks. Conclusions based on the experimental and analytical results provided the framework for field inspection recommendations and evaluation methodologies.

EXPERIMENTAL CONCLUSIONS

The eight specimens showed that the presence of a diagonal crack crossing the development length of cutoff longitudinal bars may not necessarily control specimen failure. While existing diagonal cracking was seen to increase the tensile demand in the longitudinal reinforcement, it did not serve to indicate the eventual failure location. Under service-level loads, the preformed diagonal crack produced bond stresses that were higher at the crack location. However, as load increased to failure, the eventual diagonal failure crack often developed in a different section. If the failure crack location was not the same as the initially observed diagonal crack, peak bond stresses shifted to the new crack. The location of the failure crack depended on reinforcement detailing and load patterns, not necessarily the presence of diagonal cracks observed under lower level loads. The type of failure: flexure, shear-compression, or anchorage also depended on more predictable properties such as geometry at possible cutoff locations, the number of flexural bars, and stirrup spacing rather than highly variable cracks that developed during service-level conditions.

The data showed that the required tensile demand at a diagonal crack location as predicted by AASHTO-LRFD equation 5.8.3.5-1 was reasonable. Accurately estimating the additional demands in flexural bars at crack locations required inputting coincident moment and shear values rather than using maximum attained values for these parameters.

ANALYTICAL CONCLUSIONS

Prediction of beam capacity and failure mode requires analyzing sections along the length of the specimen, not just those sections that appear to be the weak points such as at diagonal crack locations, at the support, near the loading point, and along the length of developing bars. The shear, flexural, and anchorage capacities must be checked at each section. An anchorage failure will occur when the tensile demands in the flexural reinforcing steel exceeds the force that the reinforcing bar–concrete interface can resist. This can occur at load levels less than the shear and flexural capacities of the section.

To check for anchorage failure, the predicted tensile demand calculated by AASHTO-LRFD 5.8.3.5-1 for all potential failure angles should be compared to the tensile capacity using the maximum allowable bond stress. The present experimental results exhibited average bond strength values at anchorage failure approximately 175% of those predicted using the least conservative of ACI 318 and AASHTO-LRFD development length calculations. For cases where anchorage is identified as problematic using AASHTO-LRFD development lengths, the analyst may want to consider ACI 318 detailed equations, or that proposed by Darwin (1996) as these were more representative and still conservative in the present experimental findings.

Two analysis methods were developed to predict the failure mode and capacity. These used bond strengths from any of the available sources (ACI, AASHTO, Darwin 1996). When investigating the governing failure mechanism for existing structures using Analysis Method 2, there was a slight discrepancy between the least conservative ACI 318 and AASHTO-LRFD design development length predictions and development length predicted using experimentally measured maximum average bond stresses. In many cases, the most conservative specification

2

method accurately predicted the failure mechanism. However, in scenarios where the shear-compression and shear-anchorage failure capacities were closely grouped, specification-based methods incorrectly predicted anchorage failures due to an under-prediction of bond strength in areas with developing reinforcement.

Nonlinear finite element analysis using VecTor2 predicted the ultimate capacities and load–deformation behavior of the T-beam specimens quite well. The presence or absence of a modeled preformed crack did not significantly change which characteristic diagonal crack caused failure. However, the bond-slip relationship of the cutoff affected the bond stress in the reinforcement and the failure diagonal crack. Although VecTor2 predicted the load-deformation behavior of the IT-beam specimens well at low services levels, the ultimate capacities were not as well predicted. The presence or absence of a modeled preformed crack significantly changed the predicted cracking pattern and bond stresses. The IT specimens, due to lack of confinement around the developing flexural bars and resulting nonductile bond behavior due to splitting failure of the deck as well as smaller compression zone, showed higher sensitivity to the presence of diagonal cracks compared to the T specimens.

RECOMMENDATIONS

The experimental research supports a straightforward process for analyzing beams with cutoff details interacting with diagonal cracking. Existing cracking is not a definitive indicator of the failure location; therefore, each critical section across the length of the specimen must be analyzed to locate the weakest location and controlling angle. AASHTO-LRFD specifications provide methods to calculate critical shear and moment capacities based on interaction at a selected location. Using a more refined approach to calculate the expected development length allows for a more effective prediction of the tensile capacity of the anchorages (such as Darwin 1996 or ACI 318). The critical crack angle can then be derived from the AASHTO-LRFD specifications (Chapter 5) after calculating the shear stress in the concrete at the critical location. Modified Compression Field Theory can be used in accompaniment with the calculated critical crack angle to derive a necessary applied shear that produces tensile forces in the longitudinal bars sufficient enough to induce anchorage failure. For positive moment steel (T-beams), average bond strength for Gr. 420 (Gr. 60) reinforcement and an f_c' of 24.1 MPa (3500 psi) ranged from 3.86 to 8.27 MPa (0.560-1.200 ksi) with 97.5% lower confidence level reducing this value to 4.01 MPa (0.581 ksi.). Similarly, for negative moment steel (IT-beams), average bond strength for Gr. 420 (Gr. 60) reinforcement and an f_c' of 24.1 MPa (3500 psi) ranged from 4.48-4.83 MPa (0.650-0.700 ksi) with 97.5% lower confidence limit reducing this value to 3.76 MPa (0.546 ksi.). If the applied shear for anchorage failures is less than the controlling shear strength calculated by the shear and moment interaction analysis, anchorage failure at the section can be anticipated. If this is not the case, then the analyzed specimen may be expected to fail in either shear or flexure, depending on the M/V ratio and this interaction relationship at the critical location.

The crack patterns observed in each of the specimens near the cutoff bar location gives field inspectors examples of the kind of distress to look for prior to a possible anchorage failure. Section *4.1.2 Crack Growth in Specimens* more fully describes and provides photos of the particular anchorage cracking typically noted in T-beam and IT-beams. For T-beams, it is

recommended that inspectors look for a grouping of vertical and horizontal cracks near the stem soffit at the level of the flexural reinforcing steel and focus on those locations that are near cutoff locations shown in available structural drawings. Similarly, in negative moment regions near supports, inspectors should look for horizontal and chevron cracking on the underside of the deck. These types of distress are indicative of anchorage slip and should be followed up with additional scrutiny.

If anchorage cracking is observed, crack widths and locations should be noted. Further inspections should pay special attention to these areas over time to note changes and evolution of cracks. Plans should be made for strengthening and/or posting the bridge based on limiting anchorage demands. Diagonal cracking associated with the cutoffs should be noted and compared to analytical predictions of critical failure locations using the methods described in this report. Cracking occurring in areas near the predicted critical crack location may be a cause for particular concern. However, not all visible diagonal cracking will be indicative of the ultimate failure location or angle. A full detailed analytical investigation using provisions in the AASHTO-LRFD specifications combined with the methods described in this report should be undertaken to assess the member and identify probable failure mode and anchorage demand/capacity.

Finally, it is anticipated that some cutoff anchorages may not rate well, even with the refinement of analysis methods described in this report. It will be necessary to limit anchorage demands on these members (load post the bridge) or strengthen these members. Strengthening members for anchorage will require experimental and analytical study. As these studies take time, this research should be pursued as soon as possible so that results will be available to the design community prior to the need for field implementation.

1.0   INTRODUCTION

Large numbers of reinforced concrete deck girder (RCDG) bridges were constructed during the interstate system expansion of the 1950s and are approaching the end of their originally intended design lives. Over the last 60 years, service loading has increased in terms of volume and magnitude, thereby placing a higher demand on the system than originally envisioned. Compared to the present AASHTO-LRFD standards, the provisions of the 1950s allowed for higher shear stress in the concrete, thus reducing the amount of transverse steel required. The 1950s also saw the introduction and widespread use of standardized deformed reinforcing bars. Compared to proprietary reinforcing bars, standardized deformed bars were believed to provide adequate anchorage without the need for hooks and bends. As a consequence, designers terminated flexural steel without special detailing where it was no longer needed by calculation, while in the past, proprietary reinforcing bars would have been bent to ensure anchorage. Due to the combination of age, use, and what is now understood to be poor detailing, many RCDG bridges exhibit diagonal cracking in the stems. These cracks are sometimes associated with the flexural bar terminations and have been a cause of concern from some bridge engineers and owners.

The effects of existing diagonal cracks on the bond of flexural reinforcing bars are not well understood. Diagonal cracks occurring during service level loading do not necessarily imply those cracks cause ultimate failure of the structure. The geometric and material properties of the girder greatly influence the behavior of the structure including: the type and location of anchorage details, the amount of transverse reinforcement, and the compressive strength of the concrete. The effect of a diagonal crack on anchorage response depends on its overall relationship to the other section properties of the girder and loading. Improved understanding of the interactions would enable better evaluation of the load carrying capacity of cracked girders.

Since the early 2000s, Oregon State University has conducted experimental tests of vintage RCDG bridge girders (Higgins, *et al.* 2004). The typical specimen was a T-shaped girder that was 7.92 m (26 ft) long, with a 356 x 1067 mm (14 x 42 in.) stem, and a 914 mm wide by 152 mm thick (36 x 6 in.) deck. The deck was placed in such a way as to test either T (positive moment) and IT (negative moment) conditions. The concrete strength and grade of transverse steel reasonably mimicked the materials used in the 1950s. In this previous study, it was thought that none of the T-beam specimens failed in anchorage, even those specimens that had cutoff details.

The current research program made use of similar specimen proportions to test new specimens and also used some of the previous experimental data from the earlier test program to identify shear anchorage response. Ultimately, this research intended to improve the understanding of the behavior of flexural steel anchorage in the presence of diagonal cracks in RCDG bridge girders with 1950s vintage details and present analytical methods that adequately determine the capacity of these girders. To accomplish these goals, the research methodology included a literature review, construction and laboratory testing of realistic full-scale T-beam bridge girder specimens to evaluate strength and behavior, and use of several analytical methods to assess capacity. A

portion of the analysis included modeling the test specimens using the nonlinear finite element analysis program VecTor2, which was specifically designed for reinforced concrete.

1.1   RESEARCH OBJECTIVE

The objectives of this research were to:

- Investigate the role of idealized diagonal cracks near flexural cutoff locations on the behavior and strength of vintage RC girders in positive and negative moment regions.

- Develop methods, using test data, to rate existing bridges for flexural anchorage requirements around cutoff locations.

2.0   BACKGROUND

Over the last 65 years, a number of test programs have attempted to quantify the factors that influence bond stress. Most tests were performed at small scale, using smaller size reinforcing bars, and concrete blocks. A few pullout and beam-end tests have been conducted using larger bars, but there has been a lack of research involving full-scale specimens using the most common size bars found in vintage RCDG bridges. The following subsections include: a description of the anchorage failure mechanism, summaries of previous experimental research, a brief explanation of current design specifications and their history, a list of conclusions drawn from the literature, summary of research objectives based on the findings from the literature for the present test program.

2.1   ANCHORAGE CONCERNS

Flexural reinforcement detailing of vintage RCDG girders are considered insufficient by the design standards of today. Prior to the development of standardized deformed rebar in the late 1940s, designers used hooks, bends, and transitions (such as extending positive moment steel from the bottom of the girder to the top) to ensure anchorage of the flexural steel. In continuous girders, this positive moment steel was transitioned to become the negative moment steel over the piers. At the advent of the modern deformed bars, tests showed that the presence of deformations produced mechanical engagement with the surrounding concrete with greatly improved performance compared to that of the relatively weak chemical adhesion and friction relied upon from smooth or proprietary reinforcing steel. As a result, the design specifications were relaxed and allowed straight-bar cutoffs in regions where they were no longer needed for flexural capacity. Often the flexural bars were terminated near the quarter point of the girder. Today, AASHTO-LRFD requires these same bars to be detailed so as to prevent pullout and reduce stress concentrations within the cross-section.

There are two types of anchorage failures that occur when the tensile force demand in the flexural reinforcing steel exceeds the strength of the bond between the bar and the surrounding concrete: splitting anchorage failure and pullout anchorage failure. When sufficient force is applied to the deformed bar to break the chemical bond, the bar slips just enough to cause the deformations to bear on the concrete surface (Figure 2.1a and b). Splitting anchorage failures can be abrupt. As the bars slip, the surrounding concrete splits without the presence of transverse reinforcement around the bars. Specimens are more likely to experience splitting anchorage failures where flexural reinforcement has little cover and no encasing transverse reinforcement, such as in the flanges of IT-beams. In contrast, pullout anchorage failures can be more ductile. The bars that slip are confined by the stirrups, preventing sudden failure as the bars slip (Figure 2.1c). Even as the bars slip, the demand in the bars can continue to increase to the point that the flexural bars almost yield. Pullout anchorage failures are more likely in T-beams with transverse confinement provided by stirrups. The T-beams in this research program were all designed to produce anchorage failures.
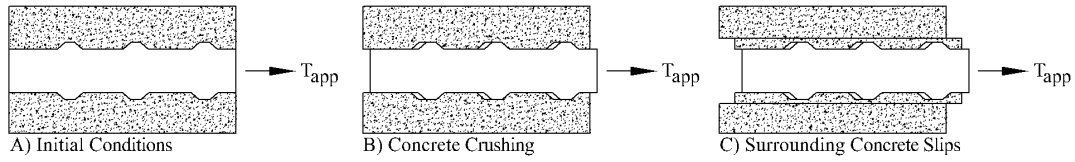
Figure 2.1: Pullout anchorage failure process

Stresses are transferred between the concrete and reinforcing steel through bond stress as illustrated in Figure 2.2. Experimentally, bond stress is difficult to measure; a wide range of factors influence the bond stress, including bar size, concrete strength, concrete cover, and confinement provided by transverse reinforcement and at supports.
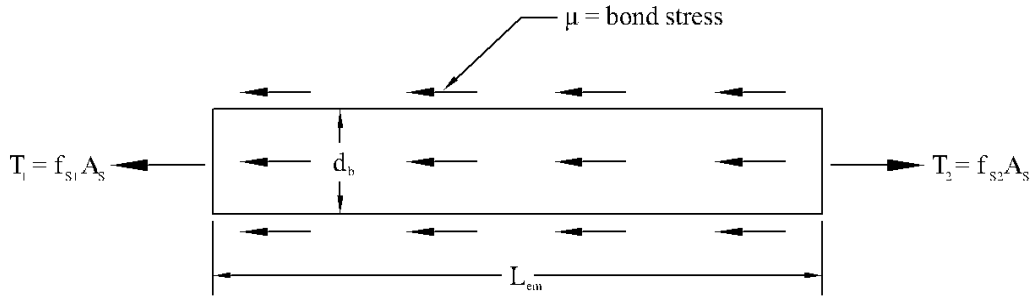
Figure 2.2: Forces acting on a segment of reinforcing steel

In theory, the average bond stress, μ_{avg}, over an incremental segment of reinforcement is:

$$\mu_{avg} = \frac{\Delta f_s d_b}{4 l_d}$$

[2.1]

where Δf_s is the change in reinforcement stress over the length of the segment which may not exceed the yield strength f_y of the steel, d_b is the bar diameter, and l_d is the segment length.

The true bond stress, μ, may be determined by taking l as a very small length, dx, such that:

$$\frac{df_s}{dx} = \frac{4\mu}{d_b}$$

[2.2]

In this report, average bond stress is used in all calculations. The average bond stress is converted to the resistive tensile force, T_μ, by multiplying the stress by the segment surface area, $\pi d_b l_{em}$, such that:

$$T_\mu = \mu_{avg} \pi d_b l_{em}$$

[2.3]

Bond stress may also be defined in terms of the minimum embedment length required to produce the yield stress in the reinforcing bar. If the average bond stress, μ_{avg}, is known from experiments, Eq [2.1] may be rewritten as:

8

$$l_d = \frac{f_y d_b}{4\mu_{avg}}$$ [2.4]

Eq. [2.4] is the basis for what modern design codes call "minimum development length."

Wherever a crack is present, the bond stress peaks as shown in Figure 2.3. Peak and average bond stress values reported in the literature vary greatly, with little information currently available regarding bond stresses of larger bars in full-size specimens in the presence of diagonal cracks.
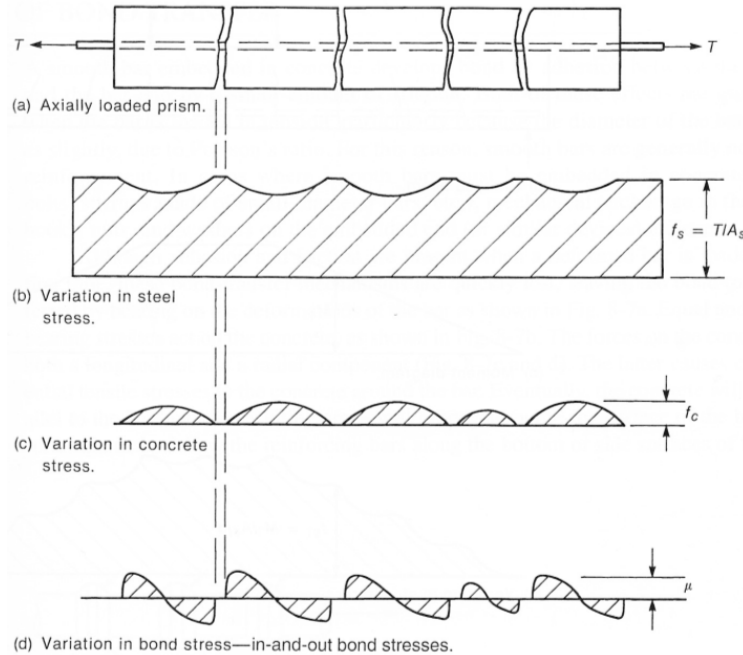
Figure 2.3: Bond stresses in a cracked prism (MacGregor and Wright 2005)

The AASHTO-LRFD Bridge Design Specifications uses an implementation of Modified Compression Field Theory (MCFT) to determine the shear capacity at a section. The theory recognizes the interaction of shear and moment on the strength of a member. AASHTO-LRFD also considers the effect of diagonal cracking on the flexural steel tensile demand, T. As shown in Figure 2.4, by summing moments around point A, the tensile demand is expressed as:
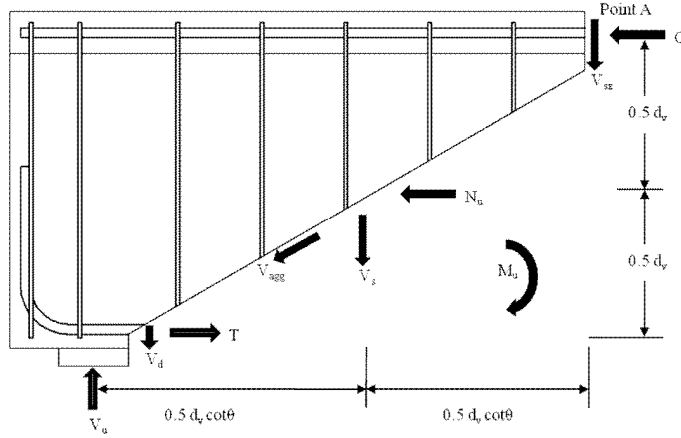
Figure 2.4: Internal forces in a diagonal cracked reinforced concrete section

$$T = \frac{M_u}{d_v} + 0.5N_u + (V_u - 0.5V_s - V_p)\cot\theta \qquad \text{AASHTO-LRFD 5.8.3.5-1} \qquad \textbf{[2.5]}$$

where M_u is the moment demand taken where the crack crosses the flexural steel; d_v is the effective section depth taken as the greater of 0.9d or 0.72h; d is the depth from the centroid of the flexural reinforcement to the top of the beam; h is the depth of the section; N_u is the axial force contribution; V_u is the shear demand; V_s is the tensile force carried by the stirrups; V_p is the shear carried by the prestressing strands; and θ is the diagonal crack angle. Other labeled forces in Fig. 2.4 are: the force in the concrete compression zone, C; the dowel action of the flexural bars, V_d; the shear carried by the concrete compression zone, V_{cz}; and the shear carried by aggregate interlock, V_{agg}. In Fig. 2.4, the V_d and V_{agg} forces are difficult to measure, are small compared to the other forces, and their inclusion in the tensile demand equation reduces the tensile demand. They are, therefore, ignored.

The current AASHTO-LRFD design specification check of tension reinforcement anchorage can control the capacity of vintage RCDG bridges. The check compares the applied tensile force in the reinforcement (Eq. [2.5]) to the tensile force developed by the bond between the reinforcement and the concrete (Eq. [2.3]). However, the crack angle considered by AASHTO-LRFD is flatter than the angle of the steeper cracks generally noted in field inspections.

2.2 LITERATURE REVIEW

Mylrea (*1948*) summarized known information regarding bond and anchorage research prior to 1947. From pullout and beams tests, engineers understood that bond stress is not uniformly distributed over the length of a bar. Further, the maximum bond stress in beam specimens is less than in pullout specimens. Bond stress varies with concrete strength, but not directly. In uncracked sections, it may be assumed that the bond is perfectly uniform, the total steel stress varying directly with the moment. However, once the section cracks under load, high bond stress occurs near the cracks, with lower stress in between the cracks as shown in Figure 2.3. As the slipping process proceeds, the bond stress at a particular point may increase with bar movement. This behavior occurs rapidly initially, then more slowly until the maximum bond stress is achieved at failure.

Clark (*1949*) conducted a number of beam and pullout tests to determine which type of deformed bar common in the 1940s developed the strongest bond. The specimens varied in bar size, embedment length and depth of concrete beneath the bar, and measured 203 x 457 x 1981 mm (8 x 18 x 78 in.). The largest bar investigated was a 28.6 mm (1-1/8 in.) square bar. Clark recommended two changes to the ASTM 305-47T standard for deformed reinforcing bars that were eventually adopted in ASTM 305-50T and are still present in the standard today (ASTM 615/A615M-09b 2009). One change specified the deformation spacing; the other, the deformation height. For a 22.2 mm ($^7/_8$ in.) bar, average bond stress values were about 2.07-2.76 MPa (300-400 psi), while peak bond stresses at crack locations were about 4.83-6.20 MPa (700-900 psi).

Mains (*1951*) used strain gages inside the reinforcing steel to quantify how bond stresses vary along the length of plain and deformed reinforcing bars. Most of the beam specimens measured 203 x 318 x 1981 mm (8 x 12.5 x 78 in.) with either straight or hooked No. 22 (No. 7) flexural bars. Both plain and non-ASTM 305-47T deformed bars were used. For the straight deformed bars, the maximum measure bond stress was 12.4 MPa (1800 psi), while the average bond stress calculated with code equations used at the time was 5.52 MPa (890 psi). The data showed that diagonal cracks caused an increase in bar forces and consequently caused a local increase in bond stresses at the crack.

Watstein and Bresler (*1974*) performed scaled beam experiments to examine the effects of shear on the tensile force and bond stresses developed in longitudinal reinforcements. Their results postulated that the discrete bond stress calculation at a point or over a given region, u_x, could be calculated as:

$$u_x = \frac{D}{4} E_s \frac{d\varepsilon_s}{dx}$$ **[2.6]**

where e_s is the measured bar strain, x is the length of bar considered, E_s is the elastic modulus of steel, and D is the diameter of the bar.

Doerr (*1978*) investigated the influence of transverse pressure on the bond stress-strain relationship by testing 25 cylinders equipped with a confining ring in pullout. Each 150 x 600 mm (5.91 x 23.6 in.) cylinder had a single No. 16 (No. 5) reinforcing bar embedded 500 mm (20.0 in.) into the concrete. Two strain gages measured the strain of the concrete and reinforcing bar. Each specimen was loaded in tension by pulling on the extended bar ends, and the transverse pressure was varied from 0 – 15 MPa (0 – 2175 psi). From the data, Doerr concluded that the bond stress $\tau(x)$ along the length of the bar could be calculated as:

$$\tau(x) = -\frac{1}{u} \frac{dP(x)}{dx}$$ **[2.7]**

where u is the bar diameter, and $P(x)$ is the force at a point x along the length of the bar.

Losberg and Olsson (*1979*) systematically tested standard and altered Swedish reinforcing bars to determine which characteristics of reinforcing bars reduced splitting failures while maximizing bond. Diameter of bar, height of lug, inclination of lug, and distance between lugs were varied. Pullout tests established the lower limit of maximum bond without splitting failure, while beam-end tests allowed realistic splitting failures to occur. Ring pullout tests were used to directly measure splitting force. The data showed that lug height and spacing made a negligible contribution to splitting failures. Splitting failures were more likely to occur with increased lug inclination rather than with transverse lugs. The amount of transverse reinforcement crossing the splitting surface greatly influenced the force developed in the reinforcing steel.

Reynolds and Beeby (*1982*) investigated the effect of transverse steel on bond stresses in lap splices. They noted in beam tests using 100 x 200 x 1220 mm (3.94 x 7.87 x 48.0 in.) specimens with No. 16 (0.63 in dia.) flexural bars and No. 8 (0.32 in dia.) stirrups that the increase in bond strength from the transverse confinement depended on lap splice location. When the splice was in a constant moment region, the increase in bond strength was slight because the stirrups were not fully engaged. However, in regions with diagonal shear cracks and the transverse steel near yield, the increase in bond strength was significant.

Soroushian, *et al.* (*1991*) reported the results of a test program investigating the slipping behavior of beam-column connections. Block specimens with No. 13 (No. 4) stirrups and No. 25 (No. 8) anchor bars projecting from the block were tested in pullout. Specimens varied in concrete strength and quantity of transverse reinforcement. Specimens with little or no transverse reinforcement failed in a brittle, splitting fashion. In contrast, the specimens with dense transverse reinforcement had ductile, pullout failures. The peak bond stress of the confined specimens was about twice that of the unconfined specimens. Also, the confined failure specimens had much higher slip values when compared to the unconfined specimens. Peak bond stress and post-peak bond stress increased with concrete compressive strength. Bond stress, τ_1, in MPa, may be calculated by:

$$\tau_1 = (20 - d_b/4)\sqrt{f_c'/30} \qquad\qquad \textbf{[2.8]}$$

where the bar diameter, d_b, is in mm, and concrete strength, f_c', is in MPa. For the typical specimen in this test program, bond stress was predicted to be about 9.91 MPa (1.44 ksi).

Malvar (*1992*) tested 12 specimens to investigate the local bond stress-slip characteristics of No. 19 (No. 6) reinforcing bars subjected to transverse confinement pressure. Each 76.2 x 102 mm (3 x 4 in.) cylinder had a single No. 19 (No. 6) bar and was confined by a steel ring. The angle of lug inclination was varied. By increasing the confinement stress from 3.45 to 31.0 MPa (500 to 4500 psi), the bond stress increased from 11.4 to 19.3 MPa (1.65 to 2.80 ksi). Comparing pre-crack and post-cracked conditions, it was noted that confinement stress was crucial to ensuring an adequate bond after cracking had occurred.

Darwin, *et al.* (*1996*) used experimental test results from 199 specimens conducted by various researchers to statically show that the ACI 318-95 design equations overestimated development and lap splice lengths. Never adopted, the proposed design equation was:

$$\frac{l_d}{d_b} = \frac{\frac{f_y}{\phi f_c^{'1/4}} - 2130\left(0.1\frac{c_M}{c_m} + 0.9\right)}{80.2\left(\frac{c + K_{tr}}{d_b}\right)} \qquad \textbf{[2.9]}$$

where f_y is longitudinal steel yield strength (psi); $f_c^{'}$ is concrete strength (psi); and ϕ is a factor of safety. The term c, taking into account concrete cover, is determined as:

$$c = \left(c_m + 0.5d_b\right)\left(0.1\frac{c_M}{c_m} + 0.9\right) \qquad \textbf{[2.10]}$$

where c_m and c_M are the minimum and maximum values of c_b or c_s. c_b is the bottom cover (in) and c_s is the minimum of one-half of the clear spacing between bars (in) or one-quarter of the side cover of the reinforcing bars (in). Lastly, the transverse reinforcement index is defined as:

$$K_{tr} = \frac{34.5t_d A_{tr}}{sn} \qquad \textbf{[2.11]}$$

where $t_d = (0.72d_b + 0.28)$, represents the effect of bar size on the confining steel force; A_{tr} is cross-sectional area of transverse reinforcement (in^2); s is transverse reinforcement spacing; and n is the number of bars being developed.

Using Eq. [2.9], the development length of the typical specimen described in subsequent chapters of this report was 1.17 m (46.7 in.), compared to the ACI 318-08 required value of 1.55 m (61.1 in.) as calculated in Section 5.3.1 Design Codes and Response 2000 Comparisons.

Abrishami and Mitchell (*1996*) researched the effect compression had on bond strength from a series of pullout and push-in tests using No. 25 (No. 8) and No. 35 (No. 11) bars. Of the specimens which failed in pullout, the average bond stress was reported as 5.86 MPa (0.85 ksi). For specimens subjected only to pullout, the ratio of maximum to average bond stress was about 1.37. Specimens tested in both pullout and push-in had a ratio of 1.10.

Jeppsson and Thelandersson (*2003*) investigated the effect of debonded, longitudinal reinforcement on shear capacity. Six small beam specimens with 6 mm stirrups and No. 10 (No. 3) flexural reinforcement were constructed with plastic pipe surrounding the majority of the flexural bars. Compared to a control specimen, the 80 percent reduction in bond only reduced the shear capacity by 33 percent, verifying that relatively little embedment length produced high bond stress.

Harajli (*2004*) conducted small beam tests using both normal and high strength concrete. It was noted that except for short development lengths, using $f_c^{'1/4}$ correlated much better for both concrete types than when correlating the data using $f_c^{'1/2}$.

Table 2.1 summarizes the average and peak bond stress values reported in the literature review documents. The value reported using Eq. [2.9] developed by Darwin, *et al*. considers the material and geometric properties of the present test program design specimen. The average bond stress value is 3.45 MPa (0.500 ksi).

Table 2.1: Reported Bond Stress Values in Literature

Data Source	μ_{avg} (MPa) [ksi]	μ_{max} (MPa) [ksi]
Clark	2.07-2.76 [0.300-0.400]	4.83-6.20 [0.700-0.900]
Mains	2.31-6.14 [0.335-0.890]	-
Darwin, *et al*.	3.52 [0.510]	-
Soroushian, *et al*.	-	9.91 [1.437]

2.3 DESIGN SPECIFICATION REVIEW

An examination of the historical and the current design specifications for determining bond strength was conducted to compare the methods used to design vintage RCDG bridges to current methods. Documents reviewed were: the Standard Specification for Highway Bridges published by the American Association of State Highway Officials Standard Specifications (AASHO 1953), ACI 318 published by the American Concrete Institute (ACI 318-08), and the AASHTO-LRFD Bridge Design Specification published by the American Association of Highway and Transportation Officials (AASHTO-LRFD).

2.3.1 AASHO Allowable Stress Design

When vintage RCDG bridges girders were designed in the 1950s, AASHO used Allowable Stress Design to design reinforced concrete structures (AASHO 1953). The applied bond stress, *u*, between concrete and reinforcing bars in beams was calculated as:

$$u = \frac{V}{jdZ_o} \qquad \text{AASHO Sec. 3.7.3.(c)} \quad \textbf{[2.12]}$$

where *V* is the total shear at section, *jd* is the arm of the resisting couple, and Z_o is the sum of perimeters of bars in one set. The code required that the allowable bond stress subjected to the flexural reinforcement be limited to:

$$u = 0.10 f_c^{'} \le 350 \, psi \qquad \text{AASHO Sec. 3.4.12} \quad \textbf{[2.13]}$$

where f'_c is the concrete compressive strength.

Starting in 1973, the AASHTO limiting bond stress equation considered bar diameter, d_b:

$$u = \frac{4.8\sqrt{f_c'}}{d_b} \leq 500\,psi \qquad\qquad \textbf{[2.14]}$$

The 1983 AASHTO Specifications gave the following equation for predicting design bond stresses, u:

$$u = \frac{9.5\sqrt{f_c'}}{d_b} \leq 800\,psi \qquad\qquad \textbf{[2.15]}$$

Based on the concrete strengths used in vintage RCDG beams (approximately 3300 psi), the allowable bond stress calculated from equations 2.12, 2.14, and 2.15 is approximately the same - 350 psi. The allowable stress method assumes that all the flexural reinforcing bars are equally sharing the stress; however, as discussed in Section *4.3 BOND STRESS*, this is not always true.

2.3.2 AASHTO-LRFD Bridge Design Specifications

Since the 1970s, an ideological shift has occurred to produce the modern day design provisions for guarding against anchorage failures. The practice of limiting bond stress in allowable stress design was replaced by the minimum development length provision required by load and resistant factor design (LRFD). The minimum development length is defined as the embedment length required to produce yield stress in the reinforcing bar. To make a comparison between modern and historical codes, the development length may be converted to an average bond stress using Eq. [2.1]. The pertinent, current design specifications are summarized as follows.

For straight No. 36 (No. 11) and smaller bars, the minimum development length is:

$$l_{db} = \frac{1.25 A_b f_y}{\sqrt{f_c'}} \qquad \text{AASHTO-LRFD Sec. 5.11.2.1.1} \quad \textbf{[2.16]}$$

but no less than *0.4d_bf_y*. The bar area, A_b, is in in^2, the steel yield strength, f_y, is in ksi, the concrete strength, f_c', is in ksi, and the bar diameter, d_b, is in inches.

For No. 36 (No. 11) and smaller hooked reinforcing bars, the development length is:

$$l_{hb} = \frac{38.0 d_b}{\sqrt{f_c'}} \qquad \text{AASHTO-LRFD 5.11.2.4-1} \quad \textbf{[2.17]}$$

and shall exceed *8d_b* or 6 inches, whichever is greater.

2.3.3 ACI 318 American Building Code for Structural Concrete

When vintage RCDG bridge girders were designed in the 1950s, ACI also required that reinforced concrete structures be designed using Allowable Stress Design as described

previously (ACI 1956). Similar to Eq. [2.12], the applied bond stress, u, between concrete and reinforcing bars in beams was calculated as:

$$u = \frac{V}{\Sigma ojd} \qquad \text{ACI 318-56 Sec 901} \quad \textbf{[2.18]}$$

where $\sum o$ is the sum of perimeters of bars in one set, j is the ratio of the distance between centroid of compression and centroid of tension to the beam depth, d. Like the contemporary AASHO code, the upper limit for bond stress was controlled by Eq. [2.13].

Like the AASHTO specification, ACI 318 shifted from allowed stress design to strength design. The current ACI 318-08 methods for determining minimum development are similar to the AASHTO-LRFD design equations.

Chapter 12.2 of ACI 318-08 describes two methods for determining the minimum development length of a straight reinforcing bar. In the simple method, for No. 22 (No. 7) and larger bars:

$$l_d = \frac{f_y \psi_t \psi_e \lambda}{20\sqrt{f_c'}} d_b \qquad \text{ACI 318-08 Sec. 12.2.2} \quad \textbf{[2.19]}$$

where the reinforcing bar yield strength, f_y, is in psi; bar diameter, d_b, is in inches; and concrete strength, f_c', is in psi. Modification factors ψ_t, ψ_e, and λ consider concrete depth below the bar, the type of bar, and the type of concrete, respectively.

The complex ACI 318-08 method considers the effects of confinement due to transverse reinforcement and concrete cover:

$$l_b = \frac{3}{40} \frac{f_y}{\sqrt{f_c'}} \frac{\psi_t \psi_e \lambda}{\dfrac{c_b + K_{tr}}{d_b}} d_b \qquad \text{ACI 318-08 12.1} \quad \textbf{[2.20]}$$

The term $(c_b+K_{tr})/d_b$ need not be taken larger than 2.5. When this term is less than 2.5, splitting failures are likely, while pullout failures are more likely when the term is greater than 2.5 (ACI 2008). c_b is the lesser of the side cover measured to the center of the bar, the bottom cover measured to the center of the bar, or half of the center-to-center adjacent bar spacing. The transverse reinforcement index, K_{tr}, is defined by:

$$K_{tr} = \frac{A_{tr} f_{yt}}{1500sn} \qquad \text{ACI 318-08 12.2} \quad \textbf{[2.21]}$$

where the area of transverse reinforcement, A_{tr} is in in^2; the stirrup yield strength, f_{yt}, is in psi; the stirrup spacing, s, is in inches; and the number of bars being developed along the plain of splitting is n. K_{tr} may be taken as zero for a conservative design.

For No. 36 (No.11) and smaller hooked bars, the development length is the greater of:

$$l_{dh} = \frac{0.02\psi_e \lambda f_y}{\sqrt{f_c'}} d_b \qquad\qquad \text{ACI 318-08 Sec. 12.5.2} \quad \textbf{[2.22]}$$

$$l_{dh} \geq 8d_b \, or \, 6" \qquad\qquad \text{ACI 318-08 Sec. 12.5.1} \quad \textbf{[2.23]}$$

ACI 318-08 Section 12.5.3 describes various reduction factors which may be taken depending on cover and transverse reinforcement. These factors are not reported here since they do not apply to the present test specimens. ACI 318-08 specifies that the design moment curve be shifted a distance, d, to the right or left (whichever produces the maximum effect) to account for effect of diagonal cracks.

2.4   CONCLUSIONS

Based on the literature and design standard reviews, several conclusions about bond stress behavior were made:

- Most experiments did not adequately represent realistic member sizes or details. Pullout and beam end tests did not account for the effects of shear, especially at diagonally-cracked locations where bond stress demands were expected to be higher. Generally, these tests were at a small scale using flexural bars sizes that were smaller than those used in bridges.

- Historically, design codes attempted to conservatively limit bond stresses. Since most data were developed from smaller bars, more information about the bond stress of specimens with larger bars is critical to assess the adequacy of present design specifications for evaluation of existing members with large size bars.

- Transverse reinforcement and concrete cover significantly increased bond stress at failure. This may be an important consideration for evaluating positive and negative moment regions of continuous bridge girders.

3.0   EXPERIMENTAL SETUP

This chapter describes the design of the experimental setup, construction, testing protocol, and instrumentation used to characterize the performance of large-size, RC girders with diagonal cracks intersecting flexural reinforcing steel near cutoff locations. Eight specimens were used in the test program, and each of these had a similar geometry with a varying number of flexural reinforcing bars and varying preformed crack orientation. Four of the specimens were T-beams for investigating the positive moment behavior, and four specimens were IT-beams for investigating the negative moment behavior. Figure 3.1 illustrates the specimen naming convention used in this study.
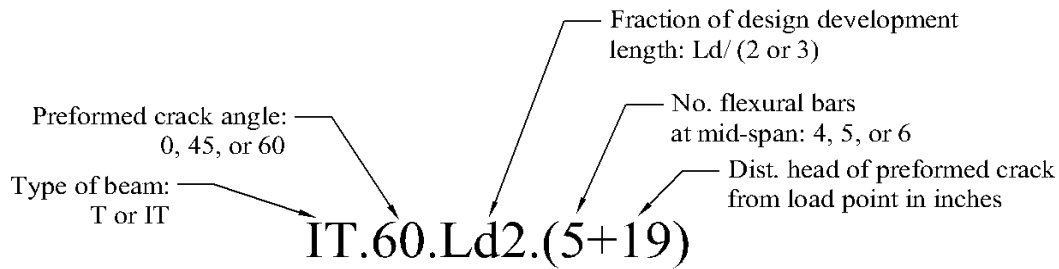
Figure 3.1: Specimen naming convention

3.1   SPECIMEN DESCRIPTION

3.1.1 Specimen Geometry

All of the test specimens were designed based on previous vintage RCDG beam tests at the Oregon State University (Higgins, *et al*. 2004). Each specimen was 7.92 m (26 ft) long, with a 356 x 1067 mm (14 x 42 in.) stem, and a 914 x 152 mm (36 x 6 in.) deck. To ensure failure of the beams where instrumentation was concentrated, half of the beam was over-reinforced with stirrups spaced at 152 mm (6 in.) and hooked flexural reinforcement extending past the support. The under-reinforced portion of each beam had stirrups spaced at 254 mm (10 in.) or 305 mm (12 in).

In the T-beams, the No. 36 (No. 11) flexural steel was arranged in two layers, located 68.6 and 162 mm (2.70 and 6.45 in.) from the bottom of the beam. Each T-beam had two cutoff bars in the top layer, two hook bars in the bottom layer, and a straight bar extending the full length of the beam in the bottom layer for specimens with five flexural bars. Two No. 36 (No. 11) bars were used as compression reinforcement to facilitate construction. The under-reinforced portion of each beam had stirrups spaced at 254 mm (10 in.). The elevation and cross-section of each T-beam specimen are shown in Figures 3.2 to 3.5.
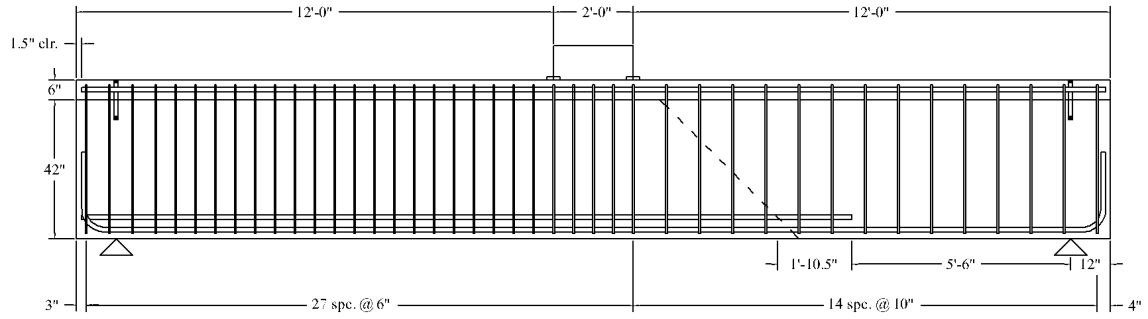
Figure 3.2: Elevation of specimens T.45.Ld3.(4) and T.45.Ld3.(5)
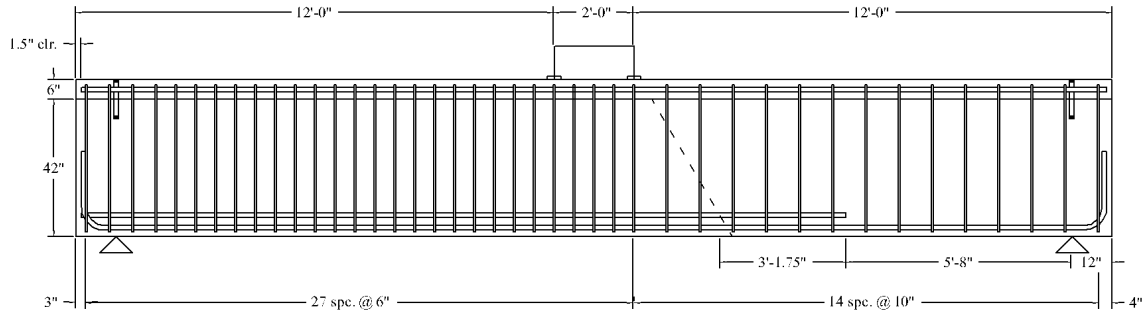
Figure 3.3: Elevation of specimen T.60.Ld3.(5)
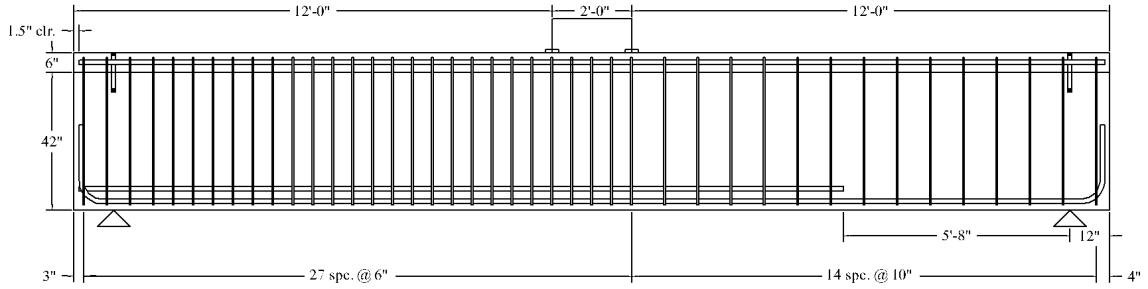
Figure 3.4: Elevation of specimen T.0.Ld3.(5)

20

a) T-beam   b) IT-Beam
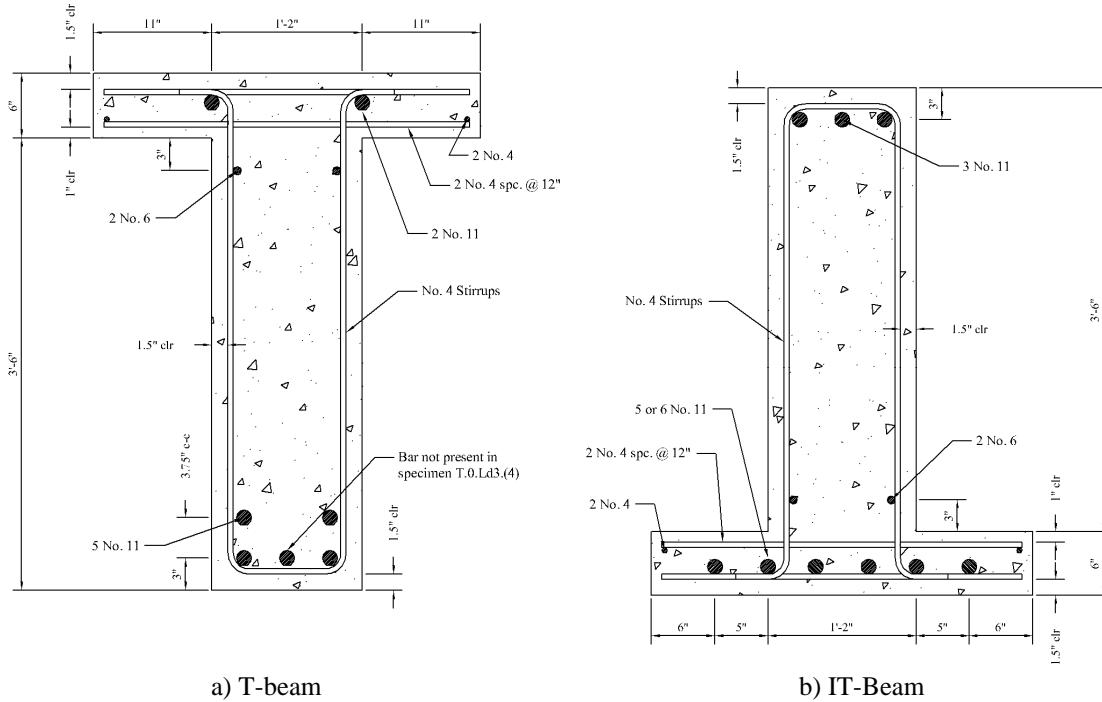
Figure 3.5: Typical specimen cross-sections

In the IT-beams, the No. 36 (No. 11) flexural steel was arranged in a single layer in the deck of the specimen. Each IT-beam had two cutoff bars, two hook bars, and either one or two straight bars extending the full length of the beam. Three No. 36 (No. 11) bars were used as compression reinforcement in the bottom of the stem to facilitate construction. The under-reinforced portion of each beam had stirrups spaced at 254 mm (10 in.) or 305 mm (12 in). The elevation and cross-section of each IT-beam specimen are shown in Figs. 3.5b to 3.9.
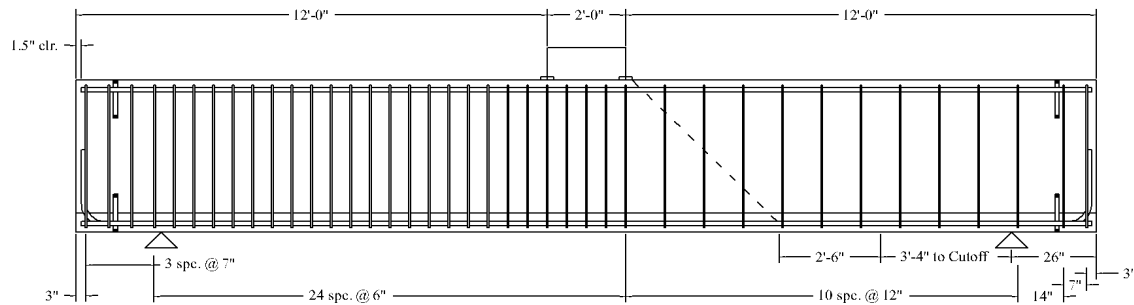
Figure 3.6: Elevation of specimen IT.45.Ld2

21
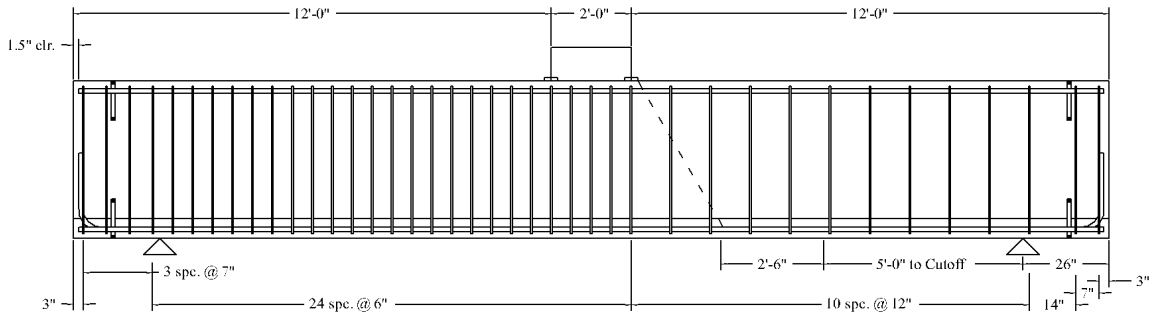
Figure 3.7: Elevation of specimen IT.60.Ld2
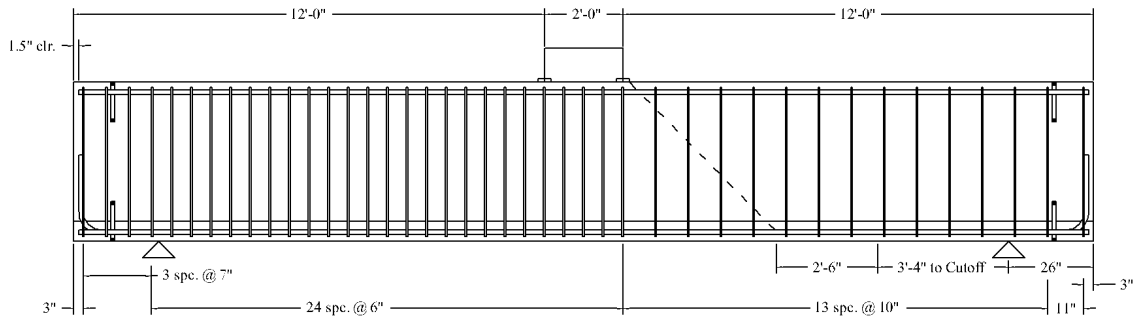
Figure 3.8: Elevation of specimen IT.45.Ld2(5)
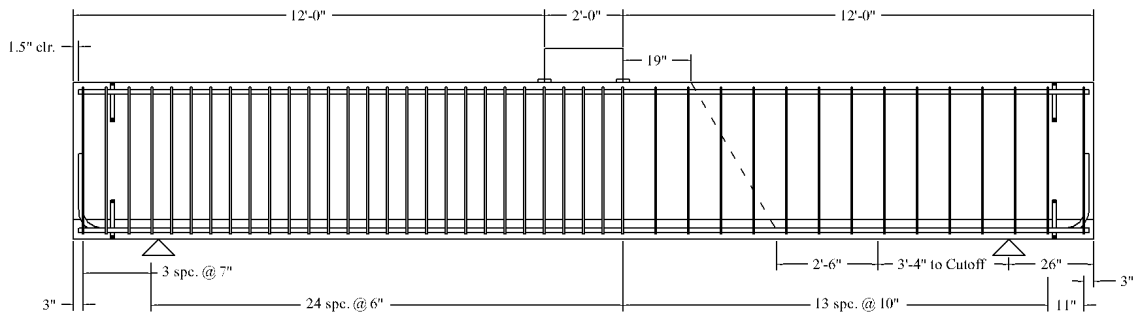
Figure 3.9: Elevation of specimen IT.60.Ld2(5+19)

It was intended that the cutoff bars extend past the preformed diagonal crack some distance short of the design minimum development length specified by ACI 318-08 (for a No. 36 Gr. 420 (No. 11 Gr. 60) reinforcing bar). For the IT-beams the minimum development length was 152 cm (60 in.) using design material properties of 22.8 MPa (3300 psi) concrete and 472 MPa (68.5 ksi) reinforcing steel. A cutoff bar embedment length past the diagonal preformed crack of one-half of the design development length was chosen for specimens IT.45.Ld2, IT.60.Ld2, and IT.45.Ld2(5) or 76.2 cm (30 in.).

The T-beam specimens were designed to have the cutoff bars extend past the preformed diagonal crack one-third the design minimum development length specified by ACI 318-08. For the design properties the minimum development length was 155 cm (61.1 in.). The specimen cutoff bars were shorter than in similar T-beam specimens tested in previous Oregon State University

22

experimental programs (Higgins, *et al*. 2004). Specimen T.45.Ld3.(4) had a cutoff bar length as described above. However, for specimen T.45.Ld3(5), the instrumentation access box shifted during the concrete placement, resulting in a development length 50.8 mm (2 in.) shorter than originally intended. Therefore, specimens T.60.Ld3.(5) and T.0.Ld3.(5) were constructed with a shorter development length to allow more direct comparison with the results of specimen T.45.Ld3.(5).

To analyze a range of crack angles observed in in-service vintage RCDG bridges, two preformed crack angles were investigated: 45°, and 60°. A 1.59 mm (1/16 in.) thick preformed diagonal "crack" was cast into each specimen using a polycarbonate sheet cut and placed at the desired crack angle. The location of the preformed diagonal crack was based on an origin at the load point on the north side of each specimen, travelling at the specified angle to the intersection of the longitudinal reinforcement. The preformed crack tip terminated at the theoretical compression zone depth (using ACI-318 analysis methods). Crack thickness was chosen to typify a relatively wide diagonal crack that would have been identified during inspection.

Preliminary analysis of the first two T-beam specimens, T.45.Ld3.(4) and T.45.Ld3.(5), showed that an anchorage failure would most likely occur when a crack angle of 45° developed with cutoff bars extending one third the ideal development length past the crack. The preformed crack angles for specimens T.60.Ld3.(5) and T.0.Ld3.(5) were then selected after the first two specimens were tested. For the initial specimens, the preformed crack was not the eventual failure crack. At failure, as the cutoff bars slipped through the concrete, new cracks formed at progressively steeper angles. Therefore, the T.60.Ld3.(5) was designed to investigate what happens when these progressively steeper cracks meet an existing weak plane. During testing, the 60° preformed crack was not mobilized at failure. To provide a control specimen without an initial preformed crack, specimen T.0.Ld3.(5) was designed.

The first two IT specimens, IT.45.Ld2.(6) and IT.60.Ld2.(6), were predicted to fail in anchorage based on cutoff reinforcement providing a specification-based allowance of one-half the capacity of well-anchored reinforcing bars. Results from these two tests indicated that cutoff reinforcement capacity exceeded specification-predicted values. The IT.45.Ld2.(5) and IT.60.Ld2.(5+19) specimens were therefore designed with fewer longitudinal reinforcing bars and tighter stirrup spacing to encourage shear-anchorage failure behavior. With the exception of crack angle, these two specimens were detailed exactly the same. This detailing fashion provided a method for determining what role existing cracking plays on failure.

The total number of flexural reinforcing bars, under-reinforced side stirrup spacing, and specific preformed diagonal crack angle for each specimen are summarized in Table 3.1.

Table 3.1: Variable parameters for each specimen

Beam Type	Specimen	Preformed Crack Angle	Faction of ld	No of Flexural Bars	Stirrup Spacing (mm) [in.]
T-beam	T.45.Ld3.(4)	45	1/3	4	254 [10]
	T.45.Ld3.(5)	45	1/3	5	254 [10]
	T.60.Ld3.(5)	60	1/3	5	254 [10]
	T.0.Ld3.(5)	0	1/3	5	254 [10]
IT-beam	IT.45.Ld2	45	1/2	6	305 [12]
	IT.60.Ld2	60	1/2	6	305 [12]
	IT.45.Ld2(5)	45	1/2	5	254 [10]
	IT.60.Ld2(5+19)	60	1/2 + 19 in.	5	254 [10]

3.1.2 Specimen Construction

The reinforcement cage was assembled after strain gages were applied to the stirrups and flexural bars. To increase the likelihood of gage operation after exposure to water and vibration during the concrete casting process, the strain gages were waterproofed and the leads were tied to the reinforcement. The preformed crack was constructed from a piece of 1.59 mm ($^1/_{16}$ in.) thick polycarbonate sheet. The polycarbonate sheet extended all the way to the stirrups and was attached at these locations to maintain the crack geometry as shown in Fig. 3.10. Also shown in Fig. 3.10, a box constructed of wood allowed access to the strain gage leads and to the ends of the cutoff bars for later instrumentation in the T-beam specimens.

Figure 3.10: Example of specimen geometry prior to concrete placement

3.2   MATERIAL PROPERTIES

Each specimen required approximately 4.59 m^3 (6 yd^3) of concrete provided by a local ready-mix supplier. The concrete design was based on the typical AASHT0 "Class A", 21 MPa (3000 psi) mix used in 1950s era bridges and has been used in previous research on similar sized specimens at Oregon State University. Standard slump tests were conducted, and water was added to achieve a 127 mm (5 in.) slump. The actual concrete compressive strengths were determined from 152 x 305 mm (6 x 12 in.) cylinders in accordance to ASTM C39M/C 39M-09a

and ASTM C617-09a. Cylinders were tested on days 7, 14, and 28 when applicable. Average test day concrete strengths are reported in Table 3.2.

Table 3.2: Average Test Day Specimen Concrete Strength

Beam Type	Specimen	Concrete Age (days)	Concrete Strength, f_c' (MPa) [psi]
T-Beam	T.45.Ld3.(4)	21	21.82 [3165]
	T.45.Ld3.(5)	30	22.77 [3303]
	T.60.Ld3.(5)	26	23.57 [3418]
	T.0.Ld3.(5)	21	24.39 [3538]
IT-Beam	IT.45.Ld2	103	27.01 [3918]
	IT.60.Ld2	155	26.63 [3862]
	IT.45.Ld2(5)	28	24.84 [3603]
	IT.60.Ld2(5+19)	40	25.26 [3664]

All of the reinforcing steel was provided by a local rebar fabricator. The Gr. 276 (Gr. 40) No. 13 (No. 4) open internal stirrups were made from the steel heat with the lowest yield-stress available. All of the remaining internal steel was ASTM A706 Gr. 420 (Gr. 60). The material properties of the internal stirrups and flexural reinforcement were determined in accordance with ASTM E8-09a as reported in Table 3.3.

Table 3.3: Average Reinforcing Steel Properties

Reinforcement Type	Bar Dia. (mm) [in.]	Grade (MPa) [ksi]	f_y (MPa) [ksi]	f_u MPa) [ksi]
Internal Stirrups	12.7 [0.50]	280 [40]	369 [53.5]	583 [84.6]
Flexural	35.8 [1.41]	420 [60]	494 [71.7]	722 [105

3.3   LOADING SCHEME

All of the specimens were tested in the Structural Engineering Research Laboratory at Oregon State University. A reaction frame constructed on the strong floor allowed for four-point loading as shown in Fig. 3.11. A 224 kN (500 kip) servo-hydraulic actuator applied load to each specimen. Illustrated in Fig. 3.11, the steel loading shoe distributed the actuator force via two 102 mm (4 in.)-wide plates space 610 mm (24 in.) apart, centered about the middle of the specimen. Both loading plates were leveled and adhered to the specimen using hydrostone to ensure uniform application of the load across the plates. The specimens were leveled in the transverse and longitudinal direction and were assumed to be perfectly straight and flat. Initial support settlements and mid-span displacements were assumed to be 0 mm (0 in.). Similarly, all other displacement sensors, strain gages, and load cells were assumed to be at a zero condition.
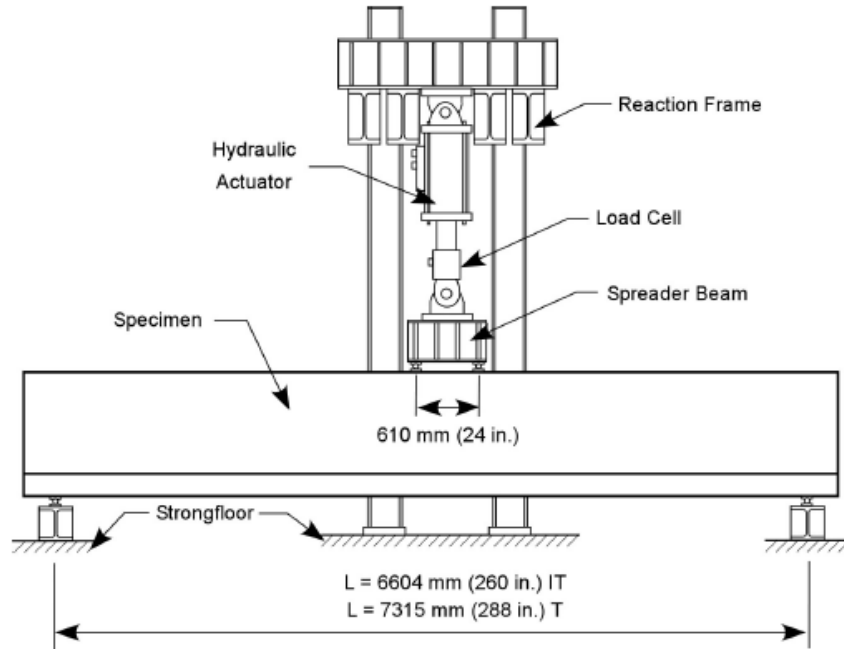
Figure 3.11: Four-point load configuration used for specimen testing

A series of cyclic tests without load reversals were performed on each specimen. Each load step increased the peak load by 111 or 222 kN (25 or 50 kips) from the previous load cycle as summarized in Table 3.4. The loading rate was 4.45 kN/sec (1 kip/sec). At each new load step, the load was reduced by 111 kN (25 kips) so cracks could be marked on the beam.

Table 3.4: Typical Load Cycle Pattern

Load Step	
(kN)	(kips)
0 – 111	0 – 25
22.2 – 222	5 – 50
22.2 – 334	5 – 75
22.2 – 445	5 – 100
22.2 – 667	5 – 150
22.2 – 890	5 – 200
22.2 –1112	5 – 250
22.2 – 1334	5 – 300
22.2 – 1556.8	5 – 350
22.2 – 1779.2	5 – 400
22.2 – to Failure	5 – to Failure

3.4   INSTRUMENTATION

A variety of instruments were used on the interior and exterior of the beam as described in the subsequent subsections. Measurements were made at a rate of 4 Hz.

3.4.1 Internal Sensor Array

Internal strain gages served two purposes. Gages applied to stirrups measured shear transfer, while gages on the flexural reinforcement served to measure tensile demand and corresponding average bond stress.

To determine the tensile force and bond stress distribution in the flexural bars, each bar had four or five strain gages. In the T-beam specimens, three gages were between the end of the bar and the location where the preformed crack crossed the bar. Two gages were between the preformed crack and mid-span. In the IT-specimens, four strain gages were between the end of the bar and the location where the preformed crack crossed the bar. Figs. 3.12 to 3.14 show the strain gage locations for the T-specimens, and Figs. 3.15 to 3.18 show the strain gage locations for the IT-specimens. Appendix A gives further information about how each gage was labeled and summarizes the data gathered from each gage.
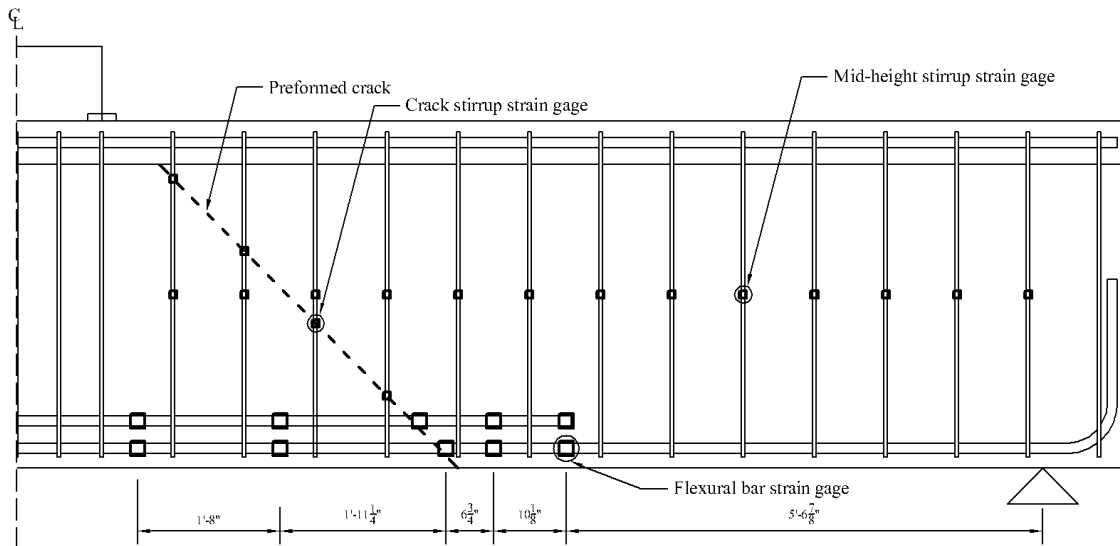
Figure 3.12: Specimens T.45.Ld3.(4) and T.45.Ld3.(5) internal sensor array
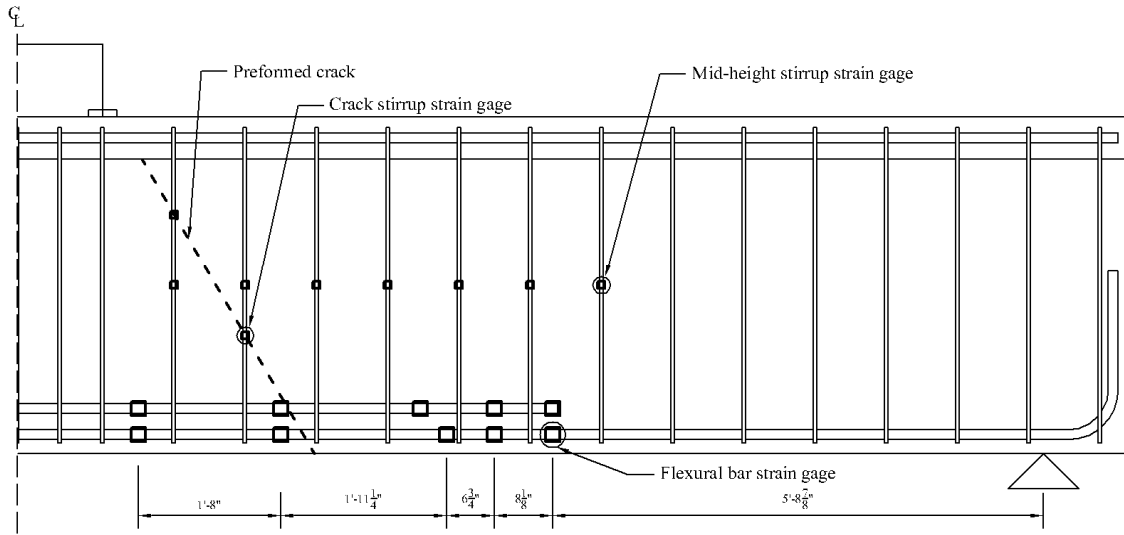
Figure 3.13: Specimen T.60.Ld3.(5) internal sensor array
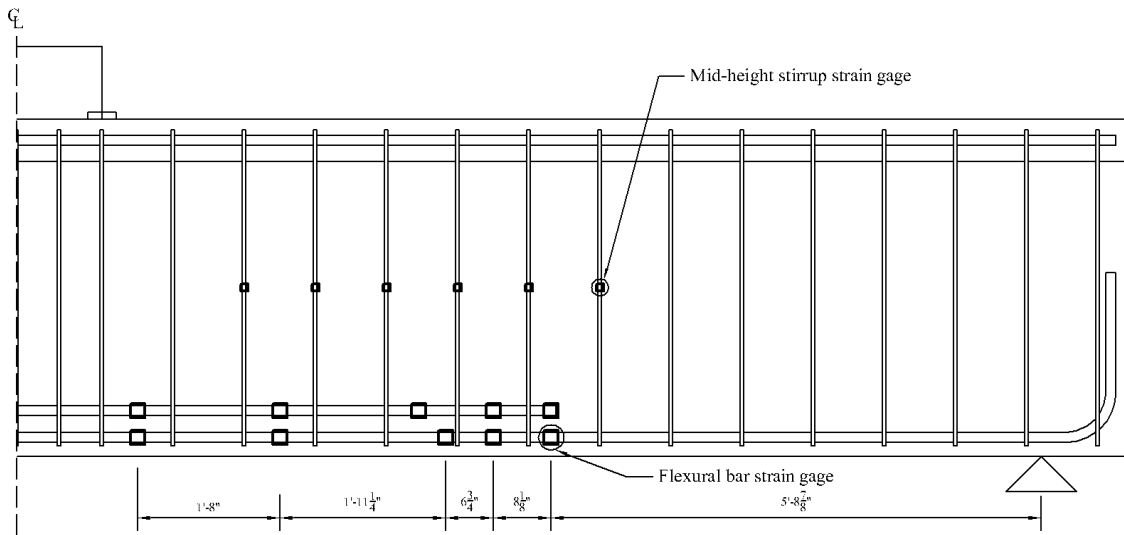
Figure 3.14: Specimen T.0.Ld3.(5) internal sensor array

28
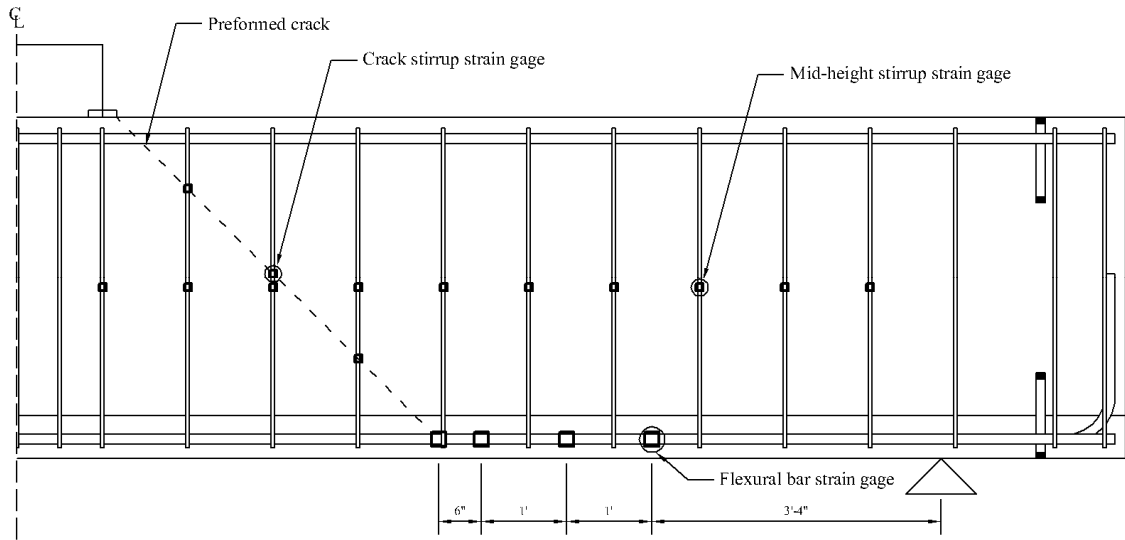
Figure 3.15: Specimen IT.45.Ld2 internal sensor array
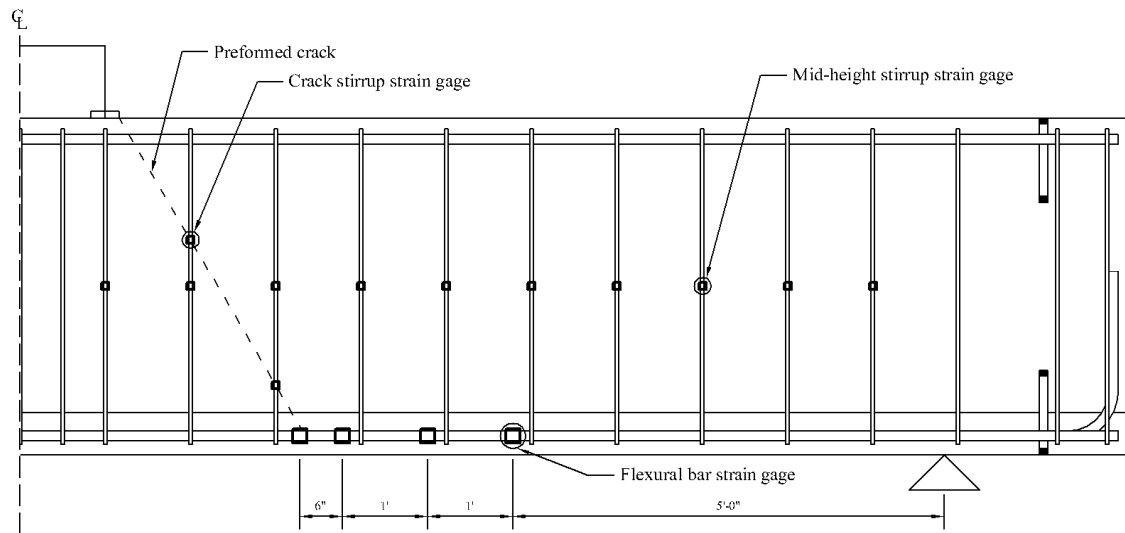
Figure 3.16: Specimen IT.60.Ld2 internal sensor array
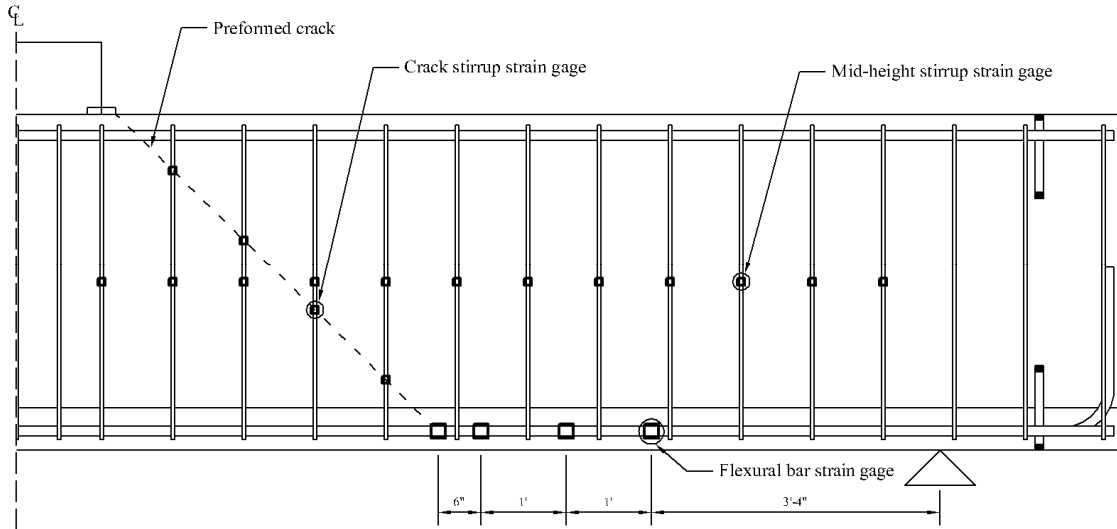
Figure 3.17: Specimen IT.45.Ld2(5) internal sensor array
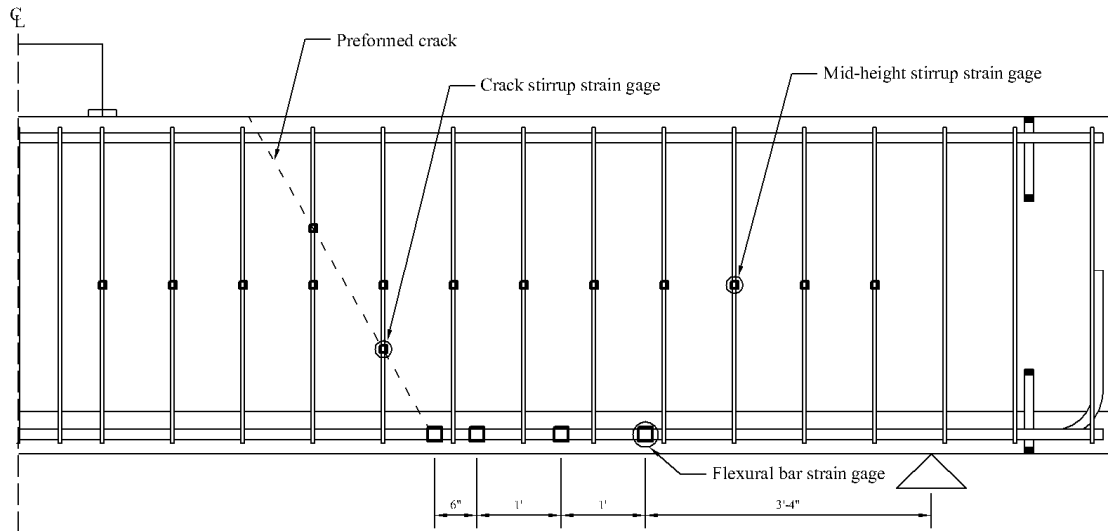
Figure 3.18: Specimen IT.60.Ld2(5+19) internal sensor array

3.4.2 External Sensor Array

Pairs of displacement sensors with a range of 12.7 mm (0.5 in.) were used to measure the shear over regions of the beam. As the cracks opened, the top sensor would measure elongation, while the bottom sensor would measure contraction. There were a total of three regions instrumented as shown in Fig. 3.19. All of the gages were located on the northwest side of the beam.

30

Beam Type	a (in)	b (in)	c (in)	d (in)
T-Beams	39	7.5	41.75	41.75
IT-Beam	40	7.5	40	46
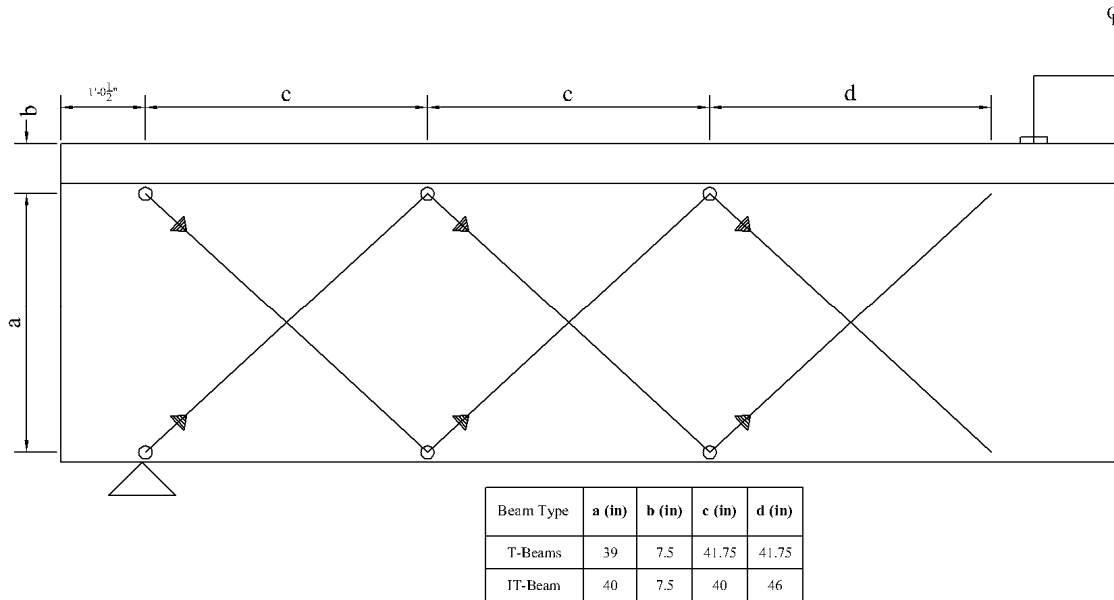
Figure 3.19: Typical specimen external displacement sensor array

To measure mid-span displacement, two 127 mm (5 in.) stroke displacement sensors were attached to opposite sides of the stem at mid-span using threaded studs glued into holes drilled 38.1 mm (1.5 in.) from the bottom of the beam.

Displacement sensors were placed under each corner of the specimen to measure the support settlement. Each 12.7 mm (0.5 in.) stroke sensor was attached to a stand resting on the floor. As photographed in Fig. 3.20, a piece of small aluminum angle, adhered to the beam surface, provided a level surface for the sensor to rest upon.

Figure 3.20: Typical vertical displacement sensor to measure support settlement

To measure the relative slip between the cutoff bar and the surrounding concrete, a 12.7 mm (0.5 in.) stroke displacement sensor was placed at the end of each cutoff bar. In specimens T.45.Ld3.(4) and T.45.Ld3.(5), each instrument was anchored to a peg exposed in the instrument access box. The measuring tip of the gage was placed flush against the exposed end of the cutoff

31

bar. Wood blocks were used to bridge the gap between the peg and center of the cutoff bar if necessary, as pictured in Fig. 3.21a. For specimens T.60.Ld3.(5) and T.0.Ld3.(5), the exposed peg did not have sufficient length to attach to a sensor. Therefore, each sensor was glued to the box via a wood spacer such that the instrument contacted the center of the cutoff bar. As shown in Fig. 3.21b, an additional sensor was added to measure the movement of the crack which formed between the box and the surrounding concrete. The horizontal movement at the crack was later subtracted from the relative movement of the cutoff bar and the concrete. For the IT-specimens, the anchorage slip sensors were placed in a precast block-out as shown in Fig. 3.218c.

| a) T.45.Ld3.(4) & T.45.Ld3(5) | b) T.60.Ld3.(5) & T.0.Ld3.(5) | c) IT-beam specimens |
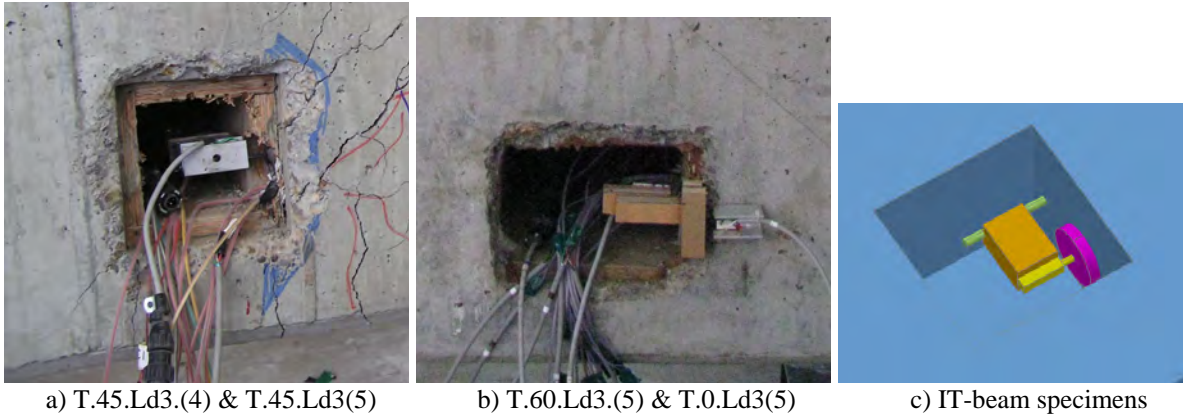
Figure 3.21: Typical anchorage slip sensor installation

Lastly, displacement sensors were used to track the change in crack width of select cracks on the northwest side of the beam as shown in Fig. 3.22. For all of the tests, the preformed crack had two instruments straddling the crack. Specimens T.45.Ld3.(5) and T.0.Ld3.(5) had two instruments at the preformed crack location, with two additional sensors crossing the major crack that developed extending from the loading plate to the end of the cutoff bar.

Figure 3.22: Typical crack width sensors

4.0 EXPERIMENTAL RESULTS

Based on the definition of anchorage failures in Section 2.1 *ANCHORAGE CONCERNS*, crack patterns, cutoff bar slippage, and load versus mid-span displacement behavior at failure, all the T-beam specimens exhibited pullout anchorage failures. All of the failures were ductile and exhibited signs of distress prior to failure. Two of the IT-beam specimens failed in shear-compression and two failed in splitting anchorage. A shear-compression failure was classified as yielding of the stirrups and crushing of the concrete compression zone prior to anchorage slip exceeding 1.27 mm (0.05 in.) or a flexural failure of the flexural reinforcement. A shear anchorage failure was determined to occur when the cutoff bars exhibited slip of 1.27 mm (0.05 in.) or greater prior to the crushing of the concrete compression zone.

The applied shear at failure, the observed failure crack angle, the as built preformed diagonal crack angle, and mid-span displacement are reported in Table 4.1. Shear forces reported in Table 4.1 include the applied shear on the specimen from the actuator, V_{APP}, the shear force from the beam self-weight acting at the failure plane, V_{DL}, and the total shear force, V_{EXP}. Assuming the unit weight of reinforced concrete was 23.6 kN/m^3 (150 lb/ft^3), V_{DL} was estimated by computing the weight of concrete acting on the diagonally cracked failure plane. Where applicable, the as-built preformed diagonal crack angle was used for comparative analyses, not the design crack angle.

Table 4.1: Summary of Specimen Condition at Failure

Beam Type	Specimen	V_{APP} (kN) [kips]	V_{DL} (kN) [kips]	V_{EXP} (kN) [kips]	Failure Crack Angle	Failure Type	Mid-span Deflection (mm) [in.]
T-Beam	T.45.Ld3.(4)	497.7 [111.9]	12.9 [2.9]	510.6 [114.8]	36	Pullout-Anchorage	36.6 [1.44]
	T.45.Ld3.(5)	661.0 [148.6]	13.9 [3.1]	674.9 [151.7]	33	Pullout-Anchorage	65.3 [2.57]
	T.60.Ld3.(5)	685.0 [154.0]	16.6 [3.7]	701.6 [157.7]	49	Pullout-Anchorage	104.0 [1.70]
	T.0.Ld3.(5)	686.8 [154.4]	13.3 [3.0]	700.1 [157.4]	35	Pullout-Anchorage	43.9 [1.73]
IT-Beam	IT.45.Ld2	1000.8 [225.0]	15.1 [3.4]	1015.9 [228.4]	32	Shear-Compression	24.6 [0.97]
	IT.60.Ld2	779.3 [175.2]	33.8 [7.6]	813.1 [182.8]	60	Shear-Compression	17.5 [0.69]
	IT.45.Ld2(5)	796.6 [179.1]	21.4 [4.8]	818.0 [183.9]	44	Shear-Anchorage	24.9 [0.98]
	IT.60.Ld2(5+19)	812.2 [182.6]	21.4 [4.8]	833.6 [187.4]	45	Shear-Anchorage	26.7 [1.05]

4.1 DISPLACEMENT RESULTS

4.1.1 Load-Deformation Response of Specimens

The load-deformation responses for all specimens are shown in Figs. 4.1 and 4.2. The deformation reported was the average mid-span displacement less the average support settlement. Each T-beam specimen exhibited softening following the 222 kN (50 kip) load cycle. At failure, the applied load was maintained as deformation rapidly increased. The apparent ductility was not due to reinforcing steel yielding (as discussed later), but due to slip of the cutoff bars. The two IT-beams that failed in shear-compression had a stiffer load-deformation response than the two IT-beams that failed in shear-anchorage.
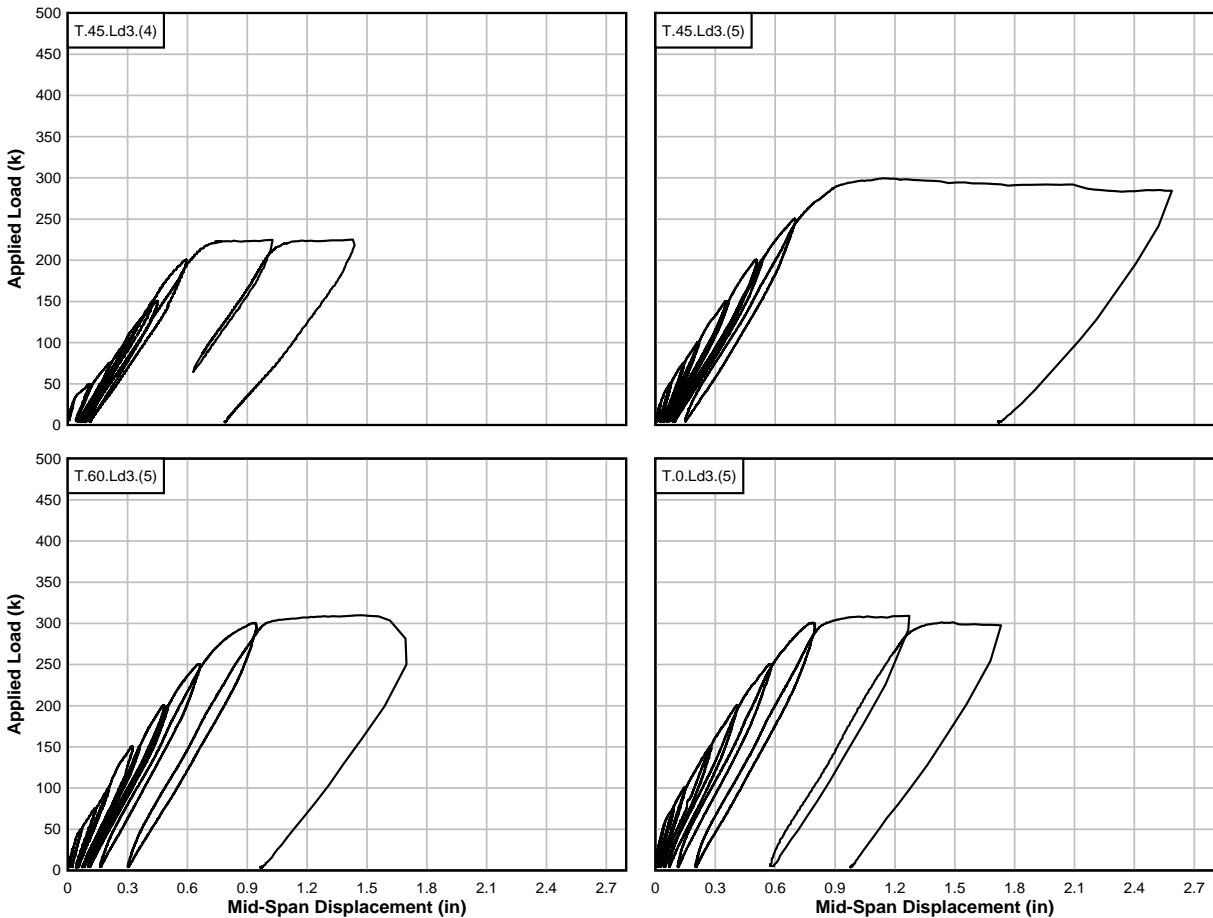
Figure 4.1: Load-displacement plots at mid-span for T-beam specimens

34
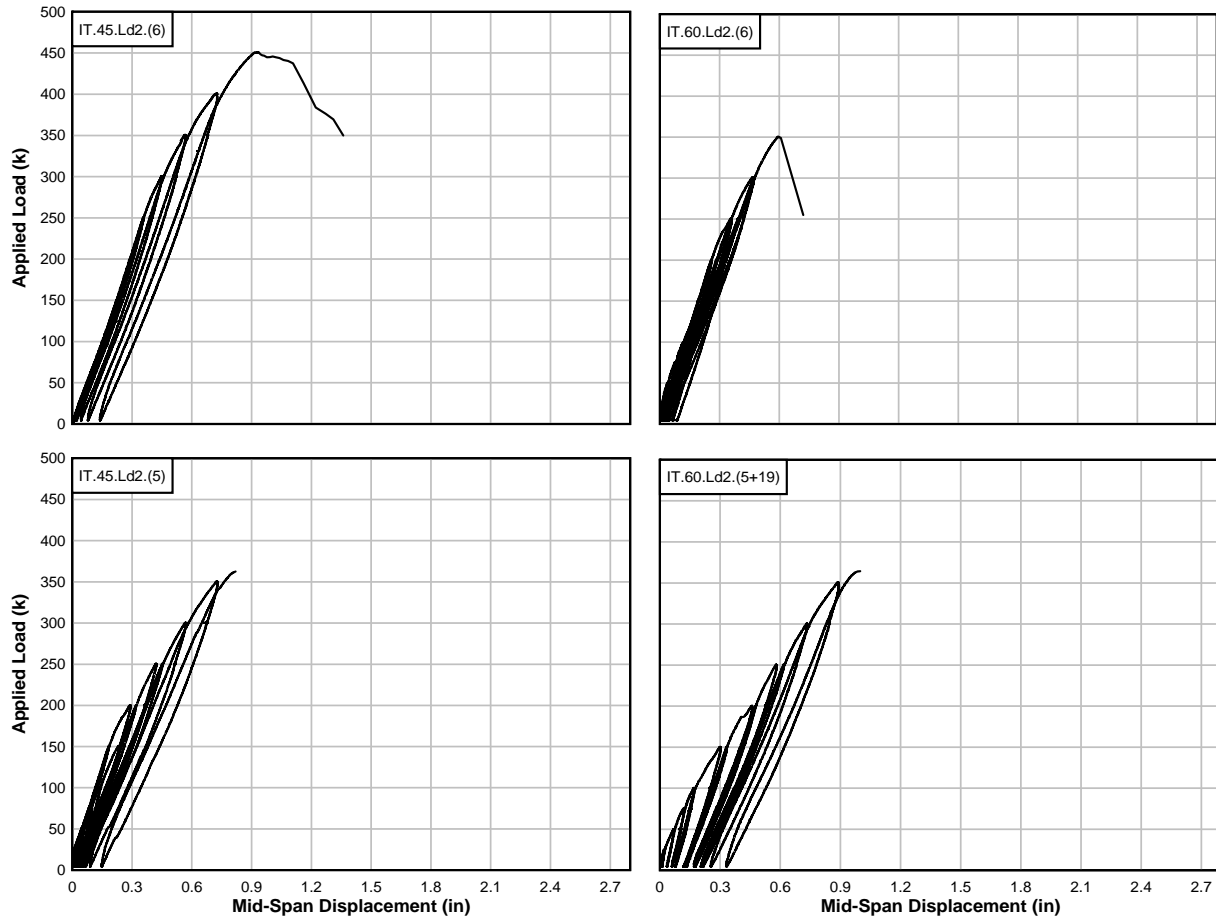
Figure 4.2: Load-displacement plots at mid-span for IT-beam specimens

4.1.2 Crack Growth in Specimens

Crack growth was monitored throughout the test. At each new load level, the applied load was reduced by 111 kN (25 kip) after achieving the target amplitude. This allowed new cracks to be traced without producing creep deformations in the specimen. The crack map records are shown in Figs. 4.3 and 4.4. Photographs were taken after mapping cracks. For all the T-beams, the crack that extended from the loading plate to the end of the cutoff bars caused failure as shown in Fig. 4.5. For the IT-beams, the location of the failure diagonal crack depended on the specimen as shown in Fig. 4.6. The anchorage failure of the IT.45.Ld2(5) and IT.60.Ld2(5+19) can be seen by the large, horizontal splitting cracks originating at the cutoff location. This cracking extended along the full length of the cutoff bar development up to the location of the diagonal failure crack. The shear-compression failure of the IT.45.Ld2 specimen was demonstrated by the shallow crack extending past the cutoff location to the supports, combined with rupture of the stirrups.

35

P/2 P/2

T.45.Ld/3.(4)

P/2 P/2

T.45.Ld/3.(5)

P/2 P/2

T.60.Ld/3.(5)

P/2 P/2

T.0.Ld/3.(5)

Failure Crack
Precast Crack
Other Cracks
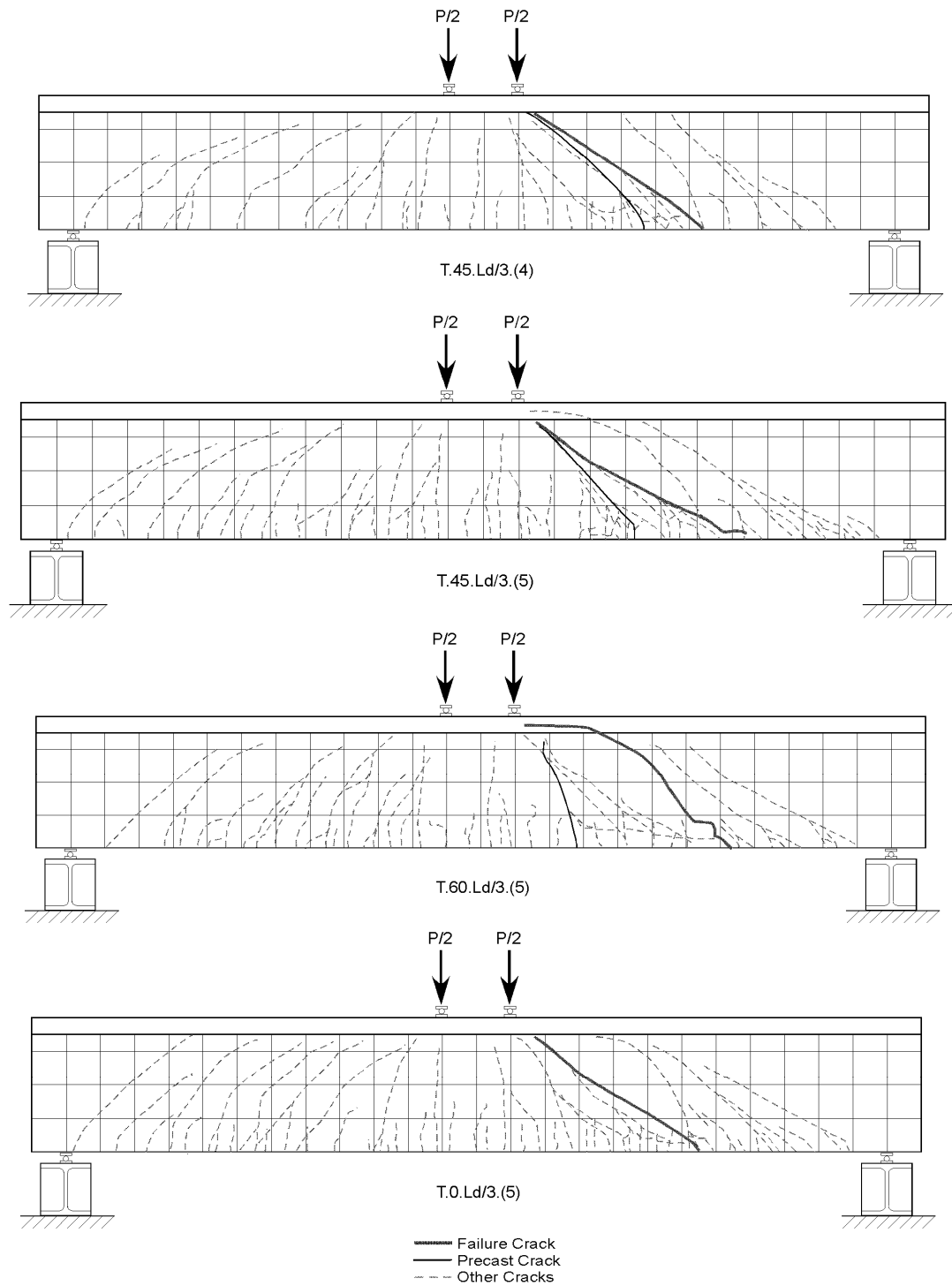
Figure 4.3: Failure crack maps for T-beam specimens
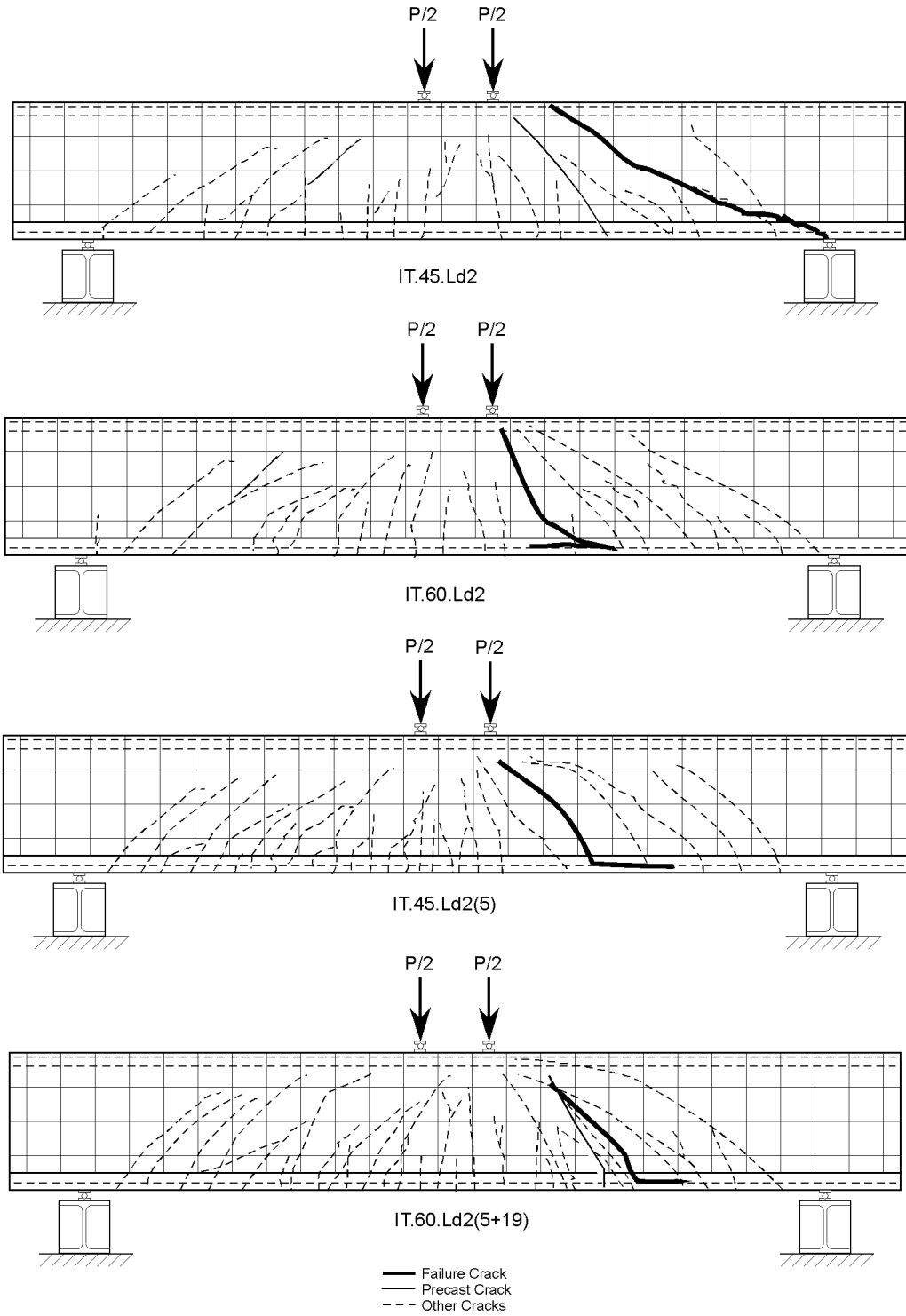
Figure 4.4: Failure crack maps for IT-beam specimens
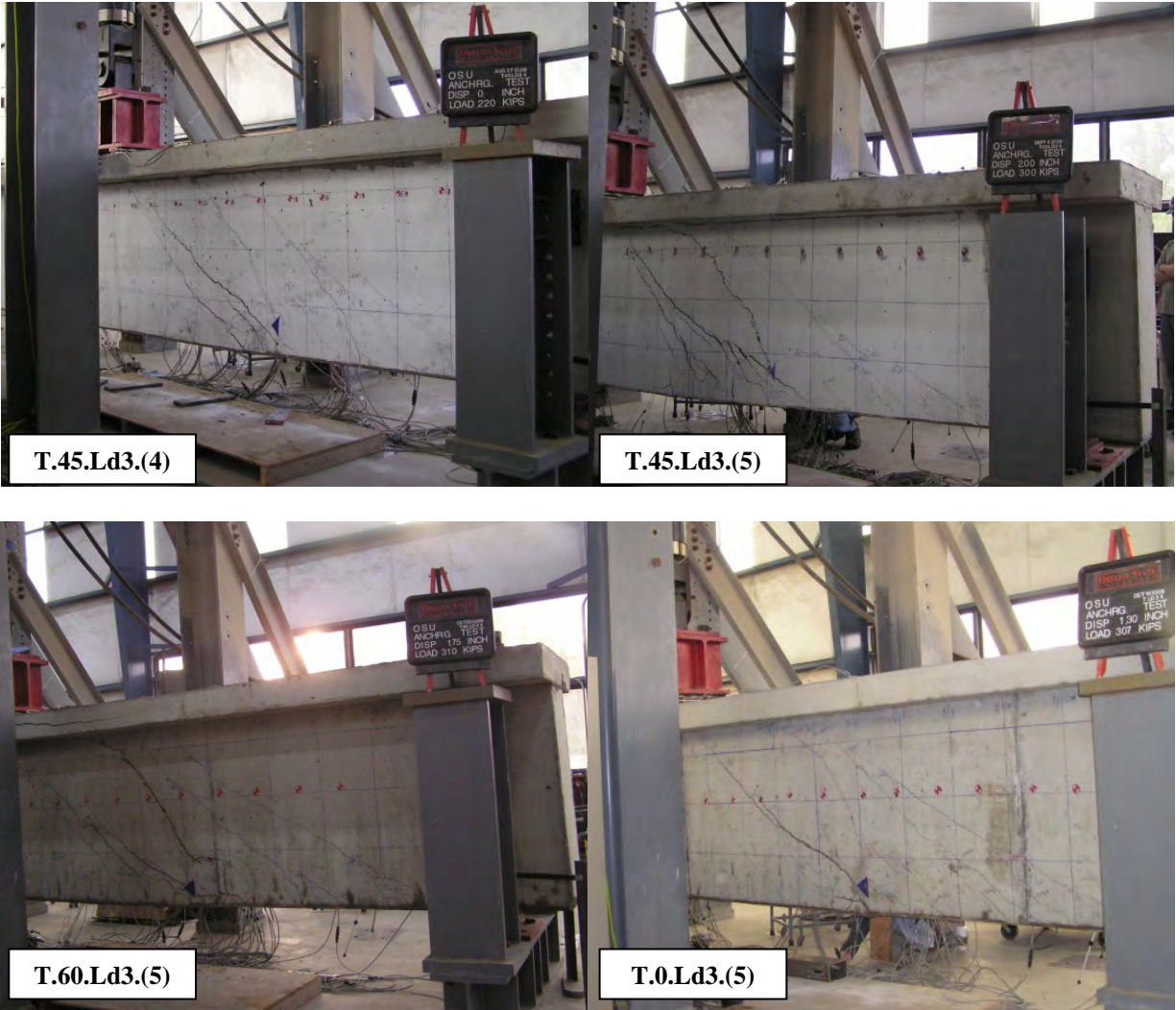
Figure 4.5: Digital photographs at failure of T-beam specimens
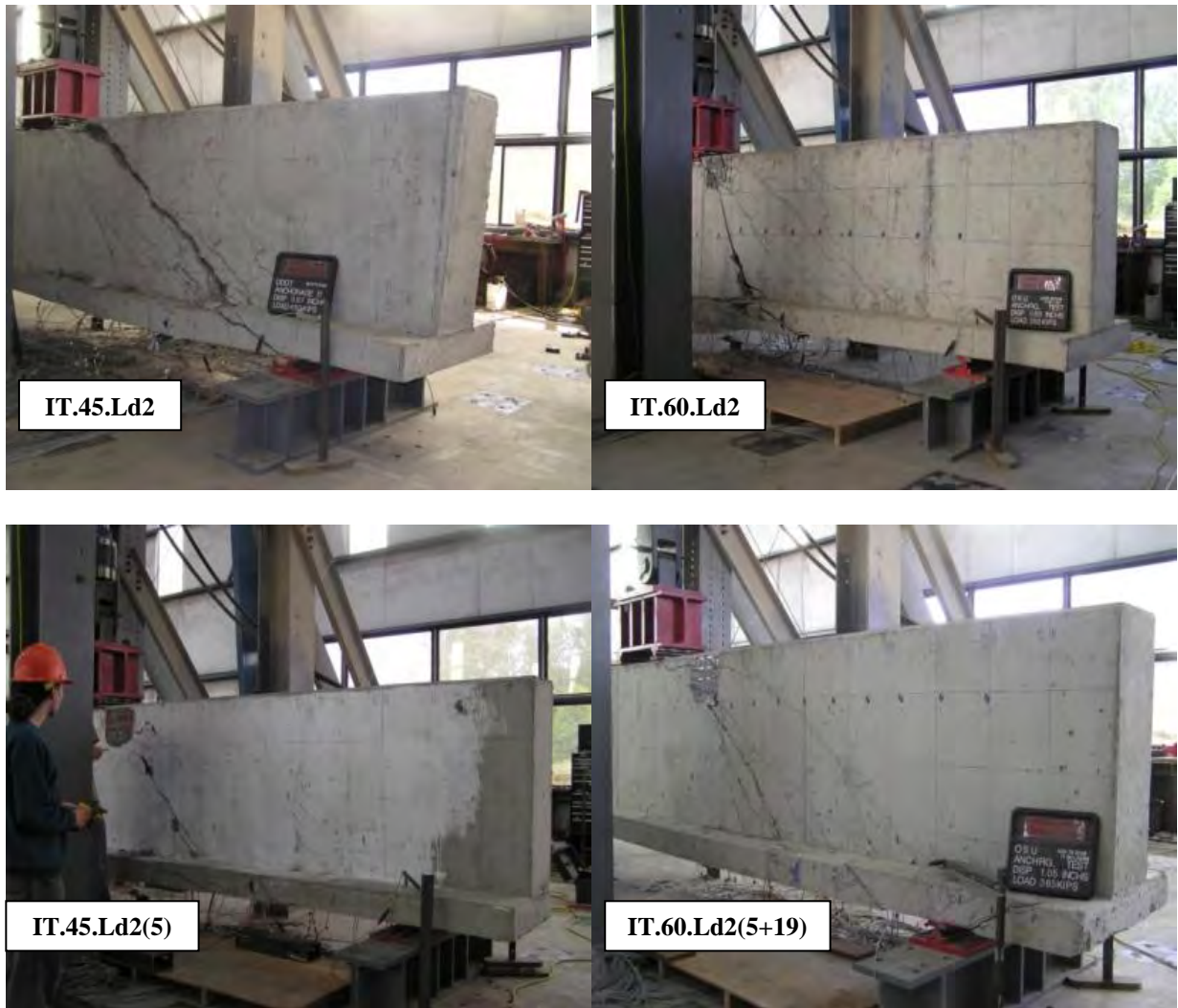
Figure 4.6: Digital photographs at failure of IT-beam specimens

Just prior to failure of all the T-beams, the largest diagonal crack in each of the specimens extended from the loading plate to the end of the cutoff bars. As the cutoff bars slipped, additional diagonal cracks formed while some of the existing cracks propagated. All of these diagonal cracks were steeper (more vertical) than the failure diagonal crack and were closer to mid-span. Evidence of this diagonal crack evolution at failure was preserved in digital videos taken during testing.

Starting at the 445 kN (100 kip) load cycle, cracks along the anchorage zone of the cutoff bars started to form in the T-beam specimens as shown in Fig. 4.7. These cracks were characterized by periodic vertical cracks extending from the location of the cutoff bar to the bottom soffit of the beam stem. The vertical cracks were connected by primary horizontal cracks at the level of the cutoff bar. As the applied load increased, the extent and density of the anchorage cracks increased. IT-beam specimens failing in shear-anchorage demonstrated similar horizontal wedge cracking located at the flange of each specimen beginning at the 667 kN (150 kip) load cycle as

shown in Fig. 4.8. This type of slip-induced cracking was clearly evident on both the bottom and top flange surfaces along the length of the developing longitudinal reinforcement.

Figure 4.7: Typical anchorage cracking caused by slip of the cutoff bars in T-beam specimens

Figure 4.8: Typical anchorage cracking caused by slip of the cutoff bars in IT-beam specimens

4.1.3 Anchorage Slip Response of Specimens

All load-cutoff bar slippage plots for the T- and IT-beam specimens are reported in Figs. 4.9 and 4.10. At early stages of loading the permanent slip in the cutoff bars was less than 0.25 mm (0.01in.) for each specimen that failed in anchorage. As loads increased toward failure, the cutoff bars slipped, and upon unloading, residual slip was observed. At failure, large slip values were observed, with as much as 12.7 mm (0.5 in.) (the limit of the instrumentation) of slip measured while additional load increased only moderately. Specimens IT.45.Ld2 and IT.60.Ld2 failed in shear-compression, with very little slip of the cutoff bars.
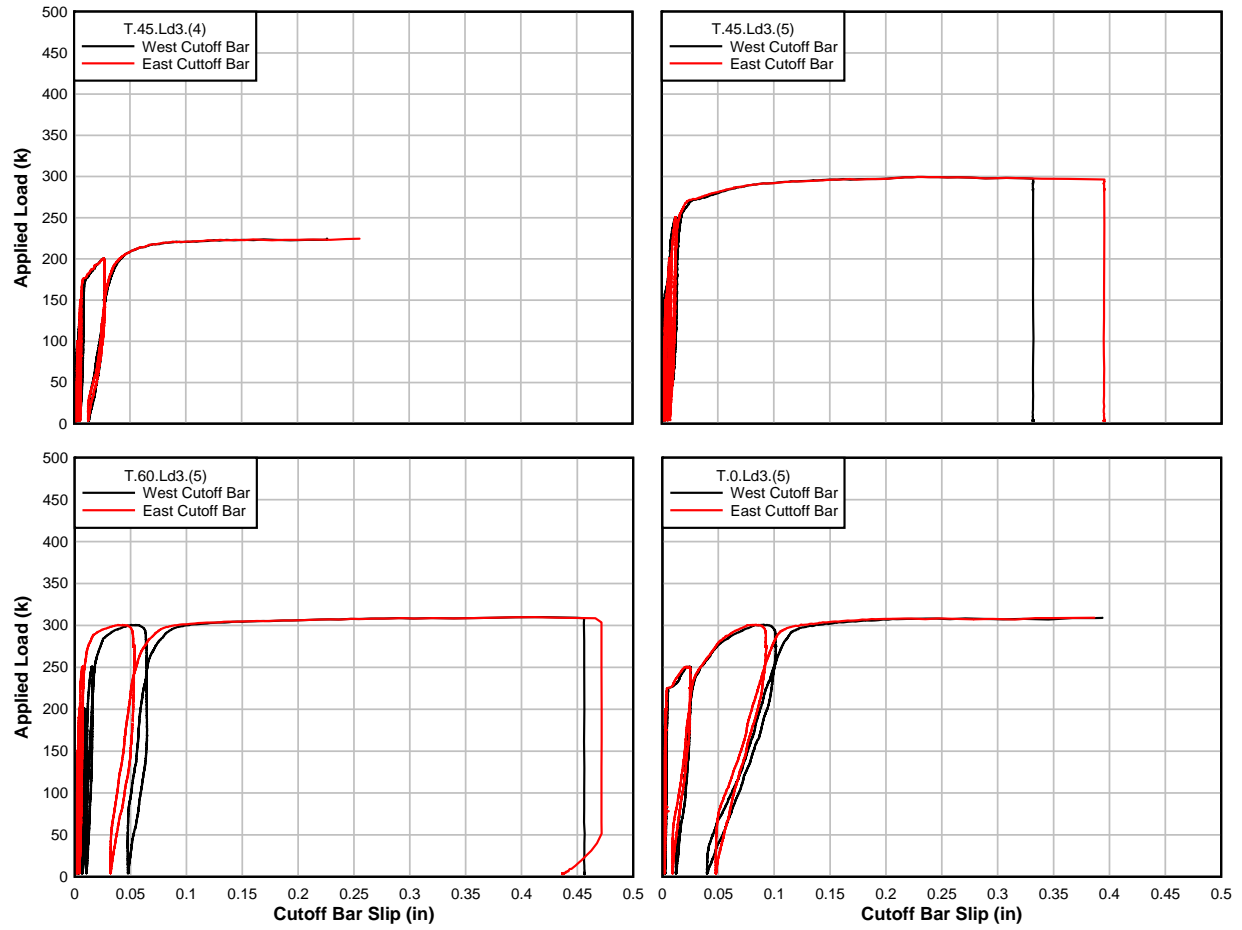
Figure 4.9: Load-cutoff bar slippage plots for T-beam specimens
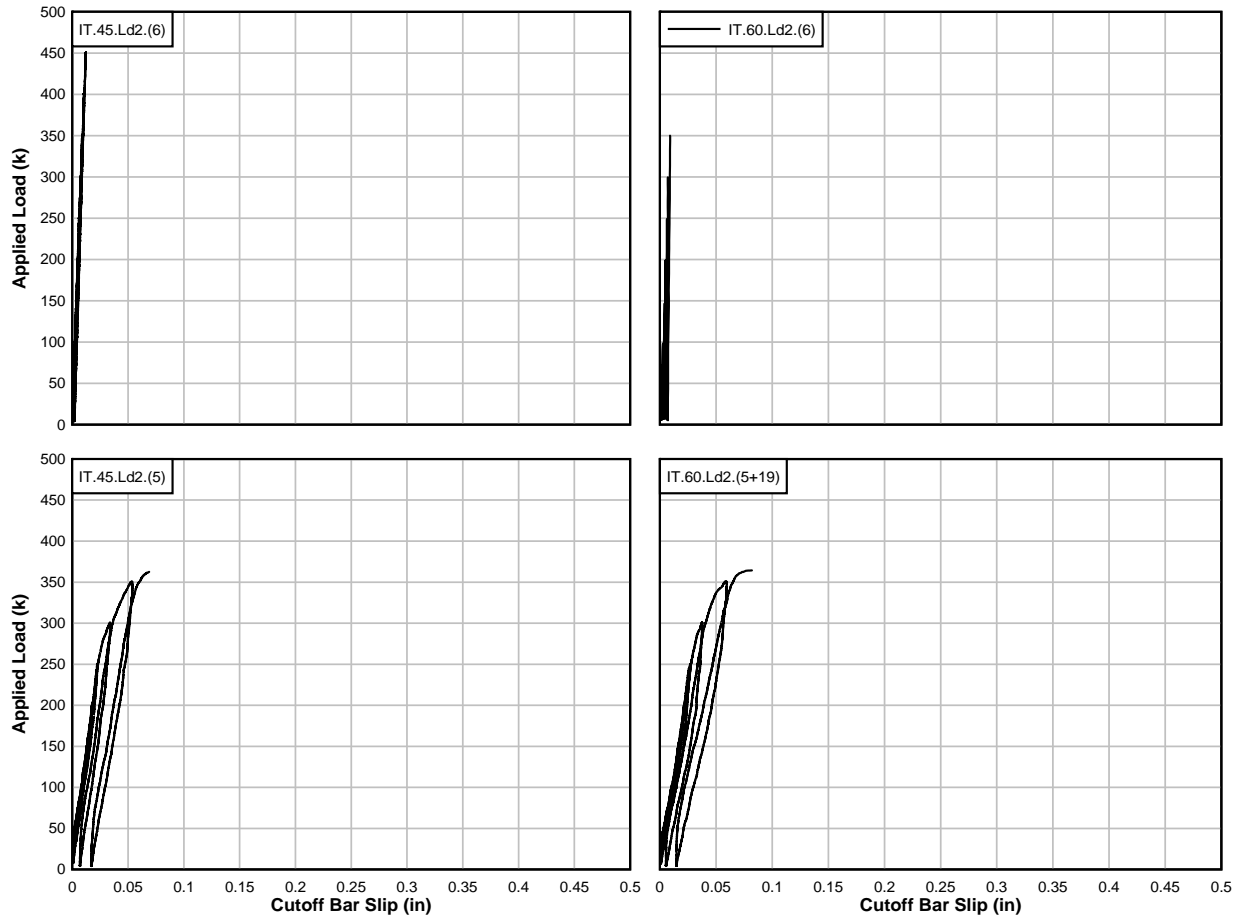
Figure 4.10: Load-cutoff bar slippage plots for IT-beam specimens

4.2   AASHTO-LRFD TENSILE CAPACITY

Tension carried by the flexural reinforcement, *T*, at any particular point along the length of the bar was calculated by converting the measured strain, ε_s, to force as:

$$T = A_s E_s \varepsilon_s \qquad [4.2]$$

where E_s is the modulus of elasticity of the flexural steel (ksi), and A_s is the cross-sectional area of the bar (in^2).

The total net tension force at the preformed diagonal crack intersection for each load step was determined by taking the sum of the tensile forces in each flexural bar. The tension in the flexural reinforcement at the preformed diagonal crack was for each specimen with a preformed crack. These values were calculated for the entirety of each test as shown in Fig. 4.11, with the peak results at each load value extrapolated.

The tensile demand for specimen T.45.Ld3.(5), T.60.Ld3.(5) and T.0.Ld3.(5) was similar during the entire load history. The three specimens had similar specimen geometry and material

properties except for the orientation of the preformed diagonal crack. The similarity of the data indicated the preformed crack had little influence on the overall behavior of the structure.
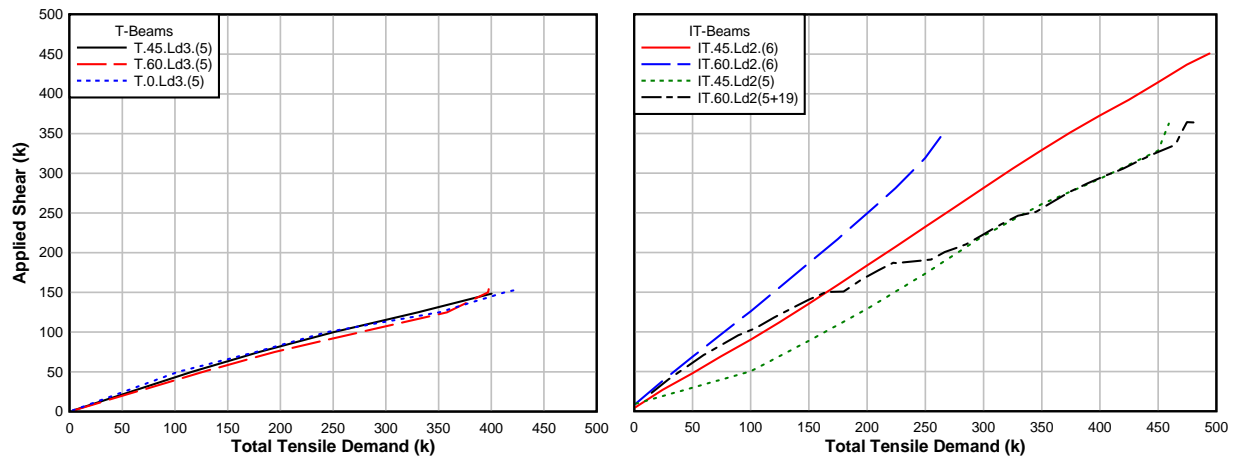
Figure 4.11: Average tensile demand at preformed diagonal crack location for T-beam specimens

The predicted AASHTO-LRFD tensile capacity of the flexural reinforcing at the preformed crack location using Eq. [2.5] was compared with the measured tension force of flexural steel at failure for all of the specimens with a preformed crack. In all cases, AASHTO-LRFD overestimated the tensile capacity.

The experimentally measured diagonal crack angle at the failure section was used as input for Eq. [2.5]. The applied moment was taken at the intersection of the flexural steel and the failure diagonal crack. The V_s term was taken as the yield stress times the number of stirrups crossing the failure diagonal crack. The experimentally measured tensile force in the flexural bars was determined from strain gages at or near the failure diagonal crack (this corresponded to the preformed crack for specimens IT.60.Ld2 and IT.45.Ld2(5)). The predicted and measured values were calculated as shown in Table 4.2.

Table 4.2: Predicted and measured tensile demands at failure

Beam Type	Specimen	AASHTO-LRFD Prediction (kN) [kips]	Measured Tensile Force (kN) [kips]	Bias T_{EXP}/T_{AASHTO}
T-Beam	T.45.Ld3.(4)	1399 [314.6]	1322 [297.2]	0.94
	T.45.Ld3.(5)	1888 [424.5]	1780 [400.3]	0.94
	T.60.Ld3.(5)	2002 [450.0]	1880 [422.7]	0.94
IT-Beam	IT.45.Ld2	2841 [638.7]	2155 [484.5]	0.76
	IT.60.Ld2	2108 [473.9]	2053 [461.4]	0.97
	IT.45.Ld2(5)	1986 [446.6]	1946 [437.4]	0.98
	IT.60.Ld2(5+19)	2091 [470.1]	2051 [461.0]	0.98

The AASHTO-LRFD predicted total (moment and shear induced) tensile demand and experimentally measured results were very close for all of the specimens accept IT.45.Ld2. All of the other specimens failed at moderate to steep crack angles and in locations with a dense array of strain gages in the flexural bars. The low correlation between AASHTO-LRFD and experimental results for specimen IT.45.Ld2 can be attributed to failure occurring in a region with small numbers of strain gages with which to determine the experimental tensile force in the flexural bars.

While the tensile demand in the flexural steel was well predicted by the AASHTO-LRFD equation for specimens with instruments located in the failure zone, it was also of interest to compare the tensile demands in the flexural reinforcing steel over the entire loading history. This included response in the service level range to better understand bond demands that could lead to possible long-term bond fatigue considerations. Using sensor data from the stirrups and flexural bars and the known crack geometry and applied loads, the experimentally measured tensile demands were compared with the AASHTO-LRFD methodology as shown in Fig. 4.12. These figures showed that AASHTO-LRFD-predicted demands were well correlated with the experimental results at service- to failure- level loads. Initial correlation was low due to the location of the neutral axis further down the specimen at low load levels. The results indicated that for existing cracks, the tensile demands on the flexural steel were indeed increased in the presence of diagonal cracks and applied shear.
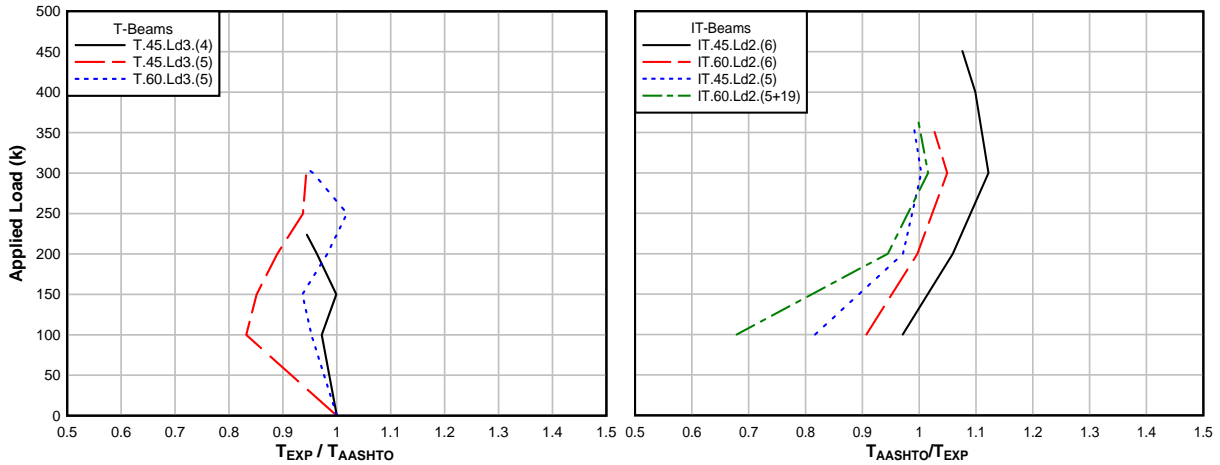
Figure 4.12: Comparison of predicted AASHTO-LRFD tensile demand to actual demand at increasing load steps

4.3   BOND STRESS

Using Eq. [2.1] the average and peak bond stress values for each cutoff bar in each specimen were determined and reported in Tables 4.3 and 4.4. For the IT-beam specimens, the peak average bond stress was coincident with failure. For the T-beam specimens, the peak values occurred prior to failure. The average bond stress was taken as the average measurement from all of the strain gages between the end of the cutoff bars and the preformed crack. The peak bond stress was taken as the maximum bond stress value along the cutoff bars. For T.0.Ld3.(5), which did not have a preformed crack, the bond stresses were determined using the first three sets of strain gages.

It can be seen from the data in Table 4.4 that bond stresses in the two IT-beam shear-anchorage failures were much higher than the bond calculated from the two shear-compression failures. Though the average bond strength in the well-anchored bars remained fairly steady throughout all tests, the cutoff bars showed a high variability in maximum bond strength based on the type of failure observed. The average maximum bond strength measured for the specimens that failed in shear-anchorage provided an estimate for bond strength necessary to produce a splitting failure in the flange of vintage RCDG beams. The two specimens that failed in shear-compression showed a range of average bond stress values that were not likely to produce anchorage failures in the flanges of RCDG beams.

45

Table 4.3: Summary of Peak and Average Bond Strength in Cutoff and Anchored Bars for T-Beam Specimens

Specimen	Cutoff Bars			Anchored Bars
	Bar	μ_{avg} (MPa) [ksi]	μ_{max} (MPa) [ksi]	μ_{avg} (MPa) [ksi]
T.45.Ld3.(4)	1	3.86 [0.560]	7.92 [1.149]	1.93 [0.280]
	2	5.05 [0.732]	12.05 [1.748]	
T.45.Ld3.(5)	1	7.57 [1.098]	19.43 [2.818]	1.98 [0.287]
	2	5.75 [0.834]	9.31 [1.964]	
T.60.Ld3.(5)	1	5.14 [0.745]	6.12 [0.887]	1.87 [0.271]
	2	5.97 [0.866]	6.41 [0.930]	
T.0.Ld3.(5)	1	7.72 [1.120]	8.62 [1.250]	2.05 [0.298]
Average		5.87 [0.851]	10.58 [1.535]	49.8 [0.284]

Table 4.4: Summary of Peak and Average Bond Strength in Cutoff and Anchored bars at Failure for IT-Beam Specimens

Specimen	Failure Mode	Cutoff Bars		Anchored Bars
		μ_{avg} (MPa) [ksi]	μ_{max} (MPa) [ksi]	μ_{avg} (MPa) [ksi]
IT.45.Ld2	Shear-Compression	2.79 [0.405]	6.74 [0.977]	2.38 [0.345]
IT.60.Ld2	Shear-Compression	3.16 [0.459]	6.60 [0.957]	2.58 [0.374]
IT.45.Ld2(5)	Shear-Anchorage	4.47 [0.648]	14.93 [2.165]	2.73 [0.396]
IT.60.Ld2(5+19)	Shear-Anchorage	4.37 [0.634]	13.88 [2.013]	2.73 [0.396]

Average bond stress versus cutoff bar slip for each cutoff bar of each specimen is presented in Figs. 4.13 and 4.14. The responses of the different specimens were all slightly different. Generally for the T-beam specimens, the maximum bond stress was achieved prior to member failure. For IT-beam specimens, maximum bond stresses were located at or near overall failure of the specimen in the case of shear-anchorage failures. It can be seen for the case of the IT.45.Ld2.(5) specimen, that one cutoff bar experienced a slightly greater bond stress, especially at or near specimen failure. For shear-compression failures, maximum bond stresses were not indicative of beam capacity, and could not, therefore, be considered with as much weight. In

cases where data were available for both cutoff bars, the maximum bond stress did not necessarily occur concurrently or at the same slip value.
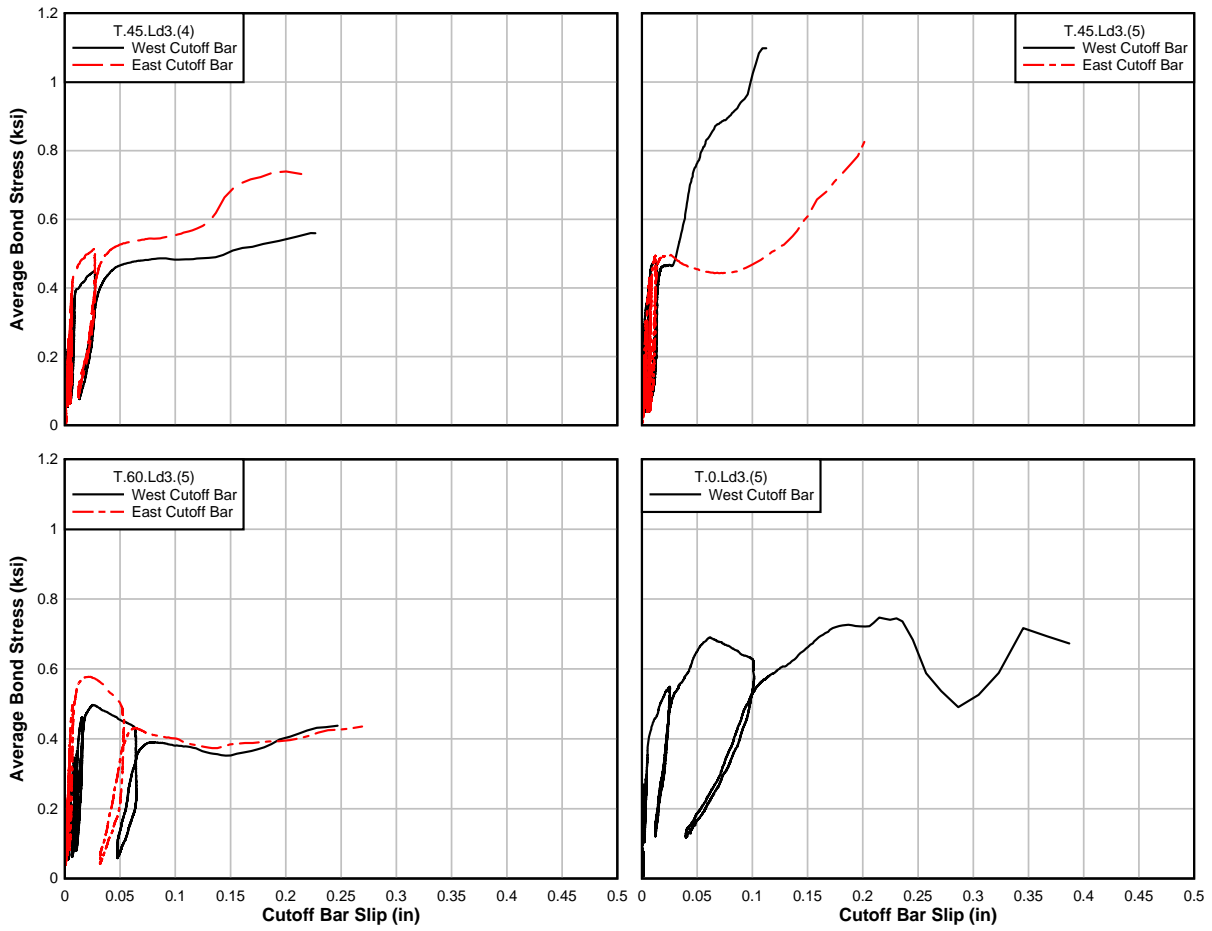
Figure 4.13: Bond stress – cutoff bar slip comparison for T-beams
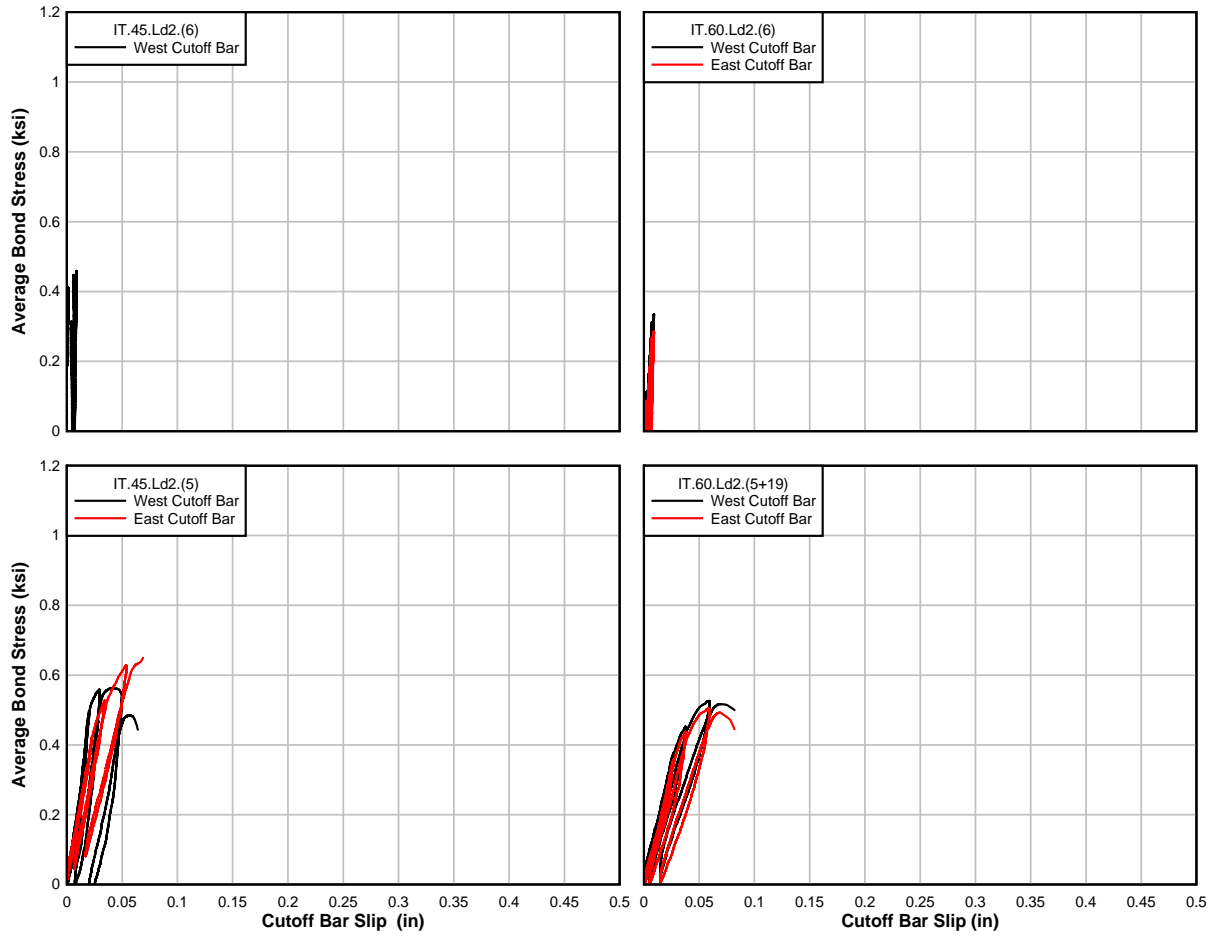
Figure 4.14: Bond stress – cutoff bar slip comparison for IT-beams

5.0   ANALYTICAL METHODS

Chapter 5 describes the methods used to analyze the experimental data. To predict the failure mode and capacity of a typical vintage RCDG girder, a Microsoft Excel Macro was developed using a combination of the AASHTO-LRFD Bridge Design Specifications, the ACI 318-08 Building Code, and literature review information. The experimental results were compared to present design specifications and archival literature sources. Nonlinear finite element analyses were performed and results were compared to the experimental results.

5.1   EXPERIMENTAL BOND STRESS ANALYSIS

5.1.1 Computing 97.5% Confidence Limit Bond Strength Values

The measured average bond stress values were higher than those calculated from ACI 318-08. While Fig. 4.10 shows the overall tension force for the specimens, it was of interest to separate the total tensile force into load carried by the anchored bars and load carried by the cutoff reinforcement in order to inspect both the relationship between the two in an effort to determine the net demand on the cutoff bars. To examine this behavior, the average tensile demand in the cutoff reinforcement was compared to the tensile demand in the anchored bars in Figs. 5.1 & 5.2.
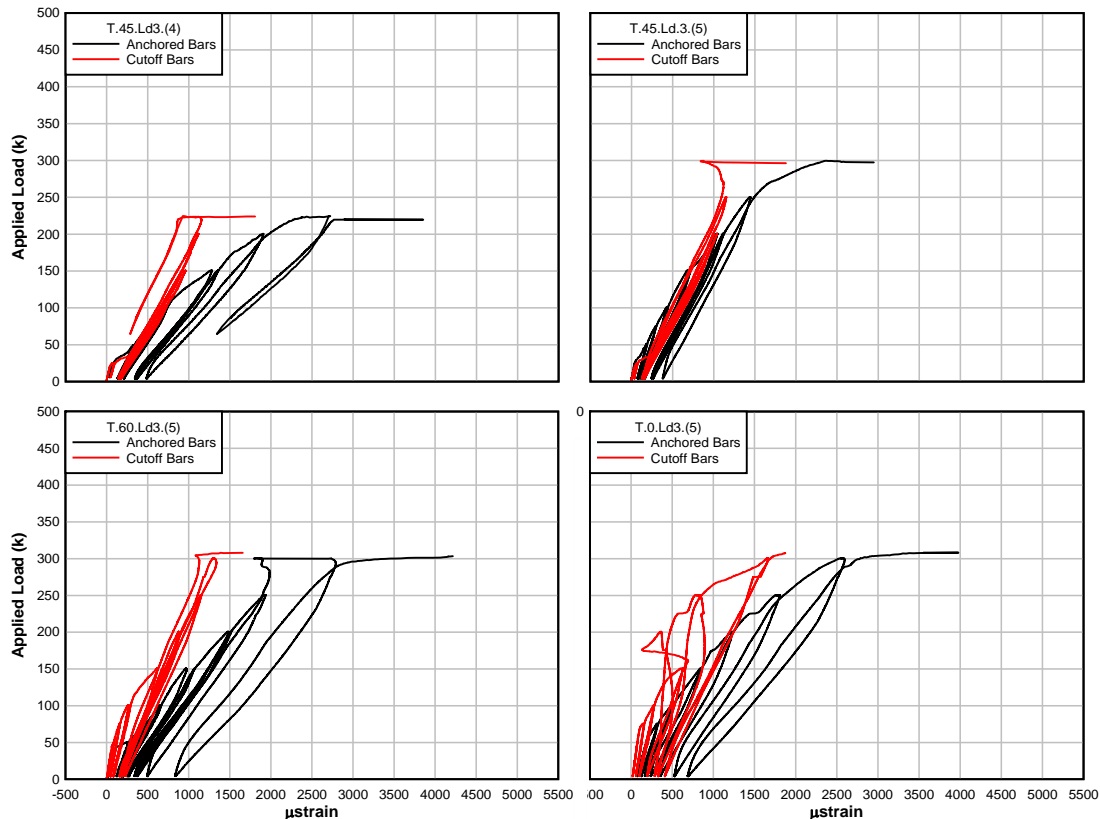
Figure 5.1: Average strain in flexural bars at the preformed diagonal crack for T-beam specimens
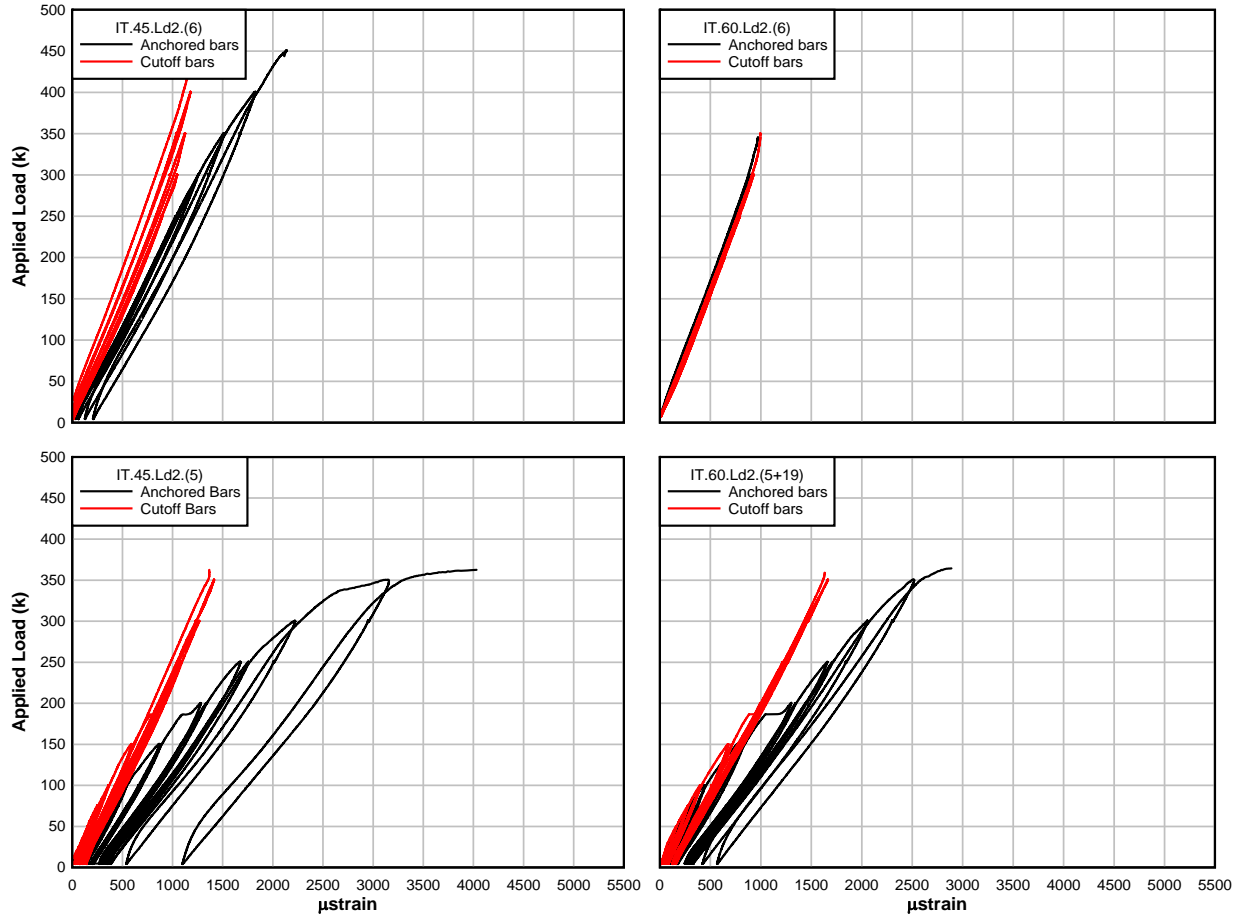
Figure 5.2: Average strain in flexural bars at the preformed diagonal crack for IT-beam specimens

From Figs. 5.1 and 5.2, it was clear that the anchored bars experienced a much higher demand throughout the failure cycle. This indicated that the cutoff reinforcement did not carry the same tension as the anchored bars at a given location along the development length of the cutoff bars. To analyze the difference in demand between the anchored bars and the cutoff bars, a tensile ratio (T_{ratio}) was considered to be the tensile demand on the cutoff bars at a given instrumented location compared to the tensile demand on the well-anchored bars at the same location:

$$T_{ratio} = \frac{T_{cutoff}}{T_{anchored}}$$

[5.1]

where T_{cutoff} is the tensile demand on the cutoff bars per bar and $T_{anchored}$ is the tensile demand on the anchored bars per bar.

The T_{ratio} was calculated for all reinforcing steel with strain gages at points between the preformed crack and the end of the cutoff bar. A linear regression of the one-sided, 97.5% lower-confidence limit for the data from the T-beam tests is shown in Fig. 5.3. The R^2 correlation was 0.8054, which was reasonable for using the data to determine the effective bond strength at a

given length of embedment. From the regression line, the maximum tensile force, $T_{97.5CL(T)}$, for the cutoff bar in T-beams was computed as:

$$T_{97.5CL(T)} = 0.0230 l_{em} A_s f_y \qquad \textbf{[5.2]}$$

where l_{em} is the length of embedment of the cutoff bar in inches; A_s is the bar cross-sectional area in in^2; and f_y is the flexural reinforcement yield strength in ksi. Eq. [5.2] must be limited by the full yield strength to indicate the bar is fully developed. Additionally, Eq. [5.2] may be converted to a maximum, permissible average bond stress, $\mu_{avg(T)}$, by:

$$\mu_{avg(T)} = 0.00574 f_y d_b \qquad \textbf{[5.3]}$$

where f_y is the flexural reinforcement yield strength in ksi and d_b is the bar diameter (in.). Using the measured material properties for the T-beam specimens, the average bond stress was 4.01 MPa (0.581 ksi) and the development length was 1.10 m (43.3 in).
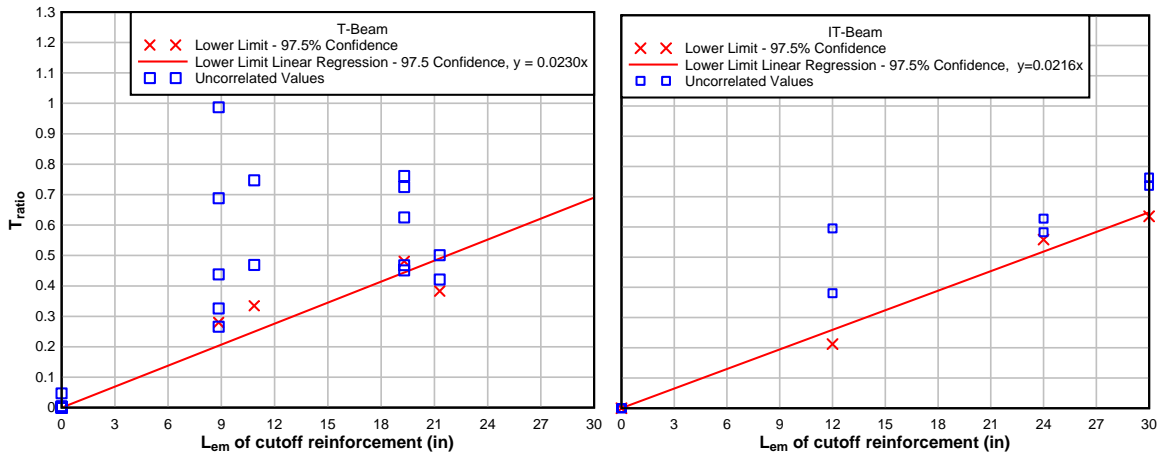
Figure 5.3: T_{ratio} analysis of the development of tension in cutoff reinforcement

Similarly, for the IT-beam data, a linear regression of the one-sided, 97.5% lower-confidence limit is shown in Fig. 5.3. The R^2 correlation was 0.9851. From the regression line, the maximum tensile force, $T_{97.5CL(IT)}$, for the cutoff bar in T-beams was computed as:

$$T_{97.5CL(IT)} = 0.0216 l_{em} A_s f_y \qquad \textbf{[5.4]}$$

Eq. [5.4] may be converted to a maximum, permissible average bond stress, $\mu_{avg(IT)}$, by:

$$\mu_{avg(IT)} = 0.00540 f_y d_b \qquad \textbf{[5.5]}$$

Using the measured material properties for the IT-beam specimens, the average bond stress was 3.76 MPa (0.546 ksi) and the development length was 1.18 m (46.3 in).

5.1.2 Comparing Bond Stress Results to Design Codes and Literature

The average bond stress values were higher than those contained in the ACI 318-08 and AASHTO-LRFD (after converting minimum development length to average bond stress). However, measured bond stress values were within the limits reported by others in the literature as described in Table. 2.1. The various methods of calculating development length in the codes and literature are compared graphically in Fig. 5.4. Where applicable, the average material properties and geometry were used to determine the development length. When only average bond stress values were reported, the development length was determined using Eq. [2.4].
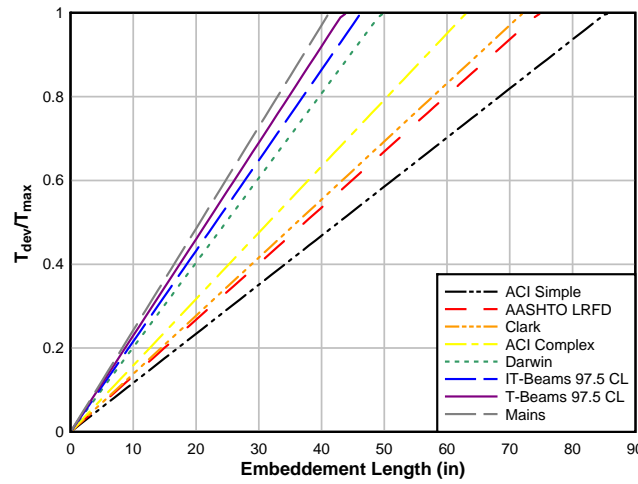
Figure 5.4: Comparison of literature, design specification, and experimental development lengths

As shown in Fig. 5.4, the specifications were highly conservative when compared to experimentally measured results. The more detailed ACI 318-08 procedure better reflected the experimentally measured response, although it remained conservative, showing that the actual maximum average bond strength available in RCDG beams was larger. From these results, it is likely that analysis of existing bridge members based on specified development lengths will under predict the maximum average bond strength and, therefore, predict shear-anchorage failures that may in fact be controlled by alternative failure mechanisms. The specified minimum development lengths calculated for straight bars using the actual material properties of each specimen are reported in Table 5.1.

Table 5.1: Comparison of Specified Minimum Development Length for Straight Bars

Beam Type	Specimen	f_c (MPa) [psi]	f_y (MPa) [ksi]	AASHTO (mm) [in]	ACI-318 (mm) [in]	
					Simplified	Complex
T-Beam	T.45.Ld3.(4)	21.8 [3165]		1996 [78.6]	2281 [89.8]	1686 [66.4]
	T.45Ld3.(5)	22.8 [3302]	494 [71.7]	1953 [76.9]	2235 [88.0]	1651 [65.0]
	T.60.Ld3.(5)	23.6 [3418]		1920 [75.6]	2197 [86.5]	1623 [63.9]
	T.0.Ld3.(5)	24.4 [3538]		1887 [74.3]	2159 [85.0]	1595 [62.8]
IT-Beam	IT.45.Ld2	27.0 [3918]		1793 [70.6]	2052 [80.8]	1415 [55.7]
	IT.60.Ld2	26.6 [3862]	494 [71.7]	1806 [71.1]	2065 [81.3]	1425 [56.1]
	IT.45.Ld2(5)	24.8 [3603]		1872 [73.7]	2139 [84.2]	1422 [56.0]
	IT.60.Ld2(5+19)	25.3 [3664]		1854 [73.0]	2121 [83.5]	1410 [55.5]

5.2   BEAM CAPACITY AND FAILURE PREDICTION METHODS

There are three likely failure modes for the specimens: "shear-compression failure", "flexure failure", or a type of "anchorage failure". The goal of the analysis was to identify the controlling shear-moment interaction point and then determine if the location had shear and moment capacities greater than the corresponding anchorage capacity. Two methods were developed to determine the failure mode and capacities.

5.2.1 MCFT Section Analysis Approach Using Response 2000

Response 2000 (R2K) is a free computer program, available on the Internet, developed by Evan Bentz and Michael Collins at the University of Toronto. (See http://www.ecf.utoronto.ca/~bentz/r2k.htm). The program performs a two-dimensional, non-linear sectional analysis for concrete beams and columns and assesses load-deformation response. R2K provides an easy-to-use input and output graphic user interface. For this investigation, the outputs of interest were the tensile demand on the flexural reinforcement and the AASHTO-99 shear-moment interaction diagram based on Modified Compression Field Theory (MCFT) as described in the AASHTO-LRFD Bridge Design Specifications. R2K provides the predicted capacity for the specified moment shear ratio. This was the value that was compared with the measured capacity of the vintage specimens. The test specimens were analyzed at key cross-sections using R2K using one of two analysis methods described in the subsequent sections.

5.2.2 Analysis Method 1

In this approach, an anchorage failure was predicted to occur if the tensile demand calculated in Eq. [2.5] exceeded the resistive tensile force determined from Eq. [2.3]. The crack angle determined from AASHTO-LRFD method analysis was not used in determining likelihood of anchorage failure for two reasons. First, AASHTO-LRFD predicted crack angles to be between 18° and 38° for specimens with at least minimum transverse reinforcement. Crack angles observed in field inspections were steeper than these values. Second, over the majority of the length of each specimen, the relatively shallow crack angles could not physically fit on the specimen in the present loading scheme. Given these two conditions, a Microsoft Excel macro program was written to search for the most likely crack angle-applied shear combination that satisfied Eq. [2.5] when limited by Eq. [2.3].

Summarized in the flowchart in Fig. 5.5, the macro worked as follows: Inputs were required for the material properties, beam geometry, and locations of flexural and shear reinforcement. At 25.4 mm (1 in.) increments along the span, the effective area of flexural steel was determined using a linear method to interpolate strength gained along the developing bar. Hooked bar development lengths were determined using the AASHTO-LRFD method. For T-beam analysis the maximum average bond strength of a straight No. 36 (No. 11) bar was defined as 4.01 MPa (0.581 ksi). Similarly, for the IT-beam analysis, the maximum average bond strength was defined as 3.76 MPa (0.546 ksi). In the end support regions, bond strength was increased by a factor of 1.3 over the 45° projection length along the straight bar as shown in Fig. 5.6 (Higgins, *et al*. 2004). The effective shear depth per AASHTO-LRFD was determined for the effective flexural steel area. Based on the effective area of flexural steel at each increment along the span, Eq. [2.3] was used to determine the maximum tensile capacity at that section.
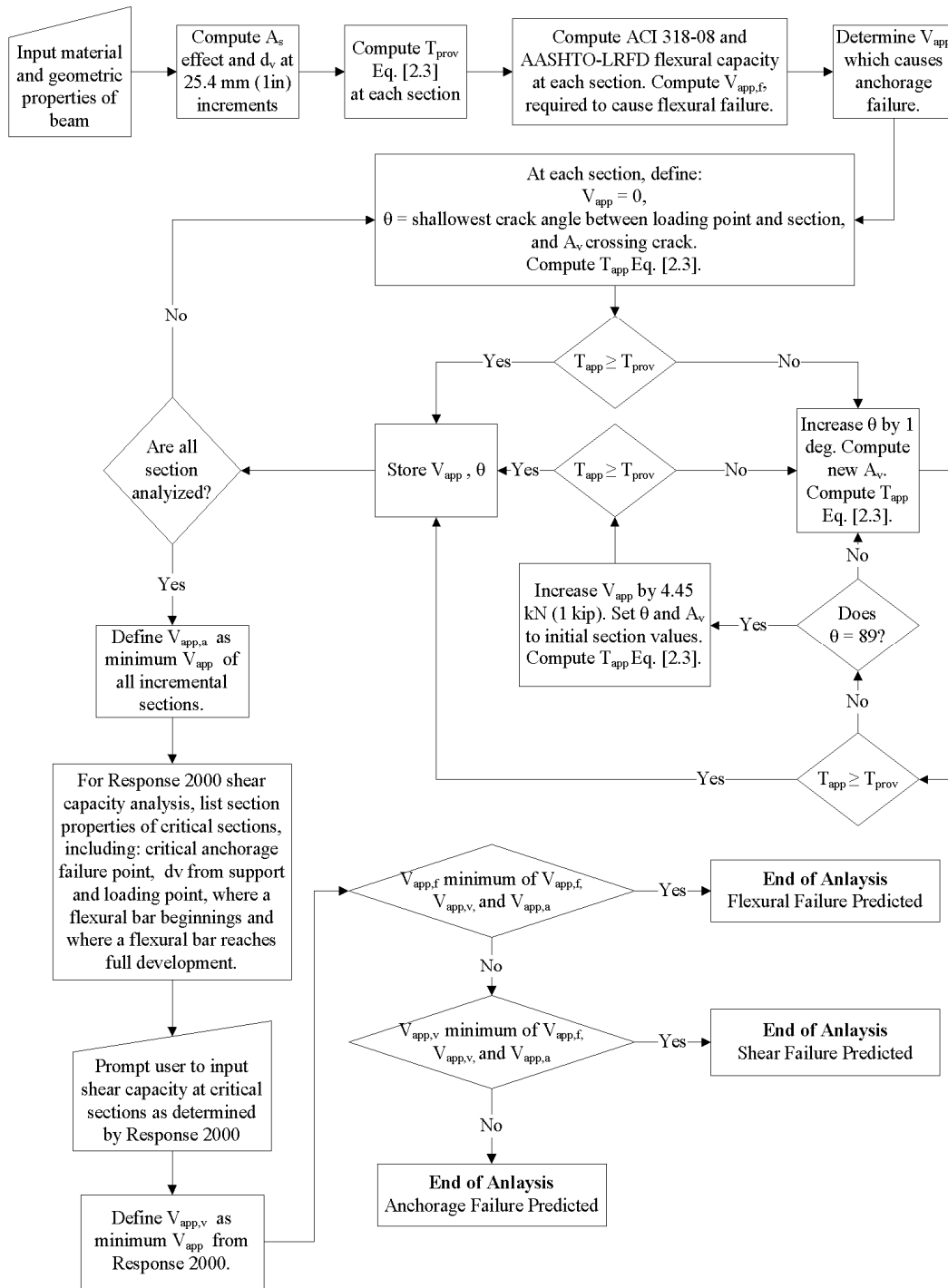
Figure 5.5: Failure load and mode solution procedure using Excel Macro
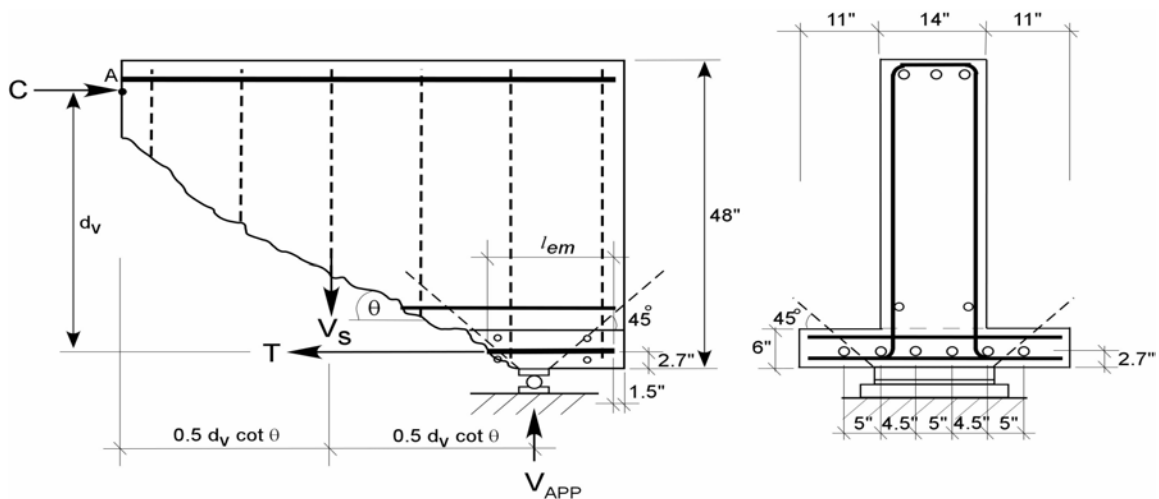
Figure 5.6: Effective region of confining stress due to supports (*Higgins, et. al 2004*)

Satisfying Eq. [2.5] was an iterative process. Starting at the support location, the applied shear was defined as 4.45 kN (1 kip) and the crack angle was defined as the shallowest crack angle that can exist between the loading point and the section in question. The number of stirrups that cross the diagonal crack was calculated. If Eq. [2.5] was not satisfied by the given applied shear-crack angle combination, the angle was increased by 1 degree. If Eq. [2.5] was not satisfied when the crack angle was 89°, the applied shear value was increased by 4.45 kN (1 kip). The process continued until an applied shear value and corresponding crack angle were reported for every 25.4 mm (1 in.) increment of the beam.

An additional feature of the macro helped the user decide if the critical anchorage failure location was also the critical failure location when also considering shear and flexure. The program automatically calculated the flexural capacity of each section specified by ACI 318-08 and AASHTO-LRFD design specifications. The moment capacity was converted to a shear load that would produce the computed moment based on the given shear-moment ratio of the applied loading. Similarly, the shear capacity as determined by ACI 318-08 and AASHTO-LRFD was also calculated. The user was prompted to input R2K predicted shear capacity at the critical locations. These locations included: where anchorage failure was identified in the above procedure; d_v from the support and loading point; where a flexural bar began; and where a flexural bar reached full development.

The applied shear at which anchorage failure may occur and the R2K predicted shear capacity and the equivalent shear to produce moment capacity is shown in Fig. 5.7. In the figure, only capacities for cross-sections on the under-reinforced section of the beam were shown and the equivalent shear to produced moment failure was not shown when the value was above 2224 kN (500 kips) for clarity. If the shear required to produce anchorage failure was below the shear strength and shear to produce moment failure, then an anchorage failure was most likely to control.

56
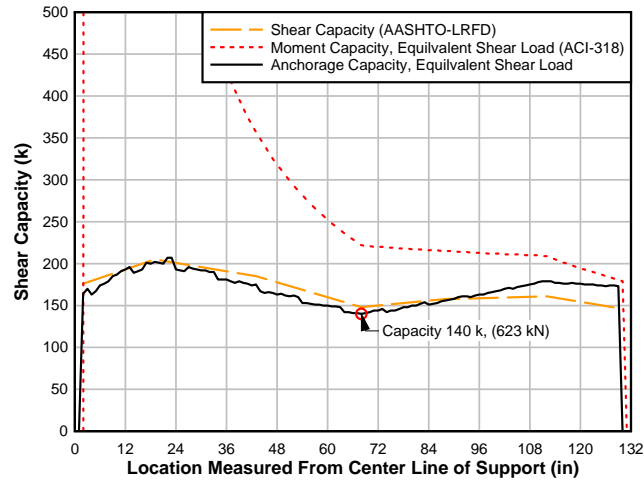
Figure 5.7: Example evaluation method one capacity and failure mode prediction for Specimen T.45.Ld3.(4)

5.2.3 Analysis Method 2

The purpose of analytical modeling for each specimen was to compare between the predicted strength of the specimens using the AASHTO-LRFD and ACI 318 codes with the experimentally measured response. It was expected that shear-anchorage failures should occur when the applied shear required to produce tensile forces (as predicted by Eq. [2.5]) in longitudinal reinforcement exceeded the maximum average bond stress and was less than the shear capacity of the specimen. The flexural demand at the locations being analyzed should be less than the flexural capacity of the section as determined by moment and shear interaction. To determine the controlling failure mode and location, the effective strength of the cutoff longitudinal reinforcement had to be determined first. After this, tensile capacity of all available flexural steel could be calculated, which was then used to determine the applied shear required to exceed this tensile capacity. Once the applied shear required to produce shear-anchorage failure was determined, the magnitude could be compared to the shear-compression and flexural capacities to determine the governing failure mode. This method established the hierarchy of failure modes for the specimens.

Shear and moment capacities were predicted using AASHTO-LRFD and ACI 318 specifications (AASHTO-LRFD 2005, ACI 318-08). As an additional check, the computer program Response 2000 (R2K) was utilized to predict shear-moment interaction capacities along the length of each test specimen. To determine the critical section at failure, multiple cross-sections throughout the length were considered. Specimens were analyzed along the cutoff bar design development length as well as at the preformed diagonal crack and support locations. The M/V ratio and effective quantity of flexural reinforcing steel were adjusted along the length of the developing bars. Effective flexural reinforcement area at each section was determined using the full nominal area of the fully developed bars plus a percentage of the nominal area for the partially developed bars. The percentage used was based on the ACI 318 predicted amount of development at the location as calculated in the Development Length section above.

57

5.2.3.1 Moment Capacity

The experimental and predicted moment capacities using ACI 318-08, AASHTO-LRFD, and R2K for all of the IT-beam specimens are shown in Table 5.2. The amount of effective flexural reinforcement at each section was calculated based on the percentage of cutoff reinforcement developed assuming a linear bond stress distribution with the design development length determined according to ACI 318. Sectional properties such as the distance between tension and compression centroids were taken from the R2K analysis. Nominal moment capacity determined by the ACI 318 and AASHTO-LRFD specifications was then compared to the predicted capacity from R2K.

Table 5.2: Predicted Moment Capacity Using Analysis Method 2

Beam Type	Specimen	Controlling Location	Predicted Shear Capacity (kN) [kips]		
			ACI-318	AASHTO	R2K
T-Beam	T.45.Ld3.(4)	Cutoff	993 [732]	956 [705]	1028 [758]
	T.45.Ld3.(5)	Cutoff	1490 [1099]	1453 [1071]	1543 [1138]
	T.60.Ld3.(5)	Cutoff	1490 [1099]	1453 [1071]	1545 [1139]
	T.0.Ld3.(5)	Cutoff	1490 [1099]	1453 [1071]	1545 [1139]
IT-Beam	IT.45.Ld2.(6)	Cutoff	2425 [1789]	2402 [1772]	2311 [1704]
	IT.60.Ld2.(6)	Cutoff	2424 [1788]	2402 [1772]	2311 [1704]
	IT.45.Ld2(5)	Cutoff	1996 [1472]	1932 [1425]	1796 [1325]
	IT.60.Ld2(5+19)	Cutoff	1995 [1473]	1932 [1425]	1796 [1325]

5.2.3.2 Shear Capacity

The experimental and predicted nominal shear capacities using ACI-318-08, AASHTO-LRFD, and R2K for all of the specimens are shown in Table 5.3. The predicted critical shear location is also reported in Table 5.3. Depending on the flexural detailing at the location of interest, the predicted shear capacities using ACI 318-08 or AASHTO-LRFD methods may be less than or greater than the R2K predictions.

Table 5.3: Predicted Shear Capacity Using Analysis Method 2

Beam Type	Specimen	Controlling Location	Predicted Shear Capacity (kN) [kips]		
			ACI-318	**AASHTO**	**R2K**
T-Beam	T.45.Ld3.(4)	Cutoff	502.6 [113.0]	509.7 [114.6]	520.4 [117.0]
	T.45.Ld3.(5)	Cutoff	682.8 [153.5]	692.6 [155.7]	707.2 [159.0]
	T.60.Ld3.(5)	Cutoff	682.8 [153.5]	692.6 [155.7]	707.2 [159.0]
	T.0.Ld3.(5)	Cutoff	682.8 [153.5]	692.6 [155.7]	707.2 [159.0]
IT-Beam	IT.45.Ld2	Support	745.9 [167.7]	744.2 [167.3]	805.1 [181.0]
	IT.60.Ld2	Cutoff	731.7 [164.5]	741.9 [166.8]	765.1 [172.0]
	IT.45.Ld2(5)	Cutoff	803.8 [180.7]	818.0 [183.9]	796.2 [179.0]
	IT.60.Ld2(5+19)	Cutoff	806.4 [181.3]	820.2 [184.4]	796.2 [179.0]

5.2.3.3 Anchorage Capacity

In order to determine if an anchorage failure is likely, it was necessary to determine applied load values that produced tensile demands in the flexural reinforcement in excess of their bond strength. Using the yield tensile capacity of the fully developed longitudinal bars as an upper limit, a tensile capacity along the length of the cutoff bars was determined based on the maximum average bond stress predicted using ACI 318, AASHTO-LRFD, and experimental results discussed previously. The required shear to produce anchorage failure at the preformed diagonal crack are tabulated in Table 5.4 for all of the specimens.

Table 5.4: Predicted Anchorage Capacity Using Analysis Method 2 (analysis at preformed crack location only)

Beam Type	Specimen	Shear Required to Produce Anchorage Failure at the Preformed Diagonal Crack (kN) [kips]		
		ACI-318	**AASHTO**	**Measured Bond**
T-Beam	T.45.Ld3.(4)	487.9 [109.7]	468.4 [105.3]	509.3 [114.5]
	T.45.Ld3.(5)	648.1 [145.7]	628.5 [141.3]	669.4 [150.5]
	T.60.Ld3.(5)	709.9 [159.6]	687.2 [154.5]	734.8 [165.2]
	T.0.Ld3.(5)	N/A	N/A	N/A
IT-Beam	IT.45.Ld2	962.5 [216.4]	929.2 [208.9]	963.5 [216.4]
	IT.60.Ld2	735.7 [165.4]	702.8 [158.0]	780.2 [175.4]
	IT.45.Ld2(5)	780.6 [175.5]	746.8 [167.9]	780.6 [175.5]
	IT.60.Ld2(5+19)	885.2 [199.0]	845.6 [190.1]	885.2 [199.0]

5.2.3.4 Results

As described in the preceding sections, governing shear-compression and moment capacities were compared to the load required to produce a shear- or pullout- anchorage failure. These results were used to determine tensile demands using AASHTO-LRFD procedures for each specimen and then converted to the corresponding shear force required to achieve failures. The shear required to produce flexural failures were highest for all specimens as seen in Table 5.5. The required applied shear forces for anchorage, shear-compression, and moment failures are given in Table 5.5. Also reported are the corresponding ratios between shear-compression and anchorage failures based on preformed diagonal crack locations. Ratios larger than unity indicated shear failure would be controlled by the anchorage (as examples: shear-compression for IT.45.Ld2 and IT.60.Ld2, shear-anchorage for IT.45.Ld2(5) and IT.60.Ld2(5+19)) with one exception. The IT.60.Ld2(5+19) specimen was predicted to fail in shear-compression. However, the analysis assumed a failure at the preformed diagonal crack angle of 60°. The actual failure occurred at 45°, which pushed the expected failure into the range of shear-anchorage. This same trend was observed for the predictions for the T specimens (shear-anchorage for all specimens) with the same exception where the preformed 60° crack was not the actual failure angle. For the case of the T.0.Ld3.(5) specimen, the load required for anchorage failure was not possible to derive based on the lack of a preformed crack. However, using the actual failure angle of 45°, this specimen was also correctly predicted to fail in shear-anchorage.

Table 5.5: Predicted Applied Shear to Produce a Given Failure Mode Using Analysis Method 2

Beam Type	Specimen	Required Applied Shear for Specified Failure Type (kN) [kips]			Ratio: Shear Compression/ Anchorage
		Moment (R2K predicted)	Shear-Compression (R2K predicted)	Anchorage (Measured Bond in Table 5.4)	
T-Beam	T.45.Ld3.(4)	612.9 [137.8]	520.4 [117.0]	509.3 [114.5]	1.02
	T.45.Ld3.(5)	920.3 [206.9]	707.2 [159.0]	669.4 [150.5]	1.06
	T.60.Ld3.(5)	921.1 [207.1]	707.2 [159.0]	734.8 [165.2]	0.96
	T.0.Ld3.(5)	921.1 [207.1]	707.2 [159.0]	N/A	N/A
IT-Beam	IT.45.Ld2	1352.6 [304.1]	805.1 [181.0]	963.5 [216.4]	0.84
	IT.60.Ld2	1064.0 [239.2]	765.1 [172.0]	780.2 [175.4]	0.98
	IT.45.Ld2(5)	1087.0 [244.4]	796.2 [179.0]	780.6 [175.5]	1.02
	IT.60.Ld2(5+19)	1087.5 [244.5]	796.2 [179.0]	885.2 [199.0]	0.90

5.3   EVALUATION OF PREVIOUS EXPERIMENTAL RESULTS

In the early 2000s, a series of vintage RCDG bridge girders were tested to evaluate shear capacity (*Higgins, el. al. 2004*). Both IT- and T-beam configurations were investigated. At the time, it was concluded that most of the T-beam specimens failed in shear-moment interaction, and several failed in flexure. However, several specimens were re-evaluated based on the findings of the present work, and it was concluded that three of the archival T-beams were susceptible to anchorage failures associated with diagonal cracking. There were two reasons for this conclusion: comparison of previous data to current experimental data and using both evaluation methods described in the previous section.

5.3.1 Visual Comparison of Previous and Current Experimental Data

Specimen 8T12-B3, 8T12-B4, and 9T12-B4 were the three archival T-beams susceptible to anchorage failure. The failure photos and load-deformation responses for each specimen are shown in Figs. 5.8 to 5.10. Specimens 8T12-B4 and 9T12-B4 had cutoff details similar to specimens T.45.Ld.3(5), T.60.Ld3.(5), and T.0.Ld3.(5) with the major differences in the specimens being that the older specimens had longer cutoff bars, wider stirrup spacing, and no hooked bars. Specimen 8T12-B3 had 6 straight bars and no cutoffs. Most likely, specimen 8T12-B4 failed in anchorage. Like the specimens in this report, the failure of specimen 8T12-B4 was ductile and characteristic anchorage cracks were observed near the bottom soffit in the anchorage zone. Although the load-deformation response of specimen 8T12-B3 was less ductile the 8T12-B4, cracks were observed in the anchorage zone near the support. Even through the macro analysis described in the subsequent paragraphs predicted an anchorage failure for specimen 9T12-B4, the experimental results did not fully corroborate this. The highly inclined diagonal crack bypassed the cutoff region entirely, with only minor diagonal cracking between mid-span and the end of the cutoff. It was likely that 9T12-B4 did not fail in anchorage.
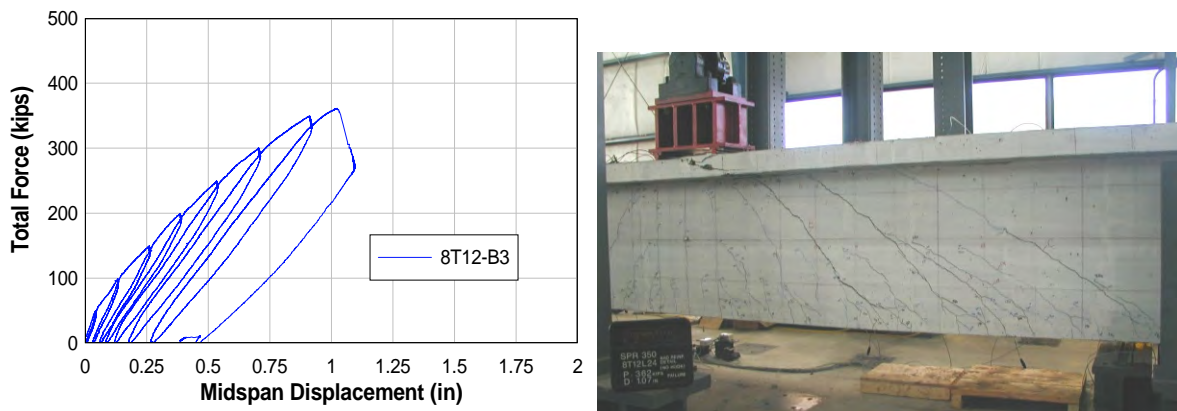
Figure 5.8: Specimen 8T12-B3 load-deflection plot and failure photo (*Higgins, et al. 2004*)
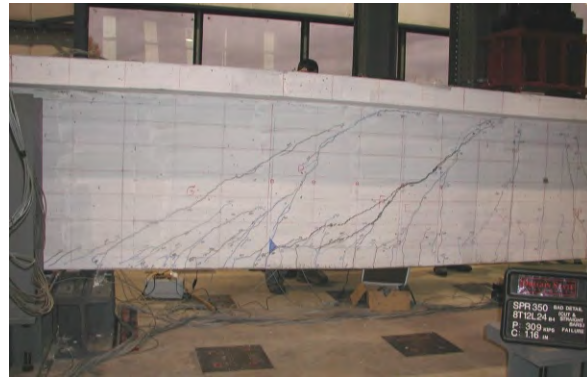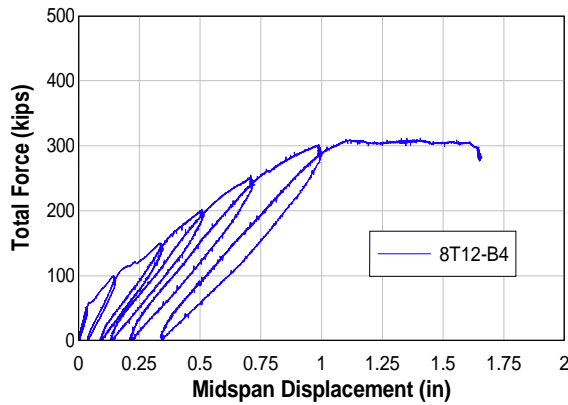
Figure 5.9: Specimen 8T12-B4 load-deflection plot and failure photo (*Higgins, et al. 2004*)
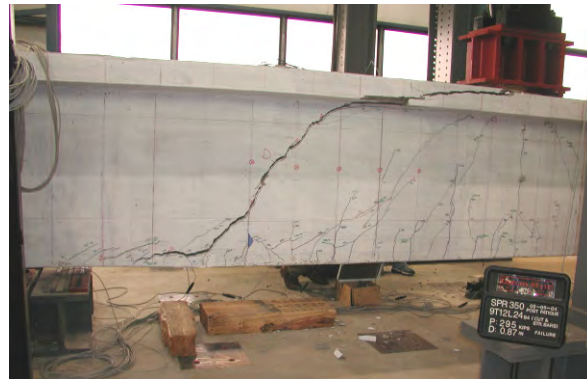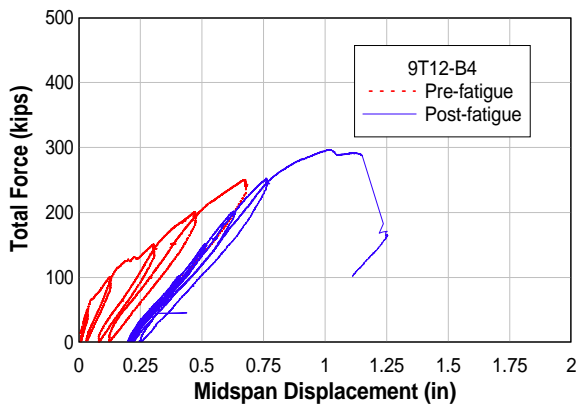
Figure 5.10: Specimen 9T12-B4 load-deflection plot and failure photo (*Higgins, et al.2004*)

5.3.2 Analytical Comparison Using Analysis Method 1

The Excel macro used to design the specimens for the current research was also used to evaluate 13 likely specimens from the SPR 350 program (Higgins, *et al.* 2004). The reported material properties in the archival report were used in the analysis. The macro analysis inputs and outputs from the investigation are described in Tables 5.6 to 5.8. To evaluate the capacity of the specimens, the 97.5 percent confidence limit average bond stress values were used. The bond stress value used for the T-beams was 4.01 MPa (0.581 ksi) as reported in Section 5.1 *EXPERIMENTAL BOND STRESS ANALYSIS*. The mean bias and the standard deviation for the T-beam specimens and the IT-beams specimens are reported in Table 5.9.

Table 5.6: Analytical Comparison of Previous and Current Experimental Data Using Evaluation Method One: Material Property Inputs

Test Program	Specimen	f'_c (MPa) [ksi]		f_y (MPa) [ksi]		f_{yv} (MPa) [ksi]
SPR 350	1T6	30.1	[4370]	463.3	[67.2]	349.6 [50.7]
	1IT6	32.9	[4775]	463.3	[67.2]	
	2T10	23.2	[3360]	540.5	[78.4]	
	2IT10	22.7	[3290]	578.4	[83.9]	
	2IT12	24.6	[3575]	588.1	[85.3]	
	5IT12-B4	28.5	[4130]	457.8	[66.4]	
	6T10	28.9	[4195]	448.8	[65.1]	
	7T12	29.7	[4310]	486.1	[70.5]	
	7IT12	28.7	[4165]	503.3	[73.0]	
	8IT12	33.4	[4840]	500.5	[72.6]	
	8T12-B3	31.5	[4570]	447.4	[64.9]	
	8T12-B4	32.6	[4725]	454.3	[65.4]	
	9T12-B4	33.8	[4910]	438.5	[63.6]	
T-Beams	T.45.Ld/3.(4)	21.8	[3165]	494.3 [71.7]		368.8 [53.5]
	T.45.Ld/3.(5)	22.8	[3302]			
	T.60.Ld/3.(5)	23.6	[3417]			
	T.0.Ld/3.(5)	24.4	[3538]			
IT-Beams	IT.45.Ld/2	27.0	[3918]	494.3 [71.7]		368.8 [53.5]
	IT.60.Ld/2	26.6	[3862]			
	IT.45.Ld/2 (5)	24.8	[3603]			
	IT.60.Ld/2 (5+19)	25.3	[3664]			

Table 5.7: Analytical Comparison of Previous and Current Experimental Data Using Evaluation Method One: Geometry Inputs

Test Program	Specimen	Span (m) [ft]	s (mm) [in]	No. Bars			Cutoff Location (m) [in]
				Hook	Straight	Cutoff	
SPR 350	1T6	7.32 [24]	152.4 [6]	3	3	0	-
	1IT6	7.32 [24]	152.4 [6]	0	6	0	
	2T10	7.32 [24]	254.0 [10]	3	3	0	
	2IT10	7.32 [24]	254.0 [10]	0	6	0	
	2IT12	7.32 [24]	304.8 [12]	0	6	0	
	5IT12-B4	6.58 [21.6]	304.8 [12]	0	6	0	
	6T10	7.32 [24]	254.0 [10]	3	3	0	
	7T12	6.58 [21.6]	304.8 [12]	3	3	0	
	7IT12	6.58 [21.6]	304.8 [12]	0	6	0	
	8IT12	6.70 [22]	304.8 [12]	0	4	2	1.22 [48]
	8T12-B3	7.32 [24]	304.8 [12]	0	6	0	-
	8T12-B4	7.32 [24]	304.8 [12]	0	3	2	1.52 [60]
	9T12-B4						
T-Beam	T.45.Ld/3.(4)	7.32 [24]	254.0 [10]	2	0	2	1.68 [66.2]
	T.45.Ld/3.(5)			2	1	2	
	T.60.Ld/3.(5)			2	1	2	1.73 [68.2]
	T.0.Ld/3.(5)			2	1	2	
IT-Beam	IT.45.Ld/2	6.58 [21.6]	304.8 [12]	2	2	2	1.02 [40]
	IT.60.Ld/2			2	2	2	1.52 [60]
	IT.45.Ld/2 (5)		254.0 [10]	2	1	2	1.02 [40]
	IT.60.Ld/2 (5+19)						

Table 5.8: Analytical Comparison of Previous and Current Experimental Data Using Evaluation Method One: Results

Test Program	Specimen	Failure Mode		V_{EXP} (kN) [kips]		Bias V_{EXP}/V_P
		Test	**Macro**	**Experimental**	**Predicted**	
SPR 350	1T6	Flexure	Flexure	918.5 [206.5]	897.6 [201.8]	1.02
	1IT6	Flexure	Flexure	1049.7 [236.0]	869.1 [195.4]	1.21
	2T10	Shear	Shear	913.2 [205.3]	944.3 [212.3]	0.97
	2IT10	Anch.	Anch.	913.2 [205.3]	858.5 [193.0]	1.06
	2IT12	Anch.	Anch.	817.5 [183.8]	782.8 [176.0]	1.04
	5IT12-B4	Shear	Shear	918.5 [206.5]	962.1 [216.3]	0.95
	6T10	Flexure	Shear	935.8 [210.4]	930.5 [209.2]	1.00
	7T12	Shear	Shear	963.0 [216.5]	958.5 [215.5]	1.00
	7IT12	Shear	Shear	909.2 [204.4]	964.8 [216.9]	0.94
	8IT12	Shear	Anch.	827.8 [186.1]	836.2 [188.0]	0.99
	8T12-B3	Shear	Anch.	818.0 [183.9]	765.0 [172.0]	1.07
	8T12-B4	Shear	Anch.	706.8 [158.9]	640.5 [144.0]	1.10
	9T12-B4	Shear	Anch.	682.8 [153.5]	613.8 [138.0]	1.11
T-Beam	T.45.Ld/3.(4)	Anch.	Anch.	510.6 [114.8]	453.7 [102.0]	1.13
	T.45.Ld/3.(5)	Anch.	Anch.	674.9 [151.7]	622.7 [140.0]	1.08
	T.60.Ld/3.(5)	Anch.	Anch.	701.6 [157.7]	622.7 [140.0]	1.13
	T.0.Ld/3.(5)	Anch.	Anch.	700.1 [157.4]	622.7 [140.0]	1.12
IT-Beam	IT.45.Ld/2	Shear	Shear	1015.9 [228.4]	926.1 [208.2]	1.10
	IT.60.Ld/2	Shear	Anch.	813.1 [182.8]	840.7 [189.0]	0.97
	IT.45.Ld/2 (5)	Anch.	Anch.	818.0 [183.9]	774.0 [174.0]	1.06
	IT.60.Ld/2 (5+19)	Anch.	Anch.	833.6 [187.4]	769.5 [173.0]	1.08

Table 5.9: Analytical Comparison of Previous and Current Experimental Data Using Evaluation Method One: Statistical Analysis

Beam Type	Bias Mean	Bias STD
T	1.07	0.058
IT	1.04	0.081

Of the 21 specimens investigated, the program indicated an anchorage failure mode for six specimens, as shown in Table 5.8, that were not observed experimentally. Five of the six specimens were said to have failed in shear, but method 1 predicted an anchorage failure. One specimen failed in flexure, but was predicted to fail in shear. As described previously, it was likely specimens 8T12-B3, 8T12-B4, and 9T12-B4 were influenced by or failed in anchorage. Similarly, specimen 8IT12 had six flexural bars, two of which were cutoff and may have been influenced by anchorage. For specimen 8IT12, the macro predicted that the critical anchorage failure would occur near the support, not the cutoff location.

The predicted difference in critical failure shear between the three possible failure modes for specimen 6T10 was less than 22.4 kN (5 kips). With the prediction window so narrow, it was possible that near-concurrent failure modes could influence outcomes due to material or analytical variability.

Lastly, specimen IT.60.Ld2 actually failed in shear at the preformed crack while an anchorage failure was predicted. Both the predicted anchorage and shear capacities were greater than the failure capacity.

Partial safety factors were calculated using the predicted and experimentally observed strengths. The results of the comparative analysis were assumed to be normally distributed so that the probability of over-predicting the experimental strength ($V_{exp}/V_p < 1$) with the Macro method depended on the outcome uncertainties and bias shown in Table 5.9. Although the bias of the T-beam data was further from unity when compared to the IT data, the standard deviation was less for the T-beam data. This was particularly clear when the data reported in Table 5.9 was shown with the confidence interval bands as in Fig. 5.11. Consequently, the T-beam data allowed a larger partial safety factor, showing that the comparative analysis results more accurately predicted T-beam failure results than IT-beams. Further, the T-beam behavior was characterized as ductile.
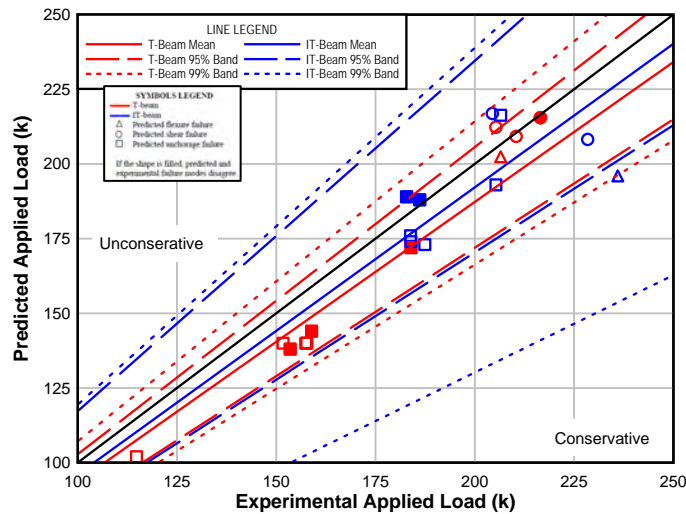
Figure 5.11: Macro analysis failure applied load predicted results bias analysis

Table 5.10: Confidence Intervals with Corresponding Partial Safety Factors

Confidence Interval	Partial Safety ϕ	
	T-Beam	IT-Beam
95%	0.97	0.91
99%	0.93	0.85

5.3.3 Analytical Comparison Using Evaluation Method 2

The tension and bond behavior discussed previously was applied to predict the failure modes and behavior of the SPR 350 specimens used for comparison. Of particular interest were the differences between failure modes predicted using ACI 318, AASHTO-LRFD, or experimental development length predictions. For these specimens, all longitudinal reinforcing bars were straight anchorage details. As a result, the development length of all bars was much higher than

the test specimens with hooked anchorage details. Therefore, shear-anchorage failures over the entire length were considered.

To determine the predicted failure mode for each SPR 350 IT-beam specimen investigated, the design development lengths using ACI 318, AASHTO-LRFD and experimental results were calculated based on the specific material properties of each specimen listed in Table 5.6. The development lengths of each specimen are reported in Table 5.11.

Table 5.11: Calculated development length using specifications and experimental results

Specimen	Calculated Development Length (mm) [in.]		
	ACI 318-08	**AASHTO-LRFD**	**Measured Bond**
2IT10	2032 [80.0]	2291 [90.2]	
2IT12	2012 [79.2]	2238 [88.1]	
5IT12-B4	1455 [57.3]	1618 [63.7]	1176 [46.3]
7IT12	1595 [62.8]	1773 [69.8]	
8IT12	1420 [55.9]	1633 [64.3]	

Since these flexural bars were developed across the supports, the effects of compression on increased bond over this region had to be accounted for to determine the effective area of flexural reinforcing steel at a given point as shown in Fig. 5.6. A modification factor of 1.3 times the calculated development length was applied to these reinforcing bars (Higgins, *et. al* 2004). Specimen material properties and failure crack angles were used to determine tensile demand at failure along the length of each specimen. The failure crack angles for each specimen are reported in Table 5.12. Using the design development length for each of the three methods, tensile capacity along the length of each specimen was compared to the predicted tensile demand to determine a failure mode. The capacity/demand ratio for each specimen from the supports to the load location is shown in Fig. 5.12. In each case, the tensile capacity predicted using experimentally derived bond strength was greater than both ACI 318-08 and AASHTO-LRFD predicted methods. The long development lengths of the specimens 2IT10 and 2IT12 resulted in a slow increase in capacity/demand ratio. Specimens 5IT12-B4 and 7IT12 exhibited a more uniform capacity/demand ratio increase with each specimen reaching maximum tensile capacity approximately 762 mm (30 in) from the supports. The development of cutoff reinforcement at 1219 mm (48 in) produced the sudden spike in additional capacity for specimen 8IT12.

Table 5.12: SPR 350 Test Specimens Failure Crack Angles (*Higgins, et. al 2004*)

Specimen	Failure Crack Angle
2IT10	30
2IT12	34
5IT12-B4	34
7IT12	32
8IT12	38
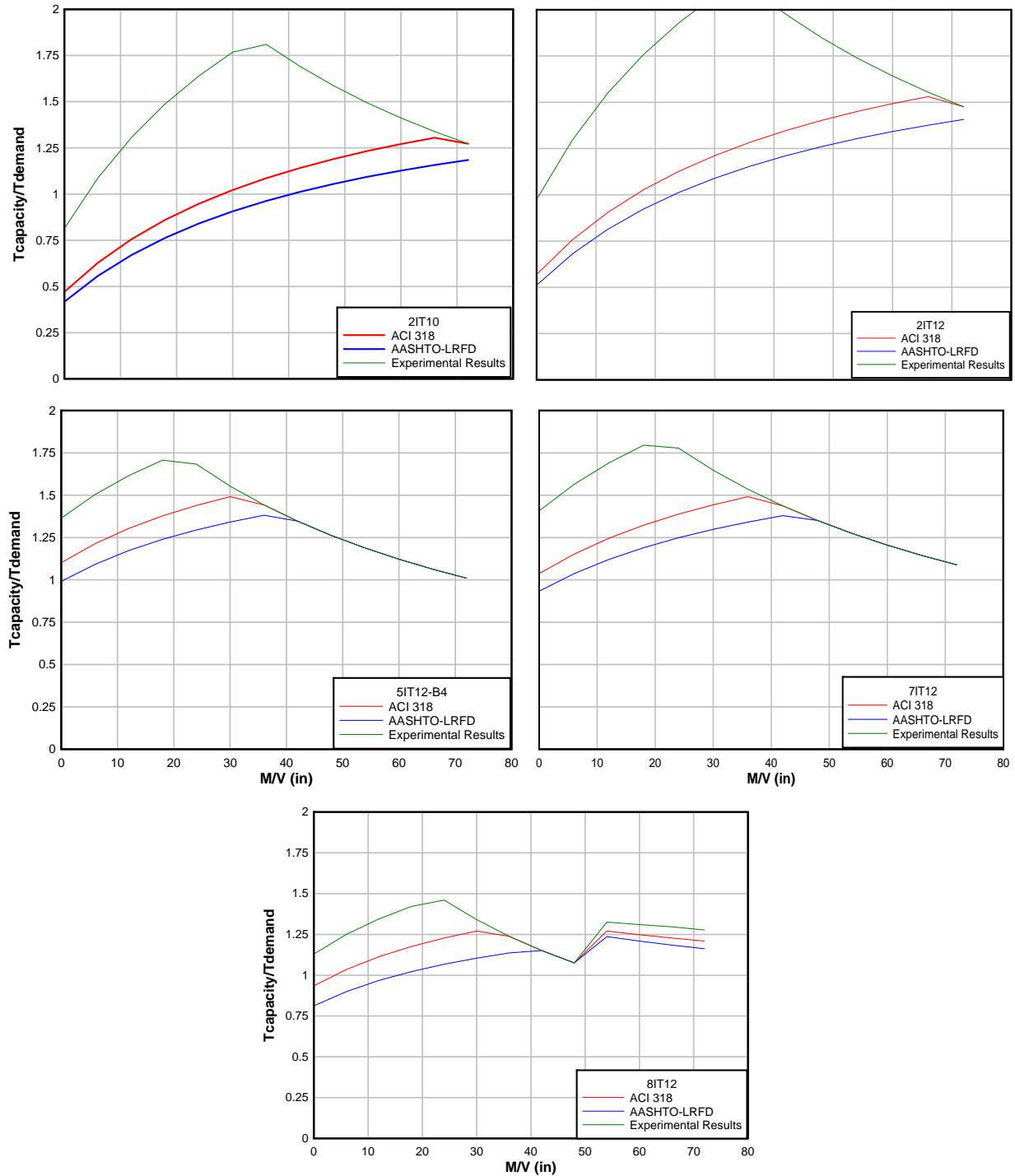
Figure 5.12: Tensile capacity - demand for each type of anchorage analysis using evaluation method two

All three methods for calculating development length correctly predicted the shear-anchorage failures for specimens 2IT10 and 2IT12. However, in the case of specimens 5IT12-B4 and 7IT12, the AASHTO-LRFD design development length incorrectly predicted a governing failure mode of shear-anchorage for these two shear-compression failures. For specimen 8IT12, which

had two cutoff longitudinal bars and a steeper failure crack, both ACI 318 and AASHTO-LRFD analysis methods incorrectly predicted a shear-anchorage failure at the supports. While the predictions from each analysis method were much more closely grouped for this specimen, only the prediction based on experimental results from this research correctly predicted the failure mode. The accuracy of each analysis method is summarized in Table 5.13.

Table 5.13: Accuracy of specification- and experimentally-based failure predictions

Specimen	Experimental Failure Mode	Predicted Failure Mode		
		ACI 318-08	AASHTO-LRFD	Measured Bond
2IT10	Shear-Anchorage	Correct	Correct	Correct
2IT12	Shear-Anchorage	Correct	Correct	Correct
5IT12-B4	Shear-Compression	Correct	Incorrect	Correct
7IT12	Shear-Compression	Correct	Incorrect	Correct
8IT12	Shear-Compression	Incorrect	Incorrect	Correct

5.4   NON-LINEAR FINITE ELEMENT ANALYSIS

The finite element method (FEM) has become a useful tool to structural engineers to analyze and predict behavior of complex structures. Successful implementation of the FEM relies on realistically representing the geometry, boundary conditions, and materials of the structure and validation of results with experimental findings.

5.4.1 Nonlinear Finite Element Analysis Using VecTor2

Reinforced concrete can be a difficult material to model due to quasi-brittle and anisotropic properties. Including realistic steel reinforcement interactions adds an additional degree of complexity. Finite element method analyses were undertaken using a program called VecTor2. VecTor2 v6.0 is the core application of a suite of programs used for finite element analysis under development at the University of Toronto since 1990. VecTor2 is a two-dimensional, membrane, nonlinear, finite element analysis program specifically intended for reinforced concrete structural modeling. Loadings schemes are static, cyclic or thermal. Two analytical models are used for predicting the results of rectangular reinforced concrete elements, Modified Compression Filed Theory (MCFT) (Vecchio and Collins, 1986) and the Disturbed Stress Field Model (DSFM) (Vecchio, 2000). The preprocessor, FormWorks v2.0, includes a graphical user interface for assigning structural geometry and material properties, an automatic mesh generator, and a bandwidth reducer to produce VecTor2 input files. The postprocessor, Augustus v5.0.6, uses a graphical user interface to display the deflected shape, the crack patterns, and the stress–strain distribution in the elements.

VecTor2 uses low-order planar triangular, rectangular, and quadrilateral elements. Reinforcing steel is modeled as either discrete or smeared. Linear truss bar elements model discrete reinforcement, with non-dimensional link or contact elements attaching the reinforcement to the concrete. The non-dimensional elements may be used to model bond-slip behavior. Alternatively, when modeled as smeared reinforcement, each element is modeled with a mixture of concrete and reinforcement material properties.

VecTor2 uses constitutive models for the concrete and steel reinforcement that account for second-order effects characteristic of reinforced concrete including: compression softening, tension stiffening, tension softening, and tension splitting. Other reinforced concrete behaviors modeled by VecTor2 include: concrete dilation and confinement, bond slip, crack shear deformations, reinforcement dowel action, reinforcement buckling, and crack propagation. Default VecTor2 material and behavioral models were used to model the concrete and reinforcing steel. Appendix D gives a brief description of each model. Further information for all models supported by VecTor2 is reported in the VecTor2 and FormWorks Manual (2002).

One of six models is used to estimate the bond behavior between the concrete and the reinforcement. Each model uses a series of reference bond slip and bond stress values for both the unconfined (splitting failure) and confined (pullout failure) cases. When the anticipated confinement pressure is somewhere between the unconfined and confined cases, a confinement pressure coefficient, β, is used to linearly interpolate between the unconfined and confined cases, where β is defined as:

$$\beta = \frac{\sigma}{7.5} \quad 0 \le \beta \le 1 \qquad \text{(in MPa)} \qquad \textbf{[5.6]}$$

where σ is the anticipated confinement pressure in MPa.

The "perfectly bonded" model assigns a large stiffness and strength to prevent deformation between the concrete and reinforcement elements. The "hooked bar" model consists of an ascending branch and sustained plateau at 22 MPa (3.19 ksi) of bond stress. The Fujii model is best suited when the expected failure is splitting. The Eligehausen, Gan, and Harajli models consider both the unconfined and confined cases. The Eligeausen and Gan models use the same algorithm for the confined case; for the unconfined case, the models calculate the same peak bond stress. The Harajli model predicts a higher confined bond stress than the Eligehausen and Gan models, and for the unconfined case, the bond stress is zero after the peak bond stress has occurred. The Fig. 5.13 compares the Eligehausen, Gan, and Harajli models using the material properties of specimen T.45.Ld3.(4). The Eligehausen model was used for the finite element analysis as explained in Section 5.4.2 *The Finite Element Model and Trial Analysis.*
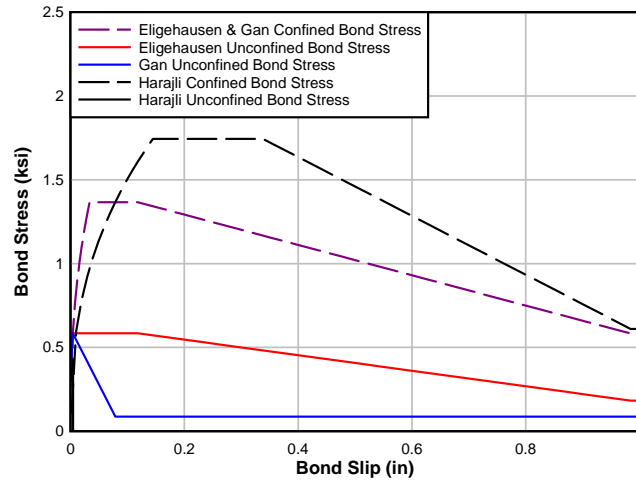
Figure 5.13: Eligehausen, Gan, and Harajli bond stress–slip response

5.4.2 The Finite Element Model and Trial Analysis

Due to the asymmetry of the reinforcement details, the full geometry of the specimens was modeled. In the experiment, both supports were friction rollers. However, to provide sufficient boundary conditions, one support was modeled as a pin and the other a roller. The pin support was modeled by constraining one node in the x and y directions, while the roller support was modeled by constraining one node in only the y-direction. Difference out of plane thicknesses were assigned for the deck and stem portions of the specimens. The concrete was modeled with rectangular and triangular elements. All reinforcement was modeled discretely using truss elements. Except for the cutoff bars, the reinforcement was assumed to be perfectly bonded to the concrete. Non-dimensional contact elements were used to connect the cutoff bar truss elements to the concrete elements to more accurately describe the bond behavior. In the IT-beam models, the cutoff bars were modeled 10 mm (0.39 in.) above their actual location to visually separate them from the well anchored bars on the output figures. In specimens with preformed cracks, the crack was modeled as a 2 mm (0.079 in.) gap between two adjacent regions. The as-built preformed diagonal crack angle was used. Using the automatic mesh generator, the element aspect ratio was limited to 1.5.

The number of rectangular and triangular elements representing the concrete, the number of truss elements representing the reinforcement, and the number of contact elements representing bond for each specimen are shown in Table 5.14. VecTor2 limits the number of elements to 6000 and the number of nodes to 5200. The finite element model for each of the specimens is shown in Figs. 5.14 to 5.21.

71

Table 5.14: Number of Elements in Each Finite Element Model

Beam Type	Specimen	Number of Elements				
		Rectangular	Triangular	Truss	Contact	Total
T-Beam	T.45.Ld3.(4)	1643	602	1152	80	3477
	T.45.Ld3.(5)	1643	602	1152	80	3477
	T.60.Ld3.(5)	1690	349	1079	82	2091
	T.0.Ld3.(5)	1630	270	1048	76	3024
IT-Beam	IT.45.Ld2	1933	492	1175	85	3685
	IT.60.Ld2	1749	654	1131	80	3614
	IT.45.Ld2(5)	1822	667	1209	85	3783
	IT.45.Ld2(5+19)	1987	464	1181	86	3718
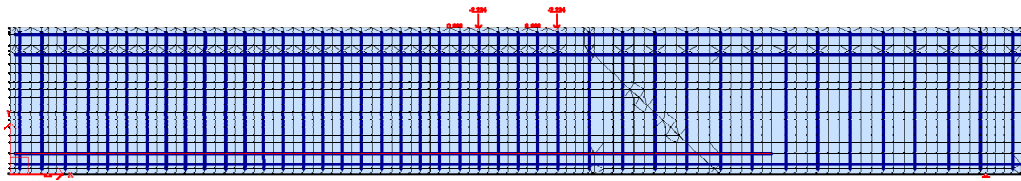
Figure 5.14: Specimen T.45.Ld3.(4) finite element model
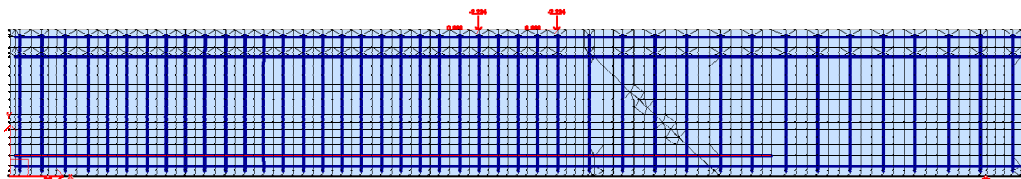
Figure 5.15: Specimen T.45.Ld3.(5) finite element model
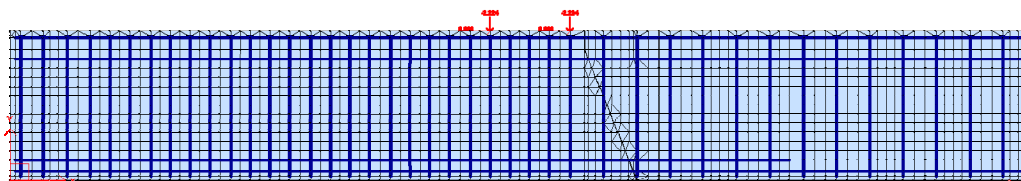
Figure 5.16: Specimen T.60.Ld3.(5) finite element model
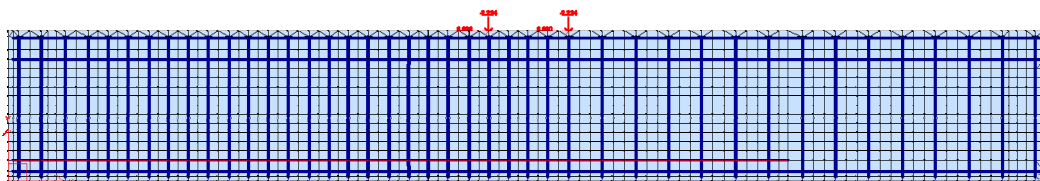
Figure 5.17: Specimen T.0.Ld3.(5) finite element model
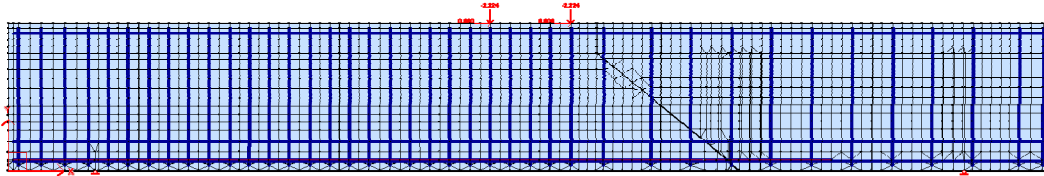
Figure 5.18: Specimen IT.45.Ld2 finite element model
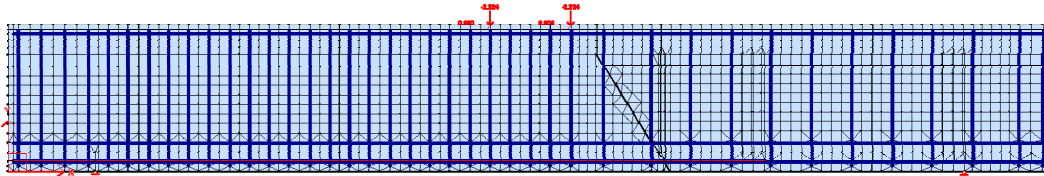
Figure 5.19: Specimen IT.60.Ld2 finite element model
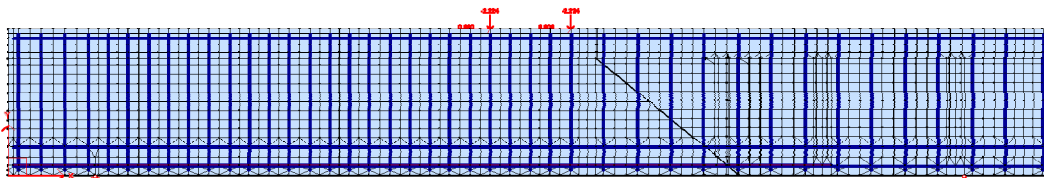
Figure 5.20: Specimen IT.45.Ld2.(5) finite element model
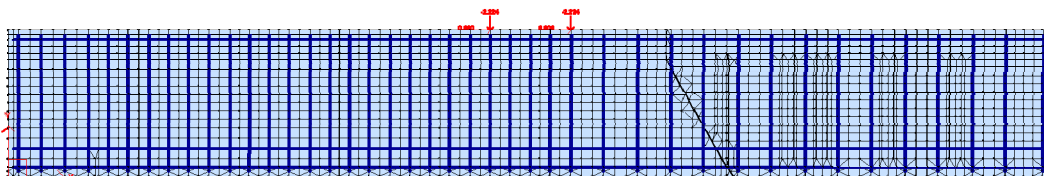
Figure 5.21: Specimen IT.60.Ld2.(5+19) finite element model

Material properties were defined using the results from material testing as described in Section 3.2 *MATERIAL PROPERTIES*. All of the derivative concrete material properties except for f_c' were determined by VecTor2. The steel elastic modulus, E_s, was taken as 200,000 MPa (29000 ksi), and the strain harding modulus, E_{sh}, was assumed to be 20,000 MPa (2900 ksi).

Three trial analyses were conducted for each beam type to determine which analysis options best captured the experimental response. These parameters were the bond model, mesh size, and load step size.

A confinement pressure coefficient study was also conducted to establish a value for *β* in Eq. [5.6] that reasonably approximated the experimental bond stress values using specimen T.45.Ld3.(4) for the T-beam calibration and IT.45.Ld2(5) for the IT-beam calibration. The predicted load-displacement for each trial is shown in Fig. 5.22 and Tables 5.15 and 5.16 summarize the *β* values and corresponding peak bond stress for each test trial analysis. VecTor2 reports the average reinforcement stress for each element. Using Eq. [2.1], taking l_d as the distance between midpoint of the element in question and the end of the cutoff, the bond stress

73

for each element between the preformed crack and the end of the cutoff was determined. The reported bond stress from VecTor2 was the average of all of the points calculated. The Eligehausen bond stress model was used for the study.
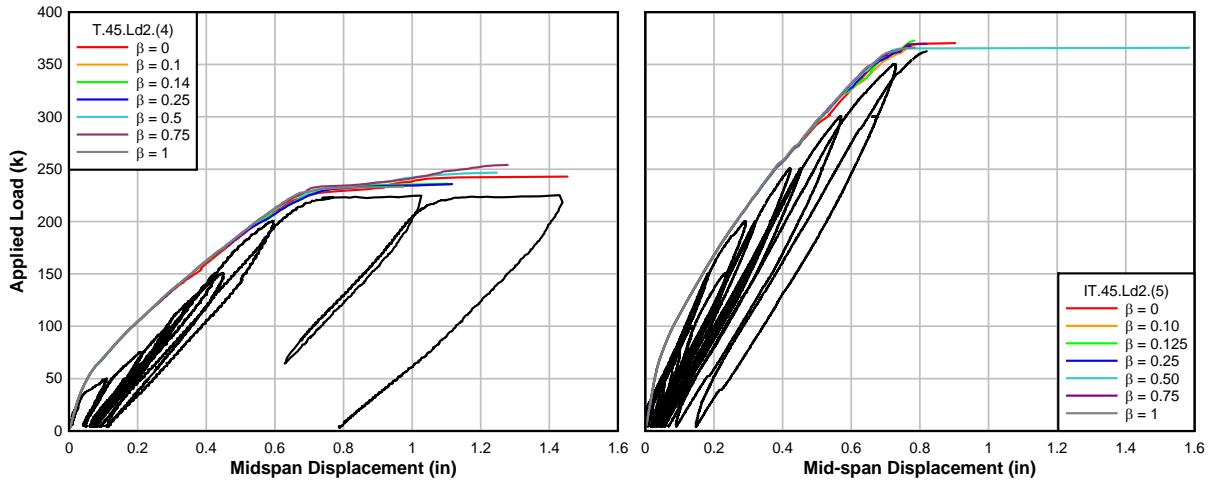
Figure 5.22: Predicted load-deformation response for different β values (specimen T.45.Ld3.(4))

Table 5.15: Predicted Bond Stress and Shear Strength for Different β Values Specimen T.45.Ld3.(4)

| β | Bond Stress | | Shear at Failure | |
	μ (MPa) [ksi]	Bias μ_{EXP}/μ_P	V_P (kN) [kips]	Bias V_{EXP}/V_P
0.000	4.08 [0.592]	1.09	540.4 [121.5]	0.94
0.100	4.36 [0.633]	1.02	525.8 [118.2]	0.97
0.140	4.71 [0.683]	0.95	525.3 [118.1]	0.97
0.250	4.72 [0.685]	0.94	525.8 [118.2]	0.97
0.500	5.09 [0.738]	0.88	548.9 [123.4]	0.93
0.750	5.54 [0.804]	0.80	565.3 [127.1]	0.90
1.00	6.03 [0.875]	0.74	518.6 [116.6]	0.98

Table 5.16: Predicted Bond Stress and Shear Strength for Different β Values Specimen IT.45.Ld2.(5)

| β | Bond Stress | | Shear at Failure | |
	μ (MPa) [ksi]	Bias μ_{EXP}/μ_P	V_P (kN) [kips]	Bias V_{EXP}/V_P
0.000	3.74 [0.542]	1.20	823.8 [185.2]	0.99
0.100	4.50 [0.652]	0.99	823.8 [185.2]	0.99
0.125	4.36 [0.633]	1.02	829.1 [186.4]	0.99
0.250	3.87 [0.561]	1.16	817.1 [183.7]	1.00
0.500	4.39 [0.637]	1.02	814.0 [183.0]	1.00
0.750	5.12 [0.742]	0.87	821.6 [184.7]	1.00
1.00	5.97 [0.866]	0.75	814.0 [183.0]	1.00

With regard to the T-beams, 4.45 MPa (0.646 ksi) was used for the experimental bond stress, which was the average of the bond stress values reported for specimen T.45.Ld3.(4) in Table 4.3.

At high β values, both the bond stress and failure load were overestimated, and at low β values the bond stress and failure load were underestimated. For the trials investigated, a β value of 0.140 most reasonably predicted the experimental load-displacement behavior, bond stress with a bias of 0.95, and failure load with a bias of 0.97. Even though using a β value of 0.10 predicted a more accurate bond stress with a bias of 1.02, the β value of 0.140 was used for the remainder of the analyses as the theoretical stirrup pressure was a practical means of estimating the β value and the results were conservative and still reasonable.

Similarly, for the IT-beams, 4.47 MPa (0.648 ksi) was used for the experimental bond stress, which was the average of the bond stress values reported for specimen IT.45.Ld2(5) in Table 4.4. Regardless of β values, the failure load was predicted well. Generally at high β values, the bond stress was overestimated, and at low β values, the bond stress was predicted well. For the trials investigated, a β value of 0.125 most reasonably predicted the experimental load-displacement behavior, bond stress with a bias of 1.02, and failure load with a bias of 0.99. Even though using a β value of 0.10 predicted a more accurate bond stress with a bias of 0.99, the β value of 0.125 was used for the remainder of the analyses.

A convergence study was performed using h-refinement. Using the automatic mesh option provided in FormWorks, five mesh sizes were investigated for the T-beam: 55 mm (2.16 in.), 70 mm (2.76 in.), 75 mm (2.95 in.), 100 mm (3.94 in.), and 200 mm (7.87 in.). Similarly, for the IT-beam, four mesh sizes were investigated: 55 mm (2.16 in.), 75 mm (2.95 in.), 100 mm (3.94 in.), and 145 mm (5.71 in.). In all cases, the initial stiffness of the specimen was the same. However, at high loads, the ultimate capacity and ultimate displacement varied. Further, when using small mesh sizes, the smallest of the elements at the cutoff location were very small compared to the nearby elements. As a consequence, a near vertical crack at the cutoff location was the cause of failure in the T-beam specimen. For these reasons, and for consistency between the T- and IT-beam analyses, a 75 mm (2.95 in.) mesh size was selected for the remainder of the analysis. Specimens T.45.Ld3.(4) and IT.45.Ld2(5) were used for the mesh convergence study. The results of the convergence trials are shown in Fig. 5.23. Similarly, the required computing time as a function of the number of elements in the model is presented in Fig. 5.24. Generally, the number of elements was proportional to the required computation time.
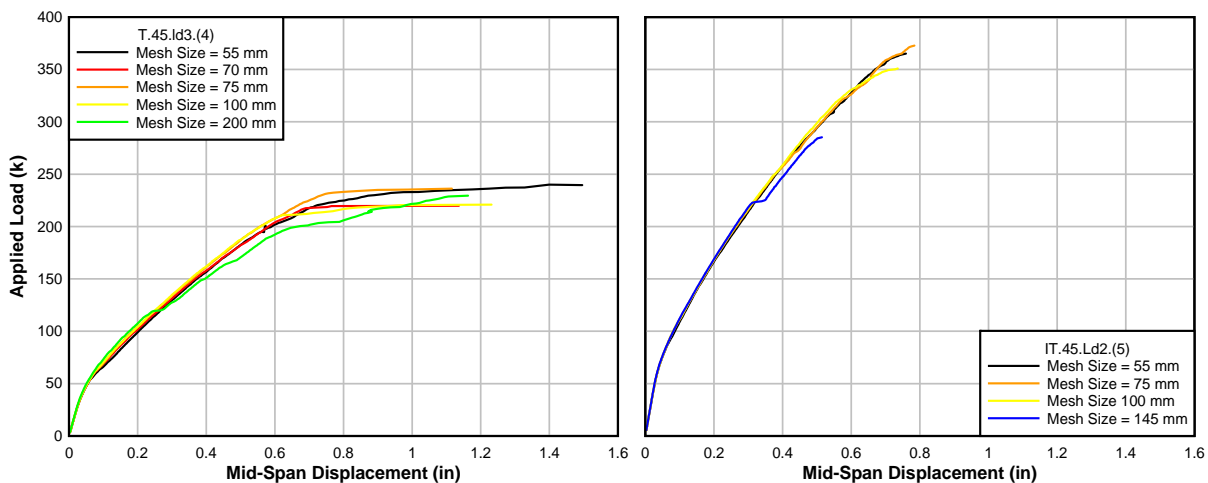
Figure 5.23: Predicted load-deformation response for different finite element mesh sizes (specimen T.45.Ld3.(4))
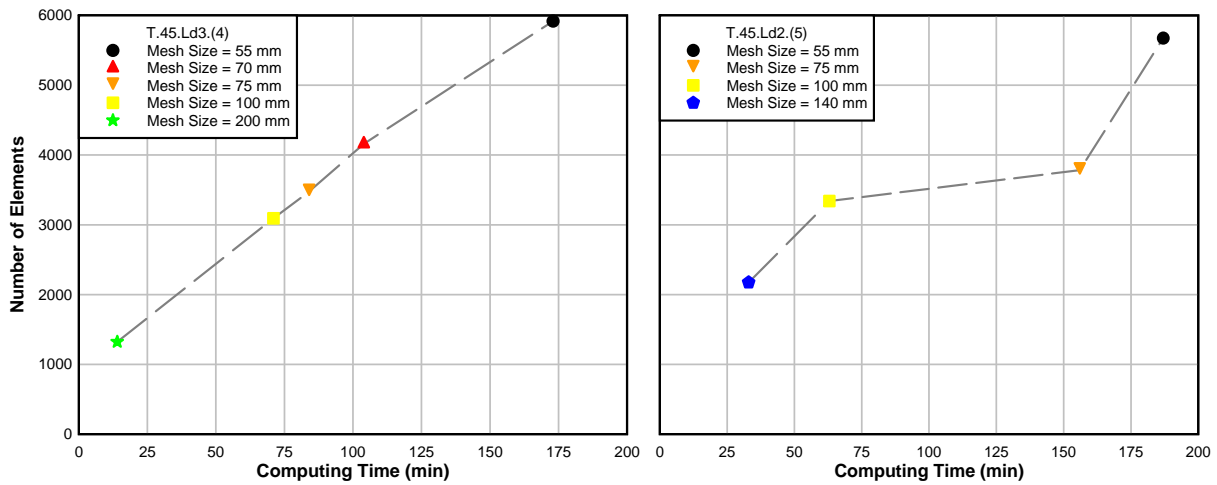
Figure 5.24: Computing time for different mesh sizes (specimen T.45.Ld3.(4))

All analyses were force controlled. It was observed that different load-step sizes affected the behavior near failure. Five load-step sizes were investigated: 2.2 kN (0.5 kip), 3.3 kN (0.75 kip), 4.5 kN (1 kip), 22.5 kN (5 kips), and 45 kN (10 kips). For the T-beam investigation, using the two largest load-steps and the two smallest load-steps, the ultimate load appeared to converge. The 4.5 kN (1 kip) trial predicted the lowest ultimate capacity. The 2.2 kN (0.5 kip) and 3.3 kN (0.75 kip) load-step converged more closely to the experimental capacity as shown in Fig. 5.25. Therefore, a load step size step of 2.2 kN (0.75 kip) was used for the remainder of the analyses. For the IT-beam study, the load appeared to converge between the three smallest load step sizes. For consistency, a load step size of 2.2 kN (0.75 kips) was also used for the remaining analyses.
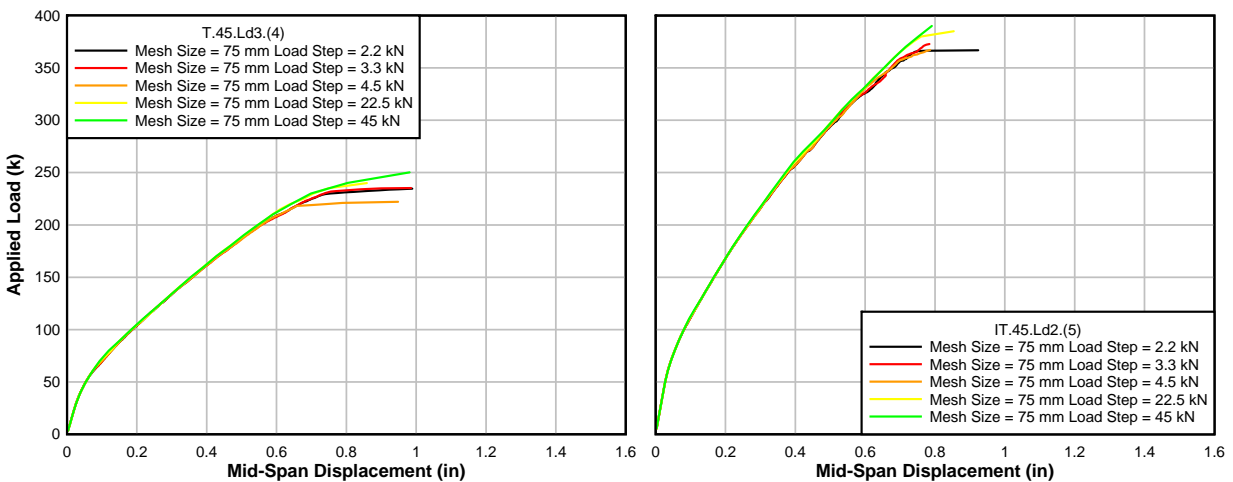
Figure 5.25: Predict load-deformation response for different load step sizes

76

5.4.3 Nonlinear Finite Element Analysis Results

After selecting the confinement pressure coefficient, the mesh size, and the load step size, further force controlled analyses were conducted using combinations of monotonic and cyclic load increments, bonded and unbonded elements, and modeled and unmodeled preformed cracks. Table 5.17 reports the parameters used in each analysis. The ultimate shear strengths predicted by VecTor2 are shown in Fig. 5.26. Analysis Series 4 with a cyclic load was not conducted for the IT-beam specimens.

Table 5.17: Finite Element Analysis Series

Beam Type	Series No.	Loading	Bonded Elements	Preformed Crack
T-Beam	1	Monotonic	Yes	Yes
	2	Monotonic	No	Yes
	3	Monotonic	Yes	No
	4	Cyclic	Yes	Yes
IT-Beam	1	Monotonic	Yes	Yes
	2	Monotonic	No	Yes
	3	Monotonic	Yes	No
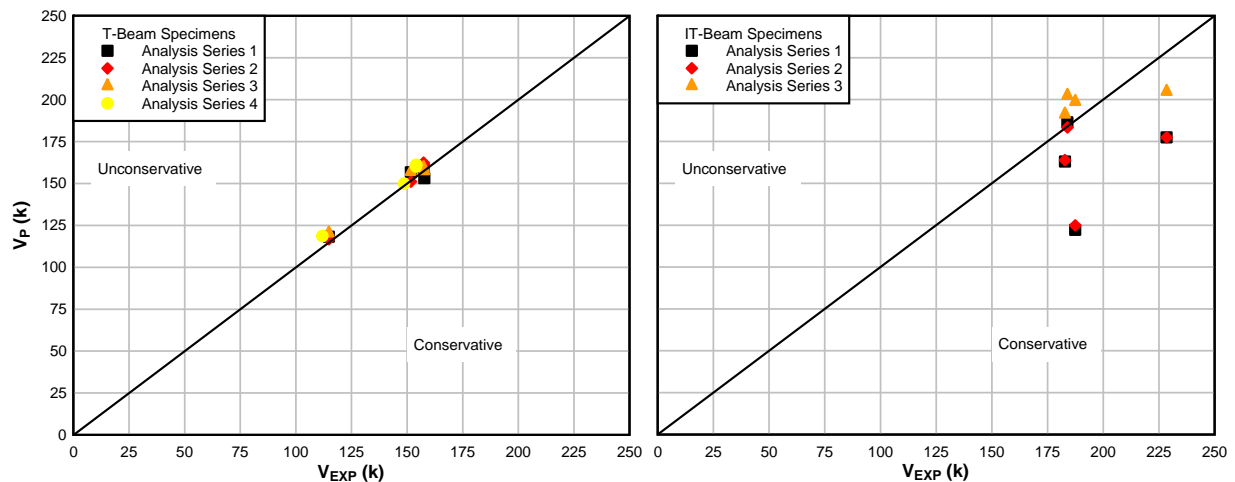
Figure 5.26: VecTor2 NLFEA ultimate shear strength prediction results

For the T-beam specimens, VecTor2 slightly over-predicted the ultimate shear strength and produced small standard deviations and coefficients of variation within the bias values. The analysis series rank orders based on standard deviation are shown in Fig. 5.27. In terms of ultimate capacity, each series had a similar bias and coefficient of variation values. Analysis Series 2 most accurately matched the experimental results with a predicted bias of 0.98 and a coefficient of variation of 1.47. The prediction biases, standard deviations, and the coefficients of variation for each analysis series are reported in Table 5.18.
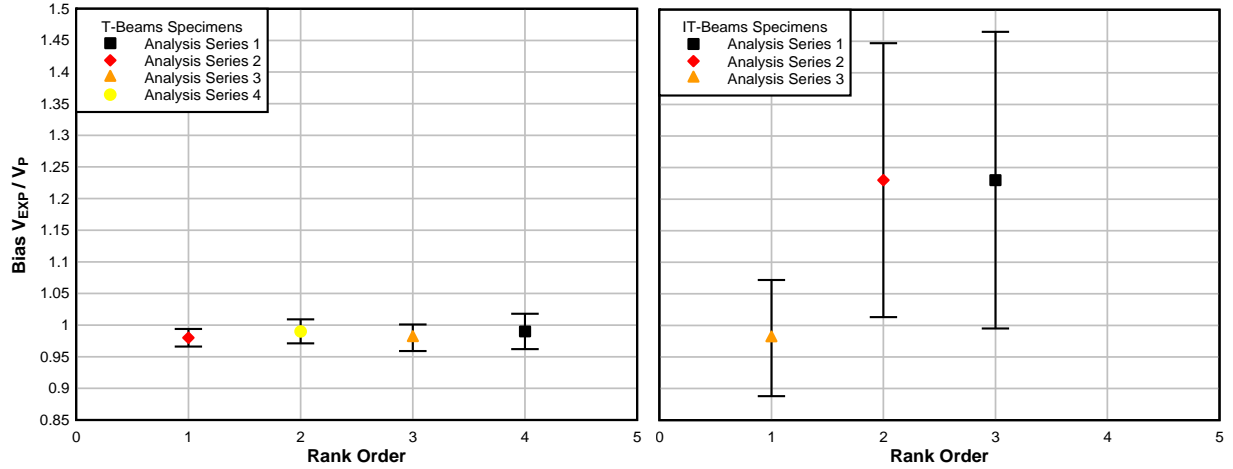
Figure 5.27: VecTor2 NLFEA ultimate shear strength prediction results

Table 5.18: VecTor2 Finite Element Analysis Prediction Results For T-Beam Specimens

Analysis Series	Specimen	V_{EXP} (kN) [kips]	V_P (kN) [kips]	Bias V_{EXP}/V_p	Mean Bias	STD Bias	COV [%]
VecTor2 NLFEA #1	T.45.Ld3.(4)	510.6 [114.8]	525.8 [118.2]	0.97	0.99	0.028	2.85
	T.45.Ld3.(5)	674.9 [151.7]	697.0 [156.7]	0.97			
	T.60.Ld3.(5)	701.6 [157.7]	681.4 [153.2]	1.03			
	T.0.Ld3.(5)	700.1 [157.4]	709.0 [159.4]	0.99			
VecTor2 NLFEA #2	T.45.Ld3.(4)	510.6 [114.8]	519.1 [116.7]	0.98	0.98	0.014	1.47
	T.45.Ld3.(5)	674.9 [151.7]	672.1 [151.1]	1.00			
	T.60.Ld3.(5)	701.6 [157.7]	715.2 [160.8]	0.98			
	T.0.Ld3.(5)	700.1 [157.4]	722.4 [162.4]	0.97			
VecTor2 NLFEA #3	T.45.Ld3.(4)	510.6 [114.8]	535.5 [120.4]	0.95	0.98	0.021	2.20
	T.45.Ld3.(5)	674.9 [151.7]	698.8 [157.1]	0.97			
	T.60.Ld3.(5)	701.6 [157.7]	700.6 [157.5]	1.00			
	T.0.Ld3.(5)	700.1 [157.4]	709.0 [159.4]	0.99			
VecTor2 NLFEA #4	T.45.Ld3.(4)	510.6 [114.8]	528.0 [118.7]	0.97	0.99	0.019	1.96
	T.45.Ld3.(5)	674.9 [151.7]	666.8 [149.9]	1.01			
	T.60.Ld3.(5)	701.6 [157.7]	712.1 [160.1]	0.99			
	T.0.Ld3.(5)	700.1 [157.4]	717.0 [161.2]	0.98			

For two of the three IT-beam analyses, VecTor2 significantly under-predicted the ultimate shear strength. All three analyses showed large standard deviations and coefficients of variation within the bias values. The analysis series rank order results according to standard deviation are shown in Fig. 5.27. In terms of ultimate capacity, the analysis with preformed cracks (Analysis Series 1 and 2) each had a similar bias (1.23) and coefficient of variation values (average 18.4). Analysis Series 3 most accurately matched the experimental results with a predicted bias of 0.98 and a coefficient of variation of 9.38. The prediction biases, standard deviations, and the coefficients of variation for each analysis series are reported in Table 5.19.

Table 5.19: VecTor2 Finite Element Analysis Prediction Results For IT-Beam Specimens

Analysis Series	Specimen	V_{EXP} (kN) [kips]	V_P (kN) [kips]	Bias V_{EXP}/V_p	Mean Bias	STD Bias	COV [%]
VecTor2 NLFEA #1	IT.45.Ld2	1015.9 [228.4]	789.2 [177.4]	1.29	1.23	0.235	19.1
	IT.60.Ld2	813.1 [182.8]	725.2 [163.0]	1.12			
	IT.45.Ld(5)	818.0 [183.9]	829.2 [186.4]	0.99			
	IT.60.Ld2(5+19)	833.6 [187.4]	543.7 [122.2]	1.53			
VecTor2 NLFEA #2	IT.45.Ld2	1015.9 [228.4]	789.1 [177.4]	1.29	1.23	0.217	17.7
	IT.60.Ld2	813.1 [182.8]	728.8 [163.8]	1.12			
	IT.45.Ld(5)	818.0 [183.9]	815.5 [183.3]	1.00			
	IT.60.Ld2(5+19)	833.6 [187.4]	555.5 [124.9]	1.50			
VecTor2 NLFEA #3	IT.45.Ld2	1015.9 [228.4]	911.0 [204.8]	1.12	0.98	0.092	9.38
	IT.60.Ld2	813.1 [182.8]	850.7 [191.3]	0.96			
	IT.45.Ld(5)	818.0 [183.9]	900.5 [202.5]	0.91			
	IT.60.Ld2(5+19)	833.6 [187.4]	884.2 [198.8]	0.94			

5.4.3.1 Load Deflection Response

For the T-beam specimens, the load-displacement curves from experimental results and Analysis Series 1 modeling are compared in Fig. 5.28. For specimen T.0.Ld3.(5), without a preformed crack, VecTor2 predicted the stiffness well at low service levels (below 155 kN (35 kips)). For the specimens with preformed cracks, VecTor2 predicted a gradual softening response compared to the observed stiffening response. This was due to the presence of the diagonal crack not being captured as well in the predicted behavior.
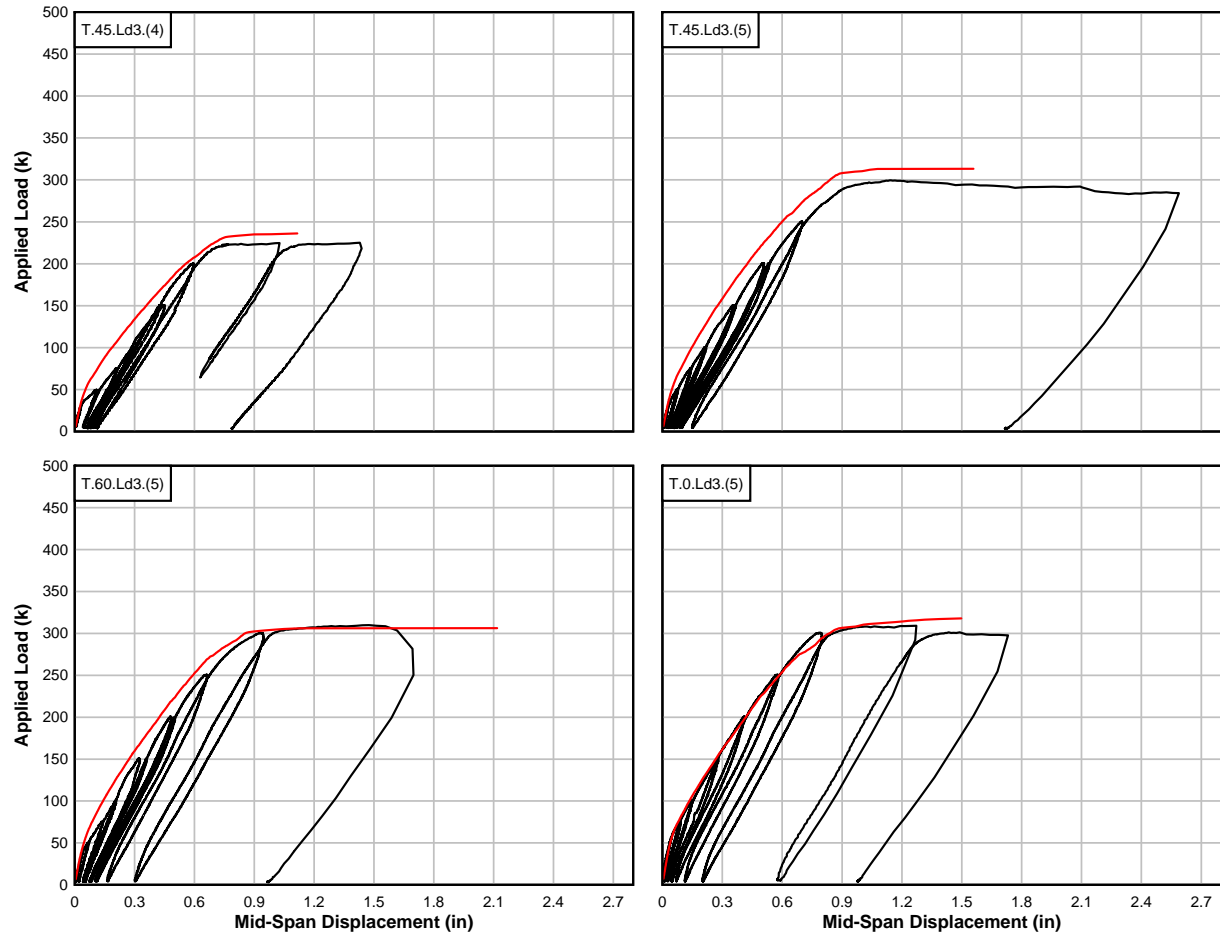
Figure 5.28: Predicted and experimental load-deformation of T-beam specimens, monotonic analysis

For the IT-beam specimens, the load-displacement curves from experimental results and Analysis Series 1 and 3 (with and without a preformed crack) modeling are compared in Fig. 5.29. For both VecTor2 analysis types, the displacement curves were similar at low service levels. For all the specimens except IT.60.Ld2.(5+19), VecTor2 predicted a gradual softening response compared to the observed stiffening response. VecTor2 predicted a much stiffer response than the actual behavior for specimen IT.60.Ld2.(5+19) at all load levels.
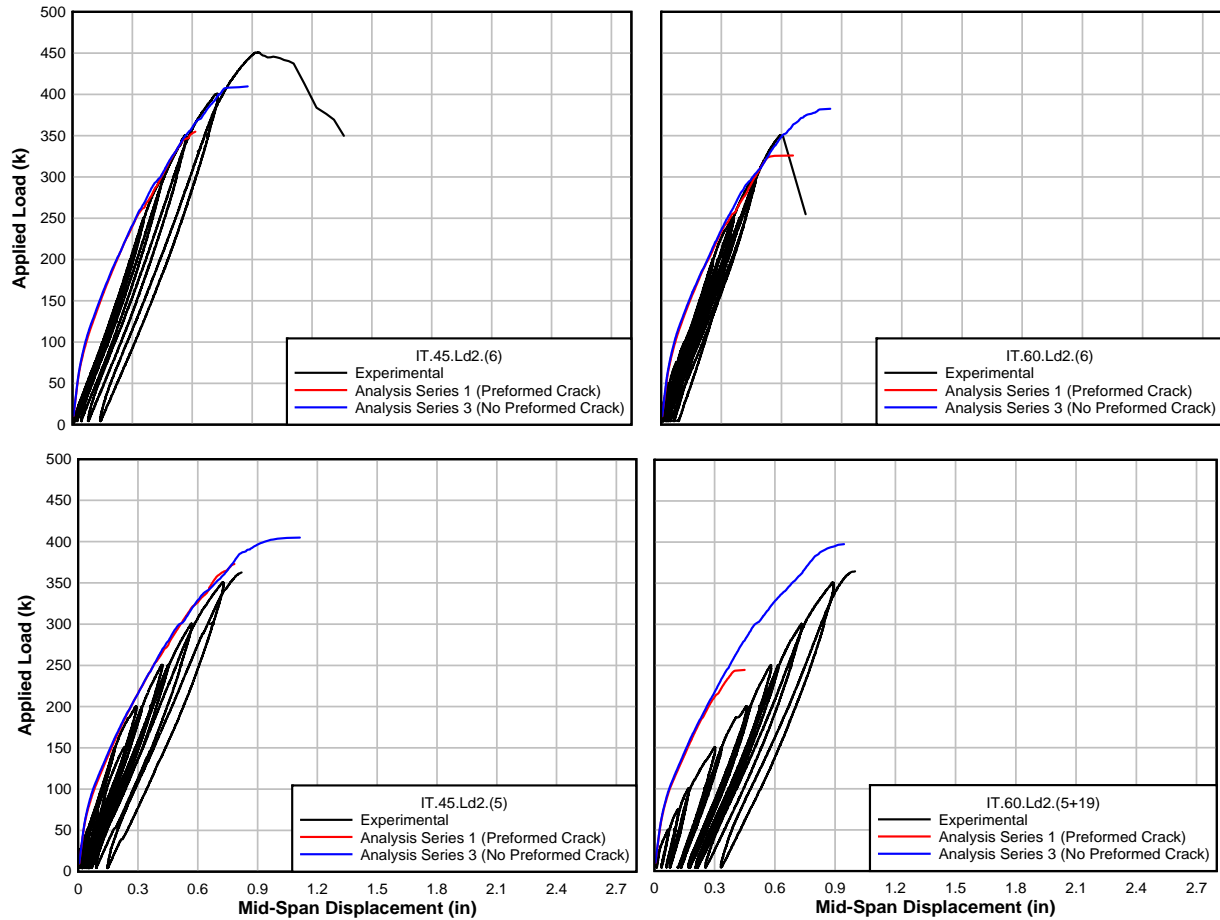
Figure 5.29: Predicted and experimental load-deformation of IT-beam specimens, monotonic analysis

To investigate the cyclic loading protocol used during the experimental testing, a cyclic finite element analysis was conducted for the T-beam specimens only. The loads were increased by 222 kN (50 kips) after each loading–unloading cycle. Except for specimen T.45.Ld3.(5), the load step size was 3.33 kN (0.75 kips). The results of specimen T.45.Ld3.(5) would not load into the Augustus postprocessor using a cyclic load step of 3.33 kN (0.75 kip), so the load step was increased to 4.45 kN (1 kip). Generally, cyclic loading did not significantly affect the predicted capacity or behavior of the load–displacement curves shown in Figs. 5.30 because the loading was not reversed. Therefore, the cyclic analysis was not conducted for the IT-beam specimens. While loading to 1334 kN (300 kips), the finite element analysis for specimen T.45.Ld3.(4) terminated at 1056 kN (237.5 kips). The failure load was reported as 1056 kN (237.5 kips), not the peak load of 1112 kN (250 kips).
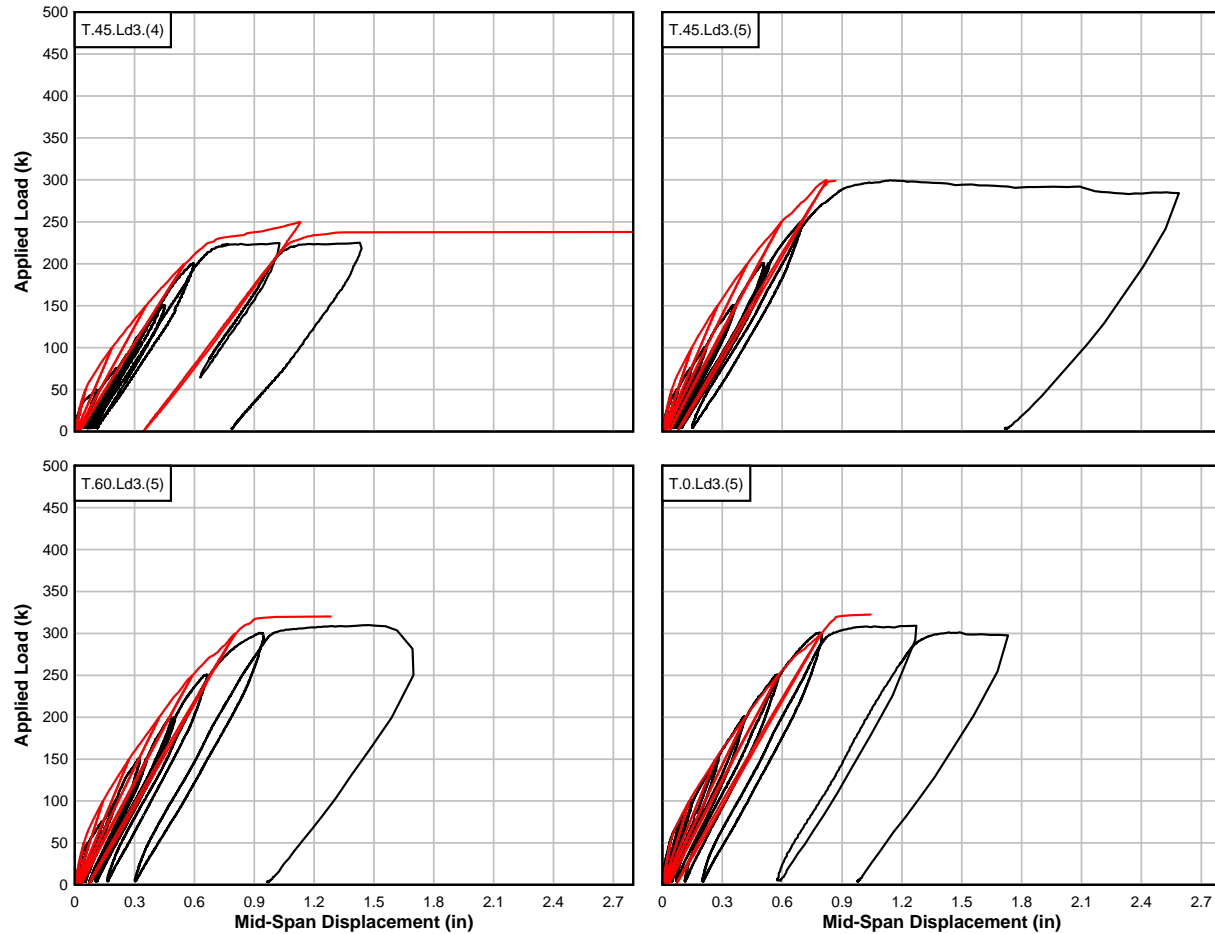
Figure 5.30: Predicted and experimental load-deformation of T-beam specimens, cyclic analysis

For the cyclic analyses, the predicted load capacity bias was 0.96, with a standard deviation of 0.021. The backbone of the cyclic load–displacement curve matched the monotonic load–displacement curve. However, the predicted plastic displacement offsets were underestimated in all cases. Unfortunately, the computation time for the cyclic analyses was as much as 545 minutes compared to the maximum of 176 minutes to complete a monotonic analysis as shown in Fig. 5.31. Generally, it was observed that monotonic finite element analysis was sufficient to predict the T-beam specimen behavior given the similarities in predicted behavior and the length of time required to compute the results.
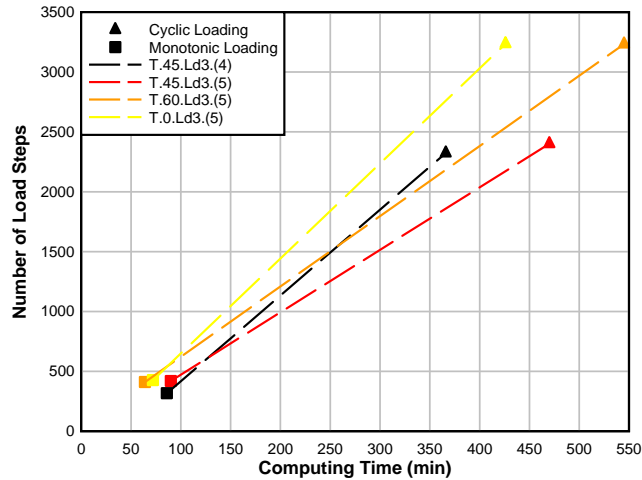
Figure 5.31: Computation time for monotonic and cyclic analyses

For the T-beam specimens, generally, the overall load–displacement results for the analysis series using perfectly bonded elements (Series 2) and not modeling the preformed crack (Series 3) were similar to Analysis Series 1. Therefore, the load–displacements plots were not shown. However, for Analysis Series 2 specimen T.0.Ld3.(5), and Analysis Series 3 specimen T.45.Ld3.(4), VecTor2 predicted a stiffer load-displacement response than in analysis series 1.

For the IT-beam specimen, the overall load–displacement results for the Analysis Series 2 using perfectly bonded elements were similar to Analysis Series 1. Not modeling the preformed crack (Series 3) did not significantly alter the load–displacement plots, but the ultimate capacities were greater than the monotonic analysis considering bond effects as shown in Fig. 5.29. Given the general similarities, the load–displacements for Analysis Series 2 were not shown.

5.4.3.2 Crack Patterns

The experimental and VecTor2 predicted crack patterns for T-beam Analysis Series 1 correlated well as shown in Fig. 5.32. Both the location and height of vertical cracks near mid-span and the locations of the characteristic diagonal cracks were reasonably predicted. When the T-beam specimens were modeled without preformed cracks, the predicted crack patterns were similar to those of Analysis Series 1. However, when all of the reinforcement was assumed to be perfectly bonded, the characteristic diagonal crack appeared at the end of the cutoff with no major diagonal cracks occurring between mid-span and the end of the cutoff. VecTor2 also reasonably captured the characteristic anchorage cracking that occurred along the cutoff bars as explained in Section 4.1.3 *Anchorage Slip Response of Specimens*.
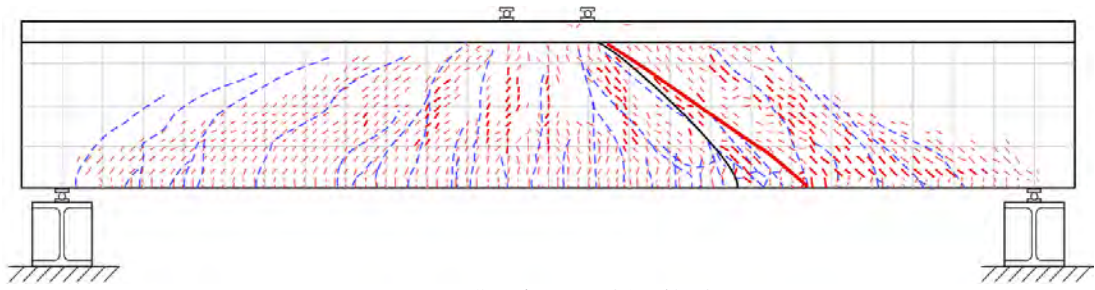
a) Specimen T.45.Ld3.(4)
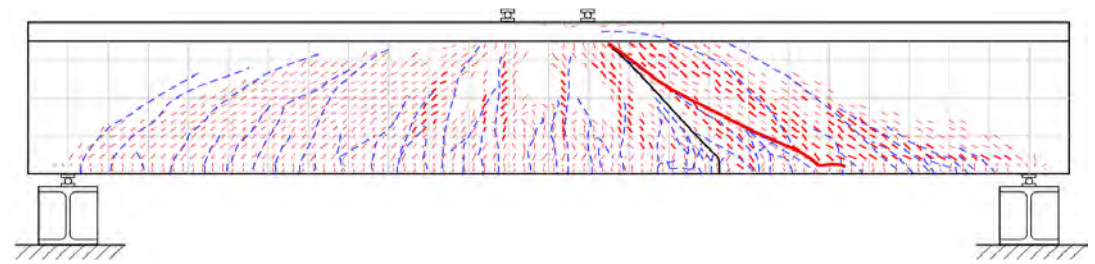
b) Specimen T.45.Ld3.(5)
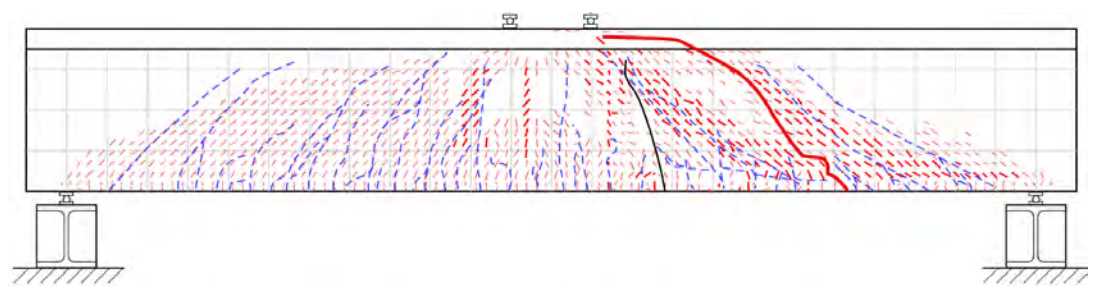
c) Specimen T.60.Ld3.(5)
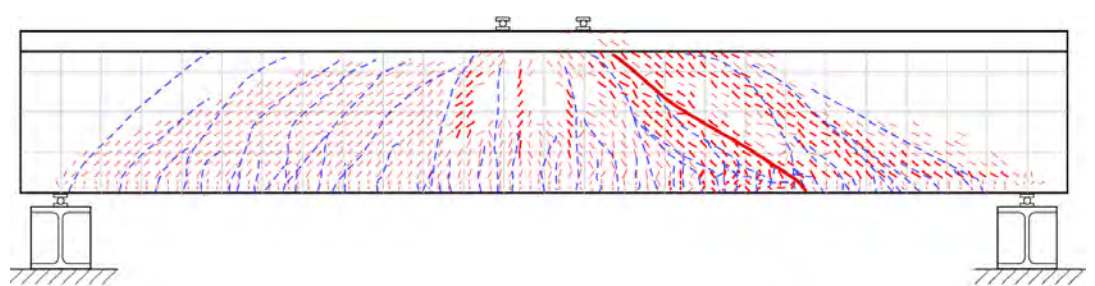
d) Specimen T.0.Ld3.(5)

Experimental Cracks
Predicted Cracks
Experimental Failure Crack
Preformed Crack

Figure 5.32: Experimental and VecTor2 predicted crack patterns for T-Beams

84

The experimental and VecTor2 predicted crack patterns for IT-beam Analysis Series 1 are shown in Fig. 5.33. Generally, VecTor2 poorly predicted the diagonal cracking patterns. In all four cases, the predicted failure crack was not the preformed crack. As reported in Table 5.19, the predicted capacity of specimen IT.60.Ld2.(5+19) was significantly lower than the experimental capacity; therefore, the predicted crack pattern did not develop the cracks that were seen during load testing. The predicted cracking patterns when perfect bond of the cutoff bars assumed in the VecTor2 model (Analysis Series 2) was similarly to the crack patterns shown in Fig. 5.33. When the specimens were modeled without preformed cracks, the predicted crack patterns showed more diagonal cracking than predicted by Analysis Series 1. VecTor2 did not capture the characteristic anchorage cracking that occurred along the cutoff bars as explained in Section 4.1.3 *Anchorage Slip Response of Specimens*.
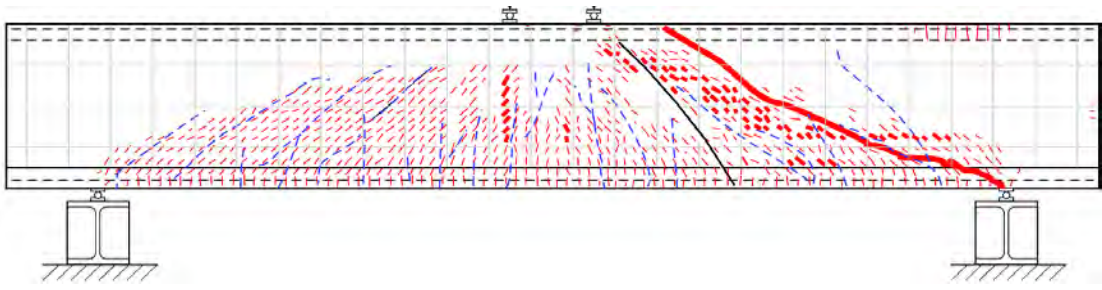
a) Specimen T.45.Ld2
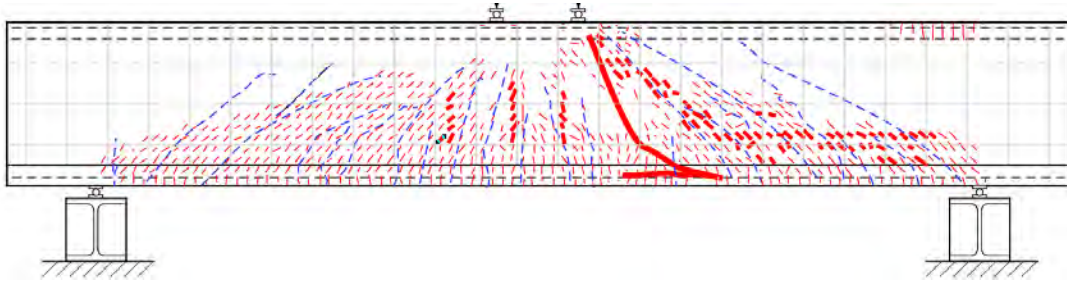
b) Specimen T.60.Ld2
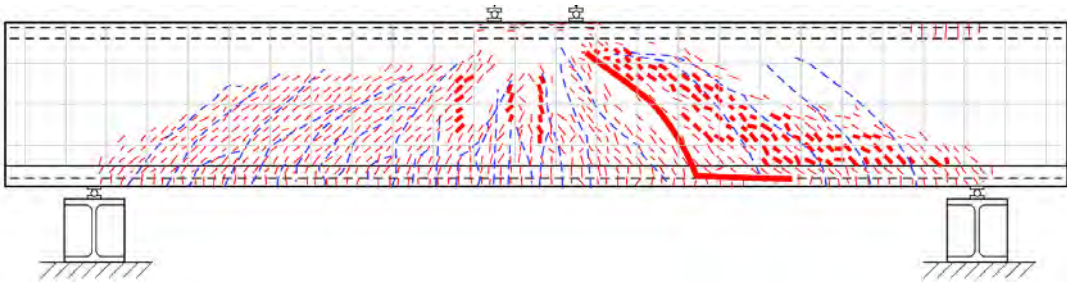
c) Specimen T.45.Ld2.(5)
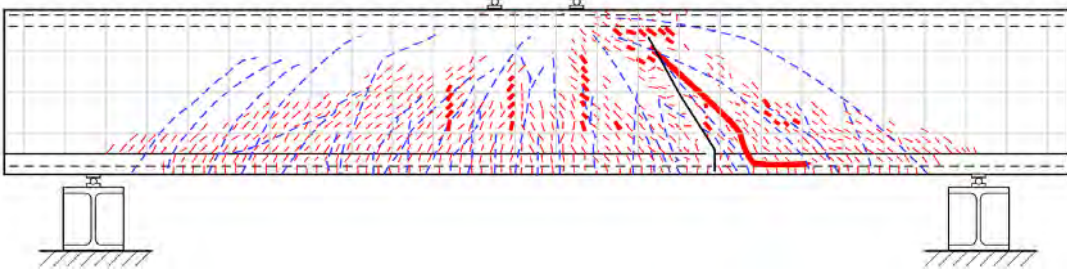
d) Specimen T.60.Ld2.(5+19)

— Experimental Cracks
— Predicted Cracks
— **Experimental Failure Crack**
— **Preformed Crack**

Figure 5.33: Experimental and VecTor2 predicted crack pattern for IT-Beams

5.4.3.3 Steel Reinforcement Stress Distribution Converted to Bond Stress

For T-beam Analysis Series 1 and 2, the predicted average bond stress, μ_{avg}, for the cutoff bars for each specimen was determined using the method described in Section 5.4.1 *Nonlinear Finite Element Analysis Using VecTor2*. In Table 5.20, the average predicted bond stresses are compared to the average experimental bond stress of 5.87 MPa (0.851 ksi) reported in Table 4.3. The peak average bond stress occurred prior to failure. Based on the observed variability, the FEM analyses using the Eligehausen bond stress model predicted a bond stress value closer to the experimental value. The steel reinforcement stress distributions are shown in Figs. 5.34 to 5.37 and were used to determine the bond stress for analysis series 1.

Table 5.20: Comparison of Experimental and VecTor2 Predicted Cutoff Bar Bond Stress for T-Beam Specimens

Analysis Series	Specimen	μ_P (MPa) [ksi]	Bias μ_{EXP}/μ_P	Mean	STD	COV (%)
1	T.45.Ld3.(4)	4.71 [0.683]	1.25	1.16	0.149	12.9
	T.45.Ld3.(5)	5.02 [0.728]	1.17			
	T.60.Ld3.(5)	6.18 [0.897]	0.95			
	T.0.Ld3.(5)	4.58 [0.664]	1.28			
2	T.45.Ld3.(4)	9.45 [1.37]	0.62	0.62	0.076	12.2
	T.45.Ld3.(5)	8.27 [1.20]	0.71			
	T.60.Ld3.(5)	11.2 [1.62]	0.52			
	T.0.Ld3.(5)	9.31 [1.35]	0.63			

Figure 5.34: Specimen T.45.Ld3.(4) predicted steel reinforcement stresses at 182 kips
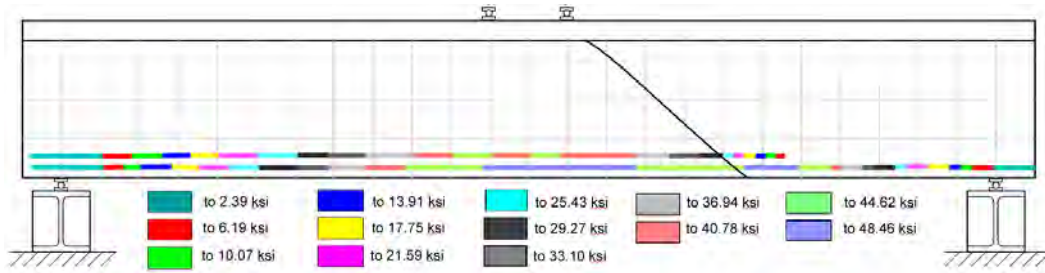
Figure 5.35: Specimen T.45.Ld3.(5) predicted steel reinforcement stresses at 234 kips
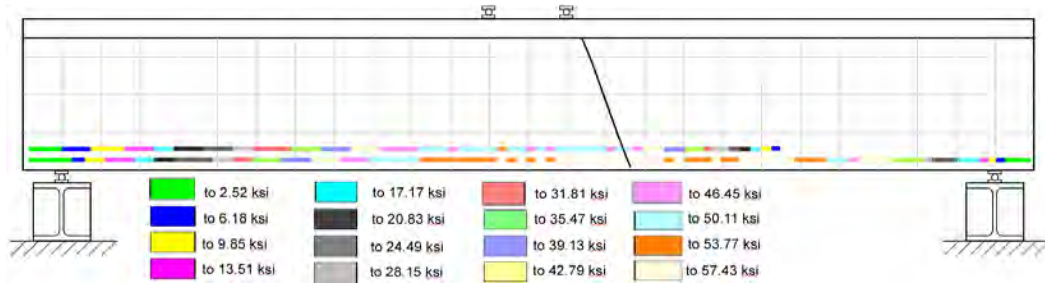
Figure 5.36: Specimen T.60.Ld3.(5) predicted steel reinforcement stresses at 274 kips
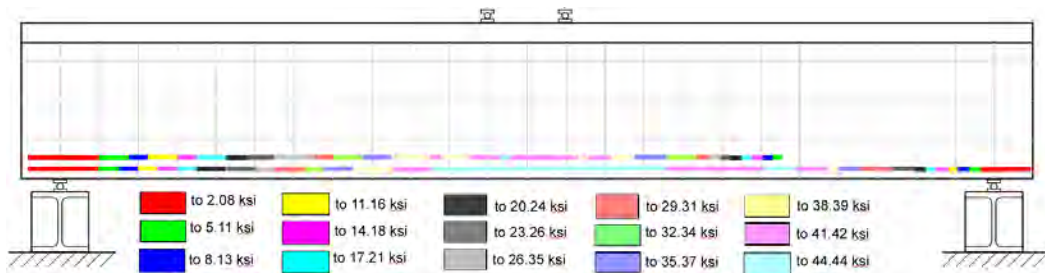
Figure 5.37: SpecimenT.0.Ld3.(5) predicted steel reinforcement stresses at 228 kips

For all the IT-beam analysis series the predicted average bond strength, μ_{avg}, for the cutoff bars for each specimen was determined using the method described in Section 5.4.1 *Nonlinear Finite Element Analysis Using VecTor2*. In Table 5.21, the average predicted bond strengths are compared to the average experimental bond strengths of each specimen as reported in Table 4.4. The peak average bond stress occurred prior at failure. For Analysis Series 1, VecTor2 closely predicted the bond stress of the two specimens with five flexural bars that failed in anchorage, but over estimated the bond strength of the other two specimens. As expected, when perfect bond was assumed (Series 2), all of the predicted bond strengths were greater than measured. When the preformed crack was not modeled, the predicted bond strengths were about half the experimental values. It was likely that the presence of a diagonal crack at a cutoff location increased the bond stresses along the embedment length of a cutoff bar. The steel reinforcement stress distributions for Analysis Series 1 at failure are shown in Figs. 5.38 to 5.41.

Table 5.21: Comparison of Experimental and VecTor2 Predicted Cutoff Bar Bond Stress

Analysis Series	Specimen	μ_{EXP} (MPa) [ksi]	μ_P (MPa) [ksi]	Bias μ_{EXP}/μ_P	Mean	STD	COV (%)
1	IT.45.Ld2	2.79 [0.405]	3.59 [0.521]	0.78	0.91	0.137	15.1
	IT.60.Ld3	3.16 [0.459]	3.94 [0.572]	0.80			
	IT.45.Ld2.(5)	4.47 [0.648]	4.36 [0.633]	1.02			
	IT.60.Ld2.(5+19)	4.43 [0.634]	4.25 [0.633]	1.03			
2	IT.45.Ld2	2.79 [0.405]	7.18 [1.041]	0.39	0.55	0.196	35.7
	IT.60.Ld3	3.16 [0.459]	7.98 [1.158]	0.40			
	IT.45.Ld2.(5)	4.47 [0.648]	7.33 [1.063]	0.61			
	IT.60.Ld2.(5+19)	4.43 [0.634]	5.47 [0.793]	0.80			
3	IT.45.Ld2	2.79 [0.405]	2.10 [0.305]	1.33	1.54	0.211	12.7
	IT.60.Ld3	3.16 [0.459]	2.25 [0.326]	1.41			
	IT.45.Ld2.(5)	4.47 [0.648]	2.50 [0.362]	1.79			
	IT.60.Ld2.(5+19)	4.43 [0.634]	2.68 [0.389]	1.63			
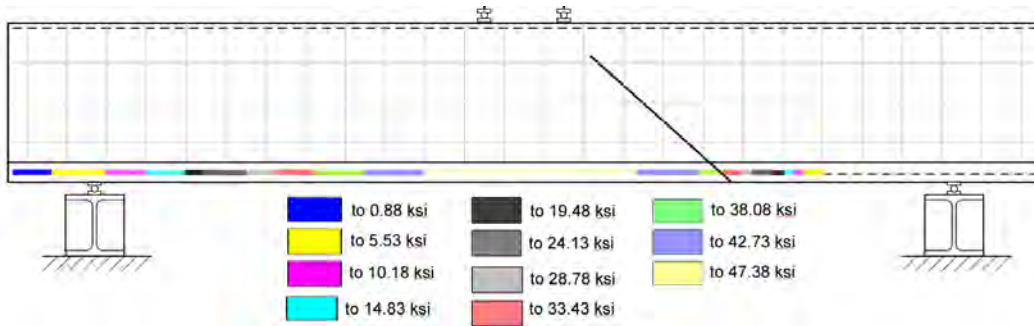
Figure 5.38: Specimen IT.45.Ld2.(6) predicted steel reinforcement stresses at failure
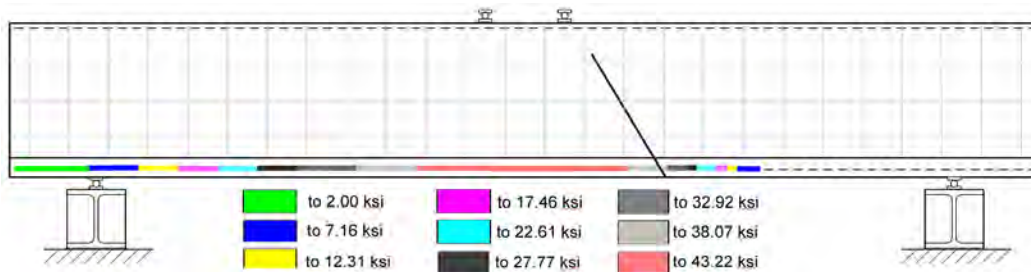
Figure 5.39: Specimen IT.60.Ld2.(6) predicted steel reinforcement stresses at failure

89
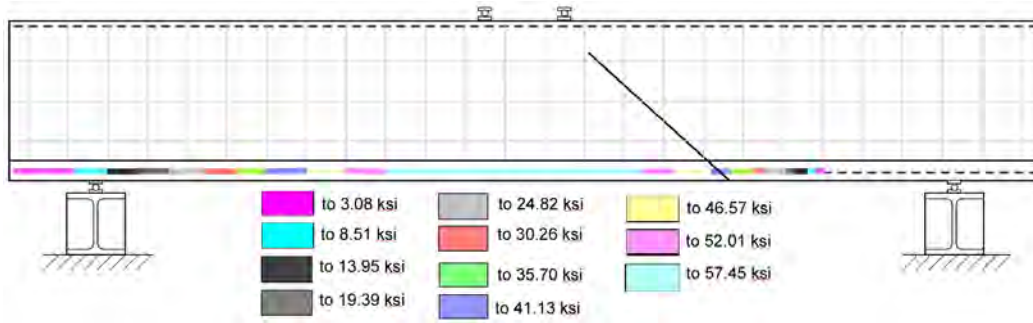
Figure 5.40: Specimen IT.45.Ld2.(5) predicted steel reinforcement stresses at failure
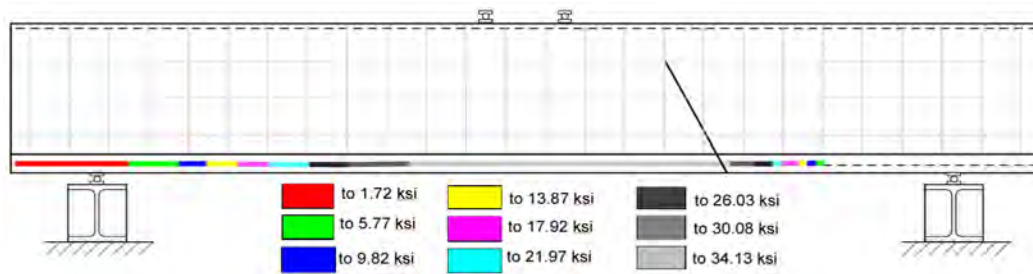
Figure 5.41: Specimen T.60.Ld2.(5+19) predicted steel reinforcement stresses at failure

5.4.4 Bounding T-Beam Specimen Finite Element Analysis

To investigate how much effect developing cutoff bars had on capacity, two analyses were conducted to bound the T-beam analysis. Using the material properties of specimen T.45.Ld3.(5), a model was developed for a beam with only three flexural bars with no cutoffs in the bottom layer of steel to show that developing bars increased ultimate capacity and limited deformations. Similarly, a second model with three flexural bars in the bottom layer of steel and two full-length bars in the top layer of bottom steel was used to show that well anchored bars increase ultimate capacity compared to the actual experimental case. For both models, all reinforcement was assumed to be perfectly bonded and the preformed crack was modeled.

The load–displacement response of the two new models and the initial VecTor2 model for the T-beam Analysis Series 1 are shown in Fig. 5.42. As expected, the predicted response of the initial VecTor2 model with the actual cutoff bar geometry fell between the bounds. The model with three flexural reinforcing bars exhibited flexural cracking with few diagonal cracks and failed in flexure. In contrast, the model with five fully anchored bars had few flexural cracks with a diagonal shear crack being the source of failure. At low service levels, the load–displacement response from the three-bar model closely matched the experimental results.

90
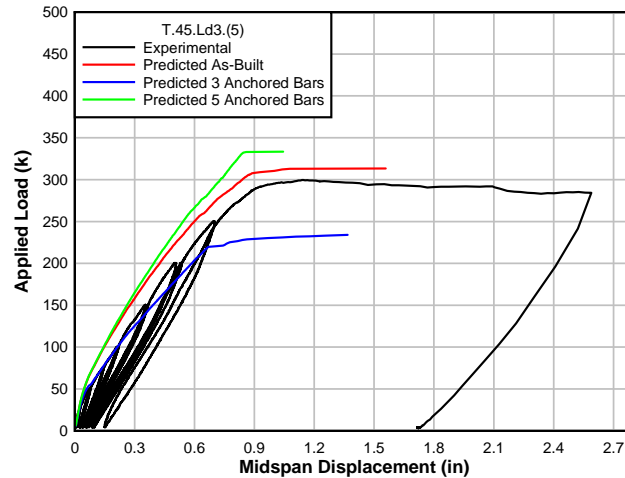
Figure 5.42 Predicted bounds of T-beam specimen with more and less flexural reinforcement than as-built

5.4.5 VecTor2 Nonlinear Finite Element Analysis Conclusions

Based on the results and comparisons between the different series of nonlinear finite element analyses using VecTor2 and experimental results, the following conclusions are presented:

For T-beams:

- Nonlinear finite element analyses provided good correlation with experimental results for overall member load–displacement response and average bond strength values. For a model with discrete reinforcement, a preformed crack, and bond elements loaded monotonically, a mean predicted bias of 0.99 with a coefficient of variation of 2.85% was obtained.

- The predicted crack patterns from the nonlinear finite element analyses agreed well with experimental observations. However, the failure diagonal cracks were not necessarily coincident.

- Generally, conducting a cyclic load analysis to take into account the hysteretic response of concrete, reinforcing steel, and bond did not significantly improve the analysis results, but significantly increased computation time.

- The use of contact elements and the Eligehausen bond-slip model reasonably predicted the experimental average bond strength. Assuming a perfect bond between the concrete and reinforcement resulted in unrealistically high bond strength values and ultimate capacities. As in the experiments, peak average bond stress was not coincident with failure.

- Additional analysis showed that developing bars contributed to the capacity of structure. When the contribution of the cutoff bars was not considered, the specimens tended to fail in flexure.

91

For IT-beams:

- Nonlinear finite element analyses provided a reasonable correlation with experimental results for initial member load–displacement response and average bond strength values, but not for ultimate capacity predictions. For a model with discrete reinforcement, preformed crack, and bond elements loaded monotonically, a mean predicted bias of 1.23 with a coefficient of variation of 19.1% was obtained.

- The predicted crack patterns from the nonlinear finite element analyses correlated poorly with experimental observations. VecTor2 predicted shear-compression failures at the preformed crack locations.

- The use of contact elements and the Eligehausen bond-slip model reasonably predicted the experimental average bond strength. Assuming the bond between the concrete and reinforcement to be perfect resulted in unrealistically high bond strength values, but had little effect on the ultimate capacities. The peak average bond stress was coincident with the failure load achieve in testing.

- When the preformed crack was not modeled, the predicted bond strengths were about half the experimental values. The presence of a diagonal crack at a cutoff location increased bond stresses along the embedment length of a cutoff bar.

6.0   CONCLUSIONS

The objectives of this research were to provide bridge inspectors and rating engineers with tools to evaluate vintage reinforced concrete deck girder bridges containing diagonal cracks interacting with flexural reinforcing steel bar cutoffs. To meet these objectives, eight large size specimens were designed, constructed, and tested to failure. Four of the specimens were T-beams and four of the specimens were IT-beams. Load application was cyclic without reversal applied in near-three-point loading over the specimen centerline.

Three T-beam specimens were constructed using a plastic sheet to create a preformed diagonal crack, which controlled the initial diagonal crack geometry and eliminated aggregate interlock. Two preformed diagonal cracks were at 45° and one crack was at 60°, common crack angles observed in the field. The fourth specimen did not have a preformed crack, but contained similar reinforcing details to the other specimens. The cutoff bar location began at about one third the minimum development length (as defined by ACI 318-08 specification) away from where the 45° crack crossed the flexural reinforcing bars. A fourth specimen, without a preformed crack, was a control.

Four IT-beam specimens were constructed with a plastic preformed diagonal crack. Two preformed diagonal cracks were at 45° and two cracks were at 60°. Cutoff bars were provided with half the minimum design development length specified by the least conservative of the ACI 318 and AASHTO-LRFD specifications past the preformed crack.

Data were collected to assess the shear and flexural-induced tensile stresses in the reinforcing steel at various locations along the span, to verify specification analysis methods, and to assist in the development of new models for assessing anchorages in the presence of diagonal cracks. Conclusions based on the experimental and analytical results provide the framework for field inspection recommendations and evaluation methodologies, while suggestions for further research are described in the following sections.

6.1   EXPERIMENTAL CONCLUSIONS

The eight specimens showed that the presence of a diagonal crack crossing the development length of cutoff longitudinal bars may not necessarily control specimen failure. While existing diagonal cracking was seen to increase the tensile demand in the longitudinal reinforcement, it did not serve to indicate the eventual failure location. Under service level loads, the preformed diagonal crack produced bond stresses that were higher at the crack location. However, as load increased to failure, the eventual diagonal failure crack often developed in a different section. If the failure crack location was not the same as the initially observed diagonal crack, peak bond stresses shifted to the new crack. The location of the failure crack depended on reinforcement detailing and load patterns, not necessarily the presence of diagonal cracks observed under lower level loads. The type of failure: flexure, shear-compression, or anchorage also depended on more predictable properties such as geometry at possible cutoff locations, the number of flexural bars,

and stirrup spacing, rather than highly variable cracks that developed during service level conditions.

The data showed that the required tensile demand at a diagonal crack location as predicted by AASHTO-LRFD equation 5.8.3.5-1 was reasonable. Accurately estimating the additional demands in flexural bars at crack locations required inputting coincident moment and shear values rather than using maximum attained values for these parameters.

6.2   ANALYTICAL CONCLUSIONS

Prediction of beam capacity and failure mode requires analyzing sections along the length of the specimen, not just those sections that appear to be the weak points such as at diagonal crack locations, at the support, near the loading point, and along the length of developing bars. The shear, flexural, and anchorage capacities must be checked at each section. An anchorage failure will occur when the tensile demands in the flexural reinforcing steel exceeds the force that the reinforcing bar–concrete interface can resist. This can occur at load levels less than the shear and flexural capacities of the section.

To check for anchorage failure, the predicted tensile demand calculated by AASHTO-LRFD 5.8.3.5-1 for all potential failure angles should be compared to the tensile capacity using the maximum allowable bond stress. The present experimental results exhibited average bond strength values at anchorage failure approximately 175% of those predicted using the least conservative of ACI 318 and AASHTO-LRFD development length calculations. For cases where anchorage is identified as problematic using AASHTO-LRFD development lengths, the analyst may want to consider ACI 318 detailed equations, or that proposed by Darwin (1996) as these were more representative and still conservative of the present experimental findings.

Two analysis methods were developed to predict the failure mode and capacity. These used bond strengths from any of the available sources (ACI, AASHTO, Darwin 1996). When investigating the governing failure mechanism for existing structures using Analysis Method 2, there was a slight discrepancy between the least conservative ACI 318 and AASHTO-LRFD design development length predictions and development length predicted using experimentally measured maximum average bond stresses. In many cases, the most conservative specification method accurately predicted the failure mechanism. However, in scenarios where the shear-compression and shear-anchorage failure capacities were closely grouped, specification-based methods incorrectly predicted anchorage failures due to an under-prediction of bond strength in areas with developing reinforcement.

Nonlinear finite element analysis using VecTor2 predicted the ultimate capacities and load–deformation behavior of the T-beam specimens quite well. The presence or absence of a modeled preformed crack did not significantly change which characteristic diagonal crack caused failure. However, the bond-slip relationship of the cutoff affected the bond stress in the reinforcement and the failure diagonal crack. Although VecTor2 predicted the load-deformation behavior of the IT-beam specimens well at low services levels, the ultimate capacities were not as well predicted. The presence or absence of a modeled preformed crack significantly changed the predicted cracking pattern and bond stresses. The IT specimens, due to lack of confinement around the developing flexural bars and resulting nonductile bond behavior due to splitting

94

failure of the deck as well as smaller compression zone, showed higher sensitivity to the presence of diagonal cracks compared to the T specimens.

6.3   RECOMMENDATIONS

The experimental research supports a straightforward process for analyzing beams with cutoff details interacting with diagonal cracking. Existing cracking is not necessarily a definite indicator of the failure location; therefore, each critical section across the length of the specimen must be analyzed to locate the weakest location and controlling angle. AASHTO-LRFD specifications provide methods to calculate critical shear and moment capacities based on interaction at a selected location. Using a more refined approach to calculate the expected development length allows for a more effective prediction of the tensile capacity of the anchorages (such as Darwin 1996 or ACI 318). The critical crack angle can then be derived from the AASHTO-LRFD specifications Chapter 5 after calculating the shear stress in the concrete at the critical location. MCFT can be used in accompaniment with the calculated critical crack angle to derive a necessary applied shear that produces tensile forces in the longitudinal bars sufficient enough to induce anchorage failure. For positive moment steel (T-beams), average bond strength for Gr. 420 (Gr. 60) reinforcement and an f_c' of 24.1 MPa (3500 psi) ranged from 3.86 to 8.27 MPa (0.560-1.200 ksi) with 97.5% lower confidence level reducing this value to 4.01 MPa (0.581 ksi.). Similarly, for negative moment steel (IT-beams), average bond strength for Gr. 420 (Gr. 60) reinforcement and an f_c' of 24.1 MPa (3500 psi) ranged from 4.48-4.83 MPa (0.650-0.700 ksi) with 97.5% lower confidence limit reducing this value to 3.76 MPa (0.546 ksi.). If the applied shear for anchorage failures is less than the controlling shear strength calculated by the shear and moment interaction analysis, anchorage failure at the section can be anticipated. If this is not the case, then the analyzed specimen may be expected to fail in either shear or flexure, depending on the M/V ratio and this interaction relationship at the critical location.

The crack patterns observed in each of the specimens near the cutoff bar location gives field inspectors examples of the kind of distress to look for prior to a possible anchorage failure. Section *4.1.2 Crack Growth in Specimens* more fully describes and provides photos of the particular anchorage cracking typically noted in T-beam and IT-beams. For T-beams, it is recommended that inspectors look for a grouping of vertical and horizontal cracks near the beam soffit at the level of the flexural reinforcing steel and focus on those locations that are near cutoff locations shown in available structural drawings. Similarly, in negative moment regions near supports, inspectors should look for horizontal and chevron cracking on the underside of the deck. These types of distress are indicative of anchorage slip and should be followed up with additional scrutiny.

If anchorage cracking is observed, crack widths and locations should be noted. Further inspections should pay special attention to these areas over time to note changes and evolution of cracks. Plans should be made for strengthening and/or posting the bridge based on limiting anchorage demands. Diagonal cracking associated with the cutoffs should be noted and compared to analytical predictions of critical failure locations using the methods described in this report. Cracking occurring in areas near the predicted critical crack location may be a cause for particular concern. However, not all visible diagonal cracking will be indicative of the

ultimate failure location or angle. A full detailed analytical investigation using provisions in the AASHTO-LRFD specifications combined with the methods described in this report should be undertaken to assess the member and identify probable failure mode and anchorage demand/capacity.

6.4   ADDITIONAL RESEARCH

The primary focus of this research was to investigate anchorage failures and interaction with diagonal cracks in vintage RCDG specimens and to provide analysis methods. As such, several future analytical and experimental projects that might further clarify anchorage behavior are suggested:

Further nonlinear finite element analysis may be conducted using VecTor2. More work may be done to improve accuracy of the bond predictions. Alternate methods of modeling cracks observed in the field may be investigated. Development of a finite element model that reproduces the experimental results of other experimental test programs performed at Oregon State University including FRP repairs could be explored.

Although the experimental program recreated vintage RCDG girders, not every possible parameter could be considered with the number of specimens available in this study. As such, future research projects could investigate the following:

- Performance of a series of specimens using all Gr. 280 (Gr. 40) reinforcing steel. With a lower steel yield strength, a comparison of bond between Gr. 420 (Gr. 60) and Gr. 280 (Gr. 40) reinforcing bars could be performed. As part of the evaluation, square bars and different deformation patterns of round bars could be used in some of the specimens.

- Influence of cutoffs in deep beams (a/d <1), where the disturbed stress fields may produce different bond demands.

- Performance of bond under repeated loading to determine possible deterioration from bond fatigue.

- Effects of scale on the bond stress development and failure modes. A comparison to how bond stress is adjusted in modeled experiments would help define scaling parameters. This could enable use of smaller specimens.

- Influence of varying bar development on maximum average bond stress.

Finally, it is anticipated that some cutoff anchorages may not rate well even with the refinement of analysis methods described in this report. It will be necessary to limit anchorage demands on these members (load post the bridge) or strengthen these members. Strengthening members for anchorage will require experimental and analytical study. As these studies take time, this research should be pursued as soon as possible so that results will be available to the design community prior to the need for field implementation.

7.0   BIBLIOGRAPHY

Abrishami, H., & Mitchell, D. (1996) Analysis of bond stress distributions in pullout specimens. *Journal of Structural Engineering*, 122 (3), 255-261.

American Concrete Institute (1956) Building code requirements for reinforced concrete (ACI 318-56). *ACI Manual of Concrete Practice*, Farmington Hills, Michigan, 927, 949.

American Concrete Institute (2008) 318-08/318R-08: Building Code Requirements for Structural Concrete and Commentary. *ACI Manual of Concrete Practice*, Farmington Hills, Michigan.

AASHO (1953) Standard specifications for highway bridges, 6th Edition, *American Association of State Highway Officials*, Washington, DC, 182, 238.

AASHO (1973) Standard specifications for highway bridges, *American Association of State Highway Officials*, Washington, DC, 57-58,93.

AASHTO (2005) AASHTO LRFD bridge design specifications, 3rd edition with 2005 interims, *American Association of State Highway and Transportation Officials*.

ASTM A305-50T (1950) Minimum requirements for the deformations of deformed steel bars for concrete reinforcement. *ASTM International*, 218-220.

ASTM A615/A615M-09b (2009) Standard specification for deformed and plain carbon-steel bars for concrete reinforcement. *ASTM International*.

ASTM C39/C39M-09a (2009) Standard test method for compressive strength of cylindrical concrete specimens. *ASTM International*

ASTM C617-09a (2009) Standard practice for capping cylindrical concrete specimens. *ASTM International*.

ASTM E8/E8M-09a (2009) Standard test methods for tension testing of metallic materials. *ASTM International*.

Bentz, E., (2000). Response-2000: Reinforced Concrete Sectional Analysis using the Modified Compression Field Theory (Version 1.0.5) [Computer software]. University of Toronto

Clark, A. P. (1949) Bond of concrete reinforcing bars. *Journal of the American Concrete Institute Proceedings*, 21 (3), 161-184.

Darwin, D., Zou, J., Tholen, M., & Idun, E. (1996) Development length criteria: for conventional and high relative rib area reinforcing bars. *ACI Structural Journal*, 93 (3), 1-13.

Doerr, K. (1978) Bond behavior of ribbed reinforcement under transversal pressure. *Nonlinear behavior of reinforced concrete spatial: contributions to IASS symposium* (pp. 13-24) Dusseldorf, Germany: International Association for Shell Structures.

Harajli M. H. (2004) Comparison of bond strength of steel bars in normal- and high-strength concrete. *Journal of Materials in Civil Engineering*, 16 (4), 365-374.

Higgins, C., Miller, T., Rosowsky, D. V., Yim, S.C., Potisuk, T., Daniels, T. K., Nicholas, B.S., Robelo, M. J., et al. (2004) *SPR 350 Assessment Methodology for Diagonally Cracked Reinforced Concrete Deck Girder.* Salem, Oregon: Oregon Department of Transportation.

Jeppsson, J., & Thelandersson, S. (2003) Behavior of reinforced concrete beams with loss of bond at longitudinal reinforcement. *Journal of Structural Engineering*, 129 (10), 1376-1383.

Losberg, A., & Olsson, P. (1979) Bond failure of deformed reinforcing bars based on the longitudinal splitting effect of the bars. *ACI Journal Symposium Paper*, 5-18.

MacGregor, J. G., & Wright, J. K. (2005) *Reinforced concrete mechanics and design.* Upper Saddle River, New Jersey: Pearson Prentice Hall.

Mains, R. M (1951) Measurement of the distribution of tensile and bond stresses along reinforcing bars. *Journal of the American Concrete Institute*, 48 (3) 225-252.

Malvar, J. (1992) Bond of reinforcement under controlled confinement. *ACI Materials Journal*, 89 (6), 593-601.

Microsoft Corporation (2006) Microsoft Office Excel 2007 [Computer software]

Mylrea, T. D. (1948) Bond and anchorage. *Journal of the American Concrete Institute Proceedings*, 44 (3), 521-552.

Reynolds, G. C., & Beeby, A. W. (1982). Bond strength of deformed bars. In P. Bartos (Ed.) *Bond in concrete*, (pp. 434-445). London: Applied Science Publishers.

Senturk, A. E. (2008) *Experimental and analytical evaluation of conventionally reinforced deck-girder bridge bent caps with vintage details*. PhD dissertation, Oregon State University.

APPENDIX A:
EXPERIMENTAL DATA

Appendix A describes the labeling of each instrument used for each specimen, with illustrations. Section 3.4 *Instrumentation* defines the purpose of each instrument. The functionality of each gage at failure is provided. Plots are provided of selected data.

Mid-Span Displacement: Mid-span displacement was measured using two potentiometers attached to each side of the stem at mid-span. The instrument on the west side of the beam was "Mid-Span W" and the instrument on the east side of the beam was "Mid-Span E."

Support Settlement: An LVDT displacement sensor was located at each of the four corners of the specimen to measure the support settlement. The instruments were identified by two letters. The first letter (N or S) noted the north or south end of the beam. The second letter (W or E) noted the west or east side of the specimen.

Cutoff Bar Slippage: A LVDT displacement sensor was located at the end of each cutoff bar. The instrument on the west cutoff bar was "Cutoff Bar Slippage W" and the instrument on the east cutoff bar was "Cutoff Bar Slippage E."

Crack Width Sensors: Displacement sensors were used to track the change in crack width of select cracks on the northwest side of the beam. All four specimens had two instruments straddling the preformed crack and were labeled as "Preformed Crack Top: or "Preformed Crack Bottom." "Top" referred to the narrower portion of the crack near the top of the beam, with "Bottom" noting the wider portion of the crack near the bottom of the beam. Additional, specimens T.60.Ld3.(5) and T.0.Ld3.(5) had two instruments crossing the dominant crack location that developed extending from the loading plate to the end of the cutoff bar. The labeling conversion was similar; except the crack was identified as "Dominant" instead of "Preformed."

Diagonal Displacement Potentiometers: Six potentiometers measured the displacement of the beam over a region. The instrument was anchored to one point on the specimen, and a wire attached to the instrument was strung to a second anchor point. Each instrument was identified by these to number anchor points. For example, the potentiometer connecting points 1 and 4 was label "1-4", as shown in Fig. A.1.
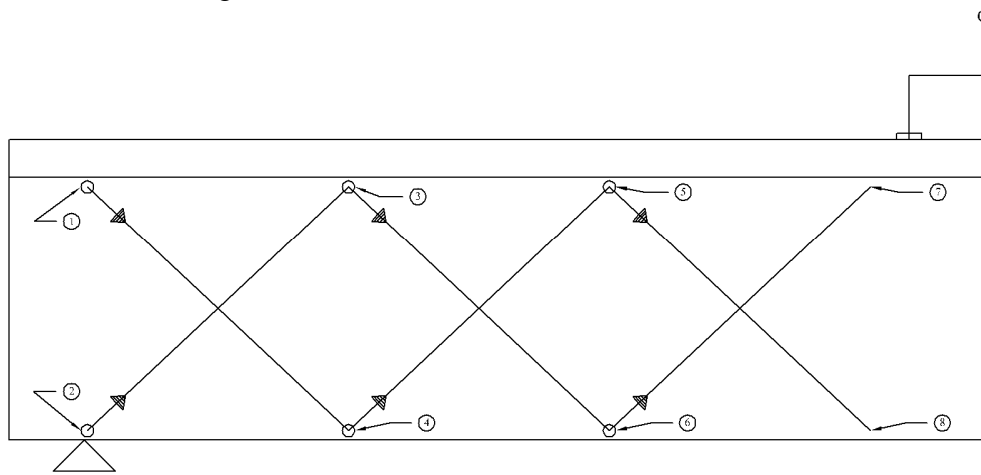
Figure A.1: Typical external displacement sensor array labeling conversion

Flexural Bar Stain Gages: Each flexural bar had five strain gages. Each gage was identified by the words "Flexural Bar" followed by two numbers. The first number signified the location as taken from the end of the cutoff bar, as shown in Fig. A.2. The second number identified the bar as located in cross-section shown in Fig. A.3.
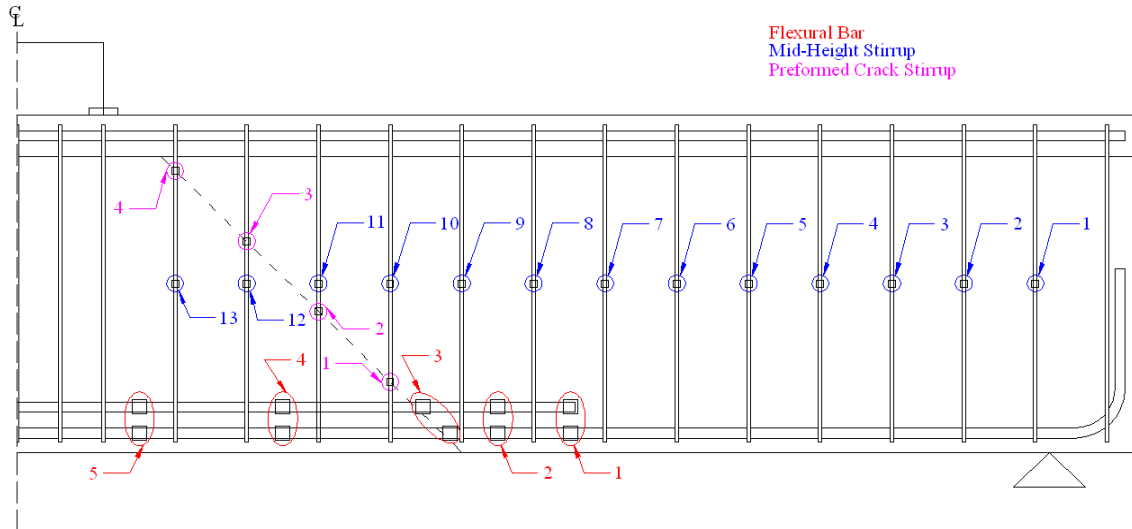
Figure A.2: Typical Specimen strain gage labeling convention
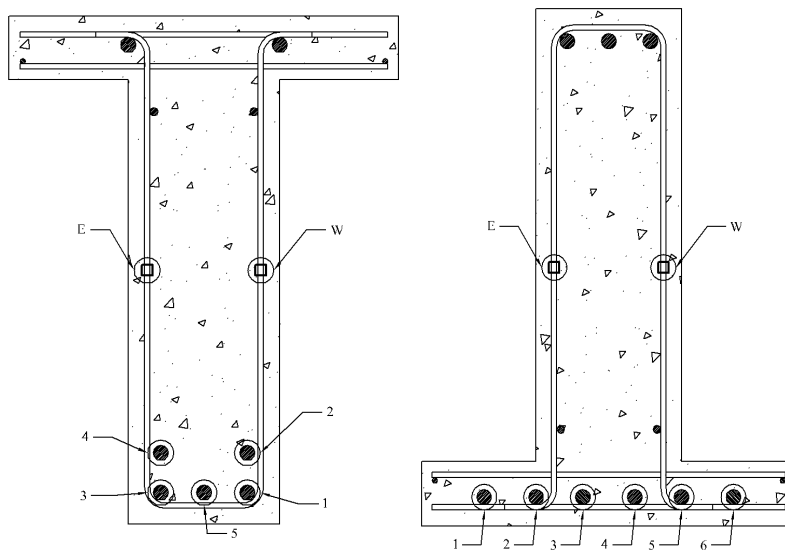
Figure A.3: Typical cross-section of specimens strain gage labeling convention

Mid-Height Stirrup Strain Gages: Strain gages were applied on each stirrup leg at the mid-height of the stirrup. Each gage was identified by the word "Stirrup" followed by a number and letter. The number identified the stirrup, with 1 being the stirrup closest to the support as shown in Fig. A.2. The letter (W or E) identified the stirrup leg as shown in the cross-section in Fig. A.3. T.45.Ld3.(4) and T.45.Ld3.(5) had gages applied to a total of 13 stirrups. Specimens IT.45.Ld2(5) and IT.60.Ld2(5+19) had 12 stirrups instrument. Specimens IT.45.Ld2 and

IT.60.Ld2 had 10 stirrups instrument. Specimens T.60.Ld3.(5) and T.0.Ld3.(5) had 7 stirrups instrumented.

Preformed Crack Stirrup: Strain gages were applied on each stirrup leg wherever the preformed crack crossed a stirrup. Each gage was identified by the words "Crack Stirrup" followed by a number and letter. The number identified the stirrup, with 1 being the stirrup closest to the support as shown in Fig. A.2. The letter (W or E) identified the stirrup leg as depicted in the cross-section in Fig. A.3. Specimen T.0.Ld3.(5) did not have any preformed crack stirrup gages.

Figs. A.4 to A.27 are graphs showing the data collected by the instrumentation.
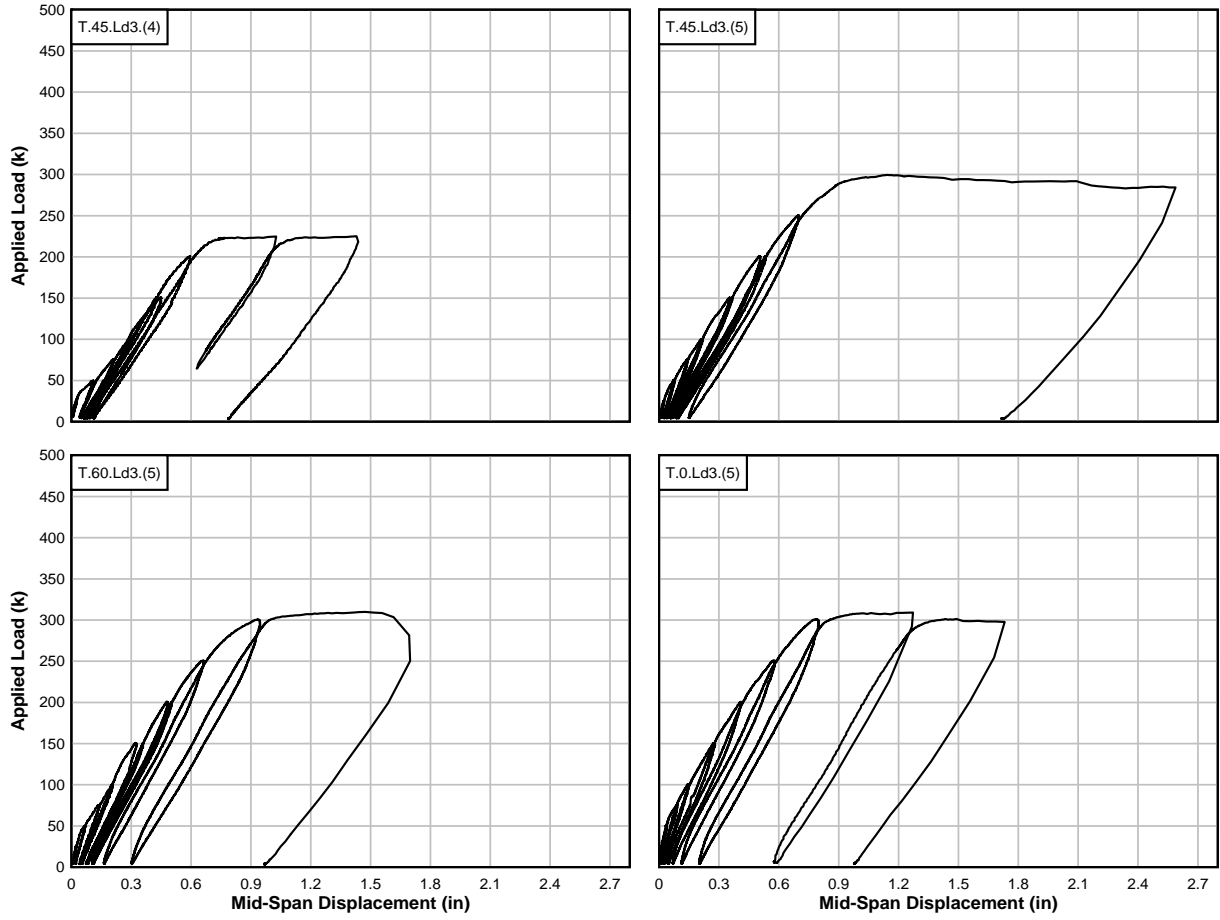
Figure A.4: Load – mid-span displacement plots for T-beam specimens
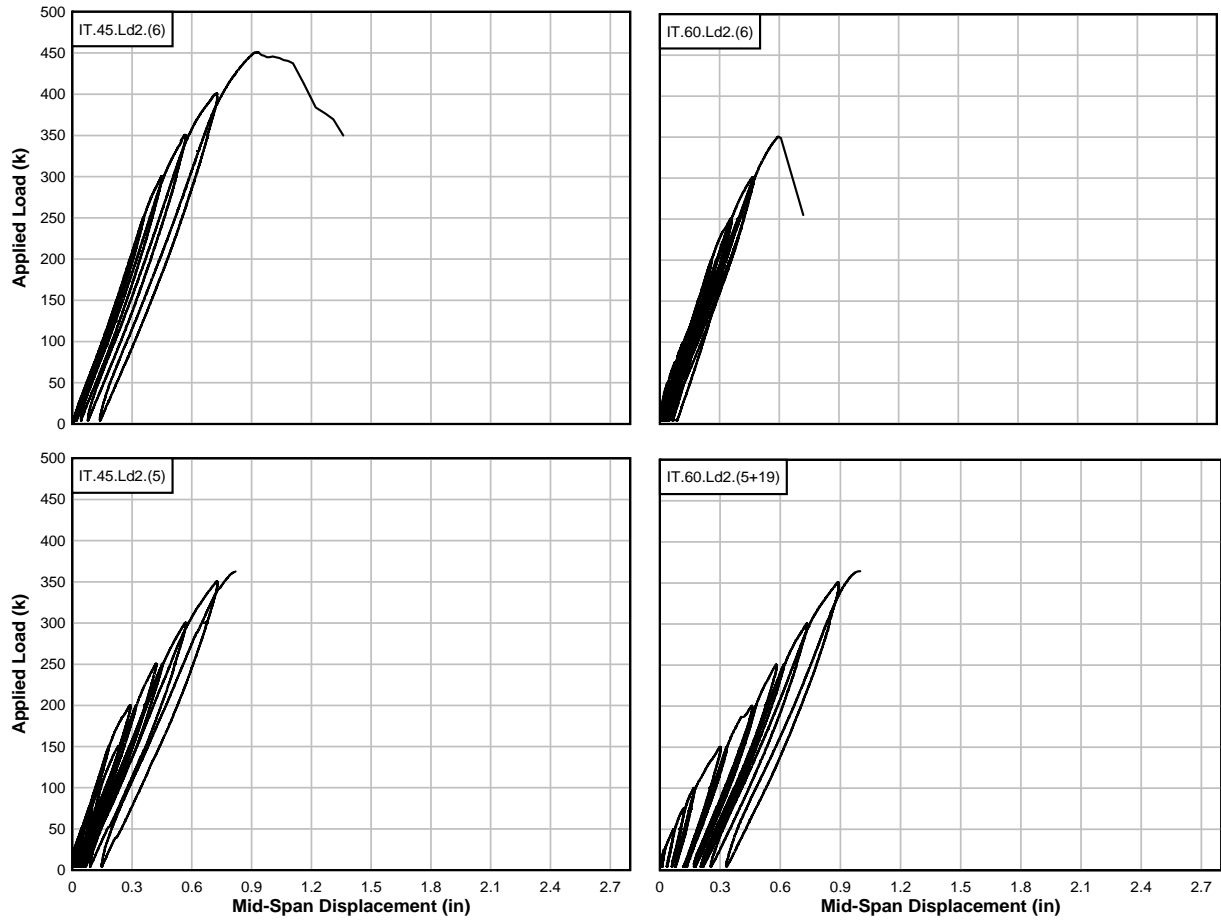
Figure A.5: Load – mid-span displacement plots for IT-beam specimens
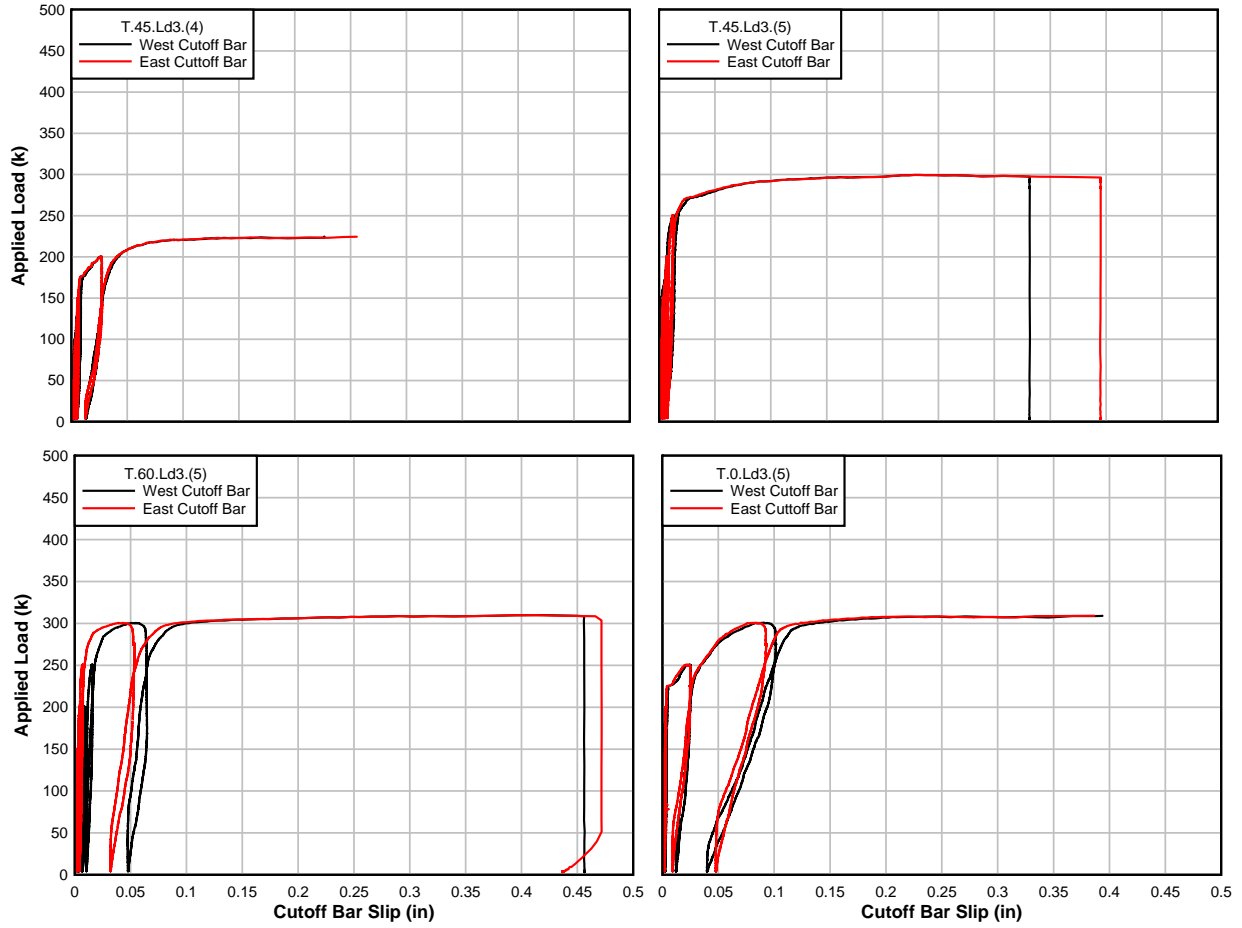
Figure A.6: Load – cutoff bar slippage plots for T-beam specimens
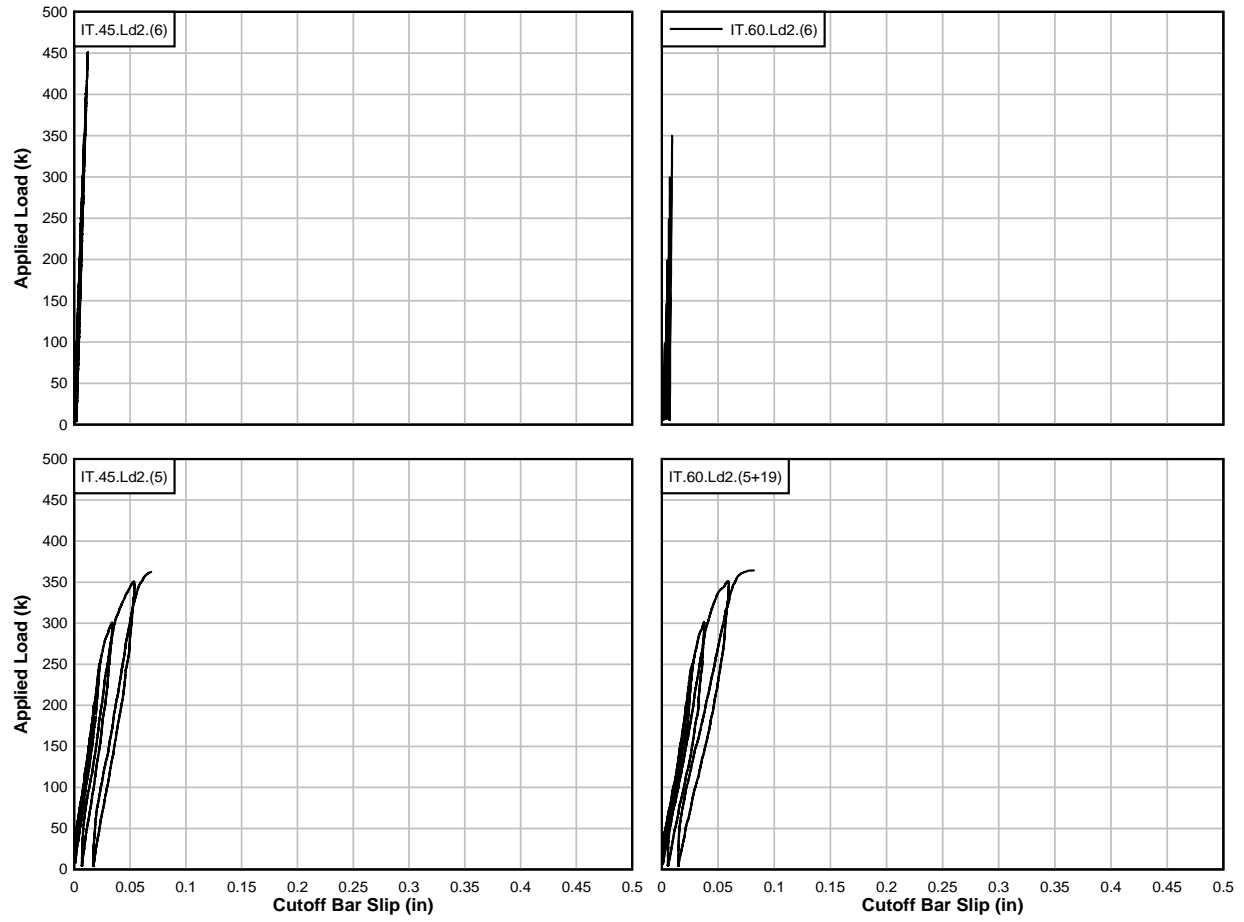
Figure A.7: Load – cutoff bar slippage plots for IT-beam specimens
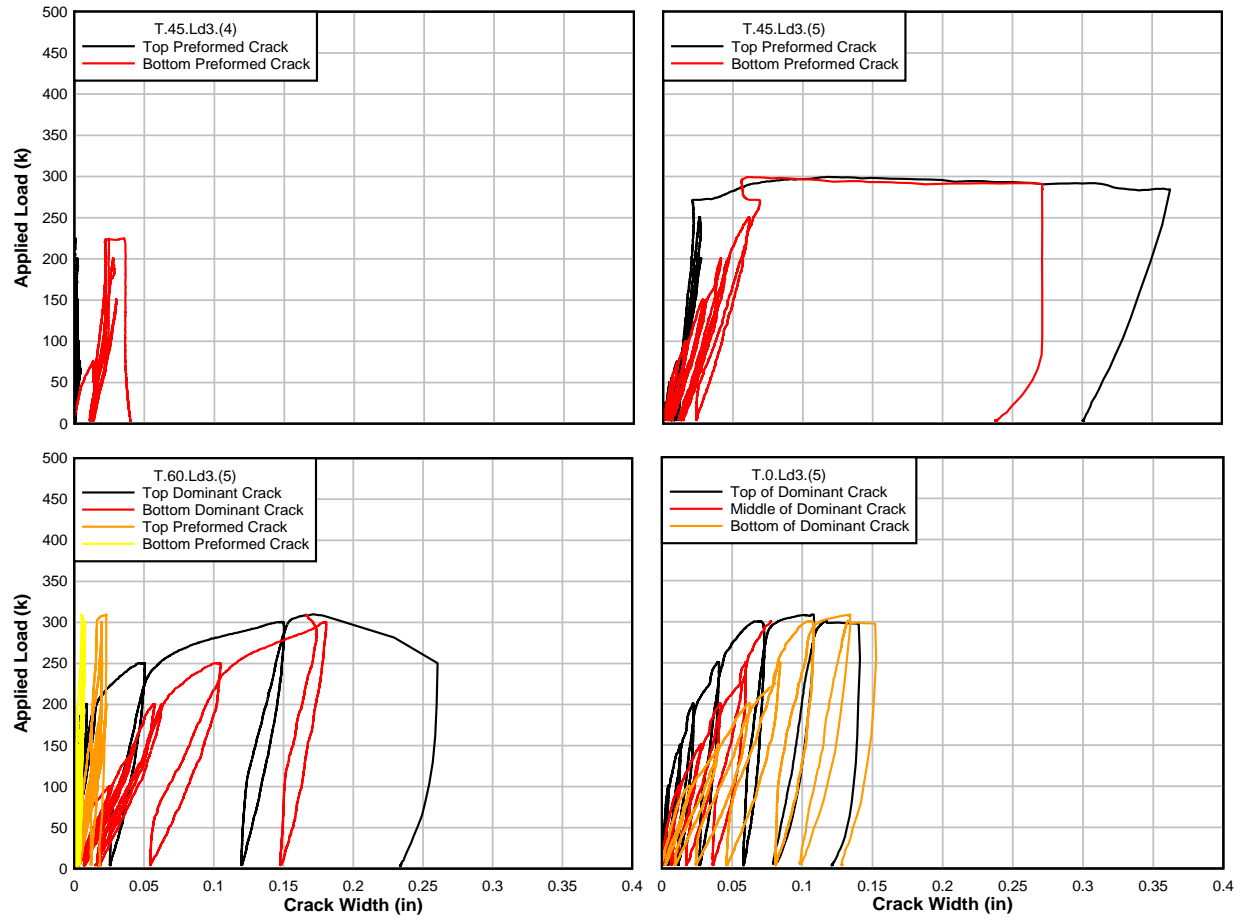
Figure A.8: Load – preformed crack width plots for T-beam specimens
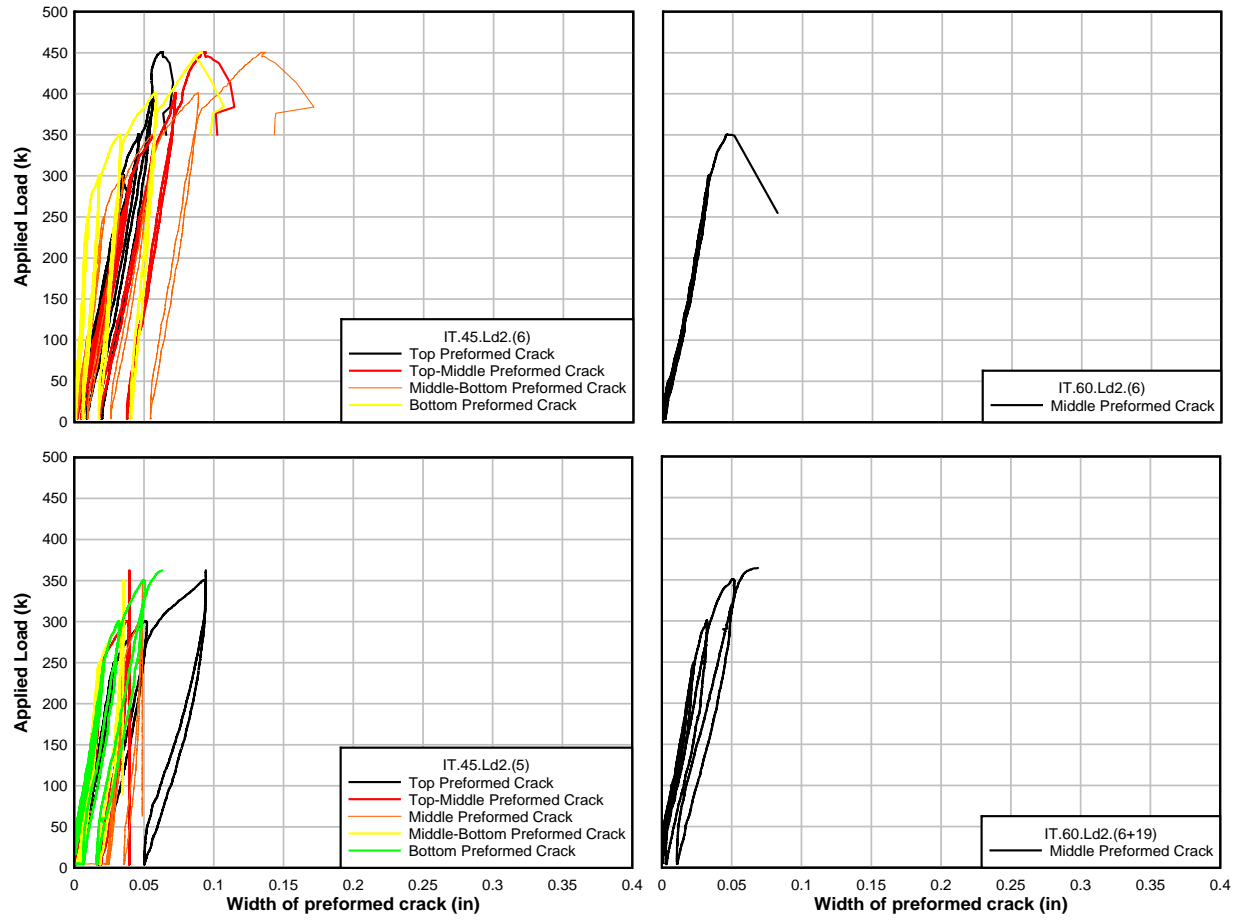
Figure A.9: Load – preformed crack width plots for IT-beam specimens
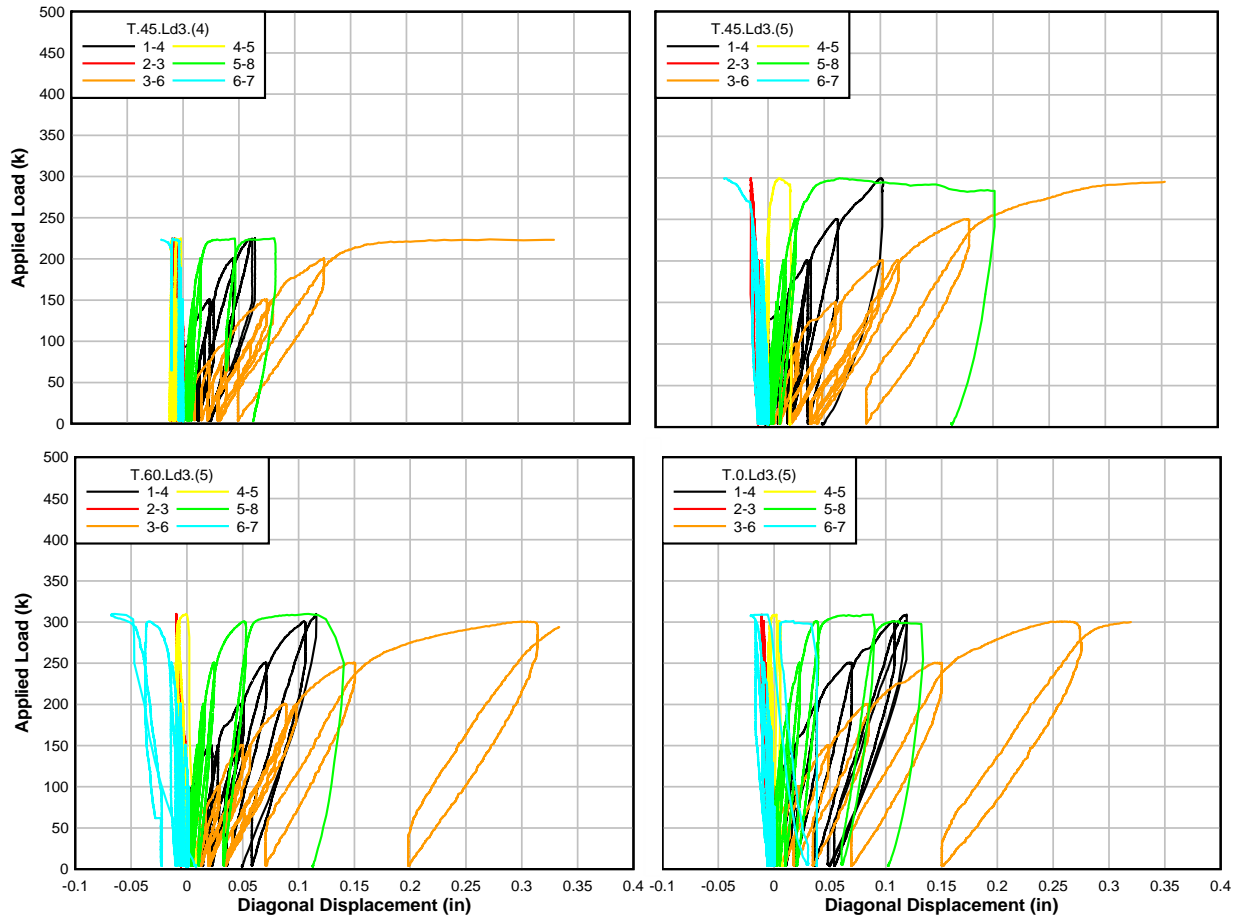
Figure A.10: Load – diagonal displacement plots for T-beam specimens
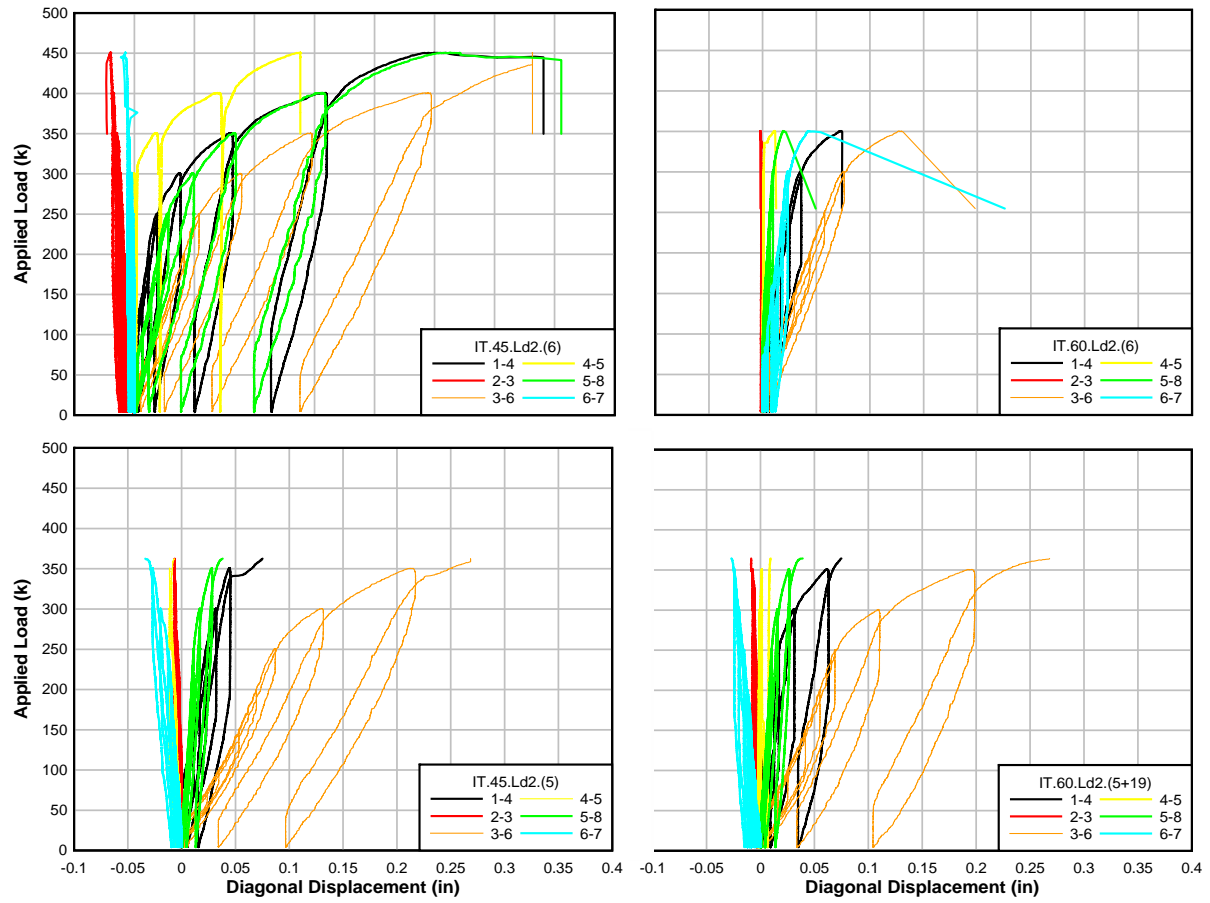
Figure A.11: Load – diagonal displacement plots for IT-beam specimens
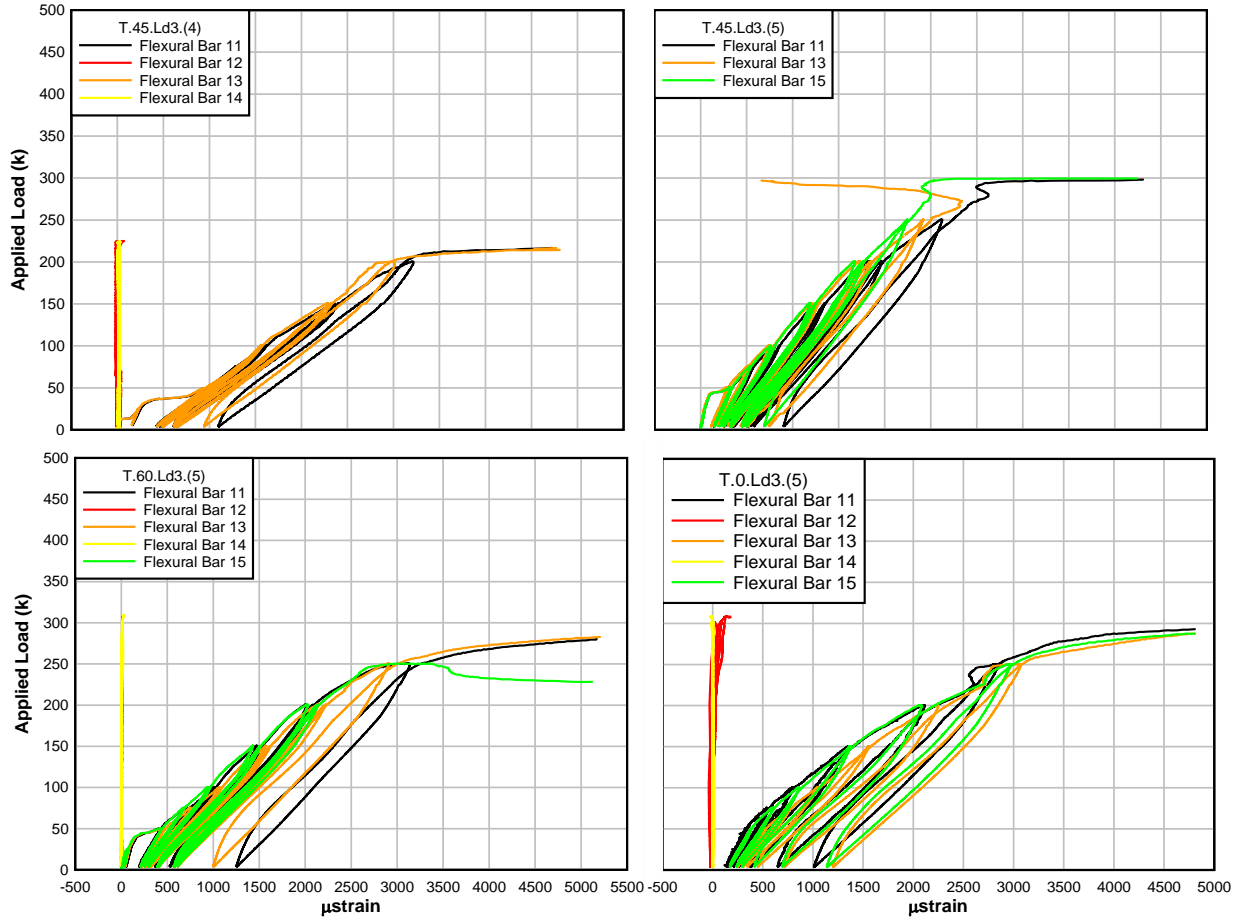
Figure A.12: Load – flexural bar location 1 strain plots for T-beam specimens
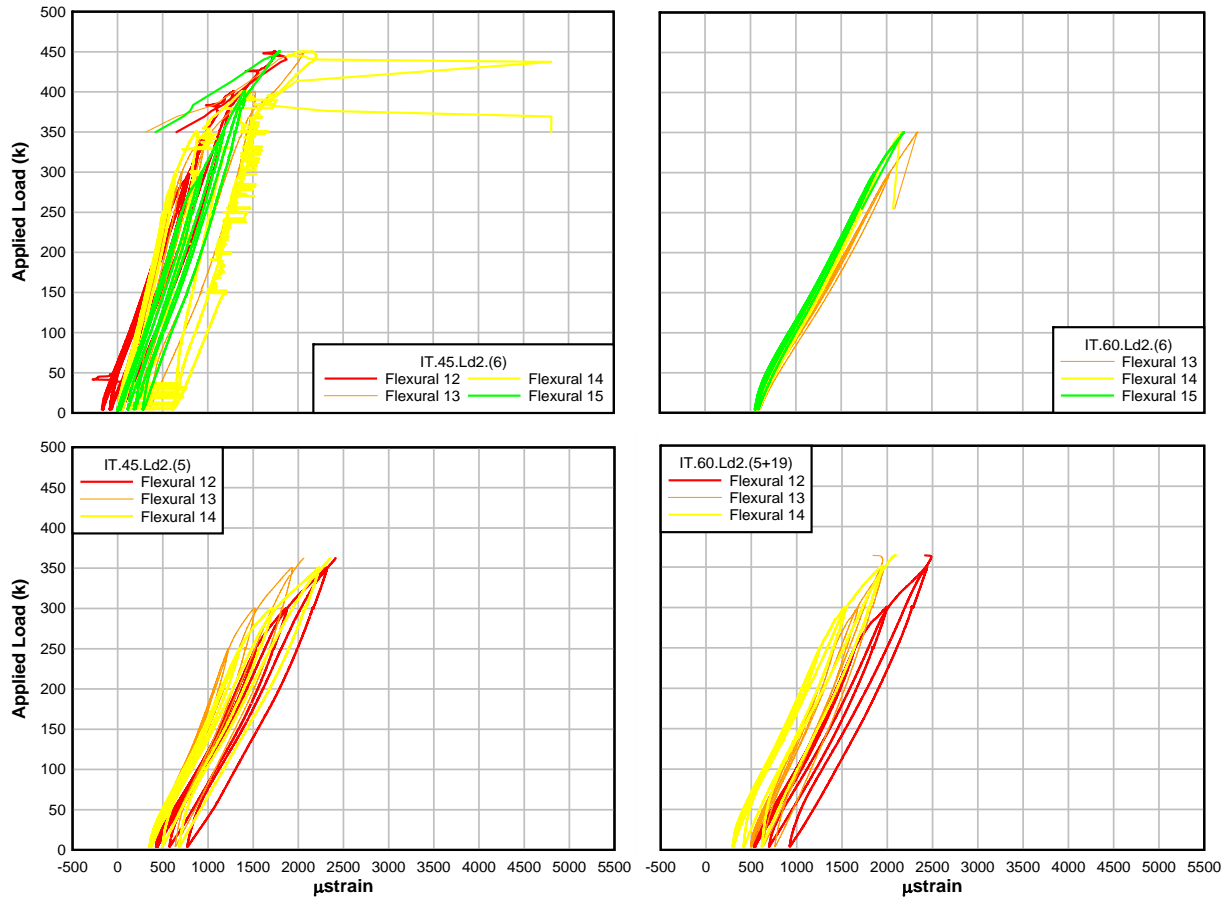
Figure A.13: Load – flexural bar location 1 strain plots for IT-beam specimens
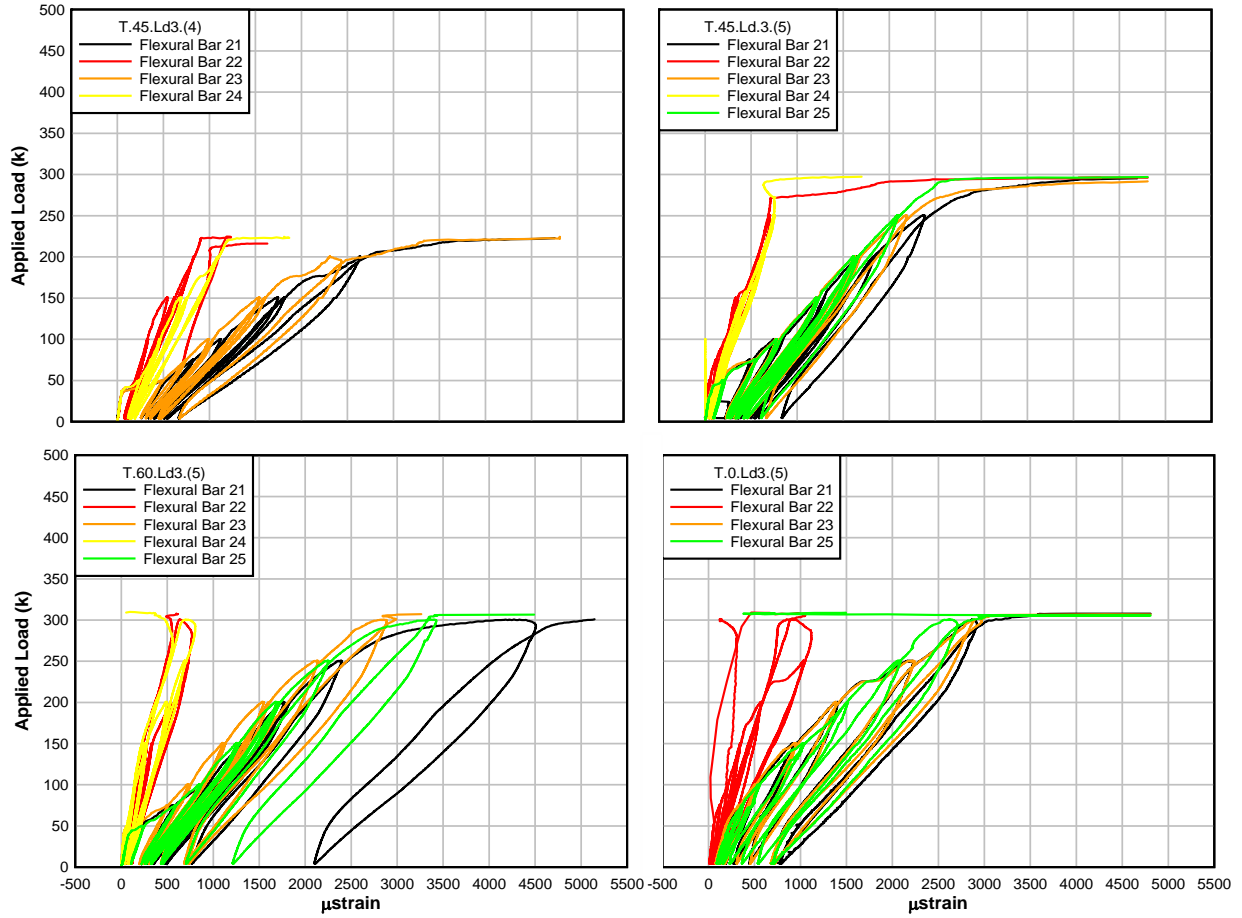
Figure A.14: Load – flexural bar location 2 strain plots for T-beam specimens
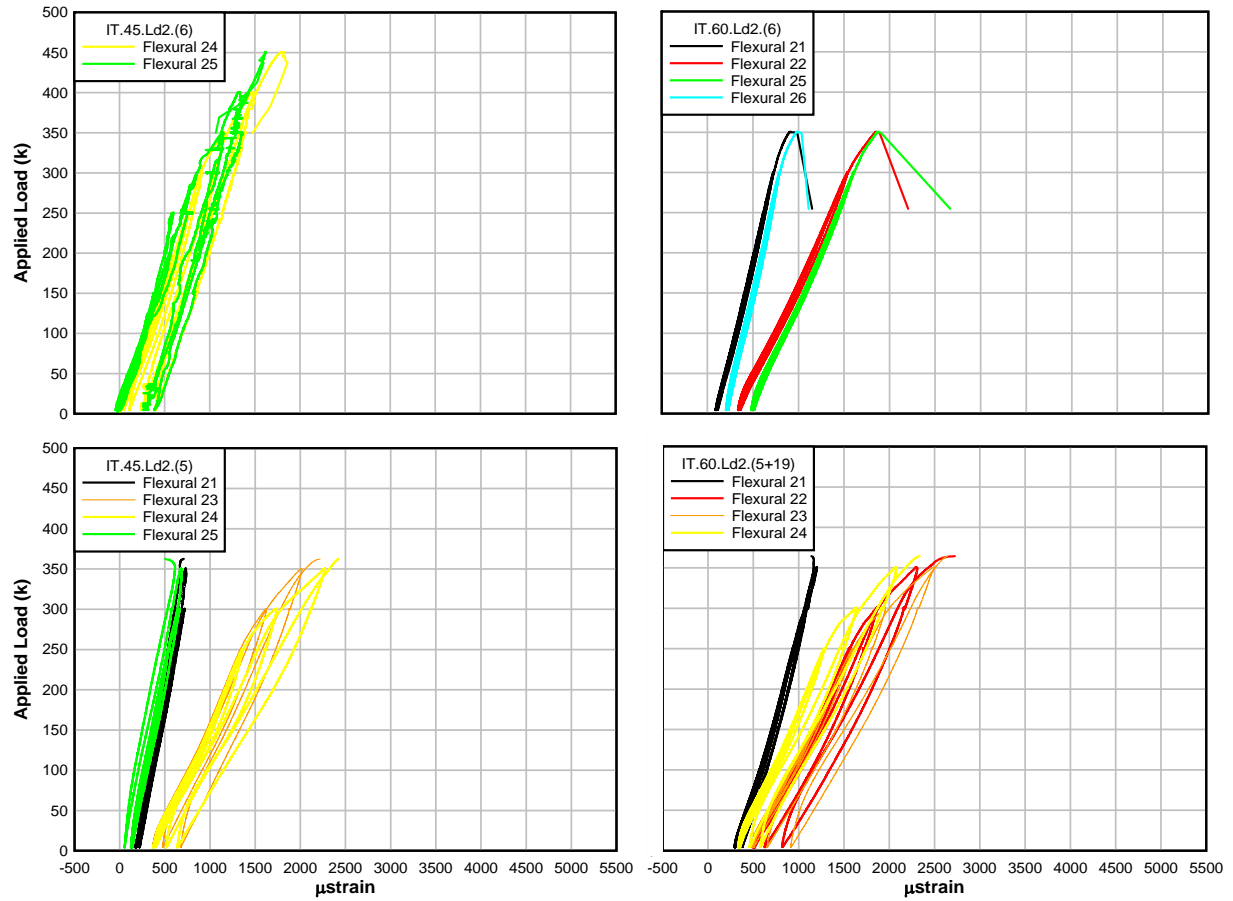
Figure A.15: Load – flexural bar location 2 strain plots for IT-beam specimens
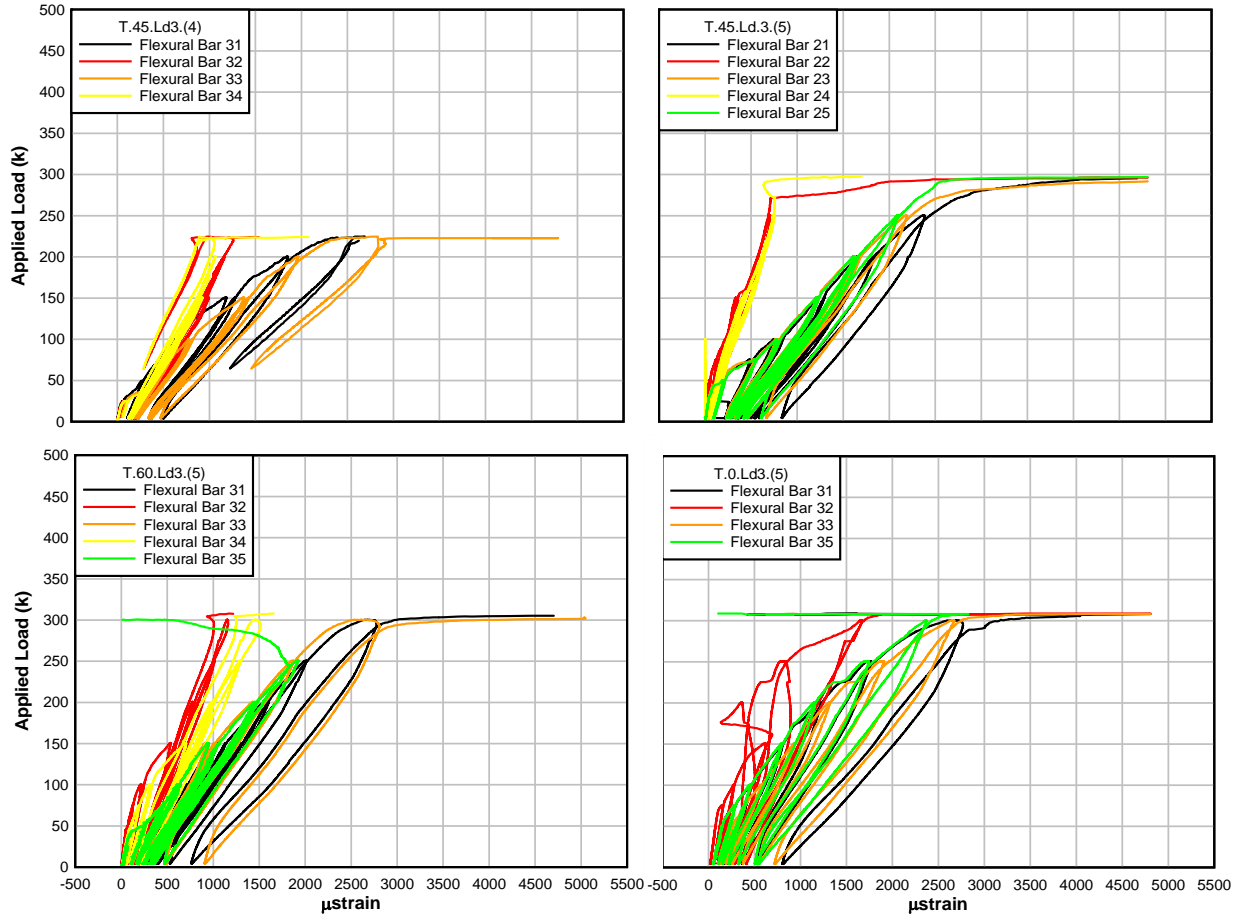
Figure A.16: Load – flexural bar location 3 strain plots for T-beam specimens
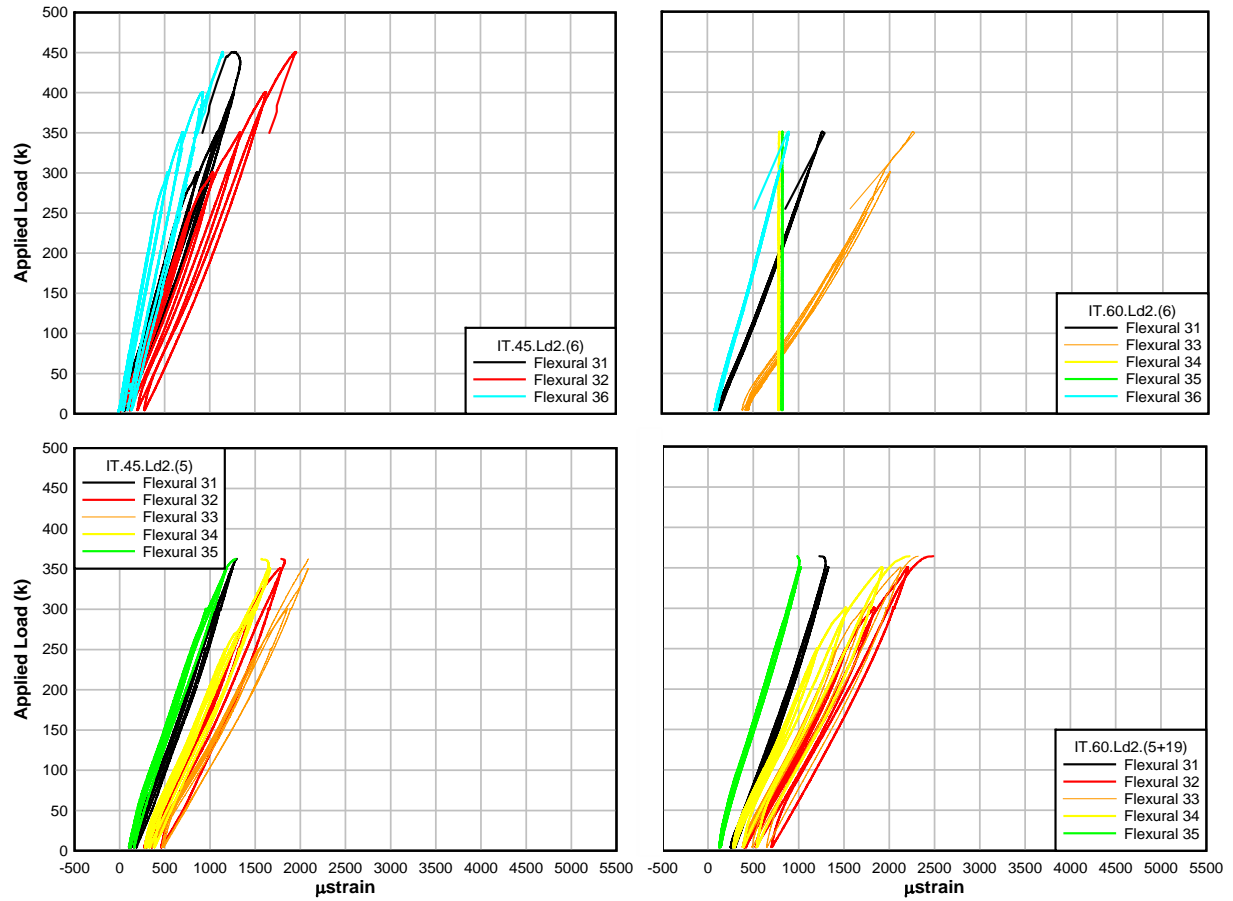
Figure A.17: Load – flexural bar location 3 strain plots for IT-beam specimens
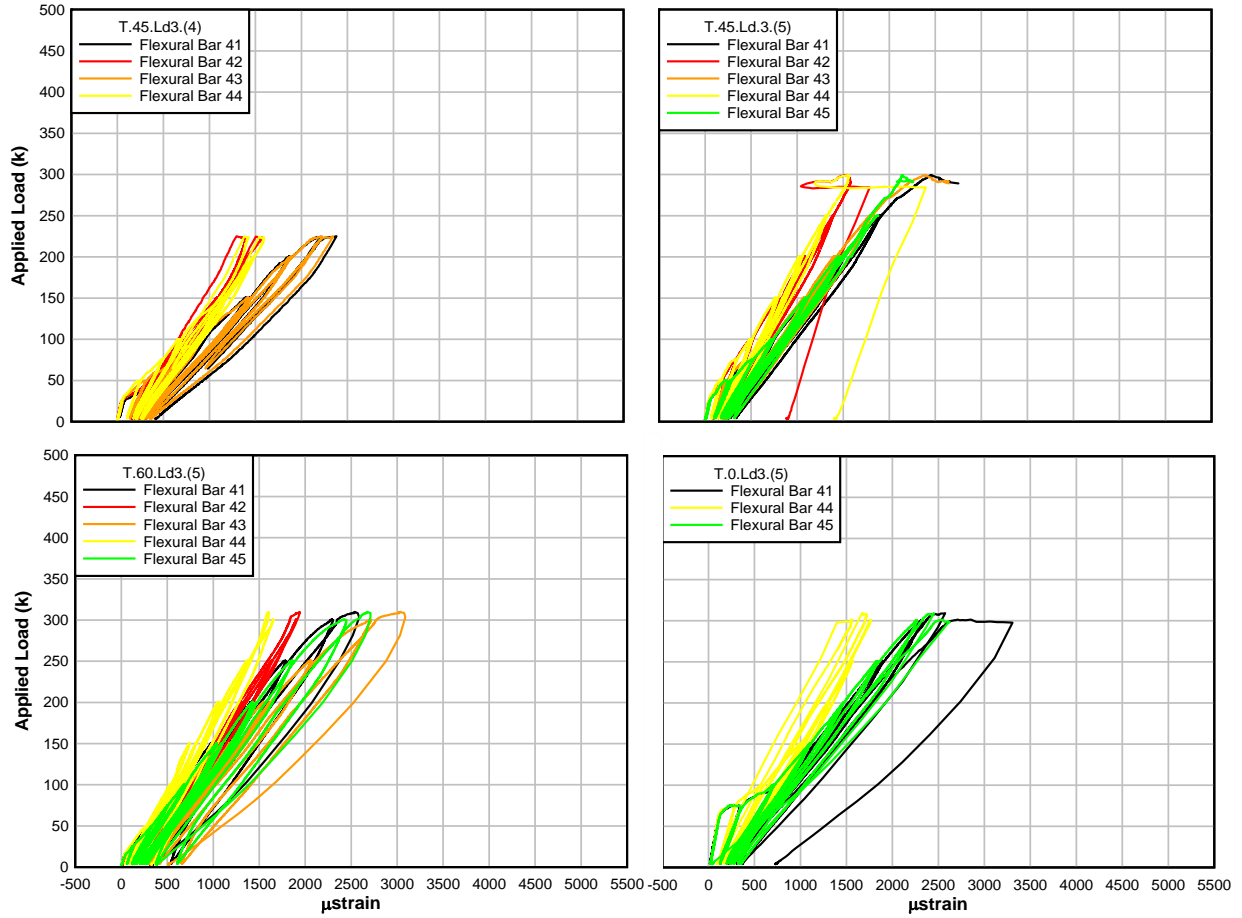
Figure A.18: Load – flexural bar location 4 strain plots for T-beam specimens
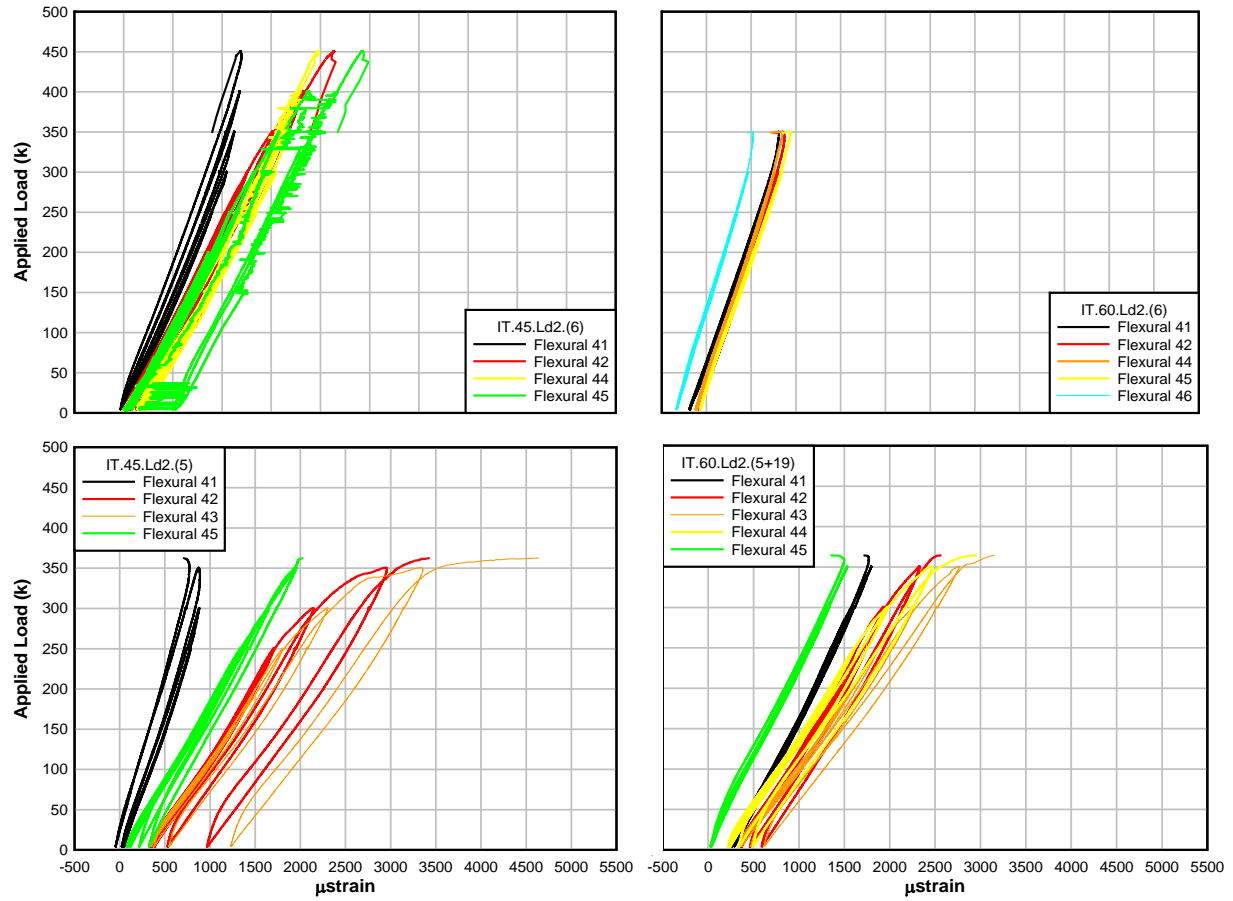
Figure A.19: Load – flexural bar location 4 strain plots for IT-beam specimens
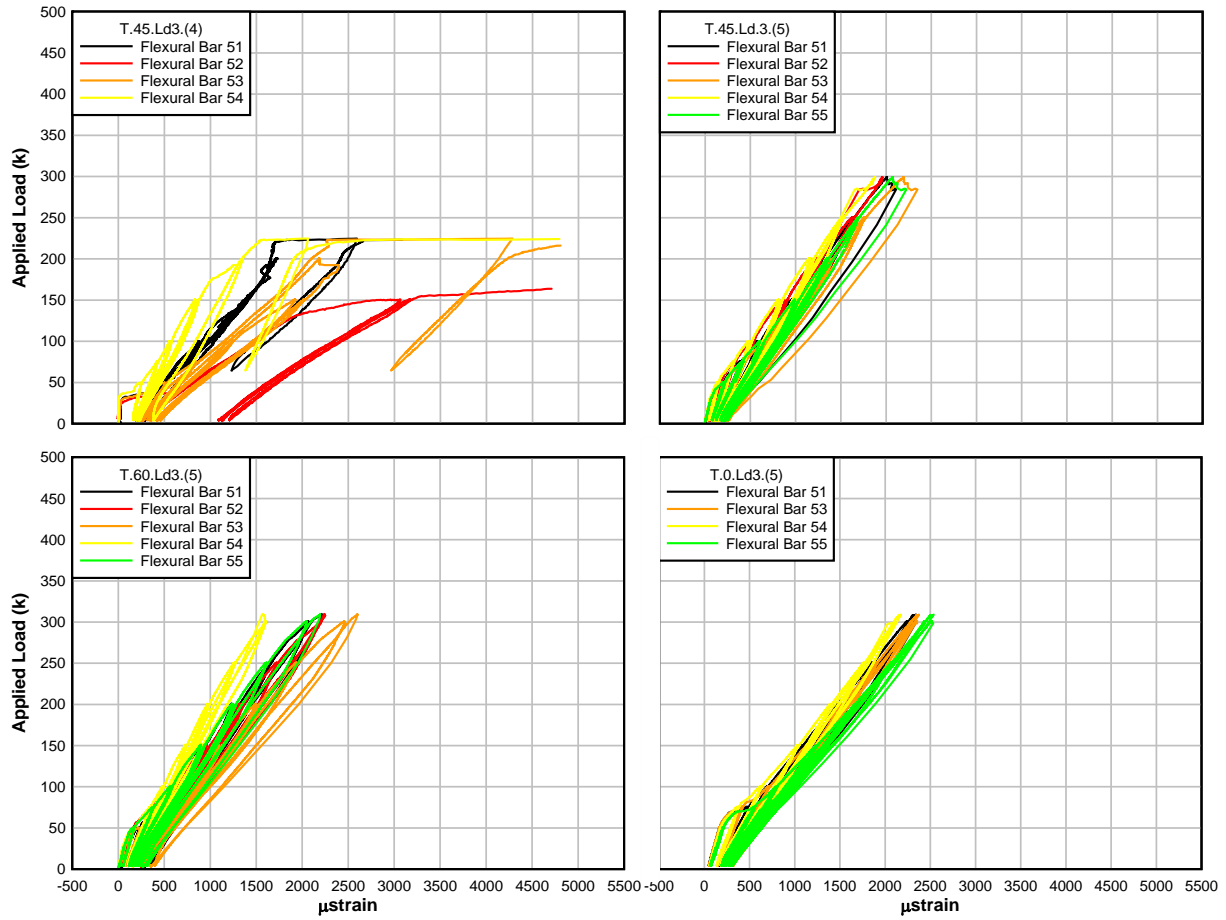
Figure A.20: Load – flexural bar location 5 strain plots for T-beam specimens
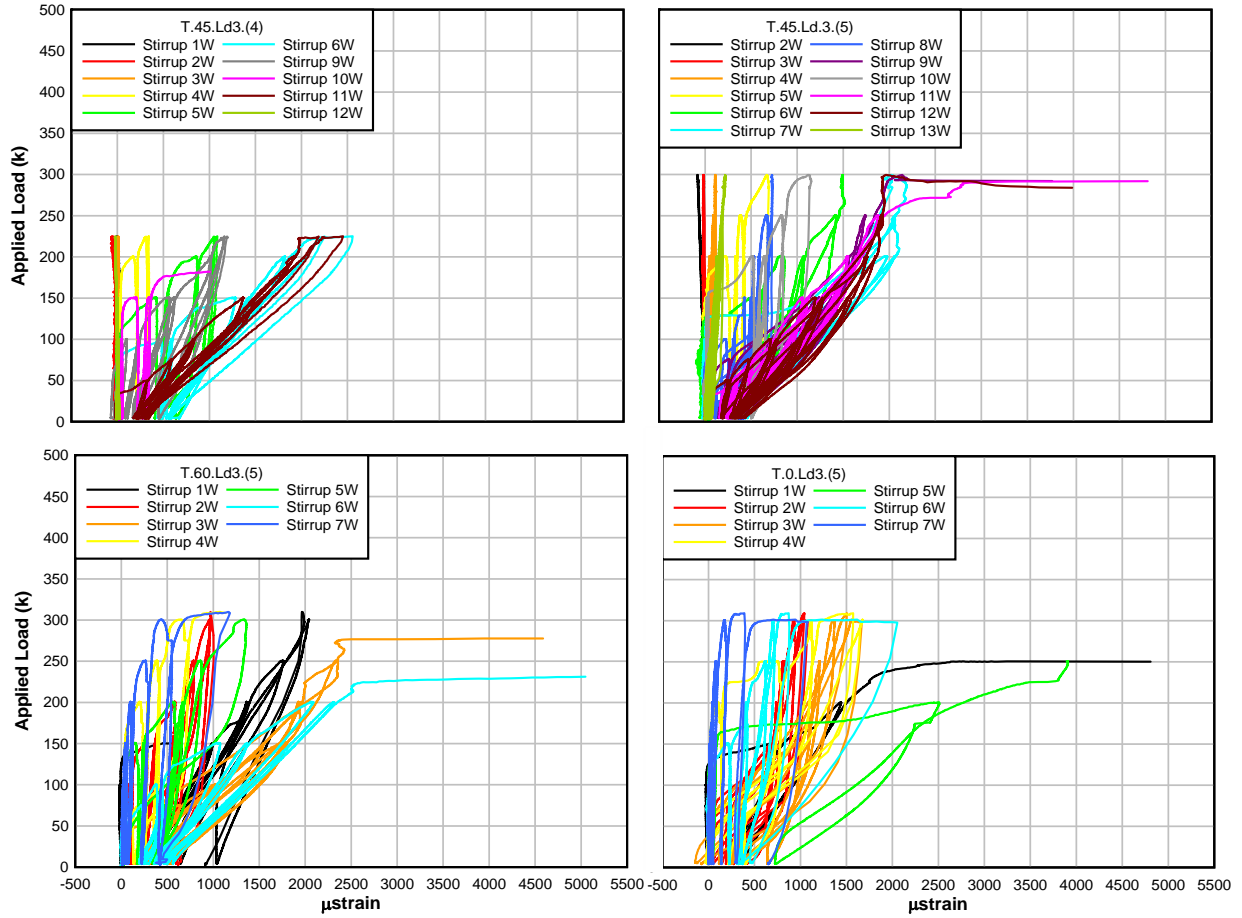
Figure A.21: Load – west mid-height stirrup strain plots for T-beam specimens
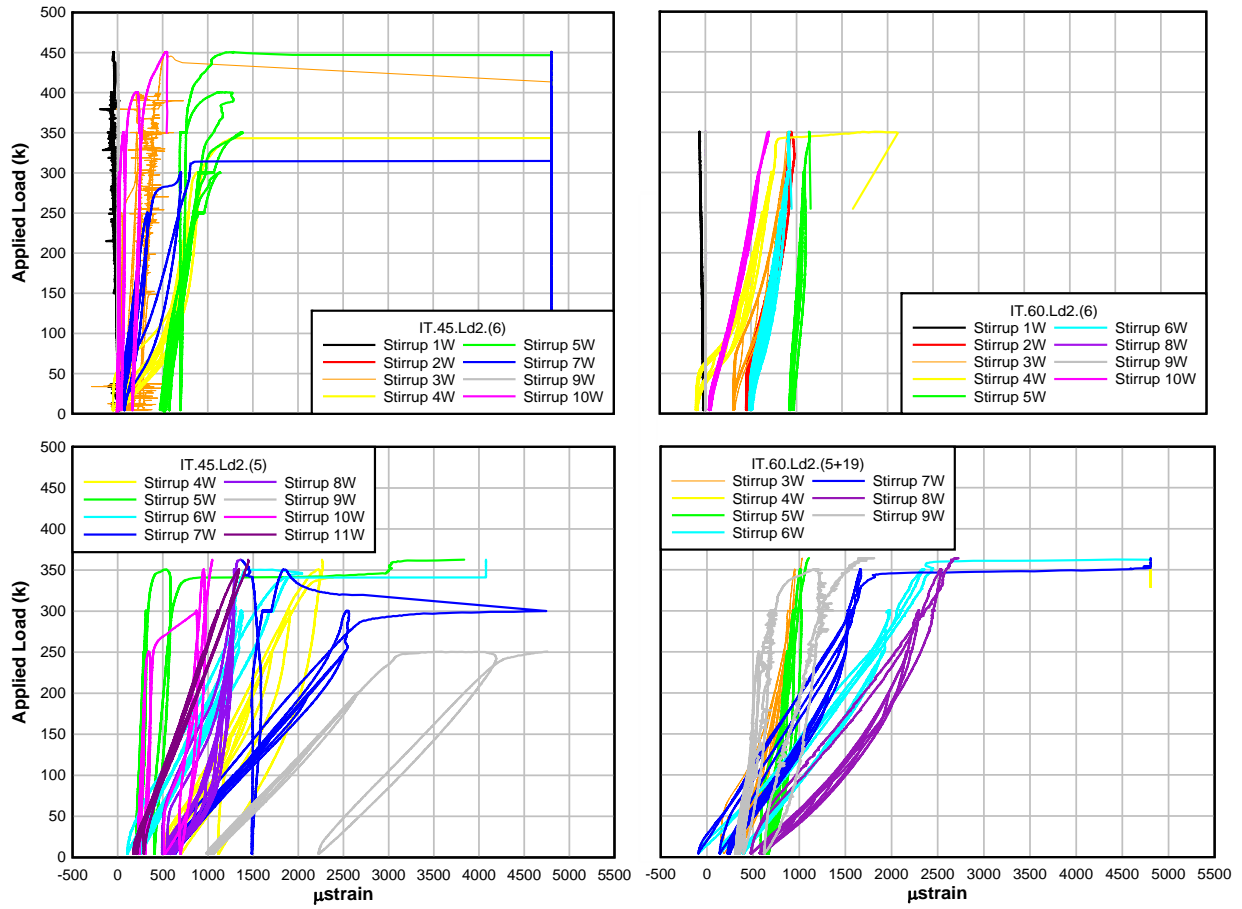
Figure A.22: Load – west mid-height stirrup strain plots for IT-beam specimens
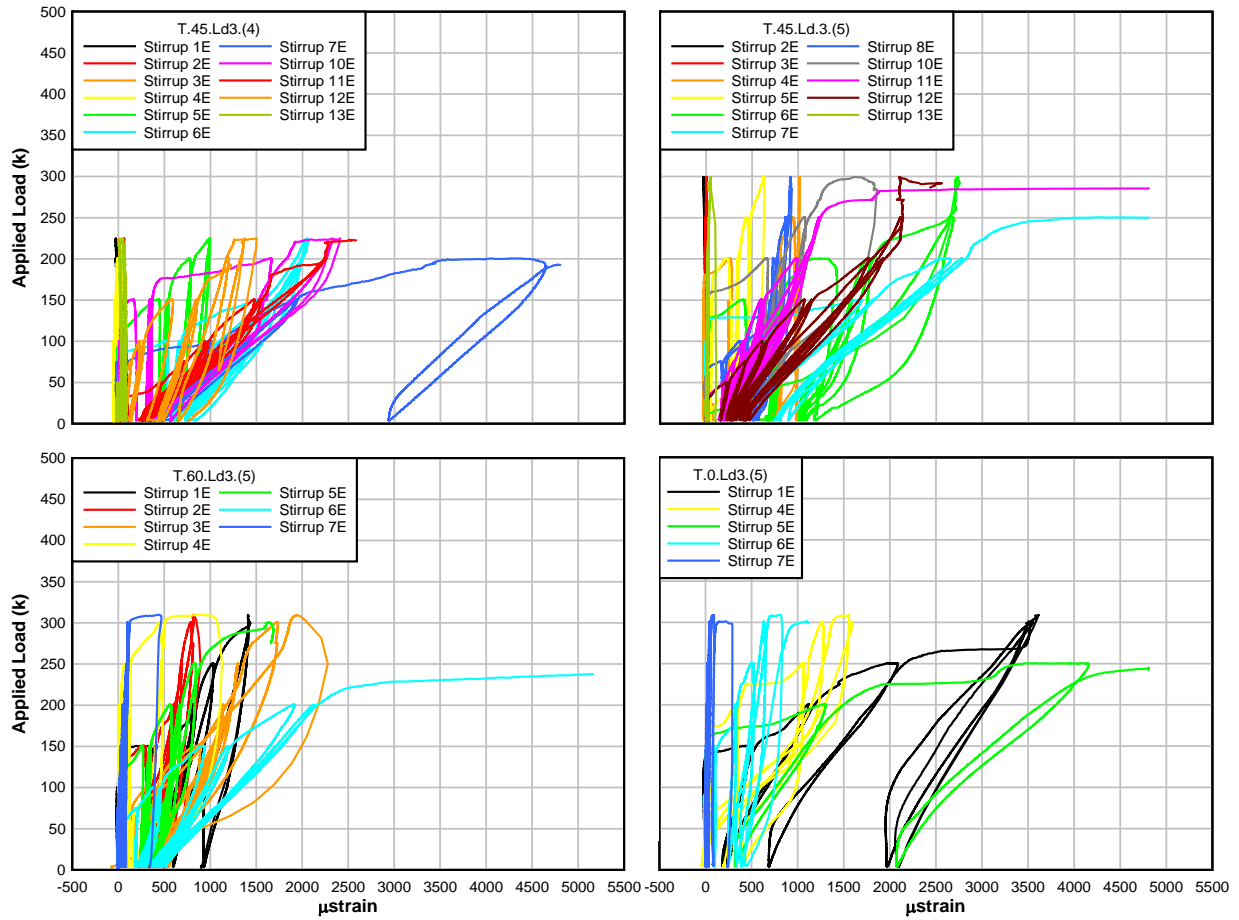
Figure A.23: Load – east mid-height stirrup stain plots for T-beam specimens
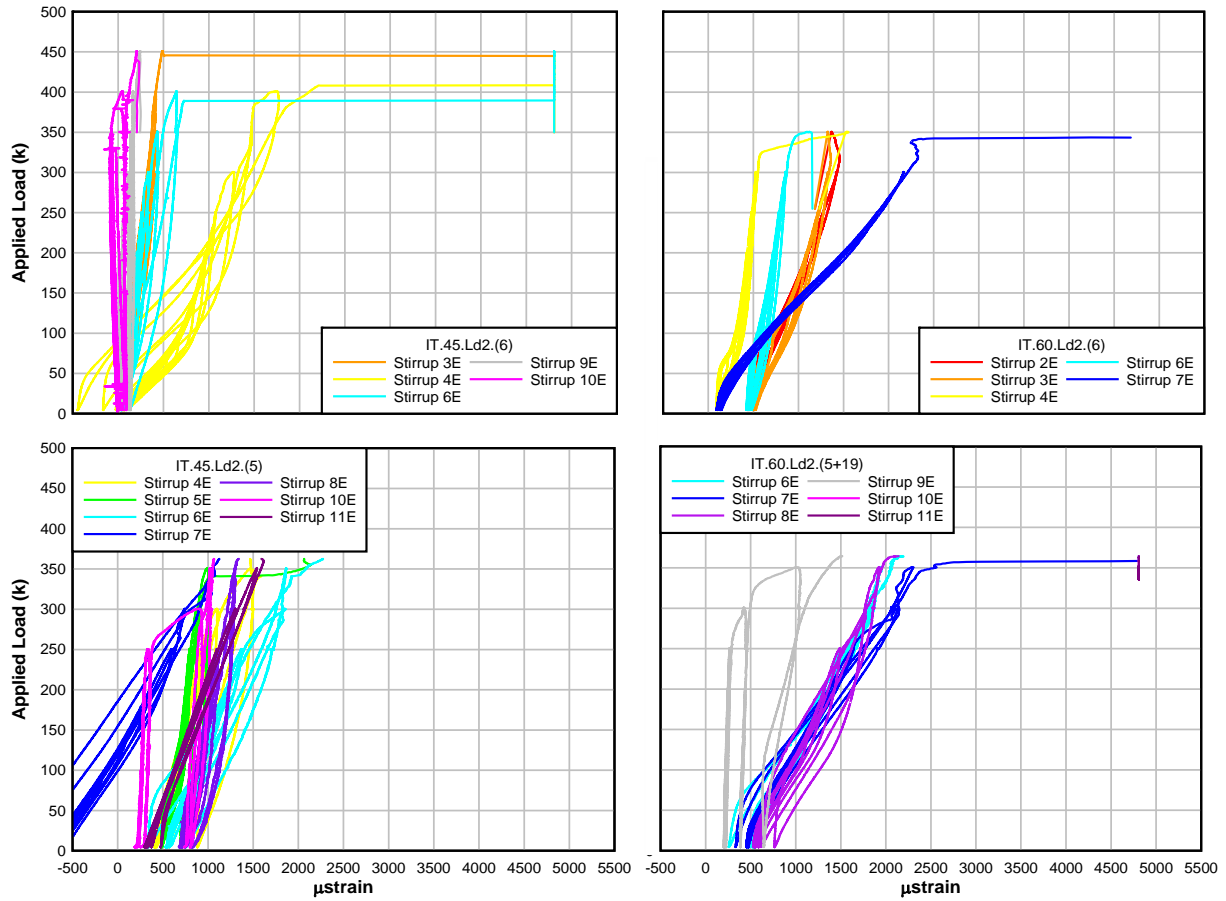
Figure A.24: Load – east mid-height stirrup stain plots for IT-beam specimens
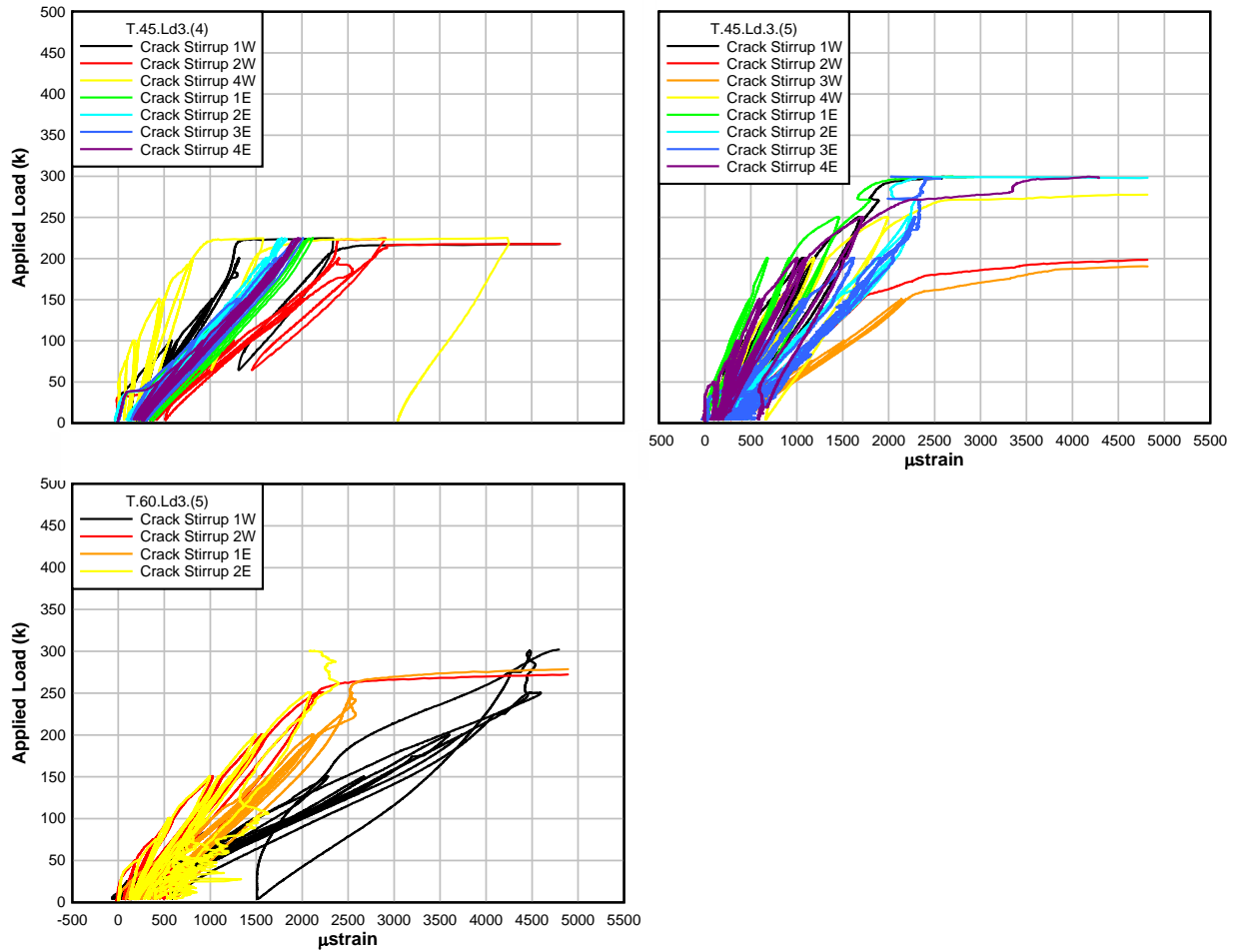
Figure A.25: Load – preformed crack stirrup stain plots for T-beam specimens
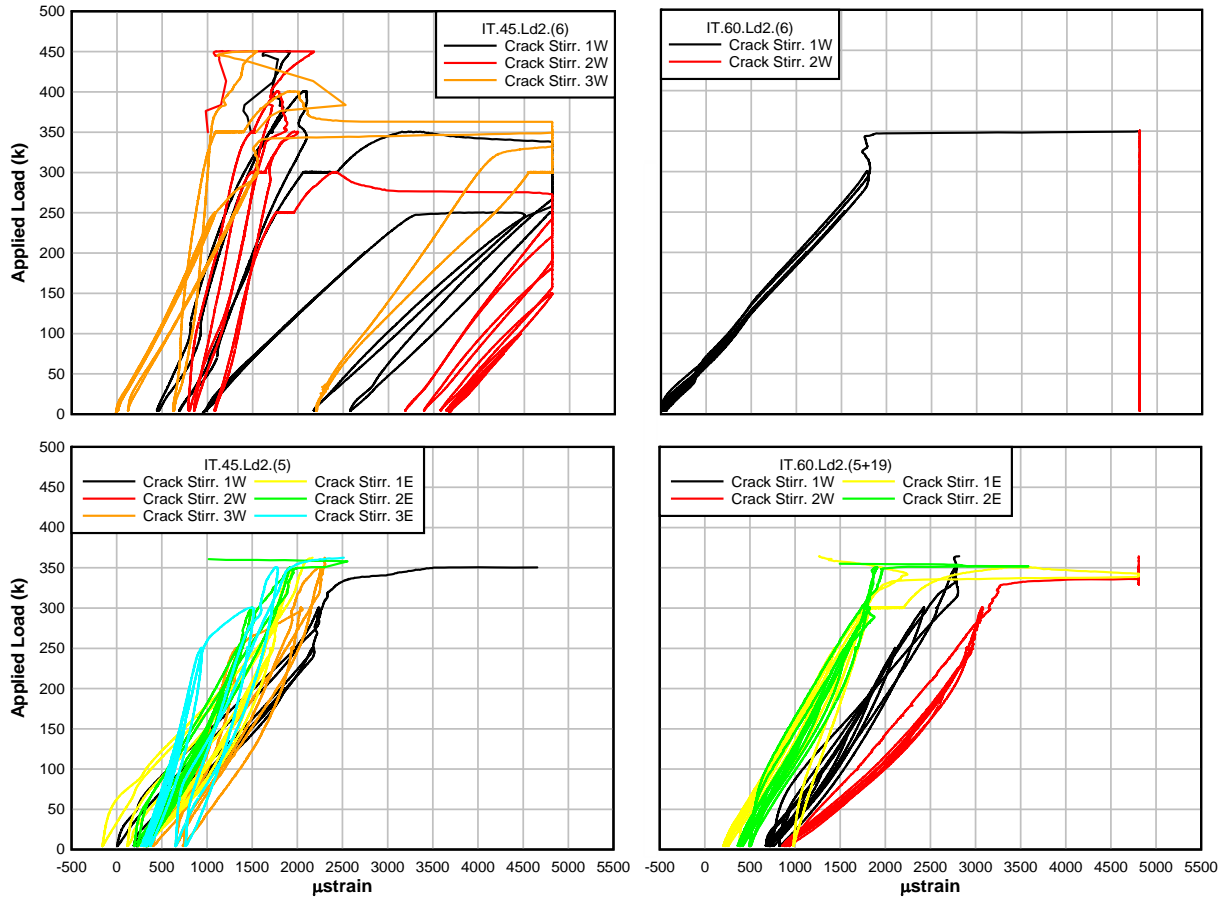
Figure A.26: Load – preformed crack stirrup stain plots for IT-beam specimens

APPENDIX B :
CASE STUDY USING ANALYSIS METHOD 2

To investigate the variation between specification-based and experimentally-derived capacity predictions, a case study was performed on the Willamette River Bridge (WRB) on OR 219. This vintage RCDG bridge, constructed in the late 1950s, featured continuous approach spans and cutoff longitudinal reinforcement details in both positive and negative moment regions. Pertinent reinforcing detailing, cross-sections, and crack angles and locations were obtained from SPR 341 ([Higgins, *et al.* 2004).

Figure B.1: South approach spans of Willamette River Bridge on OR 219 (Higgins, *et al.* 2004)

For the purpose of this case study, the positive moment region at midspan of Span 9 was selected as shown in Fig. B.1. The negative moment region near Bent 4 was selected as shown in Fig. B.2. Three crack locations were chosen for both positive and negative moment analysis at locations along the length of cutoff reinforcement. The locations of these cracks and measured crack angles were scaled from inspection drawings as reported in Table B.1. The crack location was considered from where the crack crosses the flexural steel to Bent 4.
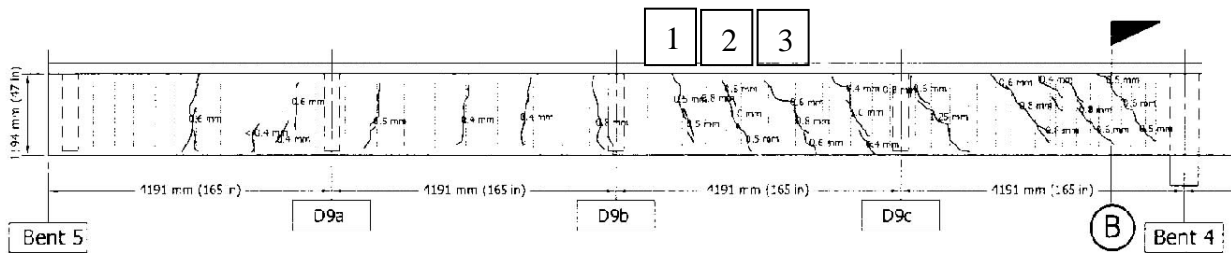
Figure B.1: Crack near midspan of Span 9
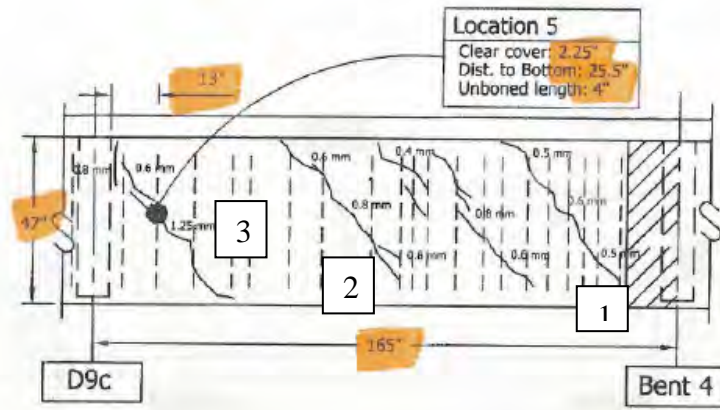
Figure B.2: Crack locations near Bent 4

Table B.1: Crack Locations and Angles Along Span 9 WRB

Moment Region	Crack Number	Distance from Center of Bent 4 to Crack Location (mm) [in]	Measured Crack Angle (deg)	Possible Failure Crack Angle (deg)
Positive	1	7292 [287.1]	69.4	43.9
	2	6454 [254.1]	71.5	43.9
	3	5448 [214.5]	54.3	43.9
Negative	1	1283 [50.5]	50.6	45.2
	2	2865 [112.8]	50.9	43.8
	3	3988 [157.0]	51.9	43.9

The measured crack angles reported are based on scaled drawings, while the possible failure crack angles are based on the possible development of additional cracking that could propagate at a shallower angle toward the bent location. Crack angles shallower than the initially measured angle should be considered based on the results of experiments described in the body of this report. The possible failure angle was determined based on AASHTO-LRFD Section 5.8.3.4 using loading parameters described below. In the event the AASHTO-LRFD crack angle is shallower than one which would physically fit on the beam between where the existing crack crosses the flexural steel and the bend location, the minimum angle which is physically possible is reported in Table B.1. Table B.2 shows the negative moment reinforcing bar details across Bent 4 and the positive moment reinforcing bar details near the midspan of Span 9. Figures B.3a and B.3b show the cross-section at each crack in question.

Table B.2: Steel Reinforcement with Cutoff Locations From Bent 4

Number of bars	Negative Moment Regions		Number of bars	Positive Moment Regions	
	A_s (mm^2) [in^2]	Length from Center of Bent to Cutoff (mm)[in]		A_s (mm^2) [in^2]	Length from Center of Bent to Cutoff (mm)[in]
2	1006 [1.56]	2286 [90.0]	1	1006 [1.56]	7620 [300.0]
2	1006 [1.56]	3353 [132.0]	2	1006 [1.56]	6401 [252.0]
2	1006 [1.56]	4572 [180.0]	1	1006 [1.56]	4877 [192.0]
2	1006 [1.56]	6553 [258.0]	2	1006 [1.56]	3353 [132.0]
2	645 [1.00]	8077 [318.0]	3	1006 [1.56]	0 [0.0]
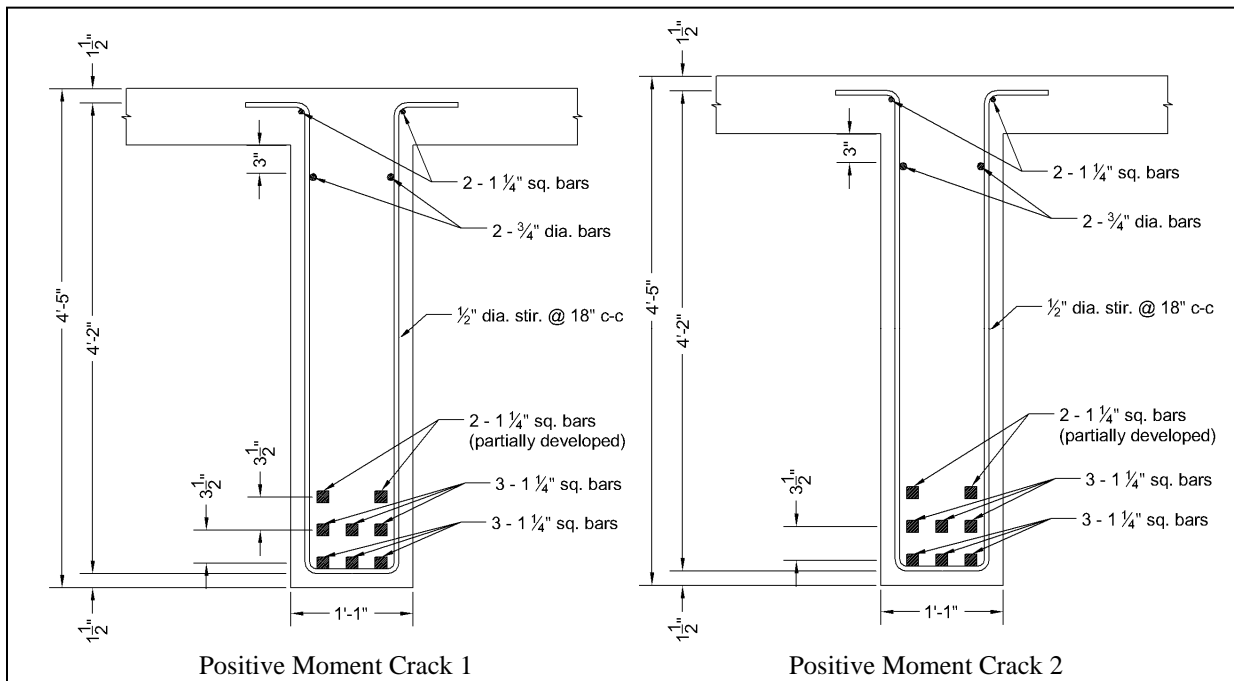
Figure B.3a: Beam Cross Sections at Crack Locations.
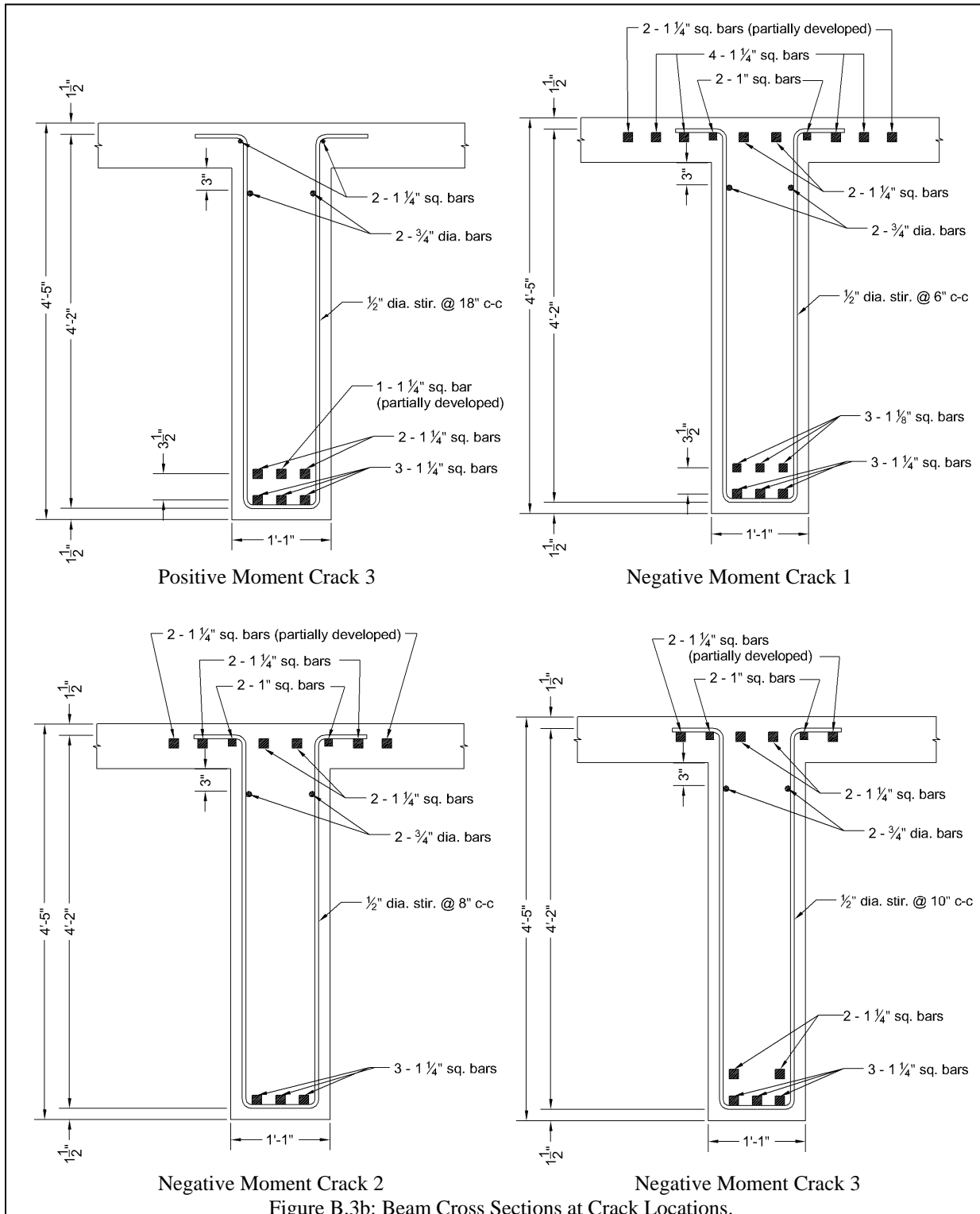
Figure B.3b: Beam Cross Sections at Crack Locations.

As a basis for analysis, bond capacity under service-level loading was evaluated using an AASHO-based allowable bond (m) of 350 psi (AASHO, 1953) to determine an equivalent development length, l_d as calculated by:

$$l_d = \frac{T}{\mu \pi d_b}$$ [B.1]

B-4

where T is the tensile capacity of reinforcement, μ is the bond strength, and d_b is the reinforcing bar diameter. The development length at strength was determined using the ACI 318 detailed development calculation (ACI 318, 2008). Although testing discussed previously indicated that bond capacity was greater than this specification-based allowance, it was intended that the analysis in this case study be performed using specification-based methods. The ACI 318 detailed calculation for development length was the more accurate method using this criterion. As a means of comparing the ACI 318 method to experimental results, a development length was also calculated using the measured maximum bond strength of 550 psi reported previously. The resultant development lengths for each method are described in Table B.3.

Table B.3: Development Lengths for Each Analysis Type

| Moment Region | No. Bars Being Developed | Tensile Bar Development Length (mm) [in] | | |
		AASHO (service)	ACI Complex (strength)	Exp. (strength)
Positive	1	1024 [40.3]	1260 [49.6]	652 [25.7]
	2		1468 [57.8]	
Negative	2	1024 [40.3]	1356 [53.4]	652 [25.7]

Based on the calculated development lengths and cutoff detailing, the effective area of steel reinforcing at each crack location was determined. This effective area of steel was then converted to an effective tensile capacity using each of the three development length considerations as described in Table B.4. Material properties were assumed to be 3300 psi for the concrete compressive strength, and 40 ksi for the yield strength of all of the reinforcing steel.

Table B.4: Tensile Capacity at Each Crack for Each Analysis Type

| Moment Regions | $\sum T_{eff}$ (kN) [k] | | | | | | | | |
| | Crack 1 | | | Crack 2 | | | Crack 3 | | |
	AASHO	ACI	Exp.	AASHO	ACI	Exp.	AASHO	ACI	Exp.
Positive	2148 [483.8]	2002 [450.9]	2220 [500.0]	1694 [381.5]	1685 [379.5]	1710 [385.2]	1542 [347.4]	1513 [340.9]	1631 [367.3]
Negative	2564 [577.5]	2431 [547.5]	2575 [580.0]	1730 [389.5]	374.9 [1665]	1881 [423.6]	1227 [276.3]	1149 [258.8]	1408 [317.1]

The factored demand, F_u, at each crack location was determined using equation B.2:

$$F_u = \gamma_{DC} F_{DC} + \gamma_{DW} F_{DW} + \gamma_{LL} \left(F_{LL} \ DF \ IMP \right) \quad\quad [B.2]$$

where: F_u = the factored demand

             γ_{DC} = loading factor for component deadload

             F_{DC} = component deadload demand

             γ_{DW} = loading factor for wearing surface deadload

             F_{DW} = wearing surface deadload demand

             γ_{LL} = loading factor for liveload

F_{LL} = liveload demand
DF = liveload distribution factor
IMP = liveload impact factor

The approach spans were modeled as simple supports at the ends and fixed at the bent. Resultant service-level shear and moment demands along the length of Span 9 are shown in Figure B.4.Both Service I and Strength I load combinations were determined for shear and moment. Maximum, shear, and moment demands, not concurrent, were used in this analysis. From design drawings, the component dead load was calculated as 1.58 kip/ft/girder. The wearing surface was assumed to be 2 in. of asphalt, which corresponds to a wearing surface dead load of 0.175 k/ft/girder. The 3S2 truck was used to determine the live load on Span 9. In a previous field experimental investigation, DF and IMP were determined as 0.542 and 1.315, respectively, as reported in SPR 341. DF for shear and moment were taken as the same. The load factors for Service I and Strength I are reported in Table B.5 using ODOT live load rating factors for state-owned bridges.

Table B.5: Service I and Strength I Load Factors

Variable	Service I	Strength I
γ_{DC}	1.00	1.25
γ_{DW}	1.00	1.50
γ_{LL}	1.00	1.35
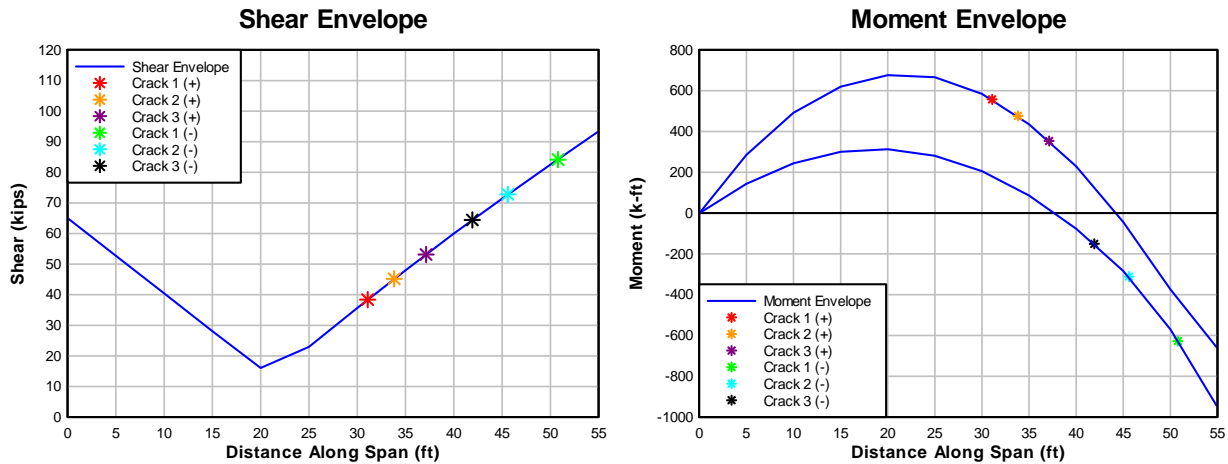
Figure B.4: Service I level shear and moment envelopes for WRB – Span 9 (similar curves developed for Strength I)

Using AASHTO LRFD equation 5.8.3.5-1 (total tensile demand on the flexural bars from flexure combined with shear) and the calculated factored shear and moment demands, the tensile demand on longitudinal reinforcement at each crack location was determined in order to predict a controlling failure mode. This calculated tensile demand was then compared to the effective tensile capacity at service (AASHO) and strength level (ACI and Experimental) conditions to derive a capacity/demand ratio at each crack location as reported in Table B.6. These ratios were considered with both the current, measured crack angles as well as potential future cracking angles. Additionally, to predict a controlling failure mode, the shear capacity of each section was

compared to the calculated shear demand at each crack location. The corresponding capacity/demand ratios are shown in Table B.7. It is possible for a specimen to be deficient in both tensile anchorage and shear capacity simultaneously. As a result, both must be determined to predict failure behavior. Strength 1 level loading only was considered with shear capacities at each crack predicted using the AASHTO-LRFD method (MCFT) and the ACI 318 method for development length. Additionally, the Willamette River Bridge has been strengthened for shear with carbon fiber reinforced polymers, which were not accounted for in this analysis.

Table B.6: Tensile Capacity/Demand at Each Crack Location

Moment Region	Θ	Crack 1			Crack 2			Crack 3		
		AASHO	ACI	Exp.	AASHO	ACI	Exp.	AASHO	ACI	Exp.
Positive	Measured	3.21	2.28	2.51	2.96	2.23	2.26	3.08	2.24	2.41
Negative		3.08	2.14	2.27	3.50	2.44	2.76	4.37	2.83	3.46
Positive	Possible	3.14	2.16	2.37	2.76	2.00	2.03	2.99	2.12	2.28
Negative		3.11	2.12	2.25	3.74	2.48	2.80	4.37	2.68	3.28

Table B.7: ACI 318 Shear Capacity vs. Demand at Each Crack Location

Moment Region	Crack	V_n (kN) [k]	V_u (kN) [k]	Ratio
Positive	1	274 [61.1]	226 [50.4]	1.21
	2	261 [58.3]	265 [59.3]	0.98
	3	273 [61.0]	312 [69.6]	0.88
Negative	1	1172 [261.7]	491 [109.7]	2.39
	2	538 [120.1]	426 [95.0]	1.26
	3	296 [66.1]	377 [84.2]	0.79

From the results in Table B.6, it can be seen that for all the crack locations, the anchorage capacities predicted using all three development lengths provide resistance larger than demand. Furthermore, using the maximum possible failure angles as opposed to only the observed diagonal crack angles provides a less conservative estimate of both failure load and mode. Although not the case for this example, if the predicted capacity is not sufficient to meet service level demands, the consideration of additional tensile capacity from framing steel may increase capacity to a point where anchorage failure is no longer a concern. From the results in Table B.7, it can be seen that for most instances, the nominal shear capacity is less than the Strength I demand (for maximum shear and moment, and refinement would warrant investigation of coincident moments and shears). Also, at all crack locations except at the negative 1 crack, a shear failure is more likely than an anchorage failure. If the partial safety factors for anchorage (Table B.6) and shear (Table B.7) failures are relatively close, the experimentally determined maximum average bond strength may better predict the failure mode. For the case study, the positive moment regions near midspan have sufficient tensile reinforcement for both service and strength level loads, but they have insufficient shear capacity at strength load conditions.

APPENDIX C:
ANCHORAGE CRACKING FIELD INSPECTION GUIDE

From the research performed as part of this examination of vintage reinforced concrete deck girders (RCDG), the following recommendations for inspection of existing bridge girders are provided.

When performing field inspection of reinforced concrete deck girder bridges with cutoff reinforcing details, inspection for anchorage failure concerns should focus on cracking near these cutoff details. Of particular interest is horizontal cracking along the developing length of the cutoff bars. If this type of horizontal cracking is observed, crack widths and locations should be noted. Further inspections should pay special attention to these areas to note changes. Research on negative moment regions indicates that for bridge girders susceptible to anchorage failure, this horizontal "wedge" cracking should become visible on the concrete face under service level loading as seen in Fig. C.1.

Figure C.1: Horizontal cracking along developing length of cutoff reinforcement in IT specimen

Research on positive moment regions demonstrated a similar cracking pattern when shear-anchorage failure is evolving. Beginning at service-level loading, cracks along the developing length of cutoff reinforcement form in the web of T-beam specimens as shown in Fig. C.2. This cracking is characterized by periodic vertical cracks extending from the location of the cutoff bar to the bottom soffit of the beam stem. The vertical cracks were connected by primary horizontal cracks at the level of the cutoff bar. Inspection should focus on the extent and density of these anchorage cracks over time. A measureable increase in this type of cracking is indicative of progressing anchorage failure.

Figure C.2: Horizontal cracking along developing length of cutoff reinforcement in T specimen

This type of crack pattern demonstrates clearly the slipping of cutoff reinforcement along the developing length. When this cracking occurs, bar slipping has already begun to occur. Plans should be made for strengthening and/or posting based on limiting capacity considering the possible diminished tensile capacity from a loss of bond of the cutoff bars. Increased occurrences of horizontal cracking accompanied by widening crack widths are an indicator of anchorage failure as seen in Fig. C.3.
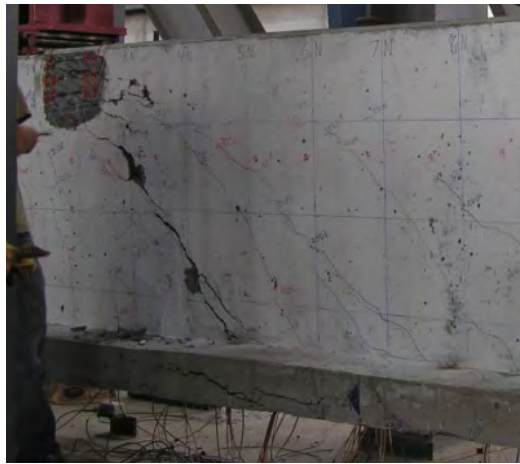
Figure C.3: Extremely wide horizontal cracking in IT specimen along developing length of cutoff bars

When inspecting regions susceptible to anchorage failure, great attention should be paid to any section exhibiting patterns of horizontal cracking. If these horizontal cracks are widening over time, urgency should be shown in determining the range of damage to the capacity of the girder. Diagonal cracking near these horizontal cracks should be carefully detailed for use in analysis. This cracking should then be compared to analytical predictions of critical failure locations using the methods described previously. Diagonal cracking occurring in areas near the predicted critical crack location may be cause for concern. However, not all visible diagonal cracking will be indicative of the ultimate failure location or angle. An analytical investigation based on provisions in the AASHTO-LRFD specifications combined with the crack conditions of inspected vintage reinforced concrete girders should assist in predicting crack locations and failure types.

APPENDIX D:
CONSTITUTIVE MODELS USED IN NLFEA

The information presented in this appendix describes the material and behavioral models implemented in the nonlinear finite element analyses using VecTor2.

D.1 CONCRETE COMPRESSION PRE-PEAK RESPONSE

The pre-peak response of the concrete was defined using the Hognestad parabola as shown in Fig. D.1. The parabola is defined as:

$$f_{ci} = -f_p \left[2\left(\frac{\varepsilon_{ci}}{\varepsilon_p}\right) - \left(\frac{\varepsilon_{ci}}{\varepsilon_p}\right)^2 \right] < 0 \quad \text{for} \quad \varepsilon_{ci} < 0 \qquad \text{[D.1]}$$

where f_p and ϵ_p are peak compressive stress and strain, respectively.
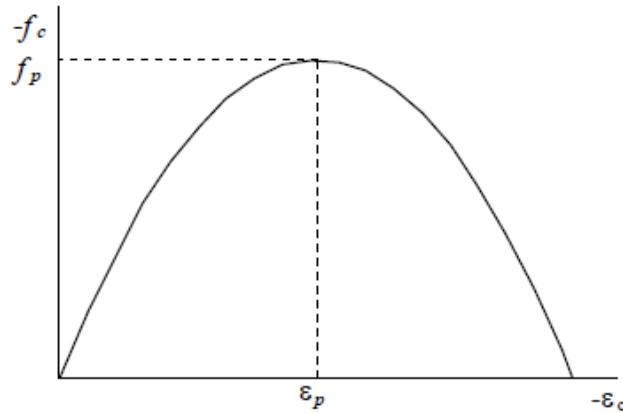
Figure D.1: Hognestad parabolic concrete compression response (Vecchio and Wong, 2002)

D.2 CONCRETE COMPRESSION POST-PEAK RESPONSE

The Modified Park-Kent post-peak response model accounts for the increased concrete strength and ductility due to transverse reinforcement confinement as shown in Fig. D.2. The Modified Park-Kent model is defined as:

$$f_{ci} = -\left[f_p + Z_m f_p \left(\varepsilon_{ci} - \varepsilon_p\right) \right] \quad \text{or} \quad -0.2 f_p \quad \text{for} \quad \varepsilon_{ci} < \varepsilon_p < 0 \qquad \text{[D.2]}$$

where

$$Z_m = \frac{0.5}{\dfrac{3 + 0.29|f_c'|}{145|f_c'| - 100} \times \dfrac{\varepsilon_o}{-0.002} + \left(\dfrac{|f_{lat}|}{170}\right)^{0.9} + \varepsilon_p} \qquad \text{[D.3]}$$

where ϵ_o is the concrete compressive strain, and f_{lat} (MPa) is the summation of principal stress, acting transversely to the direction under consideration:

D-1

$$f_{lat} = f_{c1} + f_{c2} + f_{c3} - f_{ci} \leq 0 \qquad \text{[D.4]}$$
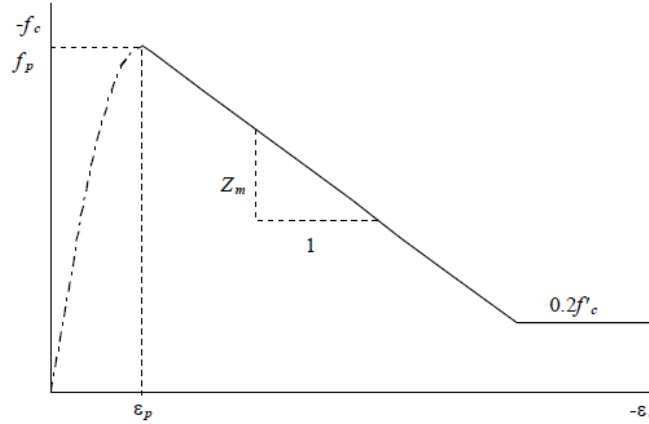
Figure D.2: Modified Park-Kent post-peak concrete compression response (Vecchio and Wong, 2002)

D.3 CONCRETE COMPRESSION SOFTENING

Compression softening refers to the reduction of compression strength and stiffness due to transverse cracking and tensile straining. VecTor2 reduces the compressive strength, f_p, and corresponding strain, ϵ_p, using a β_d factor. The Vecchio 1992-A (e1/e2-Form) model was used for this analysis as shown in Fig. D.3. The β_d factor is determined as:

$$\beta_d = \frac{1}{1 + C_s \cdot C_d} \leq 1 \qquad \text{[D.5]}$$

$$C_d = \begin{cases} 0 & \text{if} \quad r < 0.28 \\ 0.35(r - 0.28)^{0.80} & \text{if} \quad r > 0.28 \end{cases} \qquad \text{[D.6]}$$

$$r = \frac{-\varepsilon_{c1}}{\varepsilon_{c2}} \leq 400 \qquad \text{[D.7]}$$

$$C_s = \begin{cases} 0 & \text{if shear slip is not considered} \\ 0.55 & \text{if shear slip is considered} \end{cases} \qquad \text{[D.8]}$$

$$f_p = \beta_d f_c' \qquad \text{[D.9]}$$

$$\varepsilon_p = \beta_d \varepsilon_o \qquad \text{[D.10]}$$

where C_d is the strain softening factor, C_s is the shear slip factor, ε_{c1} is the principal tensile strain, and ε_{c2} is the principal compression strain.
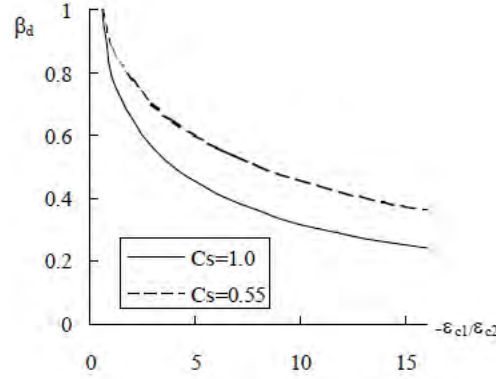
Figure D.3: Vecchio 1992-A compression softening model (Vecchio and Wong, 2002)

D.4 CONCRETE TENSION STIFFENING

Prior to cracking the response is assumed to be linear-elastic, as follows:

$$f_{c1} = E_c \varepsilon_{c1} \quad \text{for} \quad 0 < \varepsilon_{c1} < \varepsilon_{cr} \qquad \text{[D.11]}$$

where

$$\varepsilon_{cr} = \frac{f_{cr}}{E_c} \qquad \text{[D.12]}$$

ε_{cr} is the cracking strain, E_c is the initial tangent stiffness of concrete, ε_{c1} is the principal tensile strain, and f_{cr} is the cracking stress of concrete.

"Tension stiffening" refers to the phenomenon of cracked concrete still carrying tension stress between cracks through bond action. The Bentz tension stiffening model defines the average concrete tensile stress-strain response curve as:

$$f_{c1}^a = \frac{f_{cr}}{1 + \sqrt{3.6m\ \varepsilon_{c1}}} \quad \text{for} \quad 0 < \varepsilon_{cr} < \varepsilon_{c1} \qquad \text{[D.13]}$$

where the bond parameter, m, reflects the ratio of the concrete area bonded to the search of the reinforcement that is tributary to the concrete.

D.5 CONCRETE TENSION SOFTENING

"Tension softening" is a phenomenon of concrete referring to the gradual decrease of tensile stress after cracking rather than an abrupt disappearance of tensile stress. VecTor2 assumes the average post-cracked concrete tensile stress to be the larger of the concrete tensile stress due to tension stiffening, f_{c1}^b, and the average concrete tensile stress due to tension stiffening.

For this analysis, VecTor2 uses a linear tension softening base curve shown in Fig. D.4, and determined from:

$$f_{c1}^b = f_{cr}\left[1 - \frac{(\varepsilon_{c1} - \varepsilon_{cr})}{(\varepsilon_{ch} - \varepsilon_{cr})}\right] \geq 0 \quad \text{for} \quad \varepsilon_{cr} < \varepsilon_{c1} \qquad [D.14]$$

$$\varepsilon_{ch} = \frac{2G_f}{L_r \cdot f_{cr}} \quad \text{for} \quad 1.1\varepsilon_{cr} < \varepsilon_{ch} < 10\varepsilon_{cr} \qquad [D.15]$$

where ε_{ch} is the characteristic strain, G_f is the fracture energy with an assigned value of 75 N/m, and L_r is the distance over which the crack is assumed to be uniformly distributed and is assigned a value of half the crack spacing.

Figure D.4: VecTor2 linear tension softening response (Vecchio and Wong, 2002)

D.6 CONCRETE CONFINEMENT STRENGTH

To account for the enhanced strength and ductility of confined concrete, VecTor2 uses a strength enhancement factor, β_1, modify the uniaxial compressive strength, f_c', and the corresponding strain, ϵ_o, to determine the peak compressive strength, f_p', and the corresponding strain, ϵ_p, as follows:

$$f_p = \beta_d \beta_1 f_c' \qquad [D.16]$$

$$\varepsilon_p = \beta_d \beta_1 \varepsilon_o \qquad [D.17]$$

where β_d accounts for compression softening.

The Kupfer/Richart model was used to calculate the strength enhancement factor. The model is a combination of work conducted by Kupfer and Richart. For the direction of largest compressive stress, f_{c3}, β_1 is calculated as:

$$\beta_l = \left[1 + 0.92\left(\frac{f_{c2}}{f_c'}\right) - 0.76\left(\frac{f_{c2}}{f_c'}\right)^2\right] + 4.1\left(\frac{f_{cl}}{f_c'}\right) \quad \text{for} \quad f_{c2} < f_{c1} < 0 \qquad \text{[D.18]}$$

where

$$f_n = -(f_{c2} - f_{c1}) > 0 \qquad \text{[D.19]}$$

$$f_{c1} = -f_{c1} > 0 \qquad \text{[D.20]}$$

The calculation for determining the strength enhancement factor for the other compressive stress directions is similar.

D.7 CONCRETE DILATION

VecTor2 calculates Poisson's ratio for concrete in tension as:

$$\nu_{12} = \nu_{21} = \begin{cases} \nu_o & \text{for} \quad 0 < \varepsilon_{c1} < \varepsilon_{cr} \\ \nu_o\left(1 - \dfrac{\varepsilon_{c1}}{2\varepsilon_{cr}}\right) \geq 0 & \text{for} \quad \varepsilon_{cr} < \varepsilon_{c1} \end{cases} \qquad \text{[D.21]}$$

where ν_o is the initial Poisson's ratio.

For concrete in compression, the Kupfer was used. Fig. D.5 shows the nonlinear behavior of Poisson's ratio, and Posisson's ratio is defined as:

$$\upsilon_{ij} = \begin{cases} \nu_o & \text{for} \quad -0.5\varepsilon_p < \varepsilon_{cj} < 0 \\ \nu_o\left[1 + 1.5\left(\dfrac{-2\varepsilon_{cj}}{\varepsilon_p} - 1\right)^2\right] \leq 0.5 & \text{for} \quad \varepsilon_{cj} < -0.5\varepsilon_p \end{cases} \qquad \text{[D.22]}$$

where ϵ_p is the strain corresponding to the peak compressive stress.
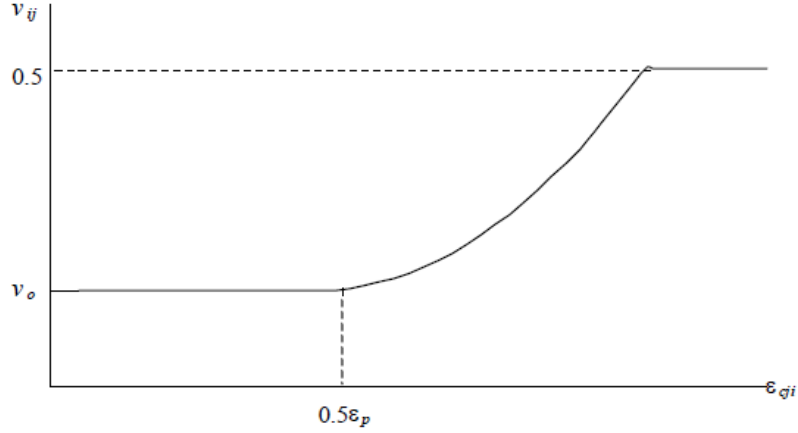
Figure D.5: Kupfer variable Poisson's ratio model (Vecchio and Wong, 2002)

D.8 CONCRETE CRACKING

The Mohr-Coulomb criterion was used to determine the concrete cracking strength, f_{cr}, as:

$$f_{cr} = f_{cru}\left(\frac{1+f_{c3}}{f_c'}\right) \quad \text{for} \quad 0.20 f_t' \leq f_{cr} \leq f_t' \quad \text{[D.23]}$$

where

$$f_{c3} = \begin{cases} -f_c'\left[2\left(\dfrac{\varepsilon_{c3}}{\varepsilon_o}\right) - \left(\dfrac{\varepsilon_{c3}}{\varepsilon_o}\right)^2\right] & \text{for} \quad \varepsilon_{c3} < \varepsilon_o < 0 \\[3mm] -f_c' & \text{for} \quad \varepsilon_o < \varepsilon_{c3} < 0 \\[3mm] 0 & \text{for} \quad 0 < \varepsilon_{c3} \end{cases} \quad \text{[D.24]}$$

$$f_{cru} = f_c' \frac{2c \cdot \cos\phi}{2\cos\phi} \quad \text{[D.25]}$$

$$c = f_c' \frac{1-\sin\phi}{2\cos\phi} \quad \text{[D.26]}$$

where c is the cohesion, and ϕ is the angle of friction with an assigned value of 37°.

The local shear stress at the crack surface, v_{ci}^{max}, was limited based on the crack check equation from Modified Compression Field Theory (Vecchio and Collins, 1986), and the work of Walraven (1981). v_{ci}^{max} is defined as:

$$v_{ci}^{max} = \frac{\sqrt{f_c'}}{0.3 + 24w/(a+26)} \qquad \text{[D.27]}$$

where w is the crack spacing (mm), and a is the maximum aggregate size (mm).

D.9 CONCRETE SLIP DISTORTIONS

Concrete slip distortions were determined using the model proposed by Vecchio and Lai The slip along the crack, δ_s, is computed as:

$$\delta_s = \delta_s^* \sqrt{\frac{\psi}{1-\psi}} \leq 2w \qquad \text{[D.28]}$$

where

$$\delta_s^* = \frac{0.5v_{cimax} + v_{co}}{1.8w^{-0.8} + \left(0.234w^{-0.707} - 0.20\right)f_{cc}} \qquad \text{[D.29]}$$

$$\psi = \frac{v_{ci}}{v_{cimax}} \qquad \text{[D.30]}$$

$$v_{cimax} = \frac{\sqrt{f_c'}}{0.31 + 24w/\left(a+16\right)} \qquad \text{[D.31]}$$

$$v_{co} = \frac{f_{cc}}{30} \qquad \text{[D.32]}$$

where v_{ci} is the local shear stress on the crack, w is the average crack width, a is the maximum aggregate size, v_{co} implements an initial offset in the crack shear-slip relationship, and f_{cc} (MPa) is the concrete cube strength, taken as $1.2f_c'$.

D.10 CONCRETE HYSTERETIC RESPONSE

The plastic offset, nonlinear loading/unloading model was used to define the hysteretic response of the concrete. This model incorporates elements from the concrete hysteresis model proposed by Vecchio and Ramsberg-Osgood formulation.

The concrete stress f_c, when unloading in compression to a strain of ϵ_c is:

$$f_c = f_{cm} + E_c \left(\varepsilon_c - \varepsilon_{cm} \right) + \frac{E_c \left(\varepsilon_c - \varepsilon_{cm} \right)^{N_c}}{N_c \left(\varepsilon_c^p - \varepsilon_{cm} \right)^{N_c - 1}} \quad \text{for} \quad 1 \le N_c \le 20 \qquad \text{[D.33]}$$

where ε_c^p is the current plastic offset strain, ε_{cm} is the maximum previously attained compress strain, f_{cm} is the corresponding stress. N_c is the Ramsberg-Osgood power term representing the deviation from linear elasticity computed as:

$$N_c = \frac{E_c \left(\varepsilon_c^p - \varepsilon_{cm} \right)}{f_{cm} + E_c \left(\varepsilon_c^p - \varepsilon_{cm} \right)} \qquad \text{[D.34]}$$

When N_c does not fall between one and twenty, f_c is:

$$f_c = E_c \left(\varepsilon_c - \varepsilon_c^p \right) \quad \text{for} \quad N_c \le 1 \text{ or } 20 \le N_c \qquad \text{[D.35]}$$

The concrete stress, f_c, when unloading in tension is:

$$f_c = f_{tm} - E_c \left(\varepsilon_{tm} - \varepsilon_c \right) + \frac{E_c \left(\varepsilon_{tm} - \varepsilon_c \right)^{N_t}}{N_c \left(\varepsilon_{tm} - \varepsilon_c^p \right)^{N_t - 1}} \quad \text{for} \quad 1 \le N_t \le 20 \qquad \text{[D.36]}$$

where ε_c^p is the current plastic offset strain, ε_{tm} is the maximum previously attained tensile strain, f_{tm} is the corresponding stress. N_t computed as:

$$N_t = \frac{E_c \left(\varepsilon_{tm} - \varepsilon_c^p \right)}{E_c \left(\varepsilon_{tm} - \varepsilon_c^p \right) - f_{tm}} \qquad \text{[D.37]}$$

When N_t does not fall between one and twenty, f_c is:

$$f_c = E_c \left(\varepsilon_c - \varepsilon_c^p \right) \quad \text{for} \quad N_t \le 1 \text{ or } 20 \le N_t \qquad \text{[D.38]}$$

D.11 STEEL REINFORCEMENT STRESS-STRAIN RESPONSE

For ductile steel reinforcement, VecTor2 uses a trilinear stress-strain response as shown in Fig. D.6. The reinforcement stress, f_s, is determined as follows:

$$f_s = \begin{cases} E_s \varepsilon_s & \text{for} \quad |\varepsilon_s| \le \varepsilon_y \\ f_y & \text{for} \quad \varepsilon_y < |\varepsilon_s| \le \varepsilon_{sh} \\ f_y + E_{sh} \left(\varepsilon_s - \varepsilon_{sh} \right) & \text{for} \quad \varepsilon_{sh} < |\varepsilon_s| \le \varepsilon_u \\ 0 & \text{for} \quad \varepsilon_u < |\varepsilon_s| \end{cases} \qquad \text{[D.39]}$$

$$\varepsilon_u = \varepsilon_{sh} + \frac{\left(f_u - f_y\right)}{E_{sh}} \tag{D.40}$$

where ϵ_s is the reinforcement strain, ϵ_y is the yield strain, ϵ_{sh} is the strain at the onset of strain hardening, ϵ_u is the ultimate strain, E_s is the elastic modulus, E_{sh} is the strain hardening modulus, f_y is the yield strength, and f_u is the ultimate strength.
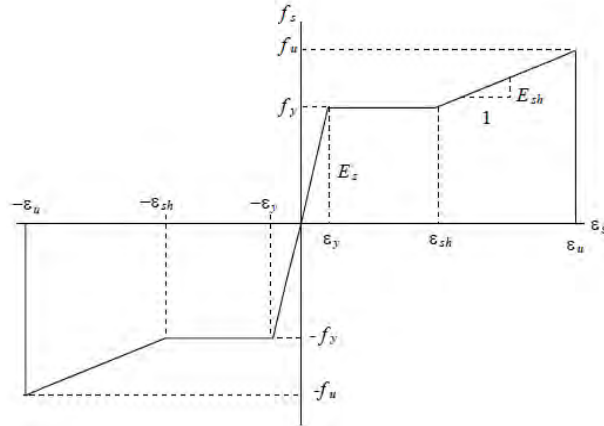
Figure D.6: Ductile steel reinforcement stress-strain response (Vecchio and Wong, 2002)

D.12 STEEL REINFORCEMENT DOWEL ACTION

Dowel action occurs at crack locations when the flexural steel must resist the shear force. In beams with light transverse reinforcement, the dowel action force may be significant. The Tassios Model for dowel action shear force, V_d, due to a relative displacement, δ_s, is:

$$V_d = E_s I_z \lambda^3 \delta_s \leq V_{du} \tag{D.41}$$

where the area moment of inertia of the reinforcement, I_z, is:

$$I_z = \frac{\pi d_b^4}{64} \tag{D.42}$$

where λ compares the stiffness of the concrete to the stiffness of the reinforcement and is calculated as:

$$\lambda = \sqrt[4]{\frac{k_c d_b}{4 E_s I_z}} \tag{D.43}$$

where k_c is the stiffness of notional concrete foundation and determined as follows:

$$k_c = \frac{127c\sqrt{f_c'}}{d_b^{2/3}} \qquad\qquad \text{[D.44]}$$

where c is experimentally defined as 0.8 and refers to the bar spacing.

$$c = 0.8 \qquad\qquad \text{[D.45]}$$

Lastly, the ultimate dowel force, V_{du}, describes the plastic hinging of the reinforcement and crushing of the surrounding concrete. V_{du} is calculated as:

$$V_{du} = 1.27d_b^2\sqrt{f_c' f_y} \qquad\qquad \text{[D.46]}$$

D.13 BOND MODEL

The confined and unconfined bond stress-slip relationship proposed by Eligehausen is shown in Fig. D.7. The confined stress-slip relationship is defined as:

$$\tau = \begin{cases} \tau_{p1}\left(\Delta / \Delta_{p1}\right)^\alpha & \text{for } \Delta \leq \Delta_{p1} \\[2mm] \tau_{p2} & \text{for } \Delta \leq \Delta_{p1} \\[2mm] \tau_{p2} - \left[\dfrac{\left(\Delta - \Delta_{p2}\right)}{\left(\Delta_{p3} - \Delta_{p2}\right)}\left(\tau_{p2} - \tau_{pf}\right)\right] & \text{for } \Delta_{p1} < |\Delta| \leq \Delta_{p2} \\[4mm] \tau_{pf} & \text{for } \Delta_{p3} < \Delta \end{cases} \qquad \text{[D.47]}$$

where

$$\tau_{pl} = \left(20 - \frac{d_b}{4}\right)\sqrt{\frac{f_c'}{30}} \qquad\qquad \text{[D.48]}$$

$$\tau_{p2} = \tau_{p1} \qquad\qquad \text{[D.49]}$$

$$\tau_{pf} = \left(5.5 - 0.07\frac{S}{H}\right)\sqrt{\frac{f_c'}{27.6}} \qquad\qquad \text{[D.50]}$$

$$\Delta_{p1} = \sqrt{\frac{f_c'}{30}} \qquad\qquad \text{[D.51]}$$

$$\Delta_{p2} = 3.0\,mm \qquad\qquad \text{[D.52]}$$

$$\Delta_{p3} = S \qquad\qquad \text{[D.53]}$$

$$\alpha = 0.4 \qquad [\text{D.54}]$$

The unconfined stress-slip relationship is defined as:

$$\tau = \begin{cases} \tau_{s1}\left(\Delta / \Delta_{p1}\right)^{\alpha} & \text{for } \Delta \leq \Delta_{s1} \\ \tau_{s2} & \text{for } \Delta \leq \Delta_{s1} \\ \tau_{s2} - \left[\dfrac{\left(\Delta - \Delta_{s2}\right)}{\left(\Delta_{s3} - \Delta_{s2}\right)}\left(\tau_{s2} - \tau_{sf}\right)\right] & \text{for } \Delta_{s1} < \left|\Delta\right| \leq \Delta_{s2} \\ \tau_{sf} & \text{for } \Delta_{s3} < \Delta \end{cases} \qquad [\text{D.55}]$$

where

$$\tau_{s1} = 0.748\sqrt{\dfrac{f_c' c}{d_b}} \leq \tau_{p1} \qquad [\text{D.56}]$$

$$\tau_{s2} = \tau_{s1} \qquad [\text{D.57}]$$

$$\tau_{sf} = 0.234\sqrt{\dfrac{f_c' c}{d_b}} \leq \tau_{sf} \qquad [\text{D.58}]$$

$$\Delta_{s1} = \Delta_{pl} \exp\left[\dfrac{1}{\alpha}\ln\left(\dfrac{\tau_{s1}}{\tau_{p1}}\right)\right] \qquad [\text{D.59}]$$

$$\Delta_{s2} = \Delta_{p2} \qquad [\text{D.60}]$$

$$\Delta_{s3} = \Delta_{p3} \qquad [\text{D.61}]$$

When the anticipated confinement pressure is somewhere between the unconfined and confined cases, a confinement pressure coefficient, β, is used to linearly interpolate between the unconfined and confined cases, where β is defined as:

$$\beta = \dfrac{\sigma}{7.5} \qquad 0 \leq \beta \leq 1 \qquad \text{(in MPa)} \qquad [\text{D.62}]$$

where σ is the anticipated confinement pressure in MPa. When a confinement stress factor, β, is defined, the bond stress-slip relationship is:

$$\tau = \begin{cases} \tau_{sp1}\left(\Delta / \Delta_{sp1}\right)^{\alpha} & \text{for} \quad \Delta \leq \Delta_{sp1} \\[2ex] \tau_{sp1} - \left[\dfrac{\left(\Delta - \Delta_{sp2}\right)}{\left(\Delta_{sp3} - \Delta_{sp2}\right)}\left(\tau_{sp2} - \tau_{spf}\right)\right] & \text{for} \quad \Delta_{sp1} < \left|\Delta\right| \leq \Delta_{sp2} \\[2ex] \tau_{sp2} - \left[\dfrac{\left(\Delta - \Delta_{sp2}\right)}{\left(\Delta_{sp3} - \Delta_{sp2}\right)}\left(\tau_{sp2} - \tau_{spf}\right)\right] & \text{for} \quad \Delta_{sp2} < \Delta \leq \Delta_{sp3} \\[2ex] \tau_{spf} & \text{for} \quad \Delta_{sp3} < \Delta \end{cases}$$ [D.63]

where

$$\tau_{sp1} = \tau_{s1} + \beta\left(\tau_{p1} - \tau_{s1}\right)$$ [D.64]

$$\tau_{sp2} = \tau_{sp1}$$ [D.65]

$$\tau_{spf} = \tau_{s1} + \beta\left(\tau_{pf} - \tau_{sf}\right)$$ [D.66]

$$\Delta_{sp1} = \Delta_{s1} + \beta\left(\Delta_{p1} - \Delta_{s1}\right) \geq \Delta_{s1}$$ [D.67]

$$\Delta_{sp2} = \Delta_{p2}$$ [D.68]

$$\Delta_{sp3} = \Delta_{p3}$$ [D.69]
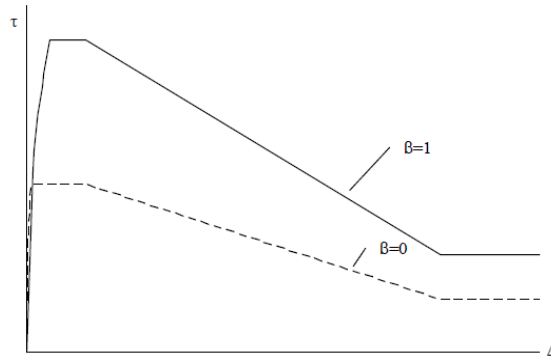
Figure D.7: Eligehausen bond stress-slip response (Vecchio and Wong, 2002)